UNIVERSITY OF SOUTHAMPTON

FACULTY OF NATURAL & ENVIRONMENTAL SCIENCES

School of Ocean & Earth Science

Modelling Macro-Nutrient Release and Fate Resulting from Sediment Resuspension in Shelf Seas

by

Christopher Charles Wood

Thesis for the degree of Doctor of Philosophy

June 2012

Abstract

Early diagenesis (ED), the physical and biogeochemical changes undergone in surficial sediments, plays an important role in the biogeochemical cycles of key elements (carbon, nitrogen and oxygen) in highly productive shelf-seas. Modelling the process uses a relatively simple set of mathematical equations to represent the transport and reaction terms. I have calibrated an existing steady-state ED model, OMEXDIA, which I have expanded to include more processes and variables (e.g. mineralisation of organic matter using iron oxide and sulphate) to examine the fate of nutrients through sediment water exchange, as well as showing how the dynamic version can be used to show how the annual variation in carbon flux to the sediment effects nutrient concentrations and fluxes across the sediment-water interface (SWI). I also discuss limitations to the model with regard to the implementation of further biogeochemical cycles, and the increased model complexity that this entails.

Observations made at the North Dogger site in the North Sea provide suitable data to calibrate the model. I have used a Genetic Algorithm (GA) approach to determine a set of parameters which is able to reflect the profiles observed. The results of the GA experiments are able to calculate sedimentary profiles that are consistently within the ranges of observations for total organic carbon, oxygen, nitrate and ammonia. I have also shown how the GA approach can act as a tool for the prediction of profiles of chemical species for the North Sea, and as such, this can lead to estimates for rates of biogeochemical processes and fluxes of chemical species that are often difficult to obtain experimentally.

Biogeochemical cycles can be affected by resuspension as a result of release or uptake of nutrients, which can also have a considerable effect on primary productivity. Resuspension is a wide-spread transport process in shallow seas due to winds, tides and biological activity. In contrast to previous diagenetic modelling, resuspension has been implemented into the dynamic version of OMEXDIA to examine its effect on nutrient cycling, and the reoxidation or burial of reduced compounds and associated nutrients. As the model results compare favourably with previously obtained experimental observations carried out both *in situ* and under controlled laboratory situations, I show it is possible to predict the effect that resuspension has both on the concentration of nutrients in the sediment, and therefore also on the flux of the nutrients across the SWI. It is also possible to calculate the length of time it takes for the sediment to re-equilibrate after a resuspension event, and I show, for the first time, the likely effect that both natural and anthropogenic resuspension events have on overall nutrient budget of the North Sea.

Contents

List of Figures

List of Tables

DECLARATION OF AUTHORSHIP

I, Christopher Charles Wood

declare that the thesis entitled

Modelling Macro-Nutrient Release and Fate Resulting from Sediment Resuspension in Shelf Seas

and the work presented in the thesis are both my own, and have been generated by me as the result of my own original research. I confirm that:

- this work was done wholly or mainly while in candidature for a research degree at this University;
- where any part of this thesis has previously been submitted for a degree or any other qualification at this University or any other institution, this has been clearly stated;
- where I have consulted the published work of others, this is always clearly attributed;
- where I have quoted from the work of others, the source is always given. With the exception of such quotations, this thesis is entirely my own work;
- I have acknowledged all main sources of help;
- where the thesis is based on work done by myself jointly with others, I have made clear exactly what was done by others and what I have contributed myself;
- none of this work has been published before submission

Signed: ……..

Date:…….

Acknowledgements

This thesis would not exist was it not for the support of a huge number of people, and so I need to initially thank all those people who I forget to mention here. The unrelenting support and patience of my supervisors, Peter Statham and Boris Kelly-Gerreyn, who have provided constant guidance and support, has been utterly invaluable, and to whom I will be forever in debt. I need to especially thank several people at NOCS, including Andrew Yool, Adrian Martin, Peter Challenor (particularly for help with both R and statistics!), Charlie Thomson, Carl Amos, John Hemmings, John Allen, Ranji Goddard and Bob Marsh who all gave up much more time than I'm sure I deserved and provided many very helpful discussions.

Thanks need to go to all the collaborators (Gary Fones, Fay Couceiro, Ruth Parker, John Aldridge, Naomi Greenwood, Elke Neubacher, Dave Sivyer, and all others who helped collect data and analyse samples and results) on the MEC project for providing me with all the data that has helped improve the model, and for letting me participate on cruise CEND 1608, which in itself taught me huge amounts about undertaking all types of oceanographic research!

I am grateful to Karline Soetaert and Filip Meysman for hosting me at NIOO-CEME on three separate occasions and for helping me understand the mechanics of diagenetic modelling. The friendliness and kind hospitality of the staff and students of NIOO (especially the residents of "*de Keete*") helped make my stays in Yerseke particularly memorable, and I will always look back upon my visits there fondly.

The friendships created in Southampton during my time here will be long-lasting, and several of these people need a special mention for always being encouraging (often in their own unique ways!); so to David, Sarah, Steve, David, Freya, Tim, Sophie, Sara, Laurie, Josh, Jenny and all other members of SUHC, the University Badminton Club and SUCC who provided some unforgettable times, which helped me to have some breaks from thinking about work, and I'm sure have kept me sane, thanks.

Finally, I need to thank my parents for their unequivocal, never-ending support, particularly through the most difficult times. My mum, especially, needs a special mention for never refusing to proof-read anything, regardless of content! However, all errors which remain in this work are, of course, my sole responsibility.

Definitions and abbreviations

1D	1-dimensional
2D	2-dimensional
3D	3-dimensional
C	Carbon
DOC	Dissolved organic carbon
DNRA	Dissimilatory nitrate reduction to ammonium
Fe_2O_3	Iron oxide
Fe^{2-}	Reduced elemental iron
GA	Genetic algorithm
Mn	Manganese
NH_3/ NH_4^+	Ammonia / ammonium
NO_3^-	Nitrate
O_2	Oxygen
OC	Organic carbon
ODE	Ordinary differential equation
ODU	Oxygen demand units
OM	Organic matter
OPD	Oxygen penetration depth
POC	Particulate organic carbon
POM	Particulate organic matter
PDE	Partial differential equation
S^{2-}	Sulphide
SCOC	Sediment community oxygen consumption
SO_4^{2-}	Sulphate
SPM	Suspended particulate matter
SWI	Sediment-water interface
TOC	Total organic carbon
TSS	Total suspended solids

1 The Significance of Shelf-Sea Systems

Due to the availability of the major nutrients (bioavailable forms of carbon, nitrogen and phosphorus) needed for the onset and continual growth of primary productivity, shelf seas and continental shelves, such as the North Sea, can be considered important areas for marine ecosystems. Shelf seas account for less than 10% of the total ocean area, but account for approximately 20% of the marine environment's total annual global production (9×10^{15} g C) and have almost double the productivity of the open ocean (250 compared to 130 g C m^{-2} yr^{-1}) (Schlesinger 1997; Knauer 1993). The importance of the recycling of nutrients was shown by the same authors, who concluded that new production on coastal shelves accounts for approximately 15% of all primary production (Eppley 1989; Knauer 1993), and more recent estimates have continued to verify this figure (Chen *et al.* 2003). Macronutrients (organic forms of carbon, nitrogen, phosphorous and silicon which can be taken up by plants for the purpose of primary production), can all exist in dissolved and particulate organic forms, with dissolved particles classed as those under 0.45 μm in size (Wright *et al.* 1995).

As this thesis will concentrate on the North Sea, it is useful to provide an explanation of the area that will be considered. Despite some apparent disagreement in the literature about the boundaries of the North Sea, this thesis will, in general, keep to the area defined by the 1993 North Sea Quality Status Report (North Sea Task Force 1993), which includes the English Channel (with the most South Westerly Corner at 48°N 5°W), the Skaggerak, the Kattegat, and the Northern Atlantic to a North Westerly point of 62°N 5°W. The area is shown in full in Figure 1.1.

As a result of the relatively high surface-area to volume ratios, large amounts of organic carbon (OC) can be adsorbed on to suspended particulate matter (SPM), and as such forms an important transport mechanism of organic matter to the sediment (de Haas *et al.* 1997), especially in shelf sea areas such as the North Sea (Bale and Morris 1998; van Raaphorst *et al.* 1998). The total mass of SPM in the southern North Sea has been estimated to be as high as 9.6×10^{6} tonnes during winter (McManus and Prandle 1997), and the total amount of dissolved organic carbon (DOC) has been estimated to be as much as 6.5×10^{11} tonnes (McNichol and Aluwihare 2007). The total amount of SPM is also deemed to be important to help understand the significance of continental shelves in the global carbon cycle, as well as to help predict the amount of organic matter that may be buried in the sediment (van Raaphorst *et al.* 1998).

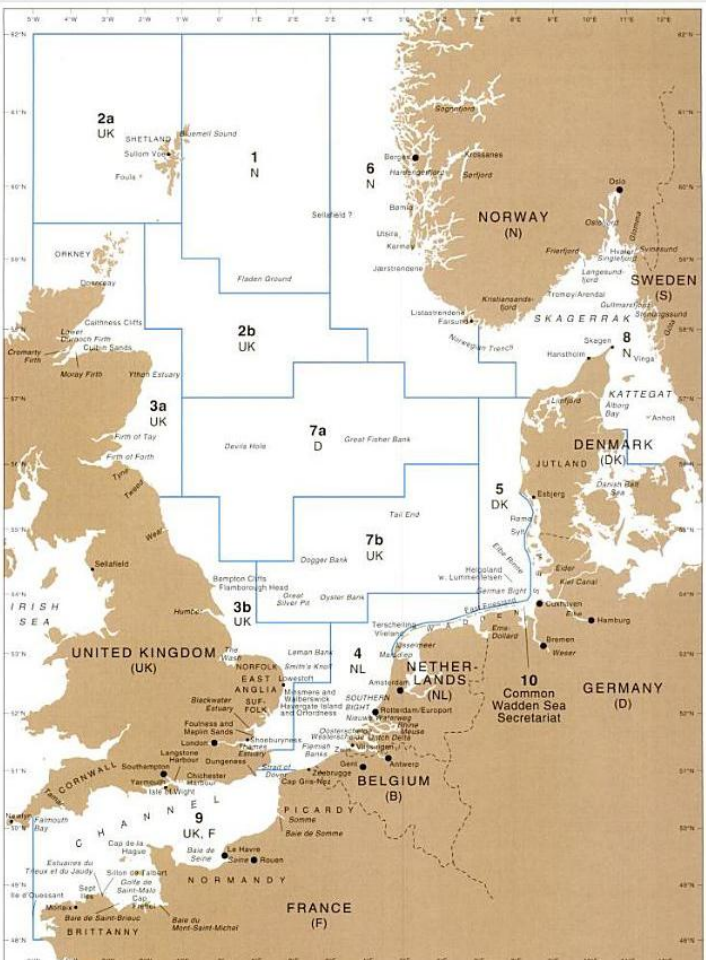

Figure 1.1: Boundaries of the North Sea for the purposes of this thesis, as defined within the North Sea Quality Status Report (North Sea Task Force 1993)

SPM size has been found to differ considerably depending on the time of year. Results from the Sediment Resuspension Experiment in the North Sea showed that the modal diameter (represented as the equivalent spherical diameter [ESD]) ranged from approximately 7 µm in January to a maximum diameter of 115 µm in May, and then fell by almost 90% in September (Jones *et al.* 1998); the largest fraction coming very soon after the spring-bloom. During the May measurements, a bimodal ESD distribution of particles was also found, with pronounced differences either side of the thermocline; measurements showed a reduction in the population of 7 µm particles below the thermocline, and an increase in the population of 35 µm particles above it. During the September sampling, the particle population showed a clear reduction in size, with the final measurements below the thermocline being 7-15 µm, resulting in little difference between particle size above and below the thermocline (Jones *et al.* 1998). Other studies, both in the North Sea and in other shelf seas, have shown similar sizes and patterns for the distribution of SPM (e.g. Eisma and Kalf 1987; Velegrakis *et al.* 1999), but with slightly larger particle sizes close to riverine inputs to the marine system (Jago and Bull 2000).

Sedimentation rates, however, are more difficult to determine, and differing methods (both direct and proxy) used to measure the rates have come to varying (and

sometimes contradictory) conclusions (de Haas and van Weering 1997). Recent studies have helped to settle previous inconsistencies, especially where new methods (such as acoustic profiling) have been used (de Haas and van Weering 1997). These more recent estimations have also been used to validate models; calculated values from coupled models coincide well with the sedimentation rates (Luff and Moll 2004). Different techniques used for estimating sedimentation rates (sediment traps, ^{210}Pb chronology, pollen studies, anthropogenic pollution, mass budget calculations of suspended sediments, foraminifera studies and ^{14}C measurements) have come to varying (and sometimes contradictory) conclusions (de Haas and van Weering 1997). One of the few comprehensive studies on sedimentation rates in the North Sea (de Haas *et al.* 1997; de Haas and van Weering 1997) estimated that the sedimentation rate in the Norwegian Channel, part of the North Sea, ranged from 30 to 280 mm 100 yr^{-1}, with total sediment accumulation being 2.8 x 10^7 tonnes yr^{-1}. The same study showed that the concentration of buried OC is approximately 0.6% and accumulates at a rate of 0.17 x 10^7 ton yr^{-1}, and, as such, is considered to be an important area within the North Sea for the sink of organic matter (de Haas and van Weering 1997). The same authors also show the importance of transport within the marine environment, by showing that the vast majority (90%) of the OC buried in the North Sea comes from outside the area studied, most likely transported by bottom and intermediate nepheloid layers. Surface nepheloid layers formed of organic material also exist.

The sources of organic matter can also be difficult to determine accurately, especially when there are differing claims as to how evenly distributed primary production is across a geographical area. The most recent estimates (Eisma and Kalf 1987) on the concentration of suspended matter in the North Sea found that it could range from 0.1 mg dm^{-3} in open channels to greater than 10 mg dm^{-3} in coastal areas, with bottom concentrations being slightly higher (occasionally up to three times higher) than in surface waters, due to tidal currents or wind-forced currents which are able to resuspend sediment. Organic matter content of the SPM also ranges widely, but not to the same orders of magnitude as concentration, and the levels are reversed; highest organic matter concentration is found in the surface water of open channels (e.g. 60% in the surface waters of the north North Sea, between Shetland and the Norwegian coast, falling to 20% in the continental coast waters). Ignoring the effect of primary productivity, organic matter concentrations do not vary significantly between surface and bottom waters (Eisma and Kalf 1987) . The methods used for data analysis have also been cited as reasons for discrepancies between results of calculations for the amount of excess OC in the marine ecosystems (Williams and Bowers 1999; Williams 1998).

1.1 Biogeochemistry of sediment

Early diagenesis, the physical, biological and chemical changes that occur to material deposited on sediments, and specifically where there is interaction with pore-water (Brown *et al.* 1989; Stumm and Morgan 1996; Froelich *et al.* 1979) is a key component of marine biogeochemical cycles (van der Weijden 1992; van Raaphorst *et al.* 1990). Early diagenesis is driven by the flux of OC to the sediment from the overlying water column.

Organic material which sinks to the sediment may be nutrient poor, due to the recycling of organic matter which often takes place further up in the water column. Faecal matter of zooplankton grazing in a phytoplankton bloom may still contain large amounts of organic matter, which itself can be grazed upon. This cycle can continue until either it has sunk out of the photic zone or that the material is too poor in nitrogen and/or phosphorous to be used. However, in shelf-sea systems, up to 12% of the sediment may be OC (Hartnett *et al.* 1998); much more than in deep oceans where it has been estimated that only 0.3% of the sediment is OC (Degens and Mopper 1976). As with the uncertainties with the concentration and total content of SPM in shelf sea environments, similar discrepancies exist with the estimates of the amount of organic material which precipitates out of the photic zone into the bottom waters, and the amount which then subsequently undergoes either diagenetic processes, or which is permanently buried in the sediments. Berner (1982) makes clear that shelf seas are especially important with regard to the diagenetic processes when compared to the global scale, with his estimates that deposition on shelf seas account for more than 80% of the global total, even though the continental margins only cover about 11.5% of the total marine environment (Gross and Gross 1996).

The proportion of the organic material that is subsequently buried relative to the quantity produced in the water column is known to vary with water depth; not only is productivity lower in open ocean environments than in coastal oceans, but the increased water depth also leads to a greater proportion of the sinking organic material to be degraded in the water column before reaching the sediment. Coastal oceans have higher rates of primary productivity and shallower water depths, leading to higher fluxes of OM to the sediment; it has been estimated that approximately 3% of surface water primary productivity reaches the benthic layer in shelf seas (Jahnke 1996). Refractory material, which is not degraded, will be permanently buried. More recently, it has been shown that relatively large proportions of organic matter that reaches the sediment can be permanently buried, with (Jørgensen *et al.* 1990) estimating that up to 50% of the settled organic material being permanently buried. If,

to a first order approximation, it is assumed that 3% of the primary production is reaching the sediment, then it follows that 1.5% of the total water column primary production is permanently buried. Separate work has estimated that 0.4% of open ocean primary production is permanently buried (Degens and Mopper 1976).

Given that recent estimates suggest that up to 180 Tg of OC is buried globally per year (Berner 1982; van der Weijden 1992), and that primary production in shelf seas can be up to ten times higher than in the open ocean (Carr *et al.* 2006), the importance of understanding the role of sediment in shelf seas is clear if we are to fully understand the global carbon and nitrogen cycles (Hydes *et al.* 1999; Thomas *et al.* 2005).

One process of early diagenesis is the microbially-mediated oxidation of organic matter (OM) using a number of oxidants, leading to a well-defined series of chemical reactions and sediment zonation. This involves two main chemical reactions, oxidation and a corresponding reduction reaction (collectively known as a redox reaction) affected by the diffusion of the species involved, sedimentation and bioturbation (Brockmann *et al.* 1990). Two further processes which affect certain chemical species are sorption and precipitation (van Raaphorst *et al.* 1990). The transport fluxes of chemical compounds that occur during the diagenetic process can also be split into four components: bioturbation, molecular diffusion in the pore water, advection in the pore water and deposition of solid particles (Stumm and Morgan 1996).

Oxidation of organic matter is mediated via chemical agents (also known as electron acceptors) in a sequence which is determined by the Gibbs Free Energy of the reaction (Froelich *et al.* 1979; Atkins and de Paula 2002). Table 1.1 shows the stoichiometric equations of oxidation, in the order of oxidants (electron acceptors) that are generally classed as the most important during diagenesis and in the order of the Gibbs Free Energy yield of each reaction (Froelich *et al.* 1979). Since Froelich's work, other oxidants, such as iodate (I_2O_5) have also been shown to be able to oxidise organic matter (Passier *et al.* 1997). In totally anoxic environments, such as where the sedimentation of OM is high enough to deplete all the oxidants listed in Table 1.1, methanogenesis can occur, in which organic matter degradation is coupled to the production of methane.

The reactions in Table 1.1 lead to zones occurring in the sediment. The zone where degradation with oxygen dominates is known as the oxic zone, with manganese reduction, denitrification, iron reduction and sulphur reduction all occurring in the suboxic zone. Methanogenesis occurs in the anoxic zone.

The direction of the fluxes of each chemical species both within the sediment porewaters and across the surface-water interface is determined by the concentration gradient created by the redox reactions. For example, in areas which have oxic bottom waters, the net flux of O_2 will often be from the water column into the sediment to meet the demand by mineralization; however, it has recently been shown that in areas with high rates of benthic primary production, the oxygen flux may be reversed (Fenchel and Glud 2000; Glud 2008).

Table 1.1: Oxidation reactions of sedimentary organic matter (Froelich *et al.* 1979) [OM = organic matter: $(CH_2O)_{106}(NH_3)_{16}(H_3PO_4)$]

Process	Reaction (oxidant & reduced species in bold)	Gibbs' Free Energy (kJ mol^{-1})
Aerobic respiration	OM + 138 **O_2** → 106 CO_2 + 16 **HNO_3** + H_3PO_4 + 122 H_2O	-3190
Manganese reduction	OM + 212 **MnO_2** → 236 **Mn^{2+}** + 106 CO_2 + 8 N_2 + H_3PO_4 + 366 H_2O	-3090
Denitrification (nitrate reduction)	OM + 84.8 **HNO_3** → 106 CO_2 + 42.4 N_2 + 16 **NH_3** + H_3PO_4 + 148.4 H_2O	-3030
Iron reduction	OM + 424 **FeOOH** → 424 **Fe^{2+}** + 106 CO_2 + 42.4 N_2 + H_3PO_4 + 148.4 H_2O	-1410
Sulphur reduction	OM + 53 **SO_4^{2-}** → 53 **S^{2-}** + 106 CO_2 + 16 NH_3 + H_3PO_4 + 106 H_2O	-380

Different environments can affect how quickly all the available organic matter is degraded. The two plots in Figure 1 of Henrichs (1992) show that the sum of total mineralisation and total burial is equal to total input; the plots estimate that in areas with relative high OM input (>100 g C m^{-2} yr^{-1}), approximately 65% of the OM is mineralised and approximately 35% is buried, which is a slightly different ratio to the one already discussed in this chapter. Henrichs (1992) estimated that in the most rapidly accumulating environments, total degradation of organic matter occurs within 50 years and that the timescales for total degradation in the slowest accumulating environments can be up to seven orders of magnitude longer. It is also worth noting that although in the majority of cases, the biogeochemical processes occurring in the benthic layer are driven by the supply of organic matter which can then be degraded. However, sediments may also lie in the photic zone, in which case primary production can also play a role in the supply of organic matter (Van Cappellen and Wang 1996). In environments where the OM accumulates less quickly, the burial efficiency rate (defined as the rate of organic matter burial / rate of organic matter input to the surface) may be much lower (Henrichs 1992).

Each of the oxidants listed in Table 1.1 will be discussed in turn in the following section, with the role each one undertakes in biogeochemical processes described.

1.2 The cycling of individual chemical species

1.2.1 Oxygen

In agreement with all previous work, Froelich *et al.* (1979) stated that the most oxidising compound is O_2, which yields -3190 KJ mol^{-1} during the reaction which forms CO_2, HNO_3, H_3PO_4 and H_2O from marine organic matter.

With high amounts (greater than 2.5% dry weight of sediment) of organic matter in sediments (Bakker and Helder 1993), oxygen consumption is high (up to 13.71 mmol O_2 m^{-2} d^{-1}), and concentration decreases to zero within a few centimetres in coastal seas such as the Skaggerak (Bakker and Helder 1993), although the relationship between TOC content and oxygen consumption is highly variable (Osinga *et al.* 1996; Van Raaphorst *et al.* 1992). North Sea sediments typically have bottom water O_2 concentrations between 230 and 337 μmol l^{-1} (Boon *et al.* 1999), although anoxic bottom waters have also been recorded in the North Sea (Lohse *et al.* 1993). Oxygen penetration depths (OPDs) in the North Sea vary between 3 and 26 mm (Bakker and Helder 1993), although these values are dependent on season, water depth and sediment type. Deeper penetration occurs during winter, on account of lower quantities of organic matter reaching the sediment. The higher porosity of sandier sediments means that OPDs are deeper than in fine sediments (Bakker and Helder 1993; Janssen *et al.* 2005; Boon *et al.* 1999).

As well as its role in mineralisation, oxygen is also the main reoxidant for the reduced species such as Mn^{2+}, NH_4^+, Fe^{2+} and S^{2-}, which are produced by OM mineralisation below the oxic zone and transported by diffusion into the oxic layer. These secondary reactions are an important part of the biogeochemical cycling and are an additional sink for O_2. Therefore, in sediments with high concentrations of reduced iron and sulphur as a result of high organic matter flux to the sediment, they could reduce the oxygen available for mineralisation (Mackin and Swider 1989).

In shelf-seas, the role of benthic fauna has the potential to have a significant impact on the transport of oxygen throughout the sediment column (Glud 2008). Two separate processes can be identified: bioturbation is the physical movement of sedimentary material by burrowing animals to an area with different nutrient characteristics, while bioirrigation is the flushing of these burrows by water from the

overlying water column. The most active burrowing animals, such as *Arenicola marina* has been shown to be able to totally turnover 15 cm of sediment and irrigate its burrows with 80 m^3 per m^2 annually, have a significant impact on both nutrient cycling in the sediment and enhancing benthic solute exchange (Glud 2008)

As a result of the cycling described above, it is clear that oxygen profiles will show a rapid decline in concentration, even in environments where the overlying bottom water has relatively high concentrations of oxygen (*e.g.* 300 mmol m^{-3}). As an example of this, Figure 1.2 shows an oxygen porewater profile typical of the ones found in the literature for North Sea cohesive sediments (Lohse *et al.* 1996).

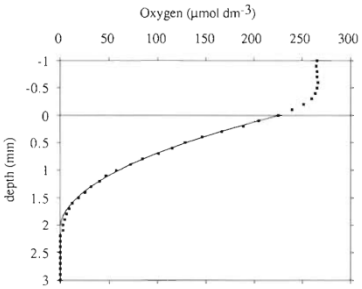

Figure 1.2: A typical example of a North Figure Sea porewater oxygen profile (Lohse *et al.* 1996)

1.2.2 Nitrogen compounds

Although dinitrogen (N_2) makes up 95.2% of the marine nitrogen content, this is biologically inert, and is not available to the majority of marine organisms (Libes 1992; Millero 2006). Therefore, nitrogen is a major limiting nutrient in marine environments (Redfield 1934, 1958). There are two bioavailable forms of nitrogen: ammonium (NH_4^+) and nitrate (NO_3^-). The links between them are shown in Figure 1.3.

NH_4^+, produced by organic matter mineralisation, is oxidised to NO_3^- by O_2 and thus, in the oxic layer of the sediment, both NO_3^- and NH_4^+ are produced. As first hypothesised in 1878 (Warington 1878), these two reactions are carried out by distinct chemoautotrophic bacteria, the former being ammonia-oxidising bacteria, and the latter being nitrite-oxidising bacteria (Bonazzi 1919; Winogradsky 1890; Mortimer *et al.* 2004).

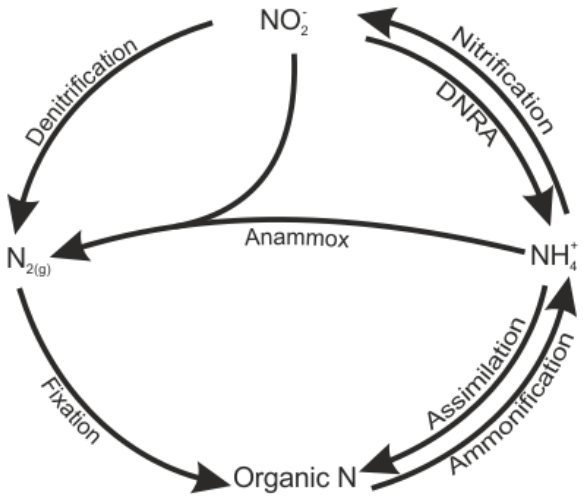

Figure 1.3: Species of nitrogen, and reactions they undergo in sediment

Other authors have also found that small concentrations of other by-products may also result from denitrification (Seitzinger *et al.* 1984). The only significant by-product being dinitrous oxide, although this has never been found to have concentrations greater than 10% relative to N_2 or $NO_3^- + NO_2^-$. The loss of nitrogen from the marine nitrogen system (and the ecosystem) by conversion to N_2 via the denitrification reaction may account for 50% of the inorganic nitrogen entering the coastal environment from terrestrial sources (Seitzinger *et al.* 1984). It has been shown that ammonia is not a significant product of denitrification, where excess oxygen is available and therefore nitrification is able to remove all available ammonia. Although experimental procedures have shown that ammonia production nearly doubled over a ten day period, the final concentration was 2.9 µg atom l^{-1}, in comparison with the NO_x concentration which reduced from nearly 30 to 0 µg atom l^{-1} over the same period (Goering and Cline 1970). Other authors have found no ammonium in the denitrification zone, and have therefore it has all been oxidised to N_2 or N_2O, or is quantitatively absorbed (Emerson *et al.* 1980).

Where the flux of OC is relatively high (such as after the spring bloom), the net flux of NH_4^+ can be out of the sediment into the water column due to the concentration gradient created when very large quantities of organic matter are mineralised. In low organic flux regions, the net flux of NH_4^+ is into the sediment (Hall *et al.* 1996; Janssen *et al.* 2005). Similarly, the net flux of NO_3^- has also been shown to be both into (Hall *et al.* 1996) and out of (Lohse *et al.* 1993) the sediment.

It is important to point out that the direct oxidation of dinitrogen to nitrate does not happen during diagenesis – this reaction only happens during high-temperature natural processes (Cowling *et al.* 2002) – and that the reduction of nitrate and nitrite to

ammonium happens only at low pH values (Stumm and Morgan 1996), so is unlikely to occur during diagenesis of organic material.

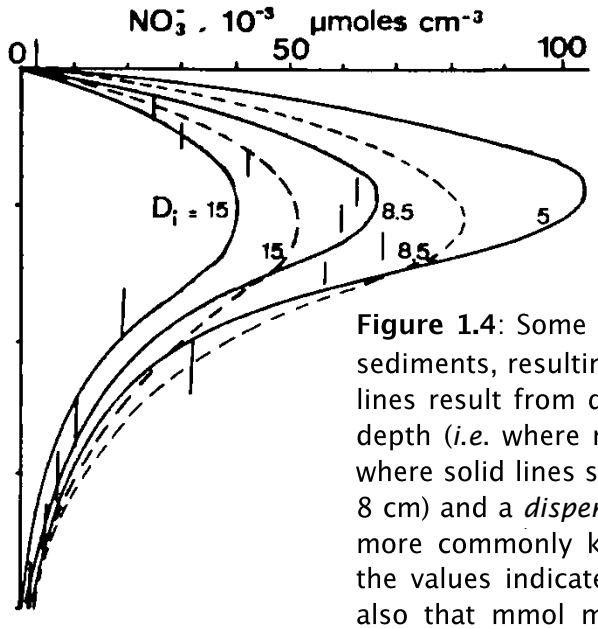

Figure 1.4: Some idealised nitrate profiles in shelf-sea sediments, resulting from a simple model; the different lines result from differing values for the denitrification depth (*i.e.* where nitrate concentration is greatest, and where solid lines signify 7 cm and dashed lines indicate 8 cm) and a *dispersion* coefficient (although this is now more commonly known as the diffusion coefficient) – the values indicated are of order $1x10^{-5}$ cm^{-2} s^{-1}; note also that mmol m^{-3} is now a more common unit for porewater nutrient concentrations, and that the depth axis is linear and extends from 0 to 20 cm (Billen 1982)

Nitrate forms distinctive profiles in sediment, with an increase of NO_3^- in the oxic zone, due to nitrification, and then a decrease of NO_3^- with depth as it is denitrified (see Figure 1.4 for some representative shelf-sea nitrate profiles). NH_4^+ concentrations generally increase with depth, but may exhibit a minima in the oxic layer due to nitrification. Although anaerobic ammonia oxidation is theoretically possible (Anschutz *et al.* 2000), there is differing opinion in the literature as to its importance (Thamdrup and Dalsgaard 2000).

Concentrations of ammonium in porewaters are also affected by sorption processes (Burdige 2006). In areas where the predominant sedimentary material is clay, such as in parts of the North Sea (Basford and Eleftheriou 1988), ion exchange processes are common due to the negatively-charged clays attracting the positively-charged ammonium molecules (Mackin and Aller 1984). As NH_4^+ is produced by all mineralisation reactions, adsorption will be an important sink process throughout the sediment.

In cases where the sediment is completely anoxic, such as areas of upwelling where there is a high POM flux (Libes 1992), nitrification will not be carried out; instead, there will be a downward positive gradient for ammonium (van der Weijden 1992), and some flux of NH_4^+ into the bottom waters will occur.

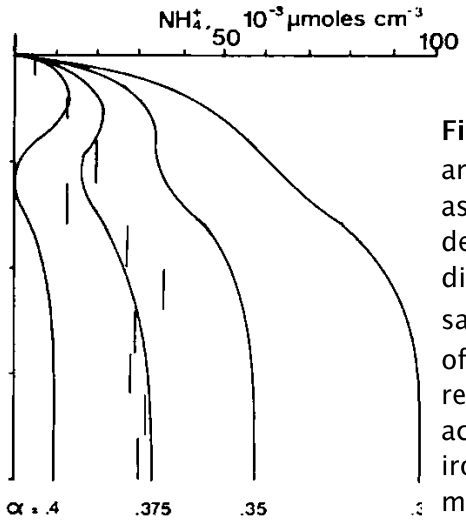

Figure 1.5: Typical modelled shelf-sea ammonia porewater profiles; α is defined as the square root of the result of the OM degradation rate constant divided by the diffusion coefficient. The y-axis is the same as in Figure 1.4. Note the build-up of ammonia in the oxic layer before it is removed by nitrification, before more accumulation in the zones dominated by iron oxide & sulphate reduction, and methanogenesis (Billen 1982)

1.2.3 Phosphate

The phosphorus component of organic matter is degraded to phosphate (PO_4^{3-}). In this form, phosphorus is in the +5 oxidation state, and is bioavailable. Phosphate is not directly involved in any of the primary diagenetic reactions, and as a result, only biological, sedimentological and the solubility of phosphate-bearing minerals, and not the sequence of redox reactions, have an impact on the availability of the phosphate (Schenau and De Lange 2001). In general, the breakdown of organic matter causes the net flux of phosphate to be out of the sediment into the water column (Hall *et al.* 1996).

It has been shown that the amount of phosphorus buried in sediments is approximately equal to the fluvial input of phosphorous (Schlesinger 1997; Froelich *et al.* 1982), Froelich *et al.* (1982) identified that phosphorus can be removed from the ecosystem when it is buried in association with OC as a component of aggregates. Phosphorus that is released as a result of OM mineralisation can either be released to the interstitial water to be taken up by the ecosystem (Froelich *et al.* 1982) or be mineralised (Fang *et al.* 2007). Recent experiments have shown that approximately 3% of phosphorus is lost from the marine system as a result of precipitation of carbonate fluorapatite (CFA), or other authigenic minerals (Vink *et al.* 1997), although the validity of data suggesting the formation of apatites as a sink for phosphorus has been recently questioned (Gunnars *et al.* 2004).

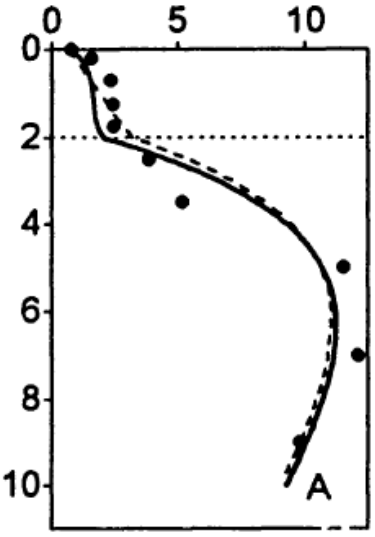

Figure 1.6: An example of typical continental margin sedimentary phosphate profiles (concentration [mmol m^{-3}] *vs.* depth [cm]), determined using a simple diagenetic model. The dashed and solid lines indicate different model parameters, while the solid circles signify experimental data; the dotted line represents the redox boundary. For full details, see Slomp *et al.* (1998)

It is known that areas where there are enhanced rates of organic matter decomposition and iron reduction provide the necessary conditions for CFA formation (van der Zee *et al.* 2002a). However, it has been shown that apatites can be formed via more than one pathway, which may be a result of, or have implications on, the diagenetic processes occurring at specific locations (Gunnars *et al.* 2004).

It has also been noted that pore-water may contain significantly higher concentrations of phosphorous than the overlying bottom water, suggesting that phosphorous, in the form of both organic and iron oxide-bound, may be remobilised diagenetically (Cha *et al.* 2005), possibly as a result of organic phosphorous being buried below the sediment surface, followed by regeneration to dissolved phosphorous, with diffusion to the overlying bottom water (Froelich *et al.* 1982). However, it seems from the current literature that neither any experimental nor modelling studies have confirmed this process. This could also be linked to the findings that although in general organic phosphorous concentration increases with depth, it has been found to fluctuate with depth near the sediment-water boundary (Cha *et al.* 2005). This again has been assumed to be due to bioturbation or resuspension of the sediments, but no studies have been carried out on the possible mechanism.

1.2.4 Other macronutrients and redox species

Silicon (SiO_2) is normally described as the fourth essential nutrient, and has been shown to be a limiting factor in the growth of diatoms, radiolaria, silicoflagellates and sponges in some areas (Libes 1992). Despite this, the role of diagenetic processes on the fate of silicon has been studied less widely than for the three other essential

nutrients, although this no doubt been partly due to the fact that silicon is only mainly found as orthosilicic acid in the marine environment, compared to the numerous organic and inorganic forms of nitrogen, carbon and phosphorous (Dugdale *et al.* 1995). Despite the limited forms that silicon has when it reaches bottom waters (i.e. orthosilicic acid, trapped in tests or as part of the chemical composition of faecal pellets), benthic effluxes have been shown, both experimentally and theoretically, to be a potential source of silicon to the marine system (Bonnin and Van Raaphorst 2004). One recent study has shown that the dissolution of biogenic silica that has sunk from the euphotic zone would produce a maximum flux of 120 μmol m^{-2} d^{-1}, although the vertical eddy diffusion coefficient showed values of orthosilicic acid as high as 1700 μmol m^{-2} d^{-1}. The difference between these two values seems to be balanced out by both an efflux from the benthic layer, which can be as high as 740 μmol m^{-2} d^{-1}, and resuspension of sediment caused by turbulent flow, contributing as much as 800 μmol m^{-2} d^{-1}; however, the features surrounding the geomorphological setting are fairly crucial for such a flux of orthosilicic acid into the water column (Bonnin and Van Raaphorst 2004) . Recent models of the flux of silicon between bottom waters and the sediment, using relatively simple equations, have shown to have good agreement with *in-situ* measurements (Ragueneau *et al.* 2000).

The low concentrations of MnO_2 (typically below $7x10^{-3}$ mmol cm^{-3}, and estimated to be an order of magnitude lower than the concentration of reducible iron) in the majority of North Sea sediments typically make the reduction of MnO_2 a relatively unimportant reaction (Jensen *et al.* 2003; Rysgaard *et al.* 2001), with manganese reduction generally contributing less than 1% of all organic matter mineralisation in studies of North Sea sediments (Bakker and Helder 1993; Rysgaard *et al.* 2001). In the North Sea, reduction by iron oxides and sulphate is generally more prevalent than manganese oxide reduction due to the low concentrations of MnO_2 (Jensen *et al.* 2003; Rysgaard *et al.* 2001). However, MnO_2 concentrations can be very high in small localised areas, with one sampling station (S9) in the Skagerrak consistently showing reducible manganese concentrations of up to 175 μmol cm^{-3} (Canfield *et al.* 1993b), leading to MnO_2 at this site being responsible for 85% of all organic matter oxidation (Rysgaard *et al.* 2001). Although there is no literature data for the proportion OM that is mineralised by MnO_2 for the whole of the North Sea, the data that is available would suggest that MnO_2 is, overall much less important than any of the other electron acceptors. As this thesis attempts to use a model to calculate both shelf-wide budgets as well as recreate profiles found in specific environments, the potential importance of MnO_2 will be discussed with each model run result. The small difference between the Gibbs' Free Energy of manganese oxide reduction and denitrification means that where MnO_2 is present, there is often spatial overlap of these reactions (van der Weijden 1992).

The reduction of iron oxides is much less favourable than denitrification and is a straight forward reduction of Fe^{3+} to Fe^{2+} (Froelich *et al.* 1979). However, the reaction drives a substantial change in porewater concentrations of total dissolved iron, since the iron oxides are solid minerals, whereas Fe^{2+} does not immediately form compounds, and hence stays as a dissolved constituent. There is some evidence (Hyacinthe and Van Cappellen 2004) that iron reacts with the constantly accumulating phosphate pool. Ferric oxyhydroxides have been found in the upper layers of sediment in shelf seas and estuaries (Jensen *et al.* 1995), and have been shown to influence the flux of dissolved reactive phosphorous (DRP) out of the sediment into the bottom waters (Jensen *et al.* 1995).

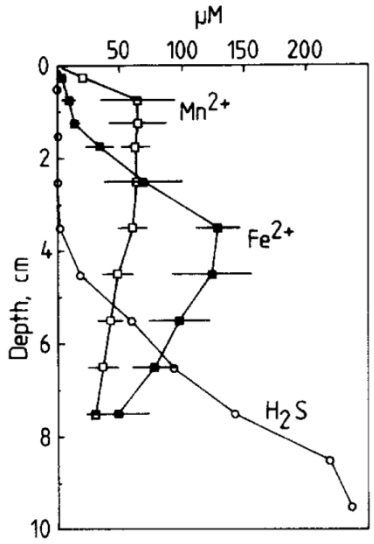

Figure 1.7: Profiles of Mn^{2+}, Fe^{2+} and H_2S from sediment taken from Aarhus Bay (Thamdrup *et al.* 1994). The concentration of Fe^{2+} decreases below the depth where iron oxide is the primary electron acceptor due to formation of iron sulphides. As Mn^{2+} does not undergo further reaction with species in the sediment, its concentration remains relatively constant. The formation of H_2S indicates excess S^{2-} after formation of iron sulphides.

The final significant oxidising agent is sulphate, which is reduced from S^{6+} to S^{2-} (Froelich *et al.* 1979). Concentrations of sulphate in shelf sea sediments are high enough to make sulphate reduction a ubiquitous process (Aplin and Macquaker 1993) with some studies showing concentrations of sulphate in North Sea surface sediments as high as 26 mmol m^{-3} (Beck *et al.* 2007; Gagnon *et al.* 1996), approximately 5000 times higher than concentrations of manganese (5 µM) (Beck *et al.* 2007). However, the reduction of sulphate to elemental sulphur during organic matter degradation only happens in suboxic environments (Froelich *et al.* 1979). In the North Sea, sulphate tends to account for between 10% (Osinga *et al.* 1996) and 50% (Upton *et al.* 1993) of total OM degradation.

Sulphide (S^{2-}) becomes the dominant sulphur species within approximately 10 cm into the sediment (Gagnon *et al.* 1996; van der Weijden 1992). The rate of the sulphate reduction pathway is positively correlated with the rate of accumulation of sediment; where sulphide is produced as a result of sulphate reduction, it is able to

react with detrital iron to form pyrite (FeS_2), or be transported back to the oxic sediment-water layer where it can be reoxidised to SO_4^{2-} or form organically bound sulphur (Aplin and Macquaker 1993; van der Weijden 1992). Where the sedimentary environment is oxic, bioturbation can cause sulphur to be transported through the sediment, thereby allowing pyrite to form in areas where the overlying sediment-water interface is oxic. The reactions that sulphur undergoes during early diagenesis, based on the amount of iron present, can also influence the chemical composition of sedimentary organic matter, acting as a potential sink for sulphur out of the ecosystem (François 1987).

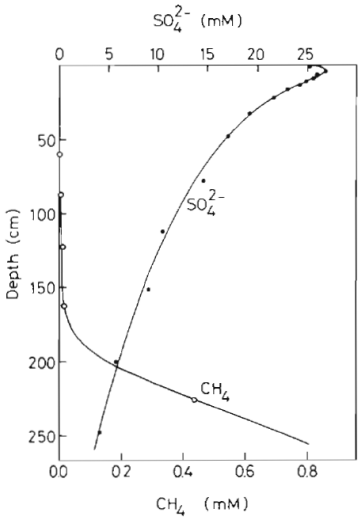

Figure 1.8: Profiles of sulphate and methane from sediment taken from a relatively shallow (water depth of 25 m) site in the Belt Sea (Jørgensen *et al.* 1990)

1.3 Anthropogenic impacts

As with the major reaction pathways, anthropogenic activities could also have an effect on the diagenetic processes. It has been estimated that the calcium flux into some shallow seas has increased by 45% as a result of human activities (Kremling and Wilhelm 1997). Although few authors have made quantitative conclusions on changes in diagenesis of calcium, they have indicated that the increase in calcium is linked to a decrease in the pH of the surrounding environments which could also indicate a change in pH of shelf-sea waters (Kremling and Wilhelm 1997).

Current scientific consensus is that increases in atmospheric CO_2 are anthropogenically driven; since the beginning of the industrial revolution, global CO_2 levels have increased from 280 ppm to 380 ppm, and the current worst case estimate is that they will increase to 1000 ppm by the end of the 21st Century (Parry *et al.* 2007). Although the oceans are able to offset some of the impact of CO_2 on global climate by taking up atmospheric CO2, this has the consequence of modifying ocean pH levels by increasing concentrations of carbonic acid. Some work has been carried out on the

effect of acidification on calcareous organisms, for example, calcifying forms of *Emiliania huxleyi* may be replaced by non-calcifying strains (Riebesell *et al.* 2000; Riebesell 2004); however, there is little understanding on the effect on the whole ecosystem by a decrease in pH levels. Using the European Regional Seas Ecosystem Model (ERSEM), (Blackford and Gilbert 2007) suggested that there may be complex direct (via denitrification) and indirect (via species-species interactions on benthic fauna) effects on shelf-sea biogeochemistry as a result of changing pH levels. However, they do conclude that the model is still too simple to quantify the impact that increased atmospheric CO_2 concentrations have on the nutrient cycles in shelf seas. As well as the more obvious effects on nutrient cycling that changes in pH may drive, it has also been suggested that varying pH levels may have more wide reaching effects on the whole ecosystem, with one study suggesting that an increase in jellyfish in the North Sea may be as a direct result of decreasing pH (Attrill and Edwards 2008; Attrill *et al.* 2007). Work has also been conducted to investigate how water mass movement will affect saturation depths, particularly with regard to shelf-sea ecosystems. Early work has found that, perhaps unsurprisingly, this is a complex set of interactions and that models predicted upwelling of water corrosive to aragonite onto the western continental shelf of North America would occur 40 years after than actually observed (Doney *et al.* 2009; Feely *et al.* 2008).

Other metals, particularly those which are known to have toxic effects on, or can bioaccumulate in, marine animals, have also been studied. Mercury bioaccumulates in fish, and can cause levels to exceed those deemed safe for consumption by humans (Fitzgerald *et al.* 2007). Mercury is known to be deposited in marine sediments as a result of being scavenged by organic-rich materials, to which mercury (II) has a natural affinity.

Within areas most affected by anthropogenic activities, such as shelf-sea and estuarine regions, other compounds may also affect the diagenetic chemical processes. Although it is known that methylamines are ubiquitous in the marine environment, their concentrations are much larger in estuarine sediments (micromolar) rather than in the open ocean (nanomolar). They are soluble in porewater, as well as having the ability to be adsorbed onto solid-phase particles in the sediment (Abdul-Rashid *et al.* 1991; Fitzsimons *et al.* 2005). Other organic compounds may also have an effect on diagenetic processes. For example, methane, which is insoluble, is known to be released from sediments, and is subsequently oxidised to carbon dioxide by microbes (Boetius *et al.* 2000; Schlesinger 1997).

Anthropogenic inputs to the marine system from surrounding terrestrial environments may have a profound influence on the health of the ecosystem, which

will also have an effect on the overall biogeochemistry of the system. Changes in farming practices and waste treatment have led to riverine concentrations of nutrients increasing over last 50 years (Diaz and Rosenberg 2008). The availability of nutrients in surface waters leads to increased phytoplankton blooms, the degradation of which in the water column leads to a lowering of oxygen concentrations, in a process known as eutrophication (OSPAR 2010). This oxygen depletion can lead to hypoxic (<2 ml of dissolved oxygen l^{-1}) or anoxic (<0.5 ml of dissolved oxygen l^{-1}) conditions, particularly in the bottom waters, limiting biological activity and changing nutrient dynamics (Radach *et al.* 1990). Although little work has been carried out on the estimates of the impact of eutrophism on diagenetic processes have been made, (Gypens *et al.* 2008) used a modelling approach to approximate the relative importance of the three mineralisation pathways modelled (oxic, denitrification, and anoxic) in a run where hypoxic bottom waters were considered, compared to a run with oxic conditions. It was found, unsurprisingly, that under hypoxic conditions, both denitrification and anoxic mineralisation dominate at much lower carbon fluxes than under oxic conditions. In particular, when the carbon flux was 10 g m^{-2} yr^{-1}, oxic mineralisation accounted for 95% of OM degradation under oxic conditions but only approximately 15% of OM degradation under hypoxic conditions. Denitrification and anoxic mineralisation accounted for only approximately 4% and 1% of OM degradation under oxic conditions, but 25% and 60% respectively when hypoxia was modelled.

1.4 The theory of diagenetic modelling

The majority of diagenetic studies are based on experimental and observational work. Although taking measurements in the natural environment is a vital approach to improving our understanding, observations can seldom describe the varied processes individually. In addition, sampling often has its own problems, either with respect to the risk of disturbing the environment that is being studied *in situ*, or with regard to the spatial and/or temporal scales of the measurements being made. It can also be argued that predictions of these environments cannot be made without a full understanding of all the individual forcing parameters (Boudreau 1997a). Ever since the basic chemistry of early diagenesis was understood, models have been developed to attempt to predict biogeochemical processes in aquatic sediments (Soetaert *et al.* 1996b; Goloway and Bender 1982; Berner 1975; Berner 1976, 1980; Boudreau 1992, 1996; Van Cappellen and Wang 1996; Dhakar and Burdige 1996; Kelly-Gerreyn *et al.* 1999; Kasih *et al.* 2008; Katsev *et al.* 2004).

Berner (1975) published a comprehensive set of equations that he deemed important within a diagenetic model. The theory of diagenetic modelling is expressed mathematically in Equations 1.1a (for solids) and 1.1b (for solutes)

$$\frac{d(1-\phi)c_i}{dt} = \frac{\partial\left((1-\phi)D_b\frac{\partial c_i}{\partial x} + \omega(1-\phi)c_i\right)}{\partial x} + (1-\phi)R(c_i,c_j) \qquad \text{Eqtn 1.1a}$$

$$\frac{d\phi c_i}{dt} = \frac{\partial\left(\phi D_s\frac{\partial c_i}{\partial x} + \omega\phi c_i\right)}{\partial x} + \phi R(c_i,c_j) \qquad \text{Eqtn 1.1b}$$

where c_i is concentration of species *i* in mass per unit volume of total sediment, ϕ is porosity in terms of volume of water per unit volume of total wet sediment, x is the depth in sediment, t is time, D_s is the bulk diffusion coefficient for the sediment (including tortuosity, but not adsorption or ion exchange), D_b is the bioturbation coefficient, ω is rate of advection (cm d^{-1}) and $R(c_i, c_j)$ is rate of addition and/or subtraction of species *i* to or from the porewater by (bio)goechemical reactions with *j*, where the rate of the reaction between *i* and *j* is dependent on the concentration, c, of both species.

Equation 1.1a shows the equation that applies to solid species in the model. Porosity in the model is defined as the fraction of the sediment that is made up of porewater. The first term, on the right-hand side of equation 1.1a, describes the transport so that the diffusion and advection of chemical species can be estimated accurately. Solid phase species, such as TOC, are part of the solid sediment mass and so the transport component needs to be treated differently. Since the amount of porewater in the sediment is just a proportion of the total amount of the sediment, the solid part is the remaining fraction, i.e. $(1-\phi)$.

Since the early models were published (Soetaert *et al.* 1996b; Dhakar and Burdige 1996; Van Cappellen and Wang 1996; Boudreau 1996), research has concentrated on developing models to deal with increased complexity, such as the coupling between chemical species and the overlap between diagenetic regions. There has also been a shift between the method in solving the model equations.

With a lack of computational power, early models could only be solved analytically. Recent models, however, have sets of more complex coupled differential equations (equations 1.1a and 1.1b) which can presently only be solved numerically.

1.5 Previous diagenetic models

Although the major contribution of Bob Berner's early work has already been briefly discussed, it wasn't until the mid-1990s, when both computational power was great enough and the sediment biogeochemistry was understood well enough for equations to be formed that took into account enough of the key processes, that diagenetic models started being developed that could accurately and reliably produce results reminiscent of observed *in-situ* experiments. Two comprehensive models of the overall process of early diagenesis, both published in 1996, had a slightly different philosophy. van Cappellen and Wang (1996) not only produced a model which included iron and manganese cycling (which, before this paper and Soetaert *et al.* (1996b), published the same month, had not been accomplished before), but also included a host of other parameters which the authors deemed important in a model of early diagenesis, such as total alkalinity, and also stated that '*there is no limit to the number of species and reactions that can be included*'. Soetaert *et al.*'s model took a more conservative approach, and modelled far fewer reactions and processes. Whereas van Cappellen and Wang took great care in setting out and solving the equation for each specific primary and secondary reaction (i.e. the reoxidation of reduced species as they are transported back to the oxic zone), Soetaert *et al.* only explicitly modelled the role of oxygen and nitrogen. The remaining species were grouped together as an Oxygen Demand Unit variable. However, unlike van Capellen and Wang, Soetaert *et al.* had separate classes of OC available for degradation, by including a fast and slow degrading, and a refractory pool, known as a multi-G model (Westrich and Berner 1984). A multi-G approach allows the quality of the OM to be controlled – with high quality (fresh) OM having a higher proportion of fast-degrading carbon; the quality of the OM settling on the sediment will be dependent on the season (Gutiérrez *et al.* 2000). Despite the different philosophies behind each of these models, they both seem to represent fairly accurately the overall results of early diagenesis and the output from the models are very similar to observed profiles taken from sediments. Two further diagenetic models were also published in 1996. *Candi* (Carbon And Nutrient DIagenesis) (Boudreau 1996) and Dhakar & Burdige (1996) had the same aims as the Soetaert *et al.* (1996b) and Wang and Van Cappellen (1996). As all the models were all developed independently at about the same time, they all formed efficient instruments for testing hypotheses and acted as a tool to check the consistency of biogeochemical datasets (Meysman *et al.* 2003b). However, they all include slightly different reactions. Dhakar & Burdige (1996), for example, include iron and manganese reduction, but do not consider sulphate reduction; and, unlike the other models, which assume that oxygen is the only oxidising agent for the reoxidation of reduced species, this model allows NO_3^- to reoxidise NH_4^+ and Fe^{2+}, and

MnO_2 to reoxidise Fe^{2+}. This model also includes a more complex bioturbation coefficient than the other models. Boudreau (1996) included methanogenesis and phosphate, which none of the other three models did, but, like Soetaert *et al*. (1996b) and Van Cappellen and Wang (1996), did include a relatively simple bioturbation coefficient.

The original publications of the models outlined above generally only described the implementation of the processes involved, with subsequent publications including applications of the models (Boudreau 1998; Soetaert *et al.* 1996a; Van Cappellen and Wang 1996; Boudreau *et al.* 1998). Despite the slightly different approaches taken by each of the model developers, the overall results of the model closely match observed profiles of the parameterised chemical species.

Models have since been developed to be either more efficient, so that they can be coupled to pelagic models but without being too computationally expensive (e.g. Gypens *et al.* 2008), or to decrease the error associated with specific processes (e.g. Khalil *et al.* 2007). Meile *et al*. (2005) improved modelled solute fluxes and reaction rates by introducing solute-specific irrigation coefficients as a result of bioturbation and bioirrigation.

1.6 The potential role of resuspension

Recent studies have shown the potential importance of resuspension on nutrient flux. Jensen *et al.* (1995) showed that resuspended sediment fluxes could be up to sixty times higher than net sedimentation. Resuspension has also been reported to increase the productivity of the overlying water by up to 200% (Pejrup *et al.* 1996). Sediments of both shelf seas and continental margins can be affected by waves (Laës *et al.* 2007), and the effect of internal waves breaking have been shown to increase the concentration of elements in the bottom water by causing resuspension of the sediment (Laës *et al.* 2007).

In terms of the potential impact on the biogeochemistry of the benthic layer, resuspension has two main impacts. Firstly, the amount of sediment that is resuspended will determine how the sedimentary chemical zones respond to the event. As previously stated, oxygen penetration can be as low as 3 mm in North Sea sediments (Bakker and Helder 1993). Almroth *et al*. (2009) estimated that 256 μm of the bed was resuspended in the Baltic Sea during natural events, and so is well within the oxic zone. This study also suggested that there was no significant role by resuspension on the overall dissolved concentrations of NO_3^-, $Si(OH)_4$, Fe or Mn, and

that although NH_4^+ concentrations are influenced by resuspension events, this appears to be the case when bottom-water oxygen concentrations are low (below 15 μM), and in an unpredictive manner. Stahlberg *et al*. (2006) and Audry *et al*. (2007) estimated how resuspension affected total mineralisation of organic matter, and they suggest that this is as a result of nutrients being released that were previously trapped within the sediment; Stahlberg *et al*. (2006) did not measure nutrient concentrations, and Audry *et al*. (2007) measured only sulphate. Low nutrient concentrations in porewater are therefore unlikely to cause resuspension to have an effect in shelf seas. Both Stahlberg *et al*. (2006) and Audry *et al*. (2006) stated that resuspension is probably only limited to the top 1 mm of sediment, but the effects of the turbulence may extend deeper by advective flow. However, neither study measured either the amount of benthic matter resuspended or the depth of erosion during resuspension. Bale and Morris (1998) found that the carbon content of SPM sampled after different resuspension events varied non-linearly, which they attributed to the mixing of high carbon content permanently suspended (or benthic fluff) material and low carbon content bed sediment, although they did not investigate how these observations affect OM degradation after resuspension. Other authors (e.g. Jago and Jones 1998; Jago *et al.* 2002) have also found high carbon content fluff which they have found is easily resuspendable.

During anthropogenic events, such as trawling or dredging, erosion is likely to be deeper, with trawling estimated to cause up to 1 cm of the bed to be resuspended (Warnken *et al.* 2003), while dredging activities will dig out up to 25 cm of sediment, with approximately 70% of this sediment resuspended (Audry *et al.* 2007). The second major effect of resuspension on biogeochemistry is the increase in sediment surface area made available for sorption processes. Specifically, clays are less than 2 μm in diameter (Winterwerp and van Kesteren 2004), and clay minerals (such as montmorillonite) tend to have a large negatively-charged framework, such as aluminosilicate; this allows substitutions of cations within the crystal lattice (Berner 1976). It is the convention (Watson and Frickers 1995; Winterwerp and van Kesteren 2004; Burdige 2006) to group all clay and silt particles together, and call this mixture *mud*, and distinguish this from *sands* with a particle size threshold of 63 μm (Winterwerp and van Kesteren 2004). Figure 1.2 shows the mud content of North Sea sediments; although this does not show the full extent of the North Sea it does show that a large proportion of the North Sea has mud content of greater than 50% (Basford and Eleftheriou 1988).

Given that different minerals have different surface charges, positive, negative and neutral species can all interact with clays, and hence adsorption is likely to be an important process in the fate of ions such as NH_4^+, Fe^{2+} and S^{2-} in solution (Berner

1976; Burdige 2006; Stumm and Morgan 1996). Based on the depth of erosion that has already been discussed, Fe^{2+} and S^{2-} are only likely to be resuspended in areas which have anoxic bottom waters. Concentrations of NH_4^+ are likely to be affected by resuspension; this would then decrease nitrification rates. Denitrification would become a less important pathway for organic matter degradation, while increasing the importance of O_2 that would have been previously used for nitrification would be free to take part in oxic mineralisation.

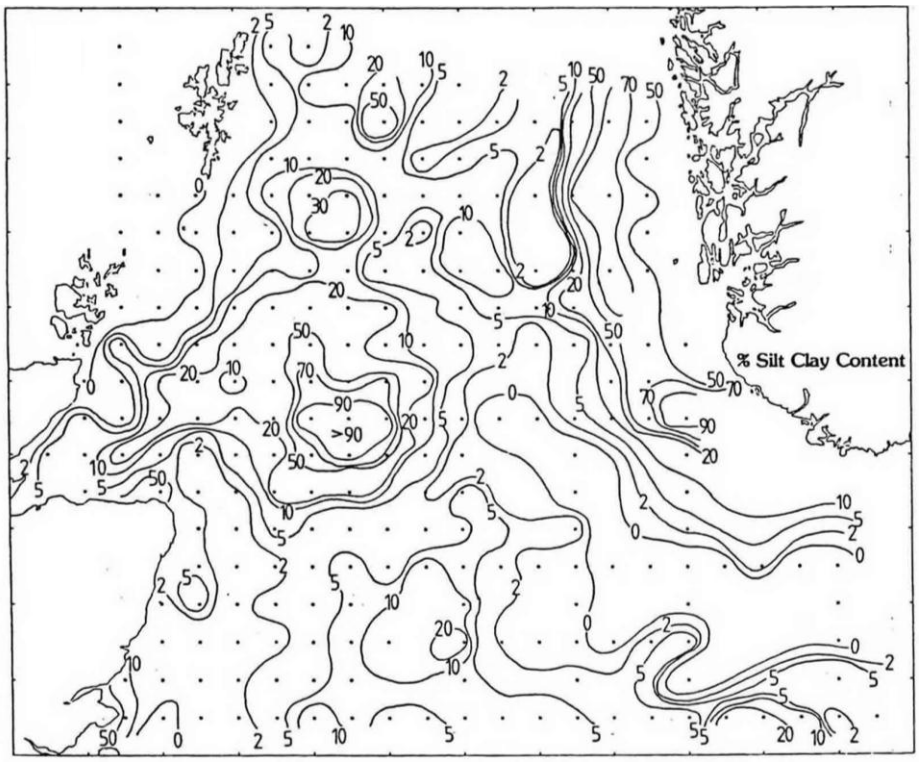

Figure 1.9: Mud content (%) of North Sea sediments
(Basford and Eleftheriou 1988)

1.7 Aims and objectives

Although models of early diagenesis have been developed for more than 30 years, to my knowledge, resuspension has not been included in a diagenetic model before. By collaborating with biogeochemists, sedimentologists and modellers as part of the NERC Partnership Marine Ecosystem Connections (MEC) Project, I aim to develop a diagenetic model which is both better constrained, due to the use of an extensive observational data set from the North Sea capable of considering the potentially important role of sediment resuspension on nutrient (NO_3^-, NH_4^+, PO_4^{3-}) exchanges between the seabed and the overlying water. The completed model will be used as a predictive tool and be used to carry out scenario testing.

Specifically, the objectives of this thesis are to:

- develop a coupled resuspension-early diagenesis model for the North Sea, based on a previously published model (OMEXDIA), developed using the R programming language.
- use the results of experiments (carried out by co-workers) undertaken both *in situ* and in the laboratory to calibrate the model.
- validate the model using literature data
- apply the model to other shelf sea environments. For upscaling purposes, I hope to implement the model into a 3D-hydrodynamic ecosystem model of the North Sea (European Regional Seas Ecosystem Model, ERSEM) so that the role of both early diagenesis and resuspension can be investigated at a shelf-sea wide scale.

2 Methods and Model Description

OMEXDIA is a mathematical 1-dimensional model describing sedimentary C, N and O_2 cycling in ocean margin environments (Soetaert *et al.* 1996b; Soetaert *et al.* 1996a). It considers the degradation of OM (organic matter) by a sequence of electron acceptors, with Table 2.1 showing the state variables. Oxic mineralisation, the first degradation reaction, is limited by oxygen; that is, the rate of degradation of OM by oxygen will decrease as concentrations of O_2 decrease. A full explanation of the kinetics surrounding this formulation can be found in Section 2.1 and the full equation describing oxic mineralisation is shown in Equation 2.1. Similarly, denitrification, the second reaction in the degradation sequence, is limited by nitrate, and is shown in Equation 2.2. However, denitrification is also inhibited by oxygen (Froelich *et al.* 1979); denitrification is therefore not favoured when there is sufficient oxygen for oxic mineralisation to occur. The second term in Equation 2.2 ensures that this does happen.

As well as describing OM oxidation by O_2 and NO_3^- OMEXDIA also considers the remaining oxidising agents (i.e. those species involved in suboxic mineralisation: MnO_2, Fe_2O_3 and SO_4^{2-}), as well as anoxic mineralisation (methanogenesis) in a combined variable known as ODU (oxygen demand units). ODU are the reduced species of suboxic and anoxic mineralisation (i.e. Mn^{2+}, Fe^{2+}, S^{2-} and CH_4) which can diffuse into the oxic layer to be reoxidised by O_2. Representing all remaining suboxic and anoxic processes within an ODU component ensures that all non-refractory OM is degraded, and mineralisation proceeds until all degradable carbon has been consumed

These mineralisation processes are not limited by the concentration of any species, but are inhibited by the presence of O_2 and NO_3^-, as shown in Equation 2.3. Although this simplifies the sequences determined by Froelich *et al*. (1979), and other work verifying Froelich's results (e.g. Emerson et al 1980, Berner 1985 Sulphate, Sorensen 1987, Canfield 1989, Henrichs 1992), it does make the model much more simple than it would otherwise be. For the environments which OMEXDIA is designed to represent, especially in this work, the simplification of the model may be a suitable compromise between model complexity and accuracy; as discussed in Chapter 1, the high productivity of coastal seas (and their sediments) ensures that the iron and sulphate diagenetic reactions are often only responsible for a relatively small proportion of the breakdown of OM, and, as such, the lack of these reactions from the model does not detract from the usefulness of its results. Although these reactions, particularly sulphate reduction, have been shown to be responsible for in excess of

80% of OM mineralisation, the current accepted opinion is that the sites where this is observed are considered relatively unique environments. In addition, the North Sea has very small quantities of manganese (e.g. Thamdrup *et al.* (1994) found that the quantities of manganese oxides in Aarhus Bay sediments were approximately 10% of those of iron oxides, while Bakker & Helder (1993) found that, on average across the Skagerrak, oxidation of OM by manganese oxides accounted for only 0.4% of the total oxidation of OM, compared with 0.8% by iron oxides, 4.5% by nitrate and 9% by sulphate; the contribution by manganese oxides to OM oxidation is only higher than the contribution by iron oxides at 1 of the 6 sites sampled), meaning that the reaction concerning the oxidation of OM by manganates can also be left out of the sequence with little worry of the effect on model output.

Table 2.1: The state variables and biogeochemical rates modelled

	Variable	Units
State variables	Concentration of fast and slow degrading carbon	mmol m^{-3} (solid)
	Concentration of oxygen	mmol m^{-3} (liquid)
	Concentration of nitrate	mmol m^{-3} (dissolved)
	Concentration of ammonia	mmol m^{-3} (dissolved)
	Concentration of ODU	mmol m^{-3} (dissolved)
Biogeochemical rates	Amount of carbon oxidised by O_2	mmol C m^{-3} solid day^{-1}
	Amount of carbon oxidised by NO_3^-	mmol C m^{-3} solid day^{-1}
	Amount of carbon oxidised by all other electron acceptors	mmol C m^{-3} solid day^{-1}
	Amount of ODU deposited (expressed as O_2 equivalent)	mmol O_2 m^{-3} solid day^{-1}
	Amount of O_2 consumed in oxidation of ODU species	mmol O_2 m^{-3} solid day^{-1}
	Amount of NH_3 nitrified (expressed as O_2 equivalent)	mmol O_2 m^{-3} solid day^{-1}

The rate of OM oxidation in the model is dependent on the flux and degradability of the OM, the availability of an oxidising agent and the presence of inhibition factors, and therefore equations can be written for the various mineralisation reactions:

$$\text{Oxic mineralisation} = \frac{O_2}{O_2 + Ks_{O_2}} * ((\kappa_f * TOC_f) + (\kappa_s * TOC_s)) * \frac{1}{\Sigma lim} \qquad \text{Eqtn 2.1}$$

$$\text{Denitrification} = \frac{NO_3^-}{NO_3^- + Ks_{NO_3}} * \left(1 - \frac{O_2}{O_2 + Kin_{O_2}^{denit}}\right) * ((\kappa_f * TOC_f) + (\kappa_s * TOC_s)) * \frac{1}{\Sigma lim} \qquad \text{Eqtn 2.2}$$

$$\text{Anoxic mineralisation} = \left(1 - \frac{NO_3^-}{NO_3^- + Kin_{NO_3}^{AnoxMin}}\right) * \left(1 - \frac{O_2}{O_2 + Kin_{O_2}^{AnoxMin}}\right) * ((\kappa_f * TOC_f) + (\kappa_s * TOC_s)) * \frac{1}{\Sigma lim} \qquad \text{Eqtn 2.3}$$

The parameters used in these equations are listed in Table 2.2. These equations are in the units of TOC. In order to couple each equation to the relevant oxidising agent, each equation needs to be multiplied by the appropriate stoichiometric ratio – 1 for oxygen, 0.8 for nitrate and 1 for anoxic mineralisation (Froelich *et al.* 1979; Emerson *et al.* 1980). Due to the presence of the oxygen demand unit parameter in the model, the remaining oxidising agents are not discretely described. From Equations 2.1 – 2.3, it is possible to see that all the degradation processes are first order with respect to OM (that is, the degradation is linearly proportional to the concentration of OM). The final term in Equations 2.1–2.3 is used to ensure that the maximum degradation rate is always achieved. As the competing pathways take place concurrently, the total mineralisation rate would be higher without this rescaling term (Soetaert *et al.* 1996b). Σlim is the sum of the first term in Equation 2.1 and the first two terms in Equations 2.2 and 2.3.

In reality, both as a result of the reactivity of OM decreasing through the sedimentary column as depth increases, due to more labile OM being mineralised preferentially (Canuel and Martens 1996; Middelburg 1989), and because of the wide range of organic substances found in sedimentary organic matter, a continuum of organic substrates is found throughout the sediment column (Middelburg 1991). It follows that the development of a generic equation to describe the degradation of organic matter should include both the ability to model the decay in reactivity with increasing depth and the decreasing reactivity with respect to time (Westrich and Berner 1984; Middelburg 1989). In response to previous models only using one or two

Table 2.2: The default parameter list for OMEXDIA

Parameter	Units	Default values
Mean carbon flux to the sediment	g C m^{-2} $year^{-1}$	20
O_2 in overlying bottom water	mmol O_2 m^{-3}	300
NO_3^- in overlying bottom water	mmol NO_3^- m^{-3}	10
NH_3 in overlying bottom water	mmol NH_3 m^{-3}	1
ODU in overlying bottom water	mmol ODU m^{-3}	0
Proportion of fast degrading organic matter	-	0.9
Nitrogen to Carbon ratio in fast degrading organic matter	moles N : moles C	0.15
Nitrogen to Carbon ratio in slow degrading organic matter	moles N : moles C	0.13
Rate of oxidation of fast degrading organic matter	day^{-1}	$1x10^{-2}$
Rate of oxidation of slow degrading organic matter	day^{-1}	$1x10^{-5}$
Rate of oxidation of oxygen demand units	day^{-1}	20
Rate of nitrification	day^{-1}	20
O_2 diffusion coefficient	cm^2 d^{-1}	1.34
NH_3 diffusion coefficient	cm^2 d^{-1}	1.18
NO_3^- diffusion coefficient	cm^2 d^{-1}	1.18
ODU diffusion coefficient	cm^2 d^{-1}	1.08
Advection rate	cm day^{-1}	$2.74x10^{-7}$
Mixed layer depth (thickness of sediment affected by bioturbation)*	cm	5
Half-saturation concentration of O_2 in oxic mineralisation	mmol O_2 m^{-3}	3
Half-saturation concentration of NO_3^- in denitrification	mmol NO_3^- m^{-3}	30
Half-saturation concentration of O_2 in nitrification	mmol O_2 m^{-3}	1
Half-saturation concentration of O_2 in oxidation of ODU	mmol O_2 m^{-3}	1
Half-saturation concentration of O_2 in inhibiting denitrification	mmol O_2 m^{-3}	1
NH_3 adsorption coefficient	-	1.3
Half-saturation concentration of NO_3^- inhibiting anoxic mineralisation	mmol NO_3^- m^{-3}	1
Half-saturation concentration of O_2 inhibiting anoxic mineralisation	mmol O_2 m^{-3}	1
Temperature	^oC	10

* The mixed layer depth is the thickness of sediment affected by bioturbation; below the mixed layer depth, the effect of bioturbation decreases exponentially with depth

carbon fractions, Boudreau & Ruddick (1991) commented: "*It would be truly astounding that the decay of all these compounds would fall neatly into a small finite number of reactivity types*". As a result, Boudreau and Ruddick (1991) determined an equation to describe reactive continuums, shown in Equation 2.4.

$$G(t) = G(0)\left(\frac{a}{a+t}\right)^{\nu} \qquad \text{Eqtn 2.4}$$

where G(t) is the amount of OM at time t, G(0) is the initial amount of OM, *a* is a measure of the average life-time of the more reactive components of the mixture of organic substances, and the exponent ν is a nondimensional parameter related only to the shape of the distribution. Equation 2.4 is similar in form to the Michaelis-Menten equations which govern the rate of breakdown of OM, as shown in Equations 2.1-2.3; however, in the Michaelis-Menten equations, the value of the half-saturation constant is the concentration of the species required to attain 50% of the maximum rate of the reaction, whereas the value of *a* here is a less well-defined value.

Boudreau and Ruddick (1991) found that they were able to use the this continuum equation to fit organic matter profiles in historical layers of marine sediments from a range of data found in the literature with some amount of success; with suitable values for *a* and ν, achieving correlation coefficients of between 0.917 and 0.978. This continuum approach has also been incorporated into a model by Middelburg (1989), which was able to satisfactorily fit experimental data from two different Long Island Sound sites. However, it should be noted that in the approach taken by both Boudreau and Ruddick (1991) and Middelberg (1989), it is assumed that the sedimentary environment is in steady-state. In practical terms, when incorporating these techniques into a full diagenetic model, van Cappellen and Wang (1996) found that the relative proportion of carbon flux across the individual sediment layers within the model (of which there are 100, and will be discussed in greater detail in 2.2) versus the sediment-water interface (SWI) flux needs to be considered (Soetaert *et al.* 1996b). Currently, it is not possible to incorporate this technique when non steady-state flux conditions are to be considered. Hence, in the model presented in this thesis, a multi-G approach (as originally described by Westrich and Berner (1984), and implemented in OMEXDIA by Soetaert *et al*. (1996b)) is used where the model has three organic carbon pools: fast degrading, slow degrading and refractory. The last pool is not modelled as such, and is therefore not found in any equations in the model, but its presence as a parameter is used to help fit the model output to experimental data in later chapters. The two degradable fractions have differing rate constants (see Table 2.2), fulfilling the criteria set out by Middelberg (1989) with regard to the degradability of OM with respect to time, which is itself directly related to depth within the sediment. Values for

the rate constants for the fast- and slow-degrading material in the default parameter set are $1x10^{-2}$ d^{-1} and $1x10^{-5}$ d^{-1} respectively, with these values being taken as representative for the environments being modelled from experimental data (Westrich and Berner 1984). The two carbon fractions also have differing carbon to nitrogen ratios, a higher ratio (106:14) for the slower degrading fraction, compared with 106:16 for the faster degrading fraction, effectively allowing the model to simulate simply the role of nitrogen as a limited resource in primary productivity, and hence becoming further limited with respect to depth as it is consumed in within the sedimentary column. This increase of C:N ratios with increasing depth is well documented (Bourgoin and Tremblay 2010; Hammond *et al.* 1996; Burdige and Zheng 1998; Stoeck *et al.* 2003).

2.1 Description of limitation functions

OMEXDIA makes use of limitation functions in Equations 2.1 – 2.3 to mathematically control the sequence of reactions. The sequence is controlled by Michaelis-Menten type kinetics, an example function of which is the second term in the denitrification equation (Equation 2.2) and the first two terms in the anoxic mineralisation reaction (Equation 2.3). Biogeochemically, the reactions are also limited by the availability of the oxidant used in the reaction. This limitation is represented by a hyperbolic function with a half-saturation constant – i.e. as the concentration of the limiting substance (e.g. O_2 in oxic mineralisation) decreases, the limitation tends towards zero, and the rate of reaction decreases. Equations of this type are known as Michaelis-Menten functions, which are a common feature of biological models (Soetaert and Herman 2009). Mathematically, this is known as a type II functional response and describes a situation where the rate increases nearly linearly at low resource density, and then levels off at higher resource densities (Holling 1959); the function has values between 0 and 1. Taking oxic mineralisation as an example, and ignoring the effect on other mineralisation pathways, this means that when O_2 concentrations are low, the reaction rate is low. The rate of reaction will then be dependent on the half-saturation constant; half-saturation constant is defined as the concentration of O_2 required to attain 50% of the rate of oxidation of OM. At high concentrations of O_2, the half-saturation constant has less of an effect, leading to high values of the rate limiting term; a value of O_2 which is relatively much greater than the value of the half-saturation constant will effectively lead to the rate-limiting term having a value close to 1. It should be noted that the higher the value of the half-saturation constant, the slower the reaction at low concentrations of the resource.

Although the anoxic mineralisation pathways are not discretely modelled, the processes that they undergo are still indirectly represented in the model; as such, the

model includes a term for the solid deposition of reduced anoxic substances. Both iron pyrite (FeS_2) (Berner 1970) and manganese carbonate ($MnCO_3$) are products of reactions embedded in the ODU variable (Soetaert *et al.* 1996b; Pedersen and Price 1982). As a result, OMEXDIA includes a term to enable the loss of these fractions when they are transported (by advection) out of the model domain.

2.2 Application of OMEXDIA in a temperate shelf-system

To start to address the initial objective of this thesis, the ODU variable was split into its individual constituent chemical reactions – manganese, iron and sulphur reduction. Iron is known to influence phosphate cycling (van der Zee *et al.* 2002a), and there is evidence that parts of the North Sea may be anoxic during certain times of the year (e.g. Pederstad *et al.* 1993). The following three microbially-mediated chemical reactions (Froelich *et al.* 1979; Soetaert *et al.* 1996b) were therefore implemented into OMEXDIA (where OM is $(CH_2O)_{106}(NH_3)_{16}(H_3PO_4)$):

$$OM + 236\ MnO_2 + 472\ H^+ \rightarrow 236\ Mn^{2+} + 106\ CO_2 + 8\ N_2 + H_3PO_4 + 366\ H_2O \quad \text{Eqtn 2.5}$$

$$OM + 424\ FeOOH \rightarrow 424\ Fe^{2+} + 106\ CO_2 + 42.4\ N_2 + H_3PO_4 + 148.4\ H_2O \quad \text{Eqtn 2.6}$$

$$OM + 53\ SO_4^{2-} \rightarrow 53\ S^{2-} + 106\ CO_2 + 16\ N_2 + H_3PO_4 + 106\ H_2O + 8H_2 \quad \text{Eqtn 2.7}$$

The reoxidation of Mn^{2+}, Fe^{2+} and S^{2-}, within the oxic layer of the sediment column, have also been implemented. It is worth noting that although methanogenesis does not appear to have been directly included, as this is the sole reaction remaining in the sequence defined by Froelich (1979), it is effectively the anoxic mineralisation defined in a modified version of Equation 2.3. Based on studies of North Sea sediment, manganese oxide reduction and menthanogenesis would appear to be, in general, least significant in the mineralisation of organic matter (e.g. van Raaphorst *et al.* 1990), although anomalies do occur; for example, in their studies of the Kattegat and the Skaggerak, Rysgaard *et al* (2001), found that at nine locations studied, manganese oxides did not contribute to OM oxidation, but at a tenth site, the Mn reduction pathways were responsible for 85% of OM oxidation.

In the following description of the model, values given to model parameters are the model defaults (Soetaert *et al.* 1996b) unless otherwise stated. The model is written in the R programming language; an open-source language with a relatively easy-to-read syntax. The open-source nature of the language enables *packages* to be developed by individuals and distributed via the R website. More detail about R, and

the usefulness of packages during the use of OMEXDIA will be discussed in more detail in Section 2.5. The model is 1D, dealing only with the change in concentrations with depth, given a constant organic matter flux to the sediment. The model domain is currently set to be the top 15 cm of sediment, with the domain divided into 100 layers. The first layer is 1 mm, and subsequent layers increase in size in an exponential fashion. The primary forcing parameter is the flux of particulate organic carbon (POC) to the top of the sediment. As the model equations are all contained within a single R program function, it is easy to set up the model to run as many times as required, by just calling the R function. The default model executes three runs of the model, using the POC fluxes 2, 15 and 50 g C m^{-2} yr^{-1} which covers the range for the North Sea presented in the literature (Lohse *et al.* 1993), with the exception of shallow coastal areas where fluxes are often higher. In later chapters in this thesis, it may be necessary to modify the POC flux to outside this range so that accurate profiles for specific environments can be generated by the model

The profiles of the chemical species studied in the model are not only affected by the biogeochemical reactions they undergo, but also by transport, chiefly by diffusion for the solutes and bioturbation for OM. Transport is approximated by finite differences. Diffusion, a function of porosity and sediment resistivity, is estimated in nearshore muds using equation 2.8 (Soetaert *et al.* 1996b). It should also be noted that although diffusion coefficients are given constant values in the table, they are calculated in OMEXDIA according to Equation 2.8.

$$D_i^T = \alpha T + D_i^0 \qquad \text{Eqtn 2.8}$$

where D_i^T is the diffusion coefficient of the species *i* at temperature T, α is an ion-specific coefficient and D_i^0 is the diffusion coefficient (cm^2 s^{-1}) at 0°C. In the calibration Soetaert *et al* (1996b) carried out, values of D_i^0 were taken from Li & Gregory (1974), while values of α were calculated by linearly interpolating between the diffusion coefficient at 0°C and 18°C for each species.

As numerous authors (including Aller (1990) and Anton *et al.* (1993)) have described, the potential role of bioturbation in coastal seas in biogeochemical cycling is considerable and can affect the rates and distribution of diagenetic reactions. Although there has been much research on the best way to model bioturbation and bioirrigation (Boudreau 1994, 2000), OMEXDIA takes a relatively simple approach by using a single depth-dependent coefficient (with units of cm^2 d^{-1}). This bioturbation coefficient is constant in the top 5 cm (the default model parameter), but decreases exponentially to zero below this depth, to reflect the depth of influence of bioturbation in marine sediments (Boudreau 2000). The approach taken here does not take into

account the advanced ideas of biodiffusion, bioirrigation or non-local transport as discussed by Meysman *et al.* (2003a; 2005; 2006); however, as shall be seen in later chapters, I believe that the relatively simple bioturbation concept implemented in this model is an adequate representation of the environment.

One of the primary concerns in the development of a biogeochemical model is whether mass is conserved. In OMEXDIA, a simple check is made after the model has run by taking the ratio of the sum of the net fluxes across the SWI and the bottom boundary of the model domain to the total consumption of each species. Mass is conserved to within 99.99%.

Finally, it is important to mention other features in the model which increases the chances of its output being realistic. The process of adsorption is likely to be significant in resuspension processes; Berner (1976) first discussed the potential of implementing adsorption in a diagenetic model based on the following ion exchange equation:

$$nA^{m+}_{(aq)} + mB^{n+}_{(s)} \rightleftharpoons mB^{n+}_{(aq)} + nA^{m+}_{(s)} \qquad \text{Eqtn 2.9}$$

where (aq) denotes ions in solution and (s) denotes ions adsorbed or in cation exchange sites (Burdige 2006). It is simple to derive an equilibrium constant for this reaction, which can then be added to either the source or sink terms of a species as necessary. Although OMEXDIA only deals with the adsorption of NH_4^+, the addition of other ions (Mn^{2+}, Fe^{2+}, S^{2-}) into the model is discussed in Chapter 3.

A minor improvement to the published (Soetaert *et al.* 1996b) version of OMEXDIA has been made. Tortuosity is the name given to the idea that diffusion in sedimentary environments is slower than it would otherwise be in water due to the convoluted path that ions have to take to avoid solid particles. Tortuosity has been studied, both experimentally and theoretically, and attempts to define it mathematically have been undertaken by a number of researchers over the last 40 years (e.g. Ullman and Aller 1982; Berner 1971; McDuff and Ellis 1979; Lerman 1979). These works led to the development of a number of relationships between porosity and tortuosity, although the ones used with most success have an adjustable parameter (Boudreau 1997a). In this work, we use a modified Weissberg relation (Weissberg 1963; Equation 2.10), using 2 as the value of *b*, leading to Equation 2.11.

$$\theta^2 = 1 - b \cdot ln(\varphi) \qquad \text{Eqtn 2.10}$$

$$\theta^2 = 1 - ln(\varphi^2) \qquad \text{Eqtn 2.11}$$

where θ is tortuosity. This relationship is used in preference to the others listed in Table 4.11 of Boudreau (1997a), due to the high r^2 value obtained when using a simple integer value with a relatively low error margin when plotting theoretical tortuosity-porosity relations with observed values found in the literature, across a range of chemical species. This relationship has therefore been included in the resuspension model (see Chapter 6) for O_2, NO_3^-, NH_3 and ODU.

Some of the parameters from Table 2.2, which shows the default parameter list for the steady-state version of OMEXDIA, along with the values used after calibration with data from continental slope and abyssal plain data (Soetaert *et al.* 1996b), need some further explanation. Diagenetic models tend to use the term 'advection rate', whereas experimental work often measures only 'sedimentation rate'. Given the lack of data in the literature for 'advection rates', for the purposes of discussion later on in the thesis, they are treated as the same parameter so that they can be compared like-for-like. However, sedimentation only takes into account that material which is accumulated at the sediment-water interface. Advection refers to the bulk flow of any environmental medium, and when thinking about the advection of sediment particles, has two components: burial and compaction. The burial component refers to the increasing distance between a specific grain and the SWI, due to the sediment accumulation and pull of gravity on that grain; compaction is the process gradually packs sediment particles closer together as a result of the increasing weight due to sediment accumulation. In OMEXDIA, advection is a depth-independent parameter, with units of cm d^{-1}. Given that sedimentation rate will include organic matter which will be degraded, whereas advection will be the integrated rate over the whole sediment column, sedimentation rate would expected to be higher than advection rate.

Using the parameter values discussed above, an example model steady-state solution can be provided to give an indication of the output provided by the model. Figure 2.1 shows the steady-state profiles generated from three separate runs with POC fluxes of 2, 15 and 50 g C m^{-2} yr^{-1}.

As can be seen in Figure 2.1, oxygen, nitrate and ammonia all respond to differing POC fluxes. The quasi step-wise decreases in the TOC profiles are due to the result of the different reactivities of the two fractions of OM (fast and slow); the fast degrading OM is oxidised more quickly, and as such, is removed from the sediment closer to the SWI than the slow degrading OM. The oxygen penetration depth (OPD) decreases as POC flux increases, as would be expected. Low POC fluxes mean that all the OM is degraded by O_2; due to sufficient concentrations of O_2 in the system to oxidise all NH_3 that is produced, and little NH_3 being produced as a result of the low

POC fluxes, NH_3 concentrations are low throughout the sediment column, but NO_3^- concentrations increase through it. With increasing fluxes of POC, the O_2 concentration is insufficient to oxidise the total inventory OM, and so there also has to be suboxic and anoxic mineralisation of OM (Libes 1992); the anoxic mineralisation is responsible for degradation of OM by NO_3^-, MnO_2, Fe_2O_3 and SO_4^{2-} (with a reminder that the latter three oxidants, and methanogenesis, are combined into a single ODU component in OMEXDIA). The model includes both nitrification and denitrification, leading to the nitrate peaks seen in the 15 and 50 g C m^{-2} yr^{-1} runs in Figure 2.1; the decreasing depth of the peak as the POC flux increases reflects the decreasing OPD (and hence the narrowing of the oxic layer). Below the oxic layer, there is no mechanism for NH_3 to be oxidised, leading to the increased concentrations seen. Mass balance calculations for these all runs show that both the O_2 and N budgets again conserve mass to within 99.99%.

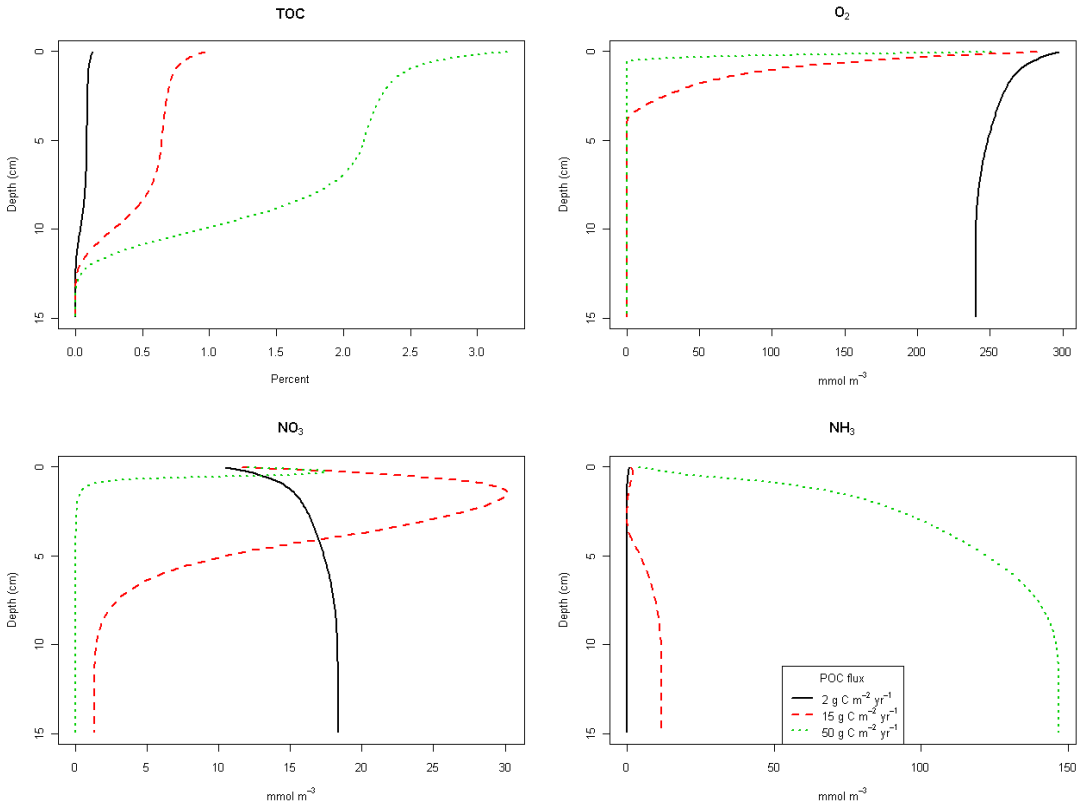

Figure 2.1: Profiles of carbon, oxygen, nitrate, and ammonia generated by the steady-state version of OMEXDIA using the default parameter set (see text) when the fluxes of OM to the sediment are 2, 15 and 50 g C m^{-2} yr^{-1}

2.3 The dynamic model

The description of the model given so far refers to the steady-state version of the model. This implies that the flux of OM to the SWI is constant over time. Although

this may hold true for some deep-sea environments (Epping *et al.* 2002; Lohse *et al.* 1998), where the water beneath the mixed-layer depth boundary is often not subjected to the effects of the seasonal dynamics that occurs in the mixed layer, this is not the case in shallow, highly productive shelf seas, particularly where the entire water column is mixed for the entire year. The dynamic version of OMEXDIA has been calibrated against POC, total particulate mass and sediment community oxygen consumption (SCOC), obtained as a time-series at a single abyssal station (Smith *et al.* 1992; Soetaert *et al.* 1996a). Using observational data for porosity, bottom water concentrations of O_2, NO_3^-, NH_3 and ODU, and temperature, Soetaert *et al.* (1996a) report that OMEXDIA was able to fit the observed data relatively well; oxygen, for example, was within the deviation of observational data from Pacific Station N/M, with the OPD also matching observed values of 1.5 - 2.5 cm. NO_3^- and NH_3 were also generally accurately represented, with nitrate showing the expected decrease with depth (decreasing to zero by 3 cm) and ammonia following the increase with depth that the observations show. Rates (fluxes and oxidation rates) between calculated values and modelled values also match well.

As discussed in Chapter 1, the general diagenetic equation does account for changes with respect to time (Eqtn 1.1; Berner 1964; Boudreau 1997a). However, in steady-state form, $dC/dt = 0$, and therefore the diagenetic equation is now a relatively simple ordinary differential equation (ODE), which can be solved numerically (such as using the Newton-Raphson method). The time-dependent version, being a more complex PDE (partial differential equation), can only be solved numerically using a more computationally-intensive method (the one used here being Runge-Kutta). The parameters for both the steady-state and dynamic versions of the model are the same (and the model has actually been designed so that it there is a simple switch between the steady-state and dynamic versions of the model).

The dynamic simulations are carried out by obtaining a steady-state solution of the model using the annual mean flux as the forcing parameter, and then running the model for two years (the first year as a *spin-up*; adequate spin-up is necessary for the model to be initialised with the changing flux). The result shown here is the second year of the model run. The steady-state solution is obtained first using the Newton-Raphson method; in this run, the difference between the inventories of the state-variables at day 1 and day 365 are approximately 1% for the state variables. This value is slightly higher than may be ideal, and I shall discuss in further detail the reasons for this discrepancy, and methods to eliminate it in Chapter 4. The technique is a fast means - taking approximately 3 seconds on a standard single processor desktop computer of obtaining a periodic steady-state solution.

The dynamic model outputs porewater concentrations and boundary fluxes of the state variables, and the rates of the organic matter pathways allowing simple plots to be generated; Figure 2.3 shows the response of the porewater concentrations of TOC, O_2, NO_3^- and NH_3 given a TOC flux to the SWI determined by Equation 2.12.

$$f_t = \overline{f} \times (1 + \sin(\frac{2\pi t}{365})) \qquad \text{Eqtn 2.12}$$

where f_t is the flux at time t and $\overline{f}$ is the mean flux over a flux cycle (in this case annual), in units of g C m^{-2} yr^{-1}. In this example, the mean flux was 15 g C m^{-2} yr^{-1}, and the resulting annual flux cycle can be seen in Figure 2.2.

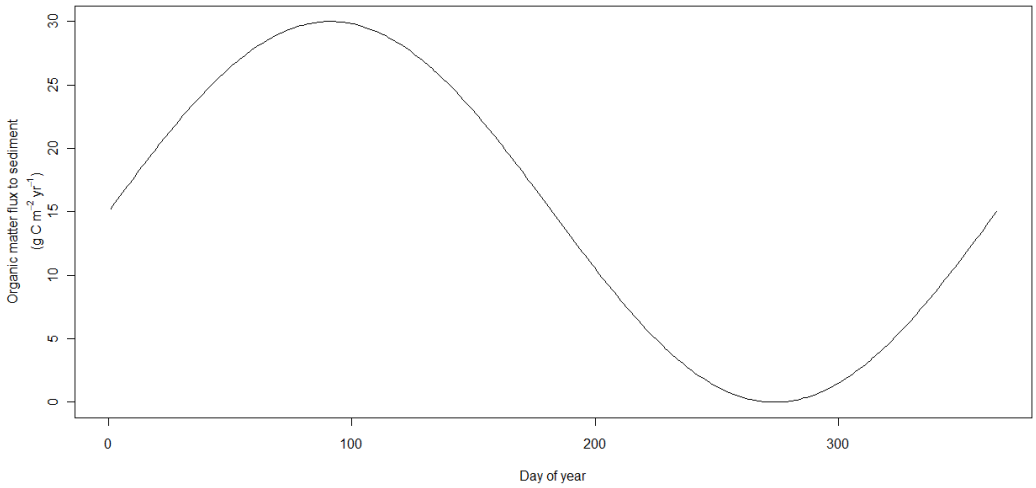

Figure 2.2: A graphical representation of Eqtn 2.1, with the value of $\bar{f}$ being 15, and when t has values of the integers 1 to 365

It should be noted that this flux equation is not a particularly realistic reflection of POC fluxes over an annual cycle, although it does provide a convenient mathematical function with which to test the dynamic model. In Chapter 4, I will demonstrate that a much more realistic POC flux can be used, although care has to be taken if using a non-continuous function, as many methods to solve PDEs are unstable if the steps between the forcing parameter values are too large (Press *et al.* 1992).

Figure 2.3 shows that O_2, NO_3^- and NH_3 all respond to a change in POC flux, with varying response times; as the POC flux increases, the oxygen consumption also increases, leading to a decrease in the OPD. Reduced oxygen concentrations subsequently lead to a decrease in nitrification, resulting in lower concentrations of nitrate and increasing concentrations of ammonia. Consequently, the relative contribution of OM oxidation by the species in the anoxic layer will increase (not

shown). When the POC flux decreases, both the OPD and concentrations of nitrate can be seen to increase, while ammonia decreases.

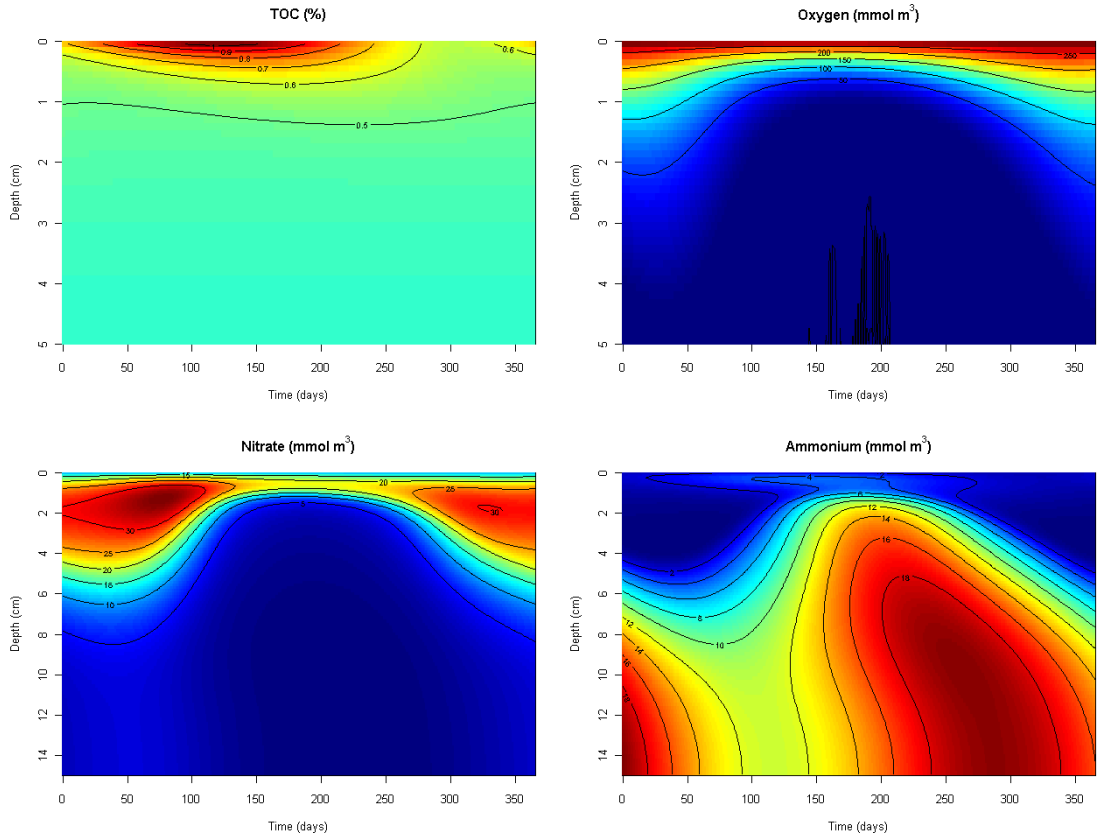

Figure 2.3: Concentration plots of carbon, oxtgen, nitrate and ammonia generated by the dynamic version of OMEXDIA using the default parameter set (see text) when the flux of OM to the sediment varies according to Eqtn 2.12 and the mean POC flux is 50 g C m^{-2} yr^{-1}

2.4 Limitations to the model

It should be noted that there are some caveats to OMEXDIA, particularly when considering its use in modelling shelf sea environments, rather than the continental slope and abyssal plain environments for which it was originally developed for, and calibrated against (Soetaert *et al.* 1996b; Soetaert *et al.* 1996a; Soetaert *et al.* 2002). The most major caveat is that OMEXDIA simplifies the sequence of oxidation of OM to enable the modelling approach to be made relatively simple. Froelich *et al.* (1979) studied three mineral phases of manganese oxide and found that the Gibbs Free Energy of two of them (birnessite and nsutite) was greater than the Gibbs Free Energy of denitrification, if the denitrification reaction causes all organic nitrogen to be released as N_2. If part of the organic nitrogen fraction is released as NH_3, then the Gibbs Free Energy of the reaction falls below that of the lower of the third manganese

oxide (pyrolusite) pathway, and so it would be expected that all manganese oxide would be reduced before denitrification occurs. However, OMEXDIA assumes that manganese oxide reduction occurs below denitrification in the sedimentary column, and hence groups it in to the ODU component.

An additional reason to not explicitly model manganese is that there is little understanding of the distribution of manganese in shelf sea environments, and particularly the North Sea. Rajendran *et al*. (1992) found concentrations of extractable manganese (which was defined as Mn carbonates and oxyhydroxides) in sediments extracted from the Skagerrak of up to 300 mmol kg^{-1}, although concentrations in the deeper, central, waters of the Skaggerak were approximately an order of magnitude higher than concentrations in shallower areas; porewater concentrations of manganese were up to 60 mmol m^{-3}. Manganese has also been studied in intertidal sediments of the southern North Sea; (Beck *et al.* 2008a), found porewater concentrations consistently below 15 mmol m^{-3}, except within deep in the sedimentary column (below 4.5 m) where concentrations rose to 30 mmol m^{-3}. These concentrations are slightly lower than the results presented by Dellwig *et al*. (2007), who found dissolved manganese concentrations of up to 40 mmol m^{-3} and reactive Mn_x concentrations of 2.5 mmol kg^{-1} in the top 5 cm of intertidal sediments of the Wadden Sea.

Soetaert *et al*. (1996b) used results from the Panama Basin (Pedersen and Price 1982), with water depths of approximately 2000 m, as justification for inclusion of $MnCO_3$ deposition within OMEXDIA. Manganese carbonate is mainly thought to be formed in anoxic sediments where there are high concentrations of carbonate ions; however, following the discussion above about the lack of information in the literature about the distribution of Mn in the North Sea, it is also difficult to estimate the amount of Mn which may be lost through deposition as $MnCO_3$. For the purposes of the work here, the original assumptions (Soetaert *et al.* 1996b) have been retained.

Although OMEXDIA does include various important transport processes, such as bioturbation, it does not include bioirrigation, which is recognised as a relatively complex mechanism to implement (Meysman *et al.* 2006), and although some models to describe bioirrigation have been published (Koretsky *et al.* 2002), to date, no diagenetic models have included bioirrigation. In addition, although porosity is modelled (and, therefore, both muddy and sandy environments can be discretely described), tortuosity is not implemented in the model.

2.5 Description of model code and development

Although originally written in FORTRAN, the R version was used for development in this work as it is the version maintained by the author of the model (K. Soetaert, personal communication, 2009). One of the main advantages of R is, due to its open-source nature, that it is easy for developers to write new functions, which can be distributed via the R website (http://www.r-project.org) as *packages*. Three such packages, *ReacTran* (Soetaert and Meysman 2011), *rootSolve* (Soetaert and Herman 2009) and *deSolve*, (Soetaert *et al.* 2010), are used directly by OMEXDIA, and as they are critical to running the model, are described in more detail below.

2.5.1 Implementation of transport equations

The model domain is defined by a series of discrete layers. Within each layer, transport and reaction equations are solved to determine fluxes and concentrations of state variables. ReacTran is a package which contains methods for creating discretised environments, so that reaction and advection-diffusion transport in one, two or three dimensions can be simulated. The package was developed with ecological and biogeochemical modelling in mind, and the majority of the examples in the *vignette*[1] reflect this; however, there is no reason why this package could not be used for any model where a discretised environment is required. The package enables a user to set up the grid that contains the layers (or cells in a 2- or 3D environment) required. To increase the efficiency of the model runs, OMEXDIA concentrates its computational efforts close to the SWI, where the majority of the biogeochemical reactions occur. To aid this, the model grid is set-up so that there is a differential in layer thicknesses. The narrowest layer (L_0, whose thickness can be prescribed) is at the top of the model domain. The thickness of the layers throughout the grid increases exponentially, yielding the thickest layer at the bottom of the model domain. ReacTran will calculate the thickness each layer needs to be based on the thickness of L_0 and number of layers, which are values supplied to the setup method.

ReacTran also calculates the transport (i.e. the rate of change due to advection and diffusion) associated with each chemical species within the model domain. This calculation includes the flux of dissolved species across the model boundaries. The package allows options for specifying values of various transport parameters (in this case diffusion coefficients and advection velocity). Both of these arguments can either be a single value (which makes most sense in biogeochemical modelling, where, for example, a diffusion coefficient would normally be considered as a constant value in a

[1] Vignette is the name given to the verbose, informal reference documents for R packages

relatively narrow model domain, where all parameters affecting diffusion would be constant) or a vector of values, providing a value for the diffusion in each layer of the grid.

2.5.2 Implementation of differential equation solvers

OMEXDIA makes use of the *deSolve* and *rootSolve* packages to solve the differential and partial differential equations that describe the reaction and transport processes.

rootSolve solves ODEs by finding the roots of non-linear functions. Roots of non-linear equations are solved using the Newton-Raphson method. The Newton-Raphson method is an iterative procedure allowing the roots of an ODE to be found when there is no analytical solution (Chen *et al.* 1999; Soetaert and Herman 2009). Using *rootSolve*, a steady-state solution of OMEXDIA can be found quickly (almost instantaneously on a modern desktop computer).

deSolve numerically solves PDEs that have been converted to ODEs by finite differencing; it is therefore suitable to solving the general diagenetic equation where a forcing parameter, such as OM deposition rate, varies over time. For performance reasons, the package provides an interface to existing FORTRAN and C implementations of solvers; the current version of *deSolve*, 1.10-3, allows the use of 1 of 13 integration methods, with the default being *lsoda*. Other well-known algorithms, such as *Runge-Kutta* and *euler*, are also available through the *deSolve* package.

The advantage in using the ReacTran, rootSolve and deSolve packages is that developers of biogeochemical models do not have to be concerned with the most efficient methods to solve the mathematical equations of the model, and can instead use their time more effectively in using their model to study the underlying science.

2.6 Summary

This chapter has outlined the basic mechanisms by which diagenetic models operate, and how the development of such models can be made easier by using existing tools and frameworks. Despite the relative complex mathematics that environmental models often require, I have introduced here some methods by which the theory can be somewhat simplified with little impact on the accuracy of the model. I have also shown how OMEXDIA can be used to produce profiles of the chemical species involved with relative ease, both when the forcing parameter, the flux of

particulate organic carbon to the sediment from the overlying water column, is constant (i.e. a steady-state model run) or changes with respect to time (a dynamic simulation).

OMEXDIA is therefore a useful starting point to model early diagenesis that incorporates many of the major advances that have been made in early diagenetic modelling since Berner's seminal 1964 paper (Berner 1964), although, as I have shown, it is also straightforward to include further slight amendments that are also likely to improve model output without having a significant impact on computational performance (such as the addition of tortuosity). In part, this is due to the programming language (R) chosen for initial model development, and the fact that many packages have already been written for the R language which have the ability to assist environmental modellers. In Chapter 3, I show how the steady-state model can be extended by increasing the number of biogeochemical processes, although this is not always a trivial task. I will also build on the dynamic version of OMEXDIA, introduced in this Chapter, in Chapter 4, showing how the forcing parameter, POC flux, can be manipulated and what affect this may have on sediments over time, and hence further our understanding of how sediments interact with the biogeochemistry of the overlying water column.

OMEXDIA was originally developed to simulate the continental slope and abyssal plain; I will build on this in Chapter 5, by showing that the model can also be applied to coastal areas and continental shelves. It can be argued that these latter two environments are more problematic for attempting to model the benthic system than the abyssal plain, due to their highly dynamic nature. However, for the purposes of initially calibrating and validating the model, I assume that the system is in quasi-steady-state. In Chapters 6 and 7, I will also describe in detail how the model has been extended to include additional physical processes; although this does affect computational performance, it provides much greater insight to processes that early diagenesis that biogeochemists now recognise is crucial to understanding the interdisciplinary nature of the marine environment.

3 The Steady-State OMEXDIA Model

Following on from the theoretical background of diagenetic modelling in Chapters 1 and 2, this chapter will examine the steady-state version of OMEXDIA, and discuss some modifications that have been implemented. Results from the default, steady-state, model will be shown initially, followed by results from various modifications made to the model. Results of how the model responds when the forcing parameters are changed to values measured during experimental work will then be shown.

3.1 Modelled porewater profiles

Figure 3.1 shows the profiles of total organic carbon (TOC), oxygen, nitrate and ammonia from the default model, which includes ODU. The three fluxes of organic carbon used to force the model (2, 15 and 50 g C m^{-2} yr^{-1}) used here reflect the range found in the literature (e.g. Anton *et al.* 1993; de Haas and van Weering 1997; Gargas *et al.* 1980; Tsunogai and Noriki 1991), and the results show that the default model is able to produce profiles are, generally, consistent with observations, as shown in Soetart et al (1996b).

In agreement with the trends in profiles that are often found in marine sediments (Bakker and Helder 1993; Lohse *et al.* 1993), increasing fluxes of organic matter cause a decrease in the oxygen penetration depth (Bakker and Helder 1993) followed by an increase in the concentration of nitrate in the upper sediment column due to increased nitrification. Below the maximum nitrate concentration there is a decrease of nitrate due to denitrification, leading to an increase of NH_3 with depth (Lohse *et al.* 1993). However, although the profiles seem realistic, there are some inconsistencies. There are several reasons why natural sediments do not behave in the same way as the system assumed in the generic model.

There is large variability in the organic carbon content between different environments; the North Sea continental shelf, being a relatively highly productive area, has high values compared with very low productivities observed in the continental slope and abyssal plain sediment. However, there is also variability within the North Sea; for example, the central North Sea, has relatively low carbon sedimentation rates compared with coastal areas, which have much high levels of sedimentation

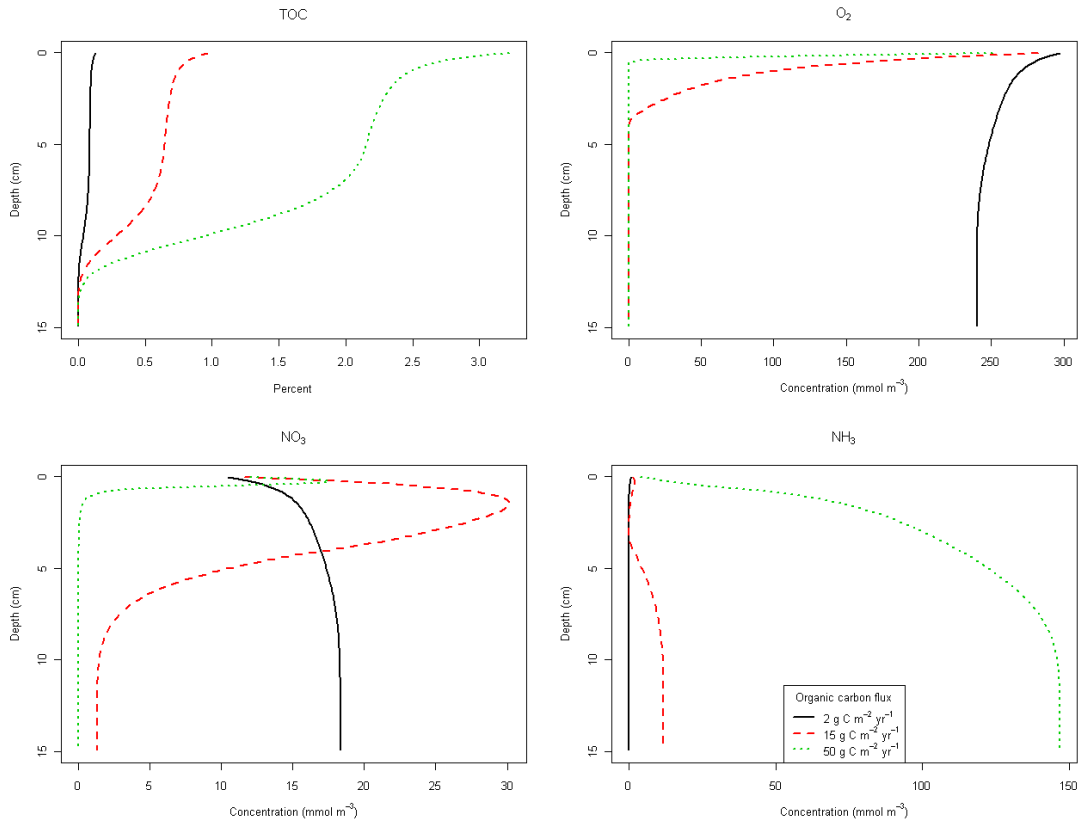

Figure 3.1: Output from the default version OMEXDIA showing carbon, oxygen, nitrate, and ammonia given three different organic carbon fluxes

It is also well known that sandy sediments, which are typically found in the southern North Sea (Postma 1981) have generally lower carbon content than more muddy sediments (Moodley 1990). However, even in silty sediments, the organic carbon content can often be below 1% (Boon and Duineveld 1998), whilst permanently deposited mud has been reported as having a carbon content as high as 4% (Salomons and Mook 1981); however, this was in the high productivity coastal region of the Wadden Sea where an unusually high carbon flux of 584 g m^{-2} yr^{-1} has been reported (Postma 1981). Typical values for carbon content in North Sea sediments are 2.5-4% (Boon *et al.* 1999; de Haas *et al.* 1997; de Haas and van Weering 1997; Salomons and Mook 1981; Van Weering *et al.* 1987).

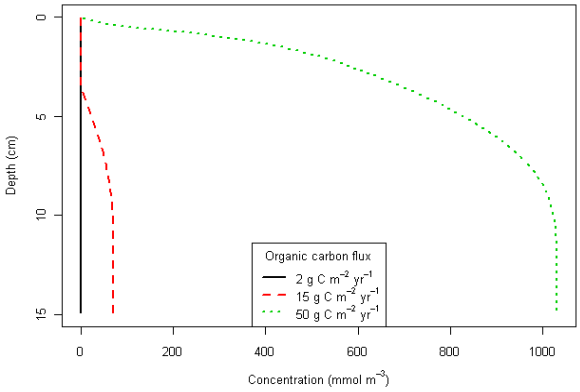

Figure 3.2: OMEXDIA ODU profiles

The results presented using show that a model can do one of two things: either generate estimations for nutrient budgets, fluxes and other large scale transport processes using a set of parameters that are likely to be averages across the whole continental shelf, or generate profiles for specific locations. It is unlikely, that with our current understanding, a model would be able to do both effectively. For example, given the high rates of productivity and carbon supply to the sediments in the Wadden Sea, a set of parameters in a 1D model which generated reasonable profiles for this location would almost certainly over-estimate fluxes and transport processes if extrapolated to the whole of the continental shelf.

Figure 3.2 shows the ODU profile from OMEXDIA, indicating that organic matter is totally degraded by approximately 7.5 cm when the organic carbon flux is 15 g C m^{-2} yr^{-1}, and by approximately 10 cm when the flux is 50 g C m^{-2} yr^{-1}. The lack of ODU confirms that all carbon is oxidised by oxygen and nitrate when the carbon flux is 2 g C m^{-2} yr^{-1}, in agreement with the nitrate profile in Figure 3.1. The concentrations of reduced species will of course depend on the concentrations of the oxidising agents in the sediment. The ODU profiles coincide with the profiles shown in Figure 3.1; the concentration of ODU increases only when nitrate decreases. The shapes (but not concentrations) of the profiles of ammonia and ODU are the same as both are products of organic carbon oxidation below the oxic zone.

3.2 Addition of iron and sulphur cycling

To enhance the realistic representation of early diagenetic processes in OMEXDIA, the constituent processes enveloped in the ODU component were explicitly included, with iron and sulphur cycling being implemented. The manganese oxide reduction pathway has not yet been included, given the low relative contribution of this pathway to the total carbon mineralisation as a result of the generally very low concentrations of manganese in the North Sea (Rajendran *et al.* 1992; e.g. Bakker and Helder 1993; Canfield *et al.* 1993b; Slomp *et al.* 1997).

$$\text{Iron oxide mineralisation} = \frac{Fe_2O_3}{Fe_2O_3+Ks_{Fe_2O_3}} * \left(1-\frac{O_2}{O_2+Kin_{O_2}^{Feox}}\right) * \left(1-\frac{NO_3^-}{NO_3^-+Kin_{NO_3^-}^{Feox}}\right) * ((\kappa_f * TOC_f)+(\kappa_s * TOC_s)) * \frac{1}{\Sigma lim} \qquad \text{Eqtn 3.1}$$

$$\text{Sulphate mineralisation} = \frac{SO_4}{SO_4 + Ks_{SO_4}} * \left(1 - \frac{O_2}{O_2 + Kin_{O_2}^{Sulph}}\right) * \left(1 - \frac{NO_3^-}{NO_3^- + Kin_{NO_3}^{Sulph}}\right) * \left(1 - \frac{Fe_2O_3}{Fe_2O_3 + Kin_{Fe_2O_3}^{Sulph}}\right) * \left((\kappa_f * TOC_f) + (\kappa_s * TOC_s)\right) * \frac{1}{\Sigma lim} \quad \text{Eqtn 3.2}$$

$$\text{Anoxic mineralisation} = \left(1 - \frac{O_2}{O_2 + Kin_{O_2}^{AnoxMin}}\right) * \left(1 - \frac{NO_3^-}{NO_3^- + Kin_{NO_3}^{AnoxMin}}\right) * \left(1 - \frac{Fe_2O_3}{Fe_2O_3 + Kin_{Fe_2O_3}^{AnoxMin}}\right) * \left(1 - \frac{SO_4^{2-}}{SO_4^{2-} + Kin_{SO_4}^{AnoxMin}}\right) * ((\kappa_f * TOC_f) + (\kappa_s * TOC_s)) * \frac{1}{\Sigma li} \quad \text{Eqtn 3.3}$$

Table 3.1: The extra parameters needed to include iron and sulphur cycling in OMEXDIA

Parameter name	Parameter description	Units	Default values
Fe_2O_3	Concentration of iron oxide species	mmol Fe_2O_3 m^{-3}	300
$Ks_{Fe_2O_3}$	Half-saturation concentration of iron oxide in iron oxide mineralisation	mmol Fe_2O_3 m^{-3}	30
$Kin_{O_2}^{Feox}$	Half-saturation concentration of oxygen in inhibiting iron oxide mineralisation	mmol O_2 m^{-3}	1
$Kin_{NO_3}^{Feox}$	Half-saturation concentration of nitrate in inhibiting iron oxide mineralisation	mmol NO_3^- m^{-3}	1
SO_4^{2-}	Concentration of sulphate	mmol SO_4^{2-} m^{-3}	2000
Ks_{SO_4}	Half-saturation concentration of sulphate in sulphate mineralisation	mmol SO_4^{2-} m^{-3}	30
$Kin_{O_2}^{Sulph}$	Half-saturation concentration of oxygen in inhibiting sulphate mineralisation	mmol NO_3^- m^{-3}	1
$Kin_{NO_3}^{Sulph}$	Half-saturation concentration of nitrate in inhibiting sulphate mineralisation	mmol NO_3^- m^{-3}	1
$Kin_{Fe_2O_3}^{Sulph}$	Half-saturation concentration of iron oxide in inhibiting sulphate mineralisation	mmol Fe_2O_3 m^{-3}	1
$Kin_{Fe_2O_3}^{AnoxMin}$	Half-saturation concentration of iron oxide inhibiting anoxic mineralisation	mmol Fe_2O_3 m^{-3}	1
$Kin_{SO_4}^{AnoxMin}$	Half-saturation concentration of sulphate inhibiting anoxic mineralisation	mmol SO_4^{2-} m^{-3}	1

The implementation of iron oxide and sulphate reduction used the same principle as for denitrification as outlined in Chapter 2 (Equation 2.2); the Michaelis-Menton equations for iron oxide and sulphate reduction are shown in Equations 3.1 and 3.2. To comply with the steady-state assumption that all OM is removed from the system, Equation 3.3 shows the necessary change to the anoxic mineralisation. The

parameters that have not already been discussed in Chapter 2 are defined in Table 3.1; with a lack of empirical data for these parameters, values were chosen to be in the same range as the values for the equivalent parameters for oxic mineralisation and denitrification in Soetaert *et al.* (1996b). The final term in Equations 3.1-3.3 were modified to include the extra processes in line with the description of the rescaling term in Chapter 2. It should be noted that iron oxide has initially been included as a solute here, instead of as a solid.

Figure 3.3 shows the output from the model following implementation of mineralisation by iron oxide and sulphate. These graphs show that the model is acting in an expected way; i.e. iron oxides are only consumed after nitrate has been depleted, and the nitrate concentrations decrease to approximately 0 mmol m^{-3}; the subsequent decrease in the concentration of iron oxides is also reflected by the expected increase in concentrations of reduced iron, a decrease in sulphate below the zone when iron oxides are used and then an increase in sulphides. Mass balances for all chemical species involved are calculated, and shown in Table 3.2. Some oxygen and nitrogen is converted to species which do not undergo further redox processes (e.g. CO_2 and N_2), accounting for the consumption values shown in Table 3.2. Unlike oxygen and nitrogen, there is no net loss of either iron or sulphur from the system at steady-state. For mass to be maintained, the net flux of iron and sulphur must therefore also be zero, although the oxic species will be prevalent in the flux across the sediment-water interface, and the reduced species will be most important across the bottom boundary of the model.

Table 3.2: Net fluxes (mmol m^{-2} yr^{-1}) & depth integrated total consumption (mmol yr^{-1}) of each of the chemical species during mineralisation and secondary reactions

	Oxygen	Nitrogen	Iron	Sulphur
Net flux	408.3	11.2	-1.3×10^{-11}	-7.0×10^{-13}
Total consumed	408.3	11.2	-1.3×10^{-11}	-7.0×10^{-13}

Despite the apparently sensible output shown in Figure 3.3 with regard to iron and sulphur cycling, these are not particularly realistic profiles and are not consistent with some published data. Van der Zee *et al.* (2002b) showed that on the Iberian Continental Margin (where the water depth was 175 metres), reduced iron increased steadily with depth from zero, reached a peak at approximately 10 cm and then decreased again, reaching a minimum at 20 cm. However, solid phase iron stayed relatively constant throughout the sediment. As the paper does not state the organic carbon flux into the sediment, it is not possible to compare like-for-like the

concentrations of reduced iron which they show in their profiles with the current model runs.

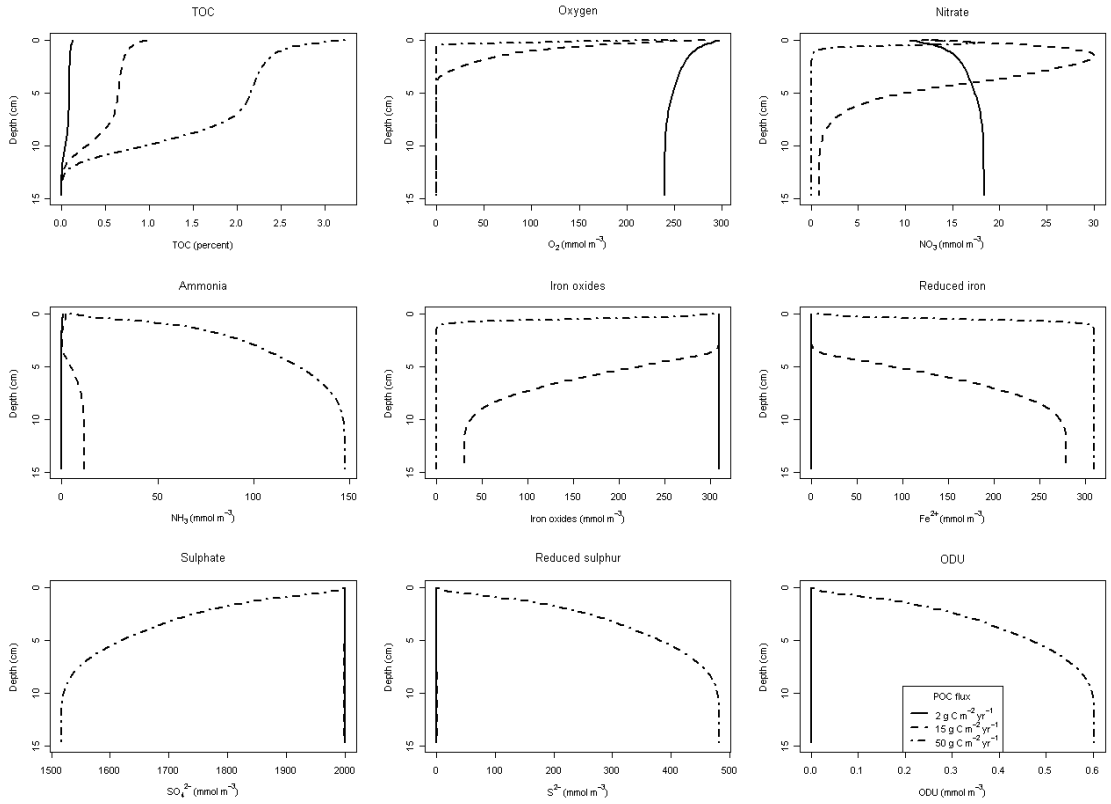

Figure 3.3: Profiles generated from a modified version of OMEXDIA when iron oxide and sulphate reduction pathways were implemented, for POC fluxes of 2, 15 and 50 g C m^{-2} yr^{-1}

The classical interpretation of this pattern would be the reduced iron and sulphur reacting to form pyrite and other iron sulphides. Beck *et al.* (2008a) studied intertidal mud flats in the Wadden Sea, and found that at one site (JS1) iron (II) concentrations were low (below 5 μM). At another site (JS2) iron (II) concentrations were below 10 μM. At both of these sites, both sulphate and sulphide concentrations were constant throughout the upper tens of centimetres (Beck *et al.* 2008b). Sedimentary organic carbon content of 1 – 1.5% appears to induce iron oxide mineralisation but not sulphate mineralisation in the upper 10 cm of the sediment column, increasing reduced iron concentrations with depth (Böttcher *et al.* 2004), which is perhaps slightly closer to the model output. Even in locations where iron profiles follow expected patterns, the rate of mineralisation, and the contribution of iron oxide to total organic matter degradation, is highly variable (Jensen *et al.* 2003); the increase of reduced iron in surface sediments can, in extreme cases, be approximately an order of magnitude (Langston *et al.* 1999). Langston *et al.* (1999) also showed that patterns of reduced iron are not always consistent even in replicate cores, leading to a conclusion that experimental conditions may not accurately reflect field conditions. Although the textbook example of an iron profile would show a decrease in reduced iron at depth to

indicate iron sulphide production, this is not always visible, even in areas where sulphate reduction is known to be an important pathway (Rajendran *et al.* 1992; Rysgaard *et al.* 2001; Arnosti and Holmer 2003).

Although mineralisation of organic matter by iron oxides does occur in shelf sea sediments (Slomp *et al.* 1996), the low concentrations of reduced iron are assumed to be a result of rapid formation of iron sulphides. This would imply that there is reworking of the sediment, either by bioturbation or by physical processes, so that the reduced iron and sulphides are able to react, as they are formed in separate distinct layers in the sediment. As iron sulphide has been observed in North Sea sediments, albeit at low concentrations, (Canfield 1993), it implies that formation of iron pyrites should be incorporated into the model to make sure it acts as realistically as possible in areas where anoxic mineralisation is likely to be important.

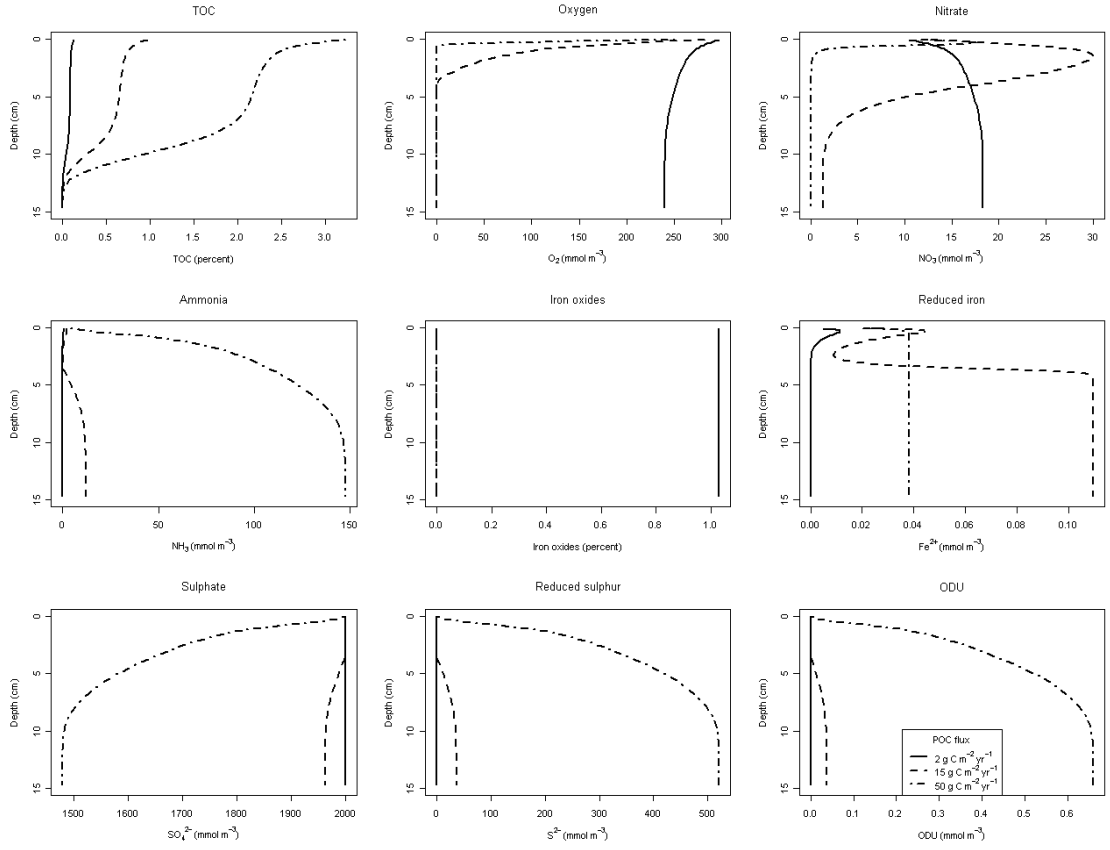

Figure 3.4: Profiles generated from a modified version of OMEXDIA when iron oxide (solid form) and sulphate reduction pathways were implemented; POC fluxes of 2, 15 and 50 g C m^{-2} yr^{-1} were used for the 3 runs

There are also further reasons why the above implementation, although on the face of it seems sensible, should be used with caution. The additional two pathways of iron oxide and sulphate reduction require an extra 10 equations to represent the

biogeochemistry, as well as the four extra transport processes (and 25 parameters); this extra complexity means that the model takes longer to run (although not prohibitively so), but the non-linearity of the model does require care in interpreting the results. The majority of the extra parameters are inhibition or half-saturation constants required for the Michaelis-Menton equations; the values for these are shown in Table 3.1. As described in Chapter 2, values for these parameters are difficult to measure experimentally, and no experimental values exist; the parameter values were chosen to be the same as the equivalent parameters for oxic mineralisation and denitrification. Finally, from a purely biogeochemical point of view, two key simplifications in this modification of the model are that iron oxides have been assumed to be a solute, and that there is no coupling of reduced iron and sulphide, to allow the formation of iron sulphide and pyrite. The bottom-water concentration of iron oxides was set to 300 mmol m^{-3}, to be a similar order of magnitude to oxygen.

A further improvement to the realism of the model was made by changing the iron oxide state variable from solute phase to solid phase. As described in Chapter 2, solid and solute constituents are defined in different ways in the model, with solid phase constituents being affected by bioturbation and a flux of the species to the top layer, whilst solute phase constituents are affected by the bottom water concentration and diffusion. Changing iron oxide from a solute to a solid in the model is a simple case of changing the declaration of the state of iron, and setting the values of the flux of iron oxide 0.01 g Fe_2O_3 m^{-2} yr^{-1}; the value of the bioturbation coefficient was the same as for organic matter. The profiles for O_2, NO_3^-, NH_3, SO_4^{2-} and S^{2-} are similar to those seen when iron oxide is modelled as a solute (Figure 3.4); however, the profiles for FeO and Fe^{2+} are different (cf. Figure 3.3). These profiles are not obviously explained, and they are likely to be artefacts of the complexity of the model and indicate that it may be difficult to model multiple solid phase species simultaneously. The concentration of reduced iron should increase, as it does when the POC flux is 2 and 15 g C m^{-2} yr^{-1}, with a decrease in the concentration in the oxic zone as a result of oxidation of Fe^{2+} to Fe^{3+}. However, this oxidation is not reflected in the iron oxide profiles. The constant values of solid iron with depth for all POC fluxes and of Fe^{2+} with a POC flux of 50 g C m^{-2} yr^{-1} cannot be explained with the current model. Additionally, when attempting to model the iron oxide component as a solid, mass is not conserved.

For the iron and sulphur cycles, the sum of the net flux and total consumption values should be zero to signify that mass is conserved and steady-state has been reached. As this is not the case it shows that the model is not able to accurately model these two solid phase species.

Table 3.3: Mass balance when solid iron is modelled – net flux (mmol m^{-2} yr^{-1}) and total amount (mmol yr^{-1}) of species consumed during mineralisation and secondary reactions, integrated through depth. (POC flux = 15 g C m^{-2} yr^{-1}). A negative value indicates a flux out of the sediment into the overlying water

	Oxygen	Total nitrogen	Total iron	Total sulphur
Net flux	419.4	14.7	-0.3	1.3×10^{-12}
Total consumed	419.4	14.7	1.3	-6.5

3.3 Inclusion of iron sulphide

In order to further improve the model, coupling of reduced iron and sulphide to form iron sulphide was implemented. For total completeness, as a result of some locations in the North Sea having significant proportions of organic matter degraded by manganese oxide (e.g. Schoemann *et al.* 1998), the manganese oxide pathway was also included. Equations 3.7 and 3.8 define these processes (note that the equations for iron oxide mineralisation, sulphate mineralisation and anoxic mineralisation, as defined in Equations 3.4-3.6, also have to be updated with the addition of the manganese oxide pathway; the resulting relationship is shown in Equation 3.9). Table 3.4 gives the values of the additional parameters.

$$\text{Manganese oxide mineralisation} = \frac{MnO_2}{MnO_2 + Ks_{MnO_2}} * \left(1 - \frac{O_2}{O_2 + Kin_{O_2}^{Mnox}}\right) * \left(1 - \frac{NO_3^-}{NO_3 + Kin_{NO_3}^{Mnox}}\right) * ((\kappa_f * TOC_f) + (\kappa_s * TOC_s)) * \frac{1}{\Sigma lim} \quad \text{Eqtn 3.7}$$

$$FeSprod = rFeSprod * Fe^{2+} * S^{2-} \quad \text{Eqtn 3.8}$$

$$\Sigma lim = \text{(oxic mineralisation) + (denitrification) + (manganese oxide mineralisation) + (iron oxide mineralisation) + (sulphate mineralisation) + (anoxic mineralisation)} \quad \text{Eqtn 3.9}$$

While the manganese oxide pathway equation (Equation 3.7) follows the standard Michaelis-Menten form, the iron sulphide production equation (Equation 3.8), as an initial step forward, uses a more simple linear form, based only on the rate of production of iron pyrite (rFeSprod, units $mmol^{-1}$ m^3, and given a value of 1 for the purposes of these runs) and the concentrations of sulphide and reduced iron. A further simplification that has been made with this implementation is that the extra equation for the formation of pyrite is not included. As described by Berner (1970,

1984), iron sulphide (FeS) reacts with reduced sulphide to form pyrite (FeS_2), with the rate of reaction being determined by the concentration of sulphate. As the work in this chapter was primarily attempting to show if the major diagenetic reactions could be included in OMEXDIA, it was decided that the additional complexity that the extra step for the formation of pyrite would require was not merited. Additionally, it is assumed that the idealised stoichiometry for all the diagenetic pathways is to be followed, as shown in Soetaert *et al*. (1996b), rather than the stoichiometry shown in Froelich *et al*. (1979), as a compromise between simplicity and realism. Future modifications of the model could attempt to include the more realistic stoichiometry, to see if this has an effect on the model output.

Table 3.4: The extra parameters needed to include manganese cycling and production of iron sulphide in OMEXDIA

Parameter name	Parameter description	Units	Default values
MnO_2	Flux of manganese oxide to the sediment	g MnO_2 m^{-2} yr^{-1}	0.01
Ks_{MnO_2}	Half-saturation concentration of manganese oxide in manganese oxide mineralisation	mmol MnO_2 m^{-3}	20
$Kin_{O_2}^{Mnox}$	Half-saturation concentration of oxygen in inhibiting manganese oxide mineralisation	mmol O_2 m^{-3}	1
$Kin_{NO_3}^{Mnox}$	Half-saturation concentration of nitrate in inhibiting iron manganese mineralisation	mmol NO_3^- m^{-3}	1
$Kin_{MnO_2}^{Feox}$	Half-saturation concentration of manganese oxide in inhibiting iron manganese mineralisation	mmol MnO_2 m^{-3}	1
$Kin_{MnO_2}^{Sulph}$	Half-saturation concentration of manganese oxide in inhibiting sulphate mineralisation	mmol MnO_2 m^{-3}	1
$Kin_{MnO_2}^{Anox}$	Half-saturation concentration of manganese oxide in inhibiting anoxic mineralisation	mmol MnO_2 m^{-3}	1
rFeSprod	Rate of formation of iron sulphide	$mmol^{-1}$ m^3	1
Fe^{2+}	Concentration of reduced iron	mmol Fe^{2+} m^{-3}	0
S^{2-}	Concentration of sulphide	mmol S^{2-} m^{-3}	0

In this run manganese oxide, iron oxide, and iron sulphide were all modelled as solid phase constituents (Cornwell and Morse 1987); manganese oxide was assumed to have a flux of 0.01 g MnO_2 m^{-2} yr^{-1}, matching the flux of iron. Fluxes of manganese oxide have been measured in shelf-sea waters, with large ranges reported; North Sea and Skaggerak fluxes were between 0 and 9 g m^{-2} yr^{-1}, although values greater than 2 g m^{-2} yr^{-1} tend to be uncommon (Slomp *et al.* 1997; Canfield *et al.* 1993b). The initial flux of FeS was 1 x 10^{-4} g m^{-2} yr^{-1}, to replicate the situation where oxic waters typically have virtually zero iron sulphide (as a result of having no reduced iron or sulphide in the water column). The mass balance of each of the species for model runs of 2 and 15 g C m^{-2} yr^{-1} are shown in Tables 3.5 and 3.6 respectively.

Table 3.5: Net flux (mmol m^{-2} yr^{-1}) and depth integrated total amount of species consumed (mmol yr^{-1}) during mineralisation and secondary reactions when organic carbon input was 2 g C m^{-2} yr^{-1} when the full iron and sulphate pathways were included (see text for details)

	Oxygen	Nitrogen	Manganese	Iron	Sulphate
Net flux	64.7	-1.3	-4.7×10^{-3}	-2.3×10^{-8}	-6.1×10^{-12}
Total consumed	64.7	-1.3	-4.7×10^{-3}	-2.3×10^{-8}	-4.7×10^{-15}

Table 3.6: Net flux (mmol m^{-2} yr^{-1}) and depth integrated total amount of species consumed (mmol yr^{-1}) during mineralisation and secondary reactions when organic carbon input was 15 g C m^{-2} yr^{-1} when the full iron and sulphate pathways were included (see text for details)

	Oxygen	Nitrogen	Manganese	Iron	Sulphate
Net flux	419.2	14.7	-3.3×10^{-2}	-3.3×10^{-8}	-2.9×10^{-10}
Total consumed	419.2	14.7	-3.3×10^{-2}	3.3×10^{-8}	2.9×10^{-10}

In Table 3.5, the three orders of magnitude difference between the net flux and consumption of sulphate leads to an apparent discrepancy when the mass balance is calculated.

Although the discussion above implies that, under certain conditions, the full set of diagenetic equations can be included within OMEXDIA, more testing is likely to be needed before a firm conclusion can be made about whether the model is entirely stable with the increased complexity. By examining the how the model reacts to an increased number of fluxes, as is done in the next section, a clearer understanding of how the complexity affects the model should help determine if the modified model can be used to accurately model specific North Sea environments in later Chapters.

3.4 Contribution of each biogeochemical pathway to OM degradation

In the model runs described so far, three different POC fluxes have been used to give an indication of how the model reacts when simulating different depositional environments. However, it is easy to increase the number of runs to attempt to gain a better understanding of the modelled diagenetic processes. For example, the contribution each electron transfer pathway makes to the overall oxidation of the organic matter is one way of judging how well the model is able to reflect the processes that occur in the natural system, when the information is available. Intuitively, when there is a very low POC flux in an oxic environment, we would expect all of the organic matter to be oxidised by oxygen. As the POC flux increases, the proportion of the total flux oxidised by oxygen will decrease, and nitrate, manganese oxide, iron oxides, and sulphate will increase in importance (depending, of course, on the total organic matter available). Methanogenesis will also need to be considered if organic matter remains after these five electron acceptors are consumed (Grunwald *et al.* 2009). By running OMEXDIA 491 times, with the only parameter change being the POC flux from 0.1 to 50 g C m^{-2} yr^{-1} (in intervals of 0.1 g C m^{-2} yr^{-1}) model output can be compared with environmental data. Figure 3.5 shows the contribution of each process when the modified model is run as described above with the manganese oxide, iron oxide, and sulphate pathways, and the formation of iron sulphide included.

From Figure 3.5 it can be seen that oxygen is the sole electron acceptor (defined here as being responsible for >99.75% of OM oxidation in the model output) when the POC flux is below 8.2 g m^{-2} yr^{-1}; it is not until the POC flux is increased to 13.3 g m^{-2} yr^{-1} that the oxygen pathway is responsible for less than 95% of the total integrated mineralisation throughout the whole sediment column. Even when the POC flux is 50 g m^{-2} yr^{-1}, O_2 is still responsible for 52.3% of the mineralisation. This result agrees with earlier calculations; for example, Bender & Heggie (1984) found that oxygen was always responsible for more than 90% of the OM mineralisation in deep ocean pelagic sediments, where POC fluxes are low. Given that the carbon flux used in their calculations was always less than 2 g C m^{-2} yr^{-1}, and that their calculations were relatively simple non-coupled concentration-depth differential calculations for each chemical species, the OMEXDIA results presented here are consistent with their interpretation. The results from the model also show similar results when comparing with environments with higher POC fluxes; in the high carbon depositional area of the Skaggerak, oxygen has been estimated to contribute less than 17.4% to the overall OM oxidation (Canfield *et al.* 1993a), while Osinga et al (1996) found the oxic mineralisation to be responsible for 19-25% of total organic matter degradation and

Cook *et al.* (2007) showing that the oxygen contribution was occasionally below 10%. It is, therefore, important to be aware that the nature of the environment can have a large influence on biogeochemical processes.

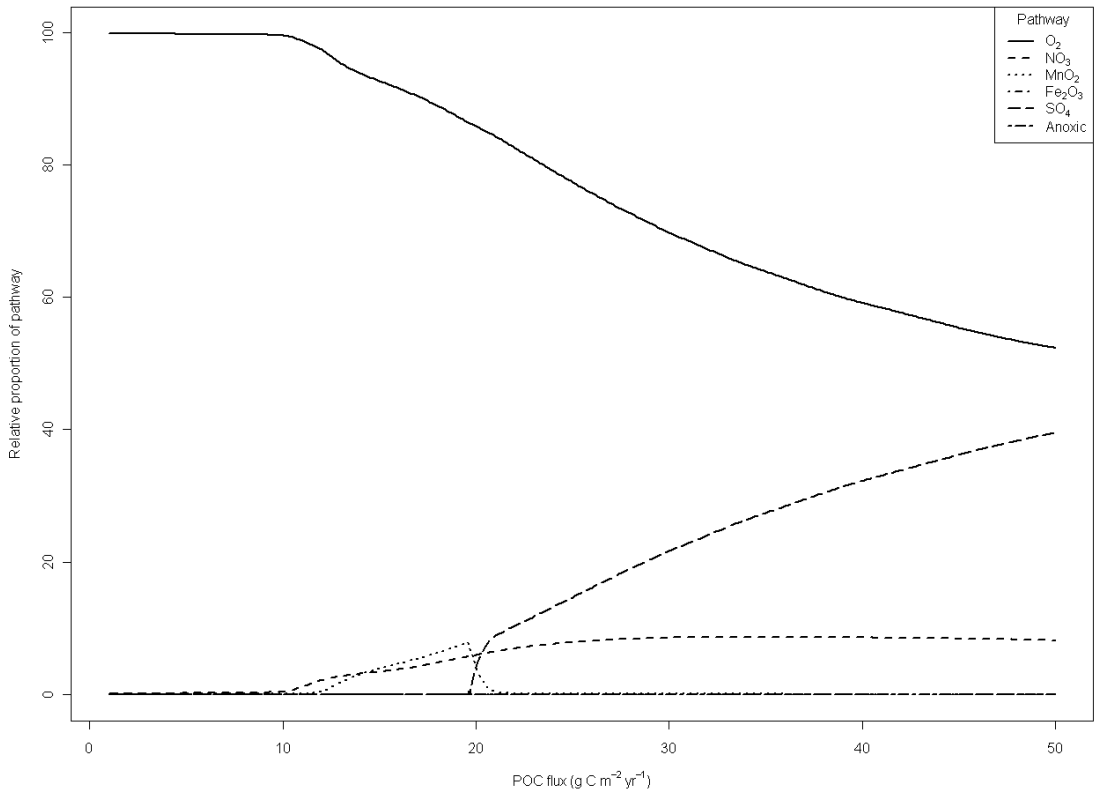

Figure 3.5: Relative contributions of each of the pathways to the overall oxidation of organic matter integrated throughout whole sediment column

In the present implementation of the OMEXDIA model, manganese mineralisation has been placed between the nitrate and iron oxide pathways in the order of electron acceptors. Froelich *et al.* (1979) suggested that the order of the nitrate and manganese pathways could vary depending on the manganese oxide mineral present, and the exact denitrification reaction (that is, whether the nitrogen is released solely as N_2, which is the more energetically favourable reaction, or whether it is released as a mix of N_2 and NH_3). However, more recent work normally implies that manganese oxide is reduced after nitrate (Bender and Heggie 1984; Schulz *et al.* 1994; Hyacinthe *et al.* 2001). Therefore, as would be expected, nitrate becomes the first electron acceptor to take over when oxygen is depleted, and NO_3^- is responsible for 5.9% of OM mineralisation when the POC flux is 20 g m^{-2} yr^{-1}. It then rises steadily to finally oxidise 8.1% of OM when the POC flux is 50 g m^{-2} yr^{-1}, comparing favourably with measured contributions of denitrification to OM oxidation (Canfield *et al.* 1993a), although with no carbon flux measurements reported, it is difficult to compare directly

our model output with the observations reported. Manganese oxide starts to oxidise OM when the POC flux is 11.8 g, and rises rapidly to oxidise 7.9% of the OM when the POC flux is 19.6 g m^{-2} yr^{-1}, before decreasing in importance and not being responsible for any OM oxidation when the POC flux is above 21.3 g m^{-2} yr^{-1}. This is likely a consequence of the importance of the SO_4^{2-} pathway. Previous estimates of the contribution of manganese oxidation have generally given values of between 0.08% and 14% (Canfield *et al.* 1993b; Bender and Heggie 1984), although they can be much higher, up to 99%, when there are localised concentrations of manganese, such as at the S9 site in the Skaggerak (Canfield *et al.* 1993b; Canfield *et al.* 1993a; Arnosti and Holmer 2003). The S9 station is fairly unique in that it is both relatively deep for a North Sea continental margin site (700m) and is a depositional area which receives comparatively large amounts of terrigenous material (Slomp *et al.* 1997). Other studies have given values for the rate of manganese oxidation, but have not given the total rate of OM oxidation, so making it difficult to compare values. For example, Slomp *et al.* (1997) reported manganese oxide reduction rates of between 0.0039 and 0.37 mmol m^{-2} d^{-1} in the Skagerrak, whilst Arnosti & Holmer (2003) report 6.4 mmol C m^{-2} d^{-1} for Mn reduction at one of these sites (S9) in the Skaggerak. These rates of reduction are orders of magnitude different to those reported in Canfield *et al.* (1993a), which reported a reduction rate of 0.027 mmol m^{-2} yr^{-1} at the Skaggerak S9 site, and was calculated to be responsible for 91% of OM oxidation. This shows how difficult it can be to compare results both spatially and temporally, particularly as both POC fluxes and manganese oxide fluxes vary widely.

With the low carbon fluxes imposed in these model runs, iron oxides have little influence in the oxidation of OM, with the maximum contribution being 0.99% when the POC flux is 19.7 g m^{-2} yr^{-1} (Figure 3.5). Sulphate, as the final electron acceptor in the diagenetic sequence considered here, does not start to contribute towards OM oxidation until the POC flux reaches 19.8 g m^{-2} yr^{-1}. It then rises steadily until it is responsible for 39.5% of OM oxidation when the POC flux is 50 g m^{-2} yr^{-1}. This is similar to previously reported contribution values at depositional sites where iron and/or manganese oxides do not dominate anoxic mineralisation (Canfield *et al.* 1993a).

It is important to note that in the majority of the experimental work cited above that is used for comparison with model output, carbon flux data is not available. However, where it has been stated that model output and observed values are comparable, model values fall in the observed range, which leads us to conclude that the model is capable of calculating sensible values. As the POC fluxes in the model are representative of carbon fluxes in the North Sea, the model should be seen as having the ability to be used as a predictive tool. However, the current caveat is that there is

still a discrepancy with mass balance in the model which contains the fully decoupled set of mineralisation and reoxidation equations. Further experiments, as discussed below, showed that there are additional reasons to question the reliability of this model.

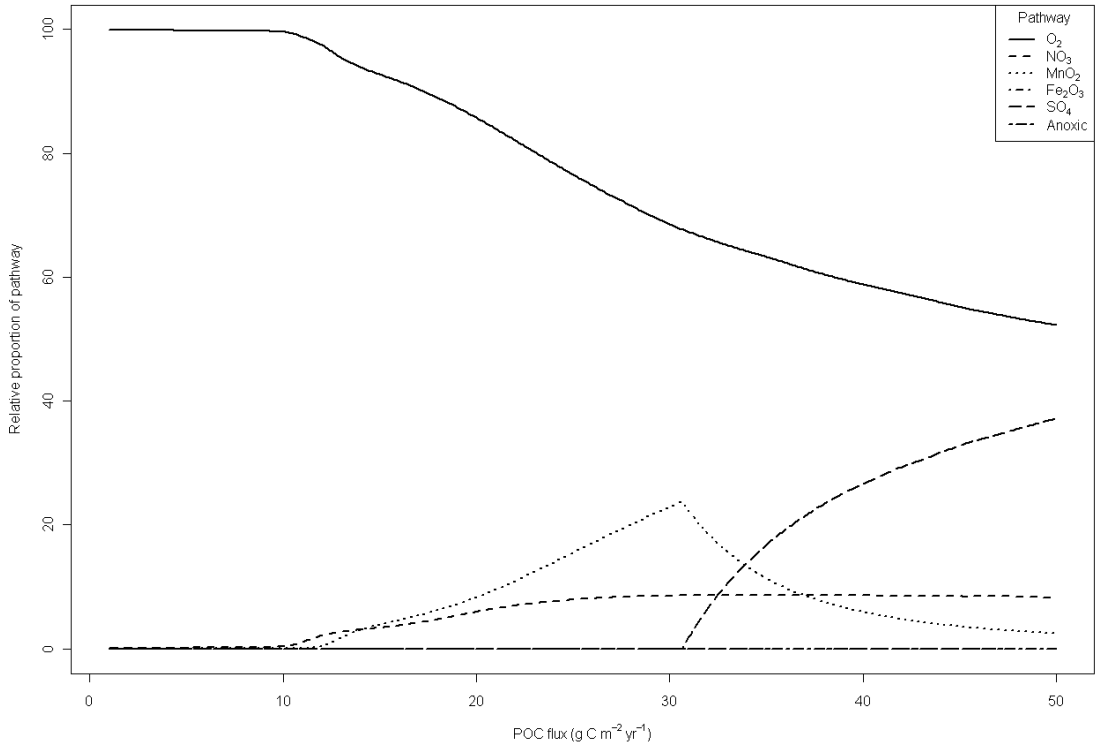

Figure 3.6: Relative contributions of each of the pathways to the overall oxidation of organic matter, when the MnO_2 flux to the sediment is increased to 1 g m^{-2} yr^{-1}

The general pattern follows what we would expect based on Figures 3.5 and 3.6. As the POC flux increases, the contribution of oxygen in organic matter degradation decreases (to have a similar contribution as the previous experiments of 53.0% at the maximum POC flux); the nitrate pathway again becomes noticeable when the POC flux reaches 8.9 g m^{-2} yr^{-1}, and, as in Figure 3.6, contributes 8.3% when the POC flux is 50 g m^{-2} yr^{-1}. However, the behaviour of the iron oxide pathway is difficult to explain. Although this pathway starts when the POC flux is 19.7 g m^{-2} yr^{-1}, which is, as expected, between the start points of the manganese oxide and sulphate pathways, the noisiness of the contribution profile between POC fluxes of 21.3 g m^{-2} yr^{-1} and 24.8 g m^{-2} yr^{-1} does not show similar behaviour to the manganese profile in Figure 3.6, as would be expected. Above a POC flux of 24.8 g m^{-2} yr^{-1}, the contribution of iron oxide to organic matter oxidation is zero, despite the high carbon flux. However, even with the unstable, oscillating, behaviour of iron oxide, the sulphate pathway appears to act as normal, as in Figures 3.5 and 3.6, with this pathway starting to have an effect when

the POC flux is 21.3 g m^{-2} yr^{-1}, while its effect continues to increase as the POC flux rises to contribute 38.6% of OM oxidation at a carbon flux of 50 g C m^{-2} yr^{-1}.

Figure 3.6 shows the contribution of different oxidants to organic matter degradation when the flux of manganese oxide was increased to 1 g m^{-2} yr^{-1}, to attempt to recreate environments with high manganese oxide concentrations. All other fluxes were kept the same. We can see that, as would intuitively be expected, the manganese oxide pathway contribution has increased, with the maximum value now 23.7% when the POC flux is 30.6 g m^{-2} yr^{-1}. Once again, the maximum organic matter oxidation associated with the manganese pathway appears just before the much larger influence of sulphate on organic matter degradation begins, and as the MnO_2 concentrations decrease. It also results in this pathway continuing to contribute to organic matter degradation as the POC flux also increases, rather than quickly falling to zero; when the POC flux is 50 g m^{-2} yr^{-1}, the manganese pathway is responsible for 2.4% of total OM oxidation (Figure 3.6).

The increase in the flux of manganese oxide from 0.01 to 1 g MnO_2 m^{-2} yr^{-1} also has an effect on the pathways that occur deeper in the sediment. As expected, the nitrate pathway starts to have an effect at the same POC flux (8.9 g m^{-2} yr^{-1}) as when the MnO_2 flux is 0.01 g m^{-2} yr^{-1}, and, additionally, has the same contribution when the carbon flux is 50 g m^{-2} yr^{-1}. The sulphate reduction pathway, however, starts much later, when the POC flux is 30.7 g m^{-2} yr^{-1}, but increases rapidly to still contribute 37.2% of OM oxidation at the maximum POC flux. Iron oxides do not contribute at all to OM oxidation, due to their low concentrations and the increased relative importance of the manganese pathway compared to the results shown in Figure 3.5.

The model run was again modified so that the manganese oxide flux was reduced to the original value of 0.01 g m^{-2} yr^{-1} but the iron oxide flux increased to 1 g m^{-2} yr^{-1}, with no other changes made. The resulting contributions graph is shown in Figure 3.7.

From the results described above, it is difficult to justify the use of the steady-state model where parts of, or the entire, ODU component is described individually. Although initial experiments imply that the model is able to recreate profiles and patterns of pathway-contributions that would be expected (e.g. Figures 3.3 and 3.5), further detailed testing revealed that the output (either by the results of mass balance calculations, or the output provided by relative contribution graphs) does not produce results which seem geochemically logical, and are frequently random in nature. For example, setting the manganese oxide flux back to 0.01 g m^{-2} yr^{-1}, but also decreasing the bottom water oxygen concentration from 300 mmol m^{-2} to 10 mmol m^{-3}, to

recreate hypoxic conditions that occasionally occur in the North Sea (Conley *et al.* 2009) generates the contributions shown in Figure 3.8. The relative contributions shown in this plot do follow the expected patterns. Due to the low relative concentrations of oxygen compared to sulphate, sulphate becomes the dominant pathway when the POC flux is greater than 2.8 g m^{-2} yr^{-1}. This behaviour seems to mimic that found at some sites in the North Sea. Jensen *et al.* (2003) for example, found through experiments that sulphate was responsible for 95% of OM oxidation in the Kattegat. This oxidation pathway can be very localised; Bakker and Helder (1993) found that the sulphate pathway contributed a maximum of 19.1% to the overall oxidation of OM at six stations in the Skaggerak.

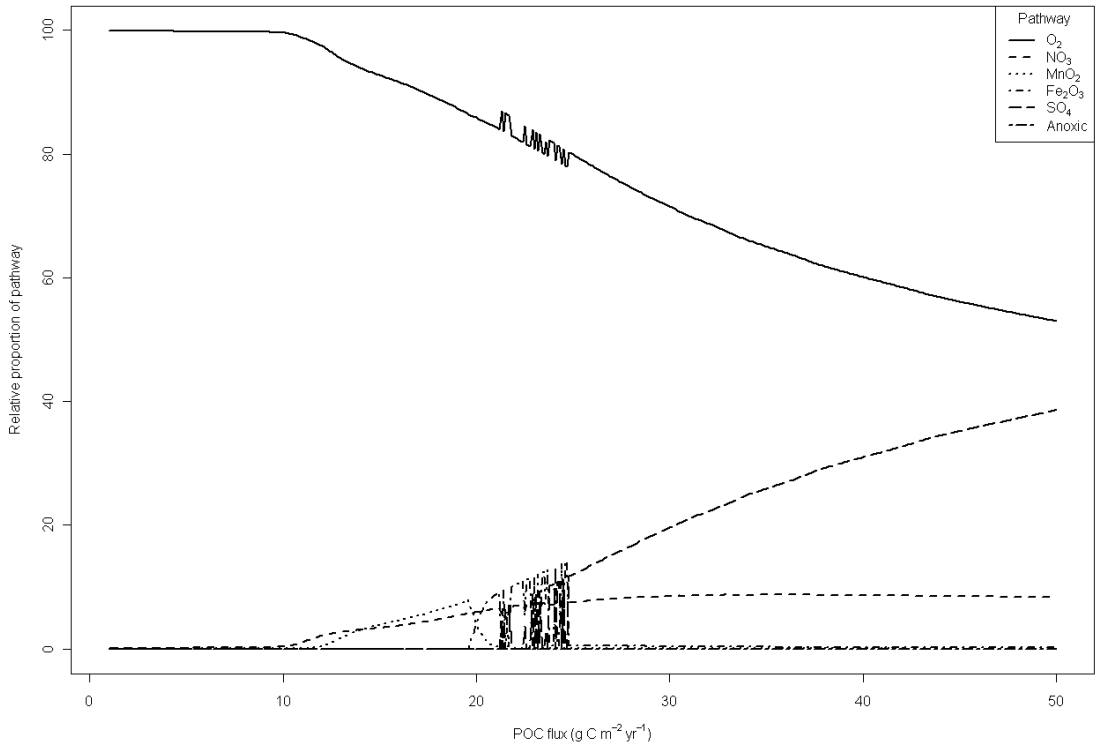

Figure 3.7: Relative contributions of each of the pathways to the overall oxidation of organic matter, when the MnO_2 flux to the sediment is reduced to 0.01 g m^{-2} yr^{-1} and the iron oxide flux increased to 1 g m^{-2} yr^{-1}

Models which are complex and attempt to simulate biological or environmental situations, often do not have an analytical solution (Kazancı 2007). Furthermore, although a model may reach steady-state, any slight deviation from this steady-state may be self-perpetuating within a model and result in steady-state not being reached, a phenomenon referred to as *unstable steady-state* (Schwarzenbach *et al.* 1993; Soetaert and Herman 2009). The *rootSolve* library as described in Chapter 2 is able to apply numerical methods to solving relatively simple models. The *rootSolve* library has

the ability to use three different equation solving techniques: two separate iterative Newton-Raphson solvers depending on the structure of the Jacobian matrix df/dy, where the ODE is of the form $dt/dy = f(t,y)$, and a solver using the DLSODE method (Soetaert *et al.* 2009). The work reported in this chapter has only used *Stode*, the Newton-Raphson method which assumes that the Jacobian matrix is banded. The alternative approaches use an arbitrary sparse structure, which are difficult and time consuming to implement.

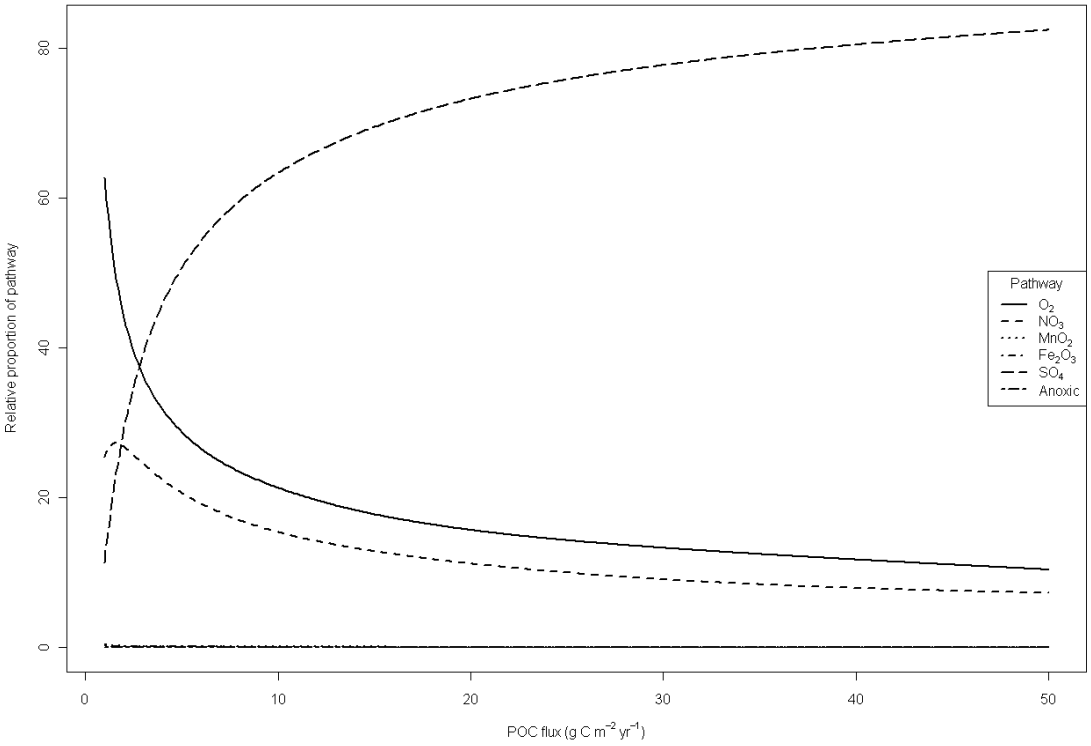

Figure 3.8: Relative contributions of each of the pathways to the overall oxidation of organic matter, when the MnO_2 and FeO fluxes to the sediment are reduced to 0.01 g m^{-2} yr^{-1}, and the bottom water O_2 concentration reduced to 10 mmol m^{-3}

Given these drawbacks to more complex approaches, it is important to consider the advantages of the original, simpler model, which only considers the oxygen and nitrate pathways, with all suboxic pathways being grouped together in the ODU component. The overall biogeochemistry of surface sediments in the North Sea lends itself to using this simpler version, as the vast majority of organic matter oxidation, when the whole of the North Sea is considered, is via the oxygen and nitrate pathways, with manganese oxides, iron oxides, and sulphate being the primary electron acceptor only in very small localised areas under relatively rare specific conditions (Dauwe and Middelburg 1998; Osinga *et al.* 1996). As shown in Table 3.1, the simpler version of the model reaches steady-state in the three runs considered (with POC fluxes of 2, 15

and 50 g m^{-2} yr^{-1}), and Figure 3.9 shows the relative contributions of the electron acceptor pathways in this model.

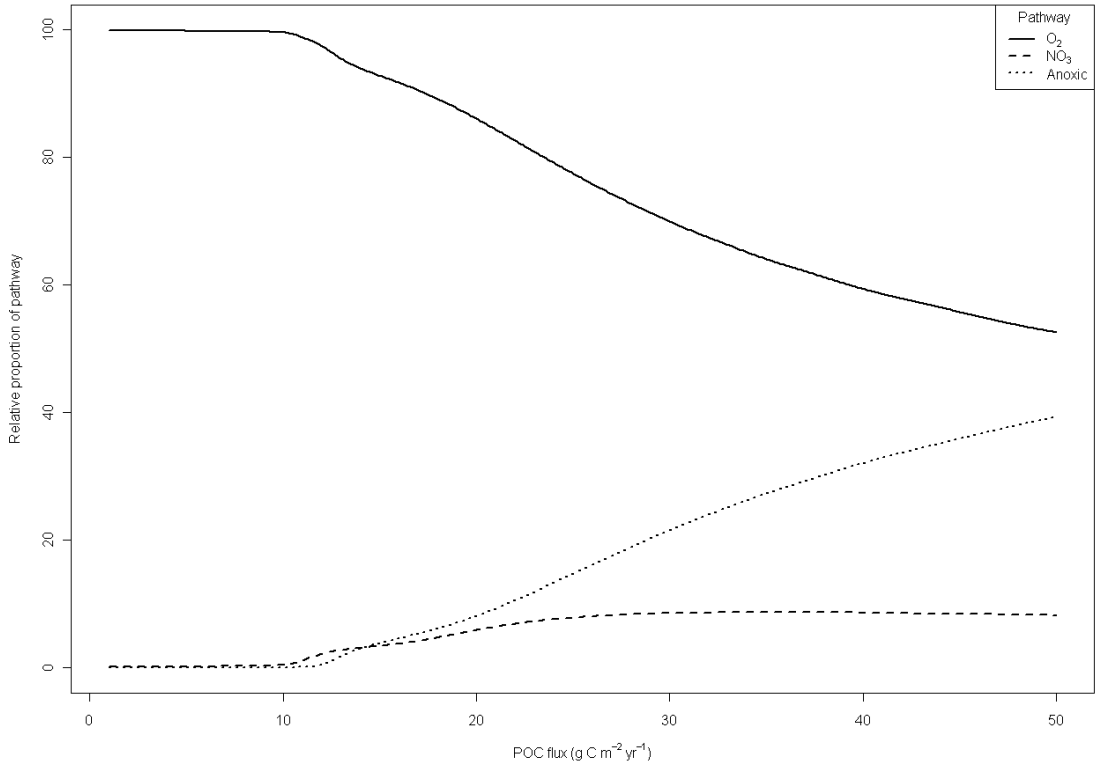

Figure 3.9: Relative contributions of each of the pathways to the overall oxidation of organic matter, when the manganese oxide, iron oxide, and sulphate pathways are combined into a single ODU component

The simpler model can therefore be used to make conclusions about aspects of the biogeochemistry of the North Sea that cannot otherwise be measured experimentally or are otherwise difficult to estimate. As demonstrated earlier in this chapter, results from the model can generate shelf-wide flux estimates, and in an analogous way to the profiles of organic matter oxidation against carbon inputs for the more complex model, similar output can be generated (Figure 3.10) for chemical species included in the simpler model.

The profiles shown in Figure 3.10 provide interesting insights into what happens to oxidative mechanisms as the POC flux changes. As the POC flux to sediments increases, the flux of oxygen across the SWI into the sediment increases approximately linearly, as anticipated from the relationship between oxygen consumption and OM mineralisation. Due to the stoichiometry of diagenetic reactions, the release of NH_3 into porewaters is also linear with respect to the degradation of organic matter, leading to an increase of nitrate flux out of the sediment with increasing carbon flux.

The lack of linearity in the nitrate flux profile in Figure 3.10 is as a result of the additional process of nitrification. At relatively low POC fluxes, not only is all organic matter degraded by O_2, but the oxygen is also able to oxidise the majority of ammonia. While these two processes are the only two significant biogeochemical processes which occur, they are linearly related. However, once the POC flux is large enough so that denitrification occurs, the non-linear Monod kinetics affects the nitrate flux. When the POC flux is low enough such that OM mineralisation occurs only via oxygen and nitrate pathways, no ODU component is produced, and thus the flux of ODU is zero. The flux of POC at which ODU starts to be released into the overlying water-column (22.9 g m^{-2} yr^{-1}) is considerably higher than that which the POC contribution rises above zero in Figure 3.9 (11.8 g m^{-2} yr^{-1}); reoxidation of the ODU component leads to a lag between the POC flux at which it is initially produced and the POC flux at which it is produced at high enough concentrations that oxygen is not able to reoxidise it totally, leading to its flux across the SWI.

Finally, the model can be used to determine additional processes occurring in North Sea sediments. Tables 3.4 and 3.5 show that at low POC fluxes, diagenetic reactions are likely to cause nitrogen to be a net contributor to the water-column, while at higher POC fluxes, the flux will be into the sediment, causing a loss of nitrogen from the water-column. Figure 3.10 shows that the nitrate flux is negative at all POC fluxes, indicating that the reoxidation of ammonia remains a more important process than denitrification, despite the presence of nitrate in bottom waters. However, the sign of the flux of ammonia changes from positive to negative when the POC flux is 4.6 g m^{-2} yr^{-1}. At relatively low POC fluxes, all NH_3 that is released as a result of the mineralisation of organic matter will be oxidised by O_2, leading to a net flux into the sediment. As the POC flux to the sediment increases, the amount of NH_3 produced increases (and hence the amount of NO_3^- via nitrification), thereby also leading to the net flux of both of these nitrogen compounds into the water-column from the sediment.

The discussion above concerning mineralisation rates focuses solely on the effect POC flux has on the mineralisation contribution pathways. However, in reality, it is likely that other factors, such as the *quality* of OM, will also have an effect. In general, quality refers to the degradability of OM, with OM that contains a high proportion of easily degradable carbon compounds being defined as high quality (Kristensen 2000). It is also possible to determine the source (*i.e.* terrestrial, riverine or produced from primary production) of OM from the relative proportions of the various carbon compounds (e.g. lignin, cellulose, proteins) present as well as the C:N ratio in the OM (Goni *et al.* 2003; Fabiano and Danovaro 1994; Baker and Spencer 2004; Thornton and McManus 1994). As a result, it is possible that the contribution of each of the

oxidation pathways may vary depending on the source of the OM, or the proportion of terrestrial, riverine and marine OM in the sediment. As it is possible to change the proportion of pFast and specify different nitrogen:carbon ratios in OMEXDIA, it is possible to mimic, albeit in a rather simplistic manner, OM quality. A further study could examine whether OMEXDIA, or a similar model, could be used to predict the contribution of different pathways based on OM quality.

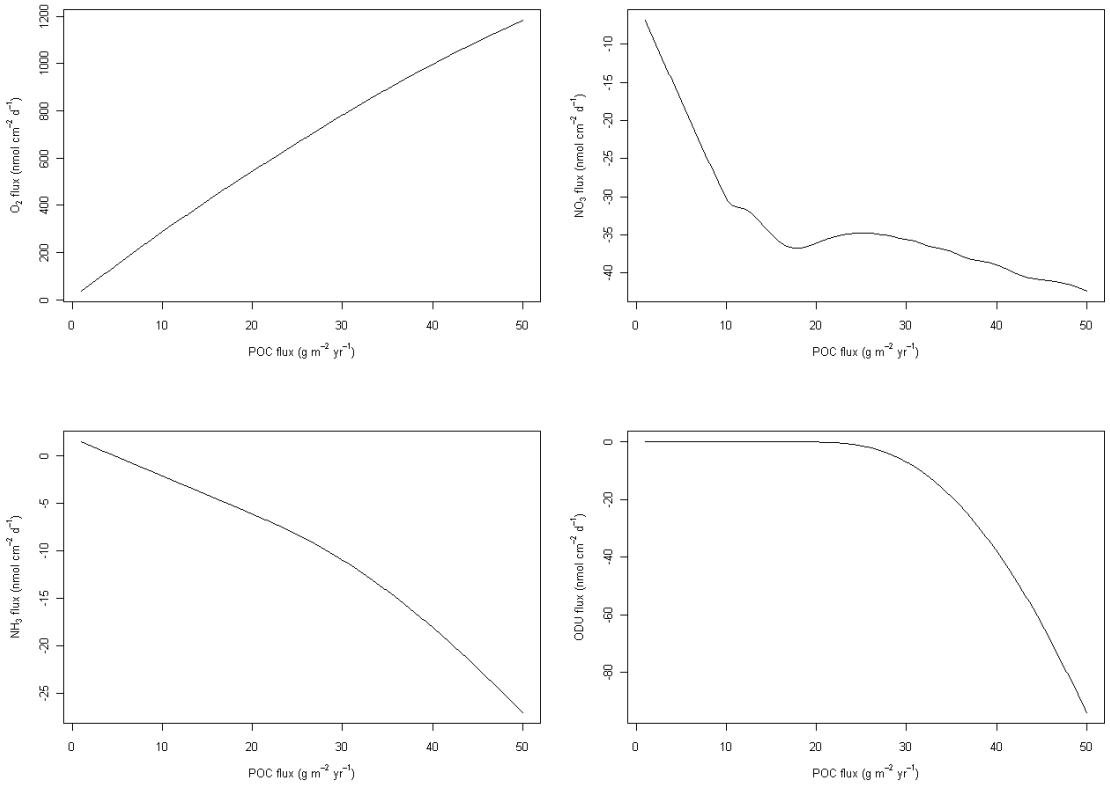

Figure 3.10: Changes in fluxes of the chemical species in the model with changing POC flux (negative fluxes indicate a flux out of the sediment into the overlying water column)

3.5 Summary

There are a variety of reasons why it has not been possible to expand the ODU component of the OMEXDIA model to include manganese oxide, iron oxide and sulphate oxidation routes. These include:

- the inability of the model both being unable to conserve mass for sulphur when pyrite is included in the model (Table 3.5)
- the noise seen in the contribution profile of Figure 3.7
- the large number of assumptions required for a full biogeochemical model including iron oxide and sulphate reduction pathways

- the highly non-linearity nature of the model leading to results which are difficult to interpret

The overarching conclusion of this chapter is therefore that the modifications made to the model are not suitable to be used in future work. As a result of the above points, it has been decided that where the steady-state model is to be used further in Chapters 5 and 6, the original model, as published by Soetaert *et al.* (1996b; 1996a), with the ODU component representing the manganese oxide, iron oxide and sulphate reduction pathways, as well as methanogenesis to fulfil the steady-state assumption, will instead be used.

As the work in this chapter shows, the OMEXDIA model has the ability, with careful modification, to behave in a way that is consistent with observations of early diagenetic processes. The profiles that it generates, and rates of processes that it calculates, are broadly similar to those presented in the literature. The model also has the potential to help quantify processes that are difficult to estimate or are not routinely measured as part of experimental work, such as the POC flux to the sediment (pers. comm. E.R. Parker); these processes are likely to be variable on both temporal and spatial scales within the North Sea, and relatively simple model runs should be able to provide estimates of these processes without the need to carry out fieldwork. It also appears that some of the assumptions made (such as the value of the bioturbation coefficient) are sufficient to allow the biogeochemistry to act in a realistic manner. Chapter 5 will show how further runs of the current implementation of the model can be used to calibrate some of the parameters known to be sensitive in the model, such as the ratio of the different pools of organic carbon, the kinetics of degradation and the bioturbation coefficient to gain further understanding about both the model and the biogeochemical processes occurring in the North Sea.

4 The Dynamic OMEXDIA Model

Further to the steady-state solutions for diagenesis that OMEXDIA can calculate, as discussed in Chapter 3, OMEXDIA is also able to find solutions to the underlying equations for non-steady-state conditions, the most obvious example being when the particulate organic carbon (POC) flux changes with respect to time. With the steady-state model, the calculated profiles are based upon a POC flux which does not vary with time. However, in coastal temperate seas, the POC flux is known to vary with time, with a sharp increase in early spring (the spring bloom) in response to increased productivity initiated by increased light and temperature that drives photosynthesis. There is a collapse in the flux of organic material in late spring due to depleted nutrient concentrations in the overlying water column (Tett *et al.* 1993; Gieskes and Kraay 1975). There is a further smaller bloom later in the year, typically during late summer or early autumn, once the nutrient concentrations have recovered, typically as a result of storm-induced mixing, and there are still favourable conditions for relatively large rates of primary productivity (Gieskes and Kraay 1975). This magnitude of this second bloom is typically limited by the length of the conditions remaining favourable.

There is therefore a clear seasonal signal in POC flux to the sediments (Leivuori and Vallius 1998; Davies and Payne 1984; Jørgensen 1996; Gieskes and Kraay 1975; Chauvand *et al.* 2000; Rauch and Denis 2008). This leads to the patterns seen in concentration isopleth plots, where, for example, nitrate concentrations are highest (and extend deeper into the sediment) in the winter, as a result of low bacterial utilisation of oxygen allowing all excess ammonia to be oxidised via the nitrification pathway (Jørgensen 1996). The cycling of the dissolved metals involved in diagenesis are also affected by the spring bloom (Ståhl *et al.* 2004), with both iron and manganese being removed from the water column during the spring bloom, thought to be primarily as a result of biogeochemical reaction pathways and adsorption onto suspended particulate matter (SPM) (Schoemann *et al.* 1998).

Unsurprisingly, the spring bloom, and the transfer of POC to the sediment, leads to the annual maximum values for the sedimentary sulphate reduction rate (SRR) and increasing porewater concentrations of Mn^{2+} (Thamdrup *et al.* 1994). Thamdrup *et al.* (1994) surmised that iron cycling was confined to the sediment (i.e. there was no net flux of iron across the sediment-water interface (SWI) on an annual timescale), whilst manganese cycling extended into the water-column, implying a flux of manganese compounds across the SWI. The spring bloom has also been speculated to have far

reaching effects, with some research suggesting that the spring bloom has the ability to sequester carbon from the atmosphere into the deep ocean (Smith *et al.* 1991).

In this chapter, I aim to show if the dynamic model is able to represent accurately the changes in porewater concentrations of oxygen, nitrate and ammonia, and rates of the biogeochemical processes represented in the model that occur as a result of the Spring Bloom and which are seen during observational work in the North Sea. Judgements can then be made about the overall usefulness of this version of the model. Although the dynamic model may be able to show a more accurate picture of the sedimentary environment over short time scales, the results gained for an assessment of the overall annual flux of the chemical species should be no different to the steady-state model. Thus the steady-state model may potentially be more useful than the dynamic model.

4.1 The mathematics of the dynamic model

Much of the theory of the dynamic simulation has been covered in Chapter 2. However, it is worth reiterating that the dynamic model uses the *deSolve* package, which solves partial differential equations (PDEs) that have been converted to ordinary differential equations (ODEs) by finite differencing. For example, Equation 4.1 shows the PDE that would describe diagenesis with a varying OM flux.

$$\frac{\delta \xi C}{\delta t} = -\frac{\delta}{\delta z}\left[\left(-\xi \text{ x } D_s \frac{\delta \text{C}}{\delta \text{z}}\right) + (w_\infty \text{ x } \xi_\infty \text{ x C})\right] + \sum \xi \text{ x } REAC \qquad \text{Eqtn 4.1}$$

where ξC is the concentration of the chemical species per volume of bulk sediment, *z* is the depth in the sediment, w_∞ is advection at depth, and REAC is the biogeochemical reaction being considered. If the chemical species is a solute then ξ is the porosity (ϕ) of the sediment, and D_s is the diffusion coefficient of the species. However, if the chemical species is a solid (i.e. OM), then ξ is ($1-\phi$) and D_s is the bioturbation coefficient, as described in Section 2.2. Equation 4.1 is a PDE as it involves changes in concentration with respect to both time (*t*) and depth. To enable this to be more easily solved, the equation needs to be converted to an ODE by numerical differencing. The *ode.1D* method in the *deSolve* package has the ability to carry out the finite differencing using one of 11 possible methods, the default being *lsoda* (Soetaert *et al.* 2010). This method was developed to efficiently solve both stiff and nonstill ODEs (Petzold 1983). Petzold (1983) notes 'The user of an ODE solver may not know whether his problem is stiff, or the solver may be called by another code (a package for solving partial differential equations or boundary value problems, for

example) where the character of the problem is not known in advance', and, as I discussed in Section 2.5.2, this is very often the case in biogeochemical modelling, and has also been applied in other natural sciences (e.g. Mendes 1993).

An example of a biogeochemical reaction, the mineralisation of OM using O_2, is described in Equation 4.2.

$$\frac{dO_2}{dt} = \varkappa - \sum_{i=1}^{2}\left\{R_{min} \text{x} \frac{O_2}{O_2 + ks_{O_2}} \text{x} \frac{\text{TOC}_\text{i}}{\sum \text{lim}} \text{x} \left[\gamma_{TOC_i}^{O_2} + \gamma_{\text{TOC}_\text{i}}^{N} + \gamma_{\text{NH}_3}^{O_2}\right]\right\} \text{x} \frac{1-\phi}{\phi} - R_{ODU_{ox}} \text{x}\, ODU \text{ x } \frac{O_2}{O_2 + ks_{ODU_{ox}}} - R_{nit} \text{ x } NH_3 \text{ x } \frac{O_2}{O_2 + ks_{nit}} \text{ x } \gamma_{NH_3}^{O_2} \quad \text{Eqtn 4.2}$$

where $\varkappa$ denotes all other biogeochemical and transport reactions (e.g. denitrification), *i* represents either the fast or slow degrading organic matter, R_{min} is the rate of oxic mineralisation, $k_s^{O_2}$ is the half-saturation concentration for O_2 limitation in oxic mineralisation, $\sum \text{lim}$ represents the limitation functions described in Section 2.1, $\gamma_{TOC_i}^{O_2}$ is the relative proportion of oxygen used in oxic mineralisation (moles of O_2 per mole of C), $\gamma_{\text{TOC}_\text{i}}^{N}$ is the N:C ratio of TOC_i, $\gamma_{\text{NH}_3}^{O_2}$ is the number of moles of O_2 per mole of NH_3 used in nitrification, ϕ is sediment porosity, $R_{ODU_{ox}}$ is the rate of oxidation of ODU, $ks_{ODU_{ox}}$ is the half-saturation concentration for O_2 limitation in ODU oxidation, R_{nit} is the rate of nitrification, ks_{nit} is the half-saturation concentration for O2 in nitrification and $\gamma_{NH_3}^{O_2}$ is the number of moles of O2 needed to oxidise one mole of NH_3 in nitrification.

4.2 Constant POC flux

To indicate that the model behaves as expected before further runs were carried out, a simple simulation consisting of a steady-state followed by, a 1 year spin-up and a 1 year model run was conducted, with no POC variation, and a constant POC input of 15 g C m^{-2} yr^{-1}. Figure 4.1 shows the concentrations of TOC, oxygen, nitrate, and ammonia for the 1 year model run, showing, that as expected, there is no variation throughout the year in the concentrations of any of these chemical species. Figure 4.2 shows the profile of the sedimentary profiles of the species at the end of the model run, showing that the dynamic run produces the same results as the steady-state model described in Chapter 3.

Due to the time lag between fluxes of chemical species and the biogeochemical processes in which they are involved, mass balance calculations are relatively

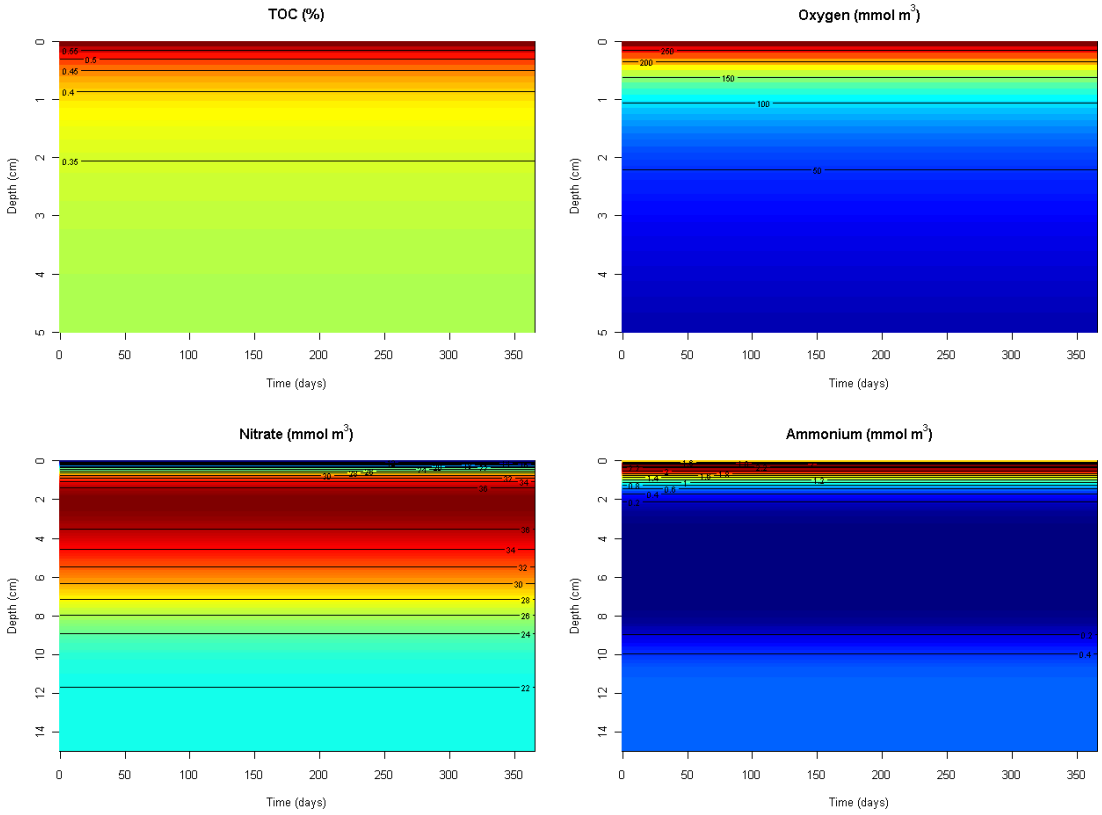

Figure 4.1: The concentrations of each of the chemical species over a 1 year model run with no POC variation; the imposed POC flux was 15 g C m^{-2} yr^{-1}

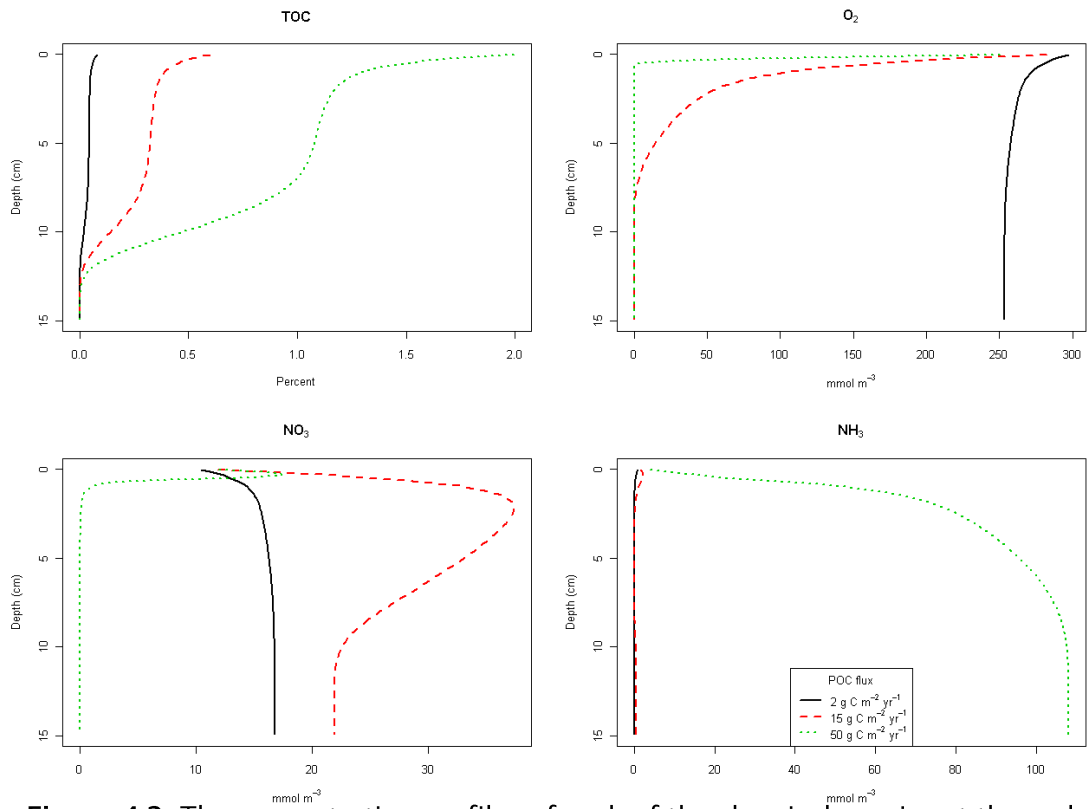

Figure 4.2: The concentration profiles of each of the chemical species at the end of a 1 year spin up + 1 year model run for 3 runs with different imposed POC flux

meaningless, and cannot be used to evaluate the stability of the model. However, the integrated concentrations of chemical species at day 1 and day 365 of the modelled year provide an equivalent metric. Table 4.1 shows the standard deviation between the output from day 1 and day 365, and the standard deviation between the output from day 365 of the 1 year model run and the steady state result, of the fluxes and concentrations, integrated over the whole sedimentary column, of the chemical species in the model.

Table 4.1: Standard deviations between output from day 1 and day 365, and from day 365 and the steady-state solution in parentheses, of integrated concentrations and fluxes of carbon, oxygen, nitrogen, ammonia and ODU over a 1 year model run, with a 1 y year model spinup, with imposed non-varying POC fluxes of 2, 15 and 50 g C m^{-2} yr^{-1}

		POC Flux (g C m^{-2} yr^{-1})		
		2	**15**	**50**
Concentrations (mmol m^{-3})	**TOC**	0 (0)	0 (0)	0 (0)
	Oxygen	4.5×10^{-13} (1.5×10^{-11})	7.2×10^{-12} (3.7×10^{-10})	0 (0)
	Nitrate	1.4×10^{-13} (1.3×10^{-11})	2.6×10^{-10} (2.1×10^{-8})	0 (0)
	Ammonia	0 (2.0×10^{-13})	9.3×10^{-12} (2.3×10^{-8})	2.5×10^{-13} (2.5×10^{-13})
	ODU	7.7×10^{-20} (1.4×10^{-13})	7.8×10^{-12} (4.8×10^{-8})	2.0×10^{-12} (2.0×10^{-12})
Fluxes (mmol m^{-2} yr^{-1})	**Oxygen**	0 (1.5×10^{-11})	9.6×10^{-13} (1.6×10^{-11})	0 (0)
	Nitrate	0 (1.2×10^{-11})	3.5×10^{-12} (1.4×10^{-11})	0 (0)
	Ammonia	0 (2.6×10^{-12})	1.3×10^{-15} (0)	0 (3.6×10^{-15})
	ODU	6.9×10^{-18} (1.9×10^{-12})	6.4×10^{-16} (2.3×10^{-15})	2.0×10^{-14} (0)

As can be seen from Table 4.1, the model does seem to have reached a steady-state after 1 year. The infinitesimally small values of the standard deviation between both day 365 and day 1 and day 365 and the steady-state solution indicates that the dynamic solution and the steady-state solution have reached essentially the same value; this is used as confirmation that the dynamic model gives the expected results before a time-varying POC flux was imposed.

4.3 Varying POC flux

The most obvious use of the dynamic model is to run simulations where the POC flux is allowed to vary over time. Initially, the POC flux used for testing the model was the same as that shown in Equation 2.12, which generates isopleths such as those shown in Figure 2.3. The mean flux used was 15 g C m^{-2} yr^{-1}. We can also use the results to generate plots of the change in flux across the SWI of each of the chemical species as a result of variation in POC flux, and how the variation affects the relative contribution of each of the electron acceptor pathways to the overall degradation of the organic matter.

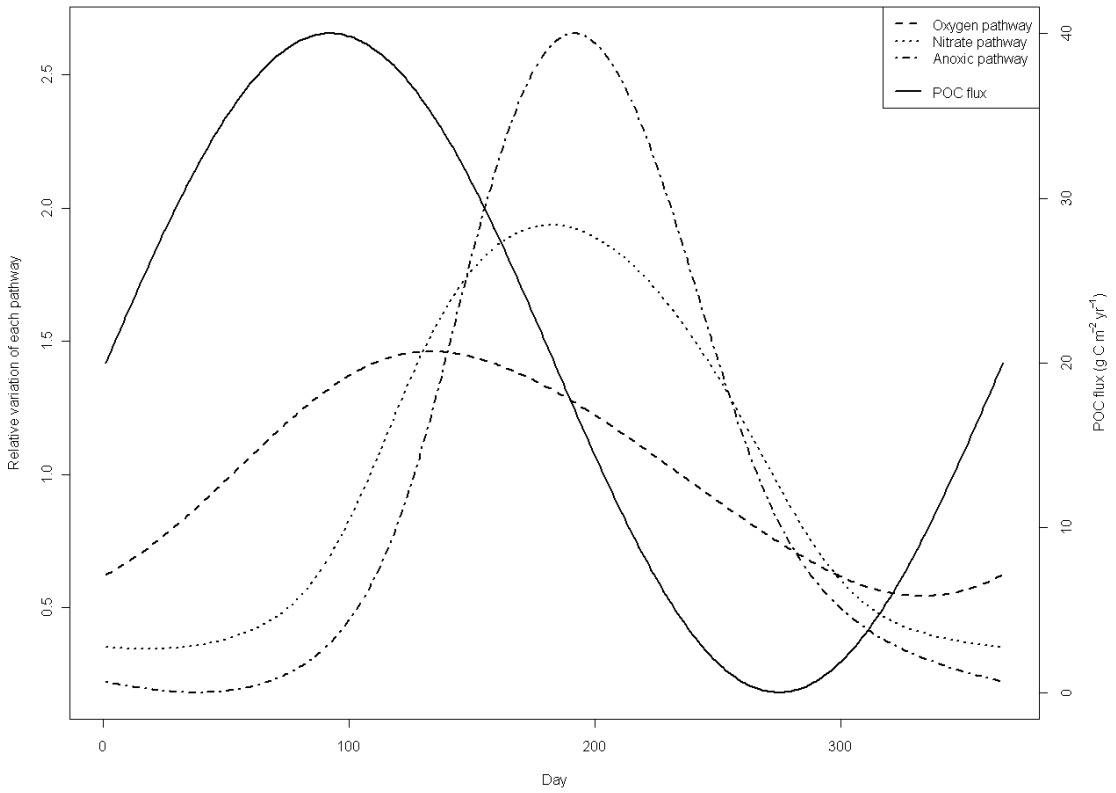

Figure 4.3: The relative contributions of each of the diagenetic pathways, as described in the text, over a one year cycle, using the POC flux described in Equation 2.12. The POC flux is also shown for reference

It was empirically found that a one year spin up was not sufficient for a subsequent one year model run to result in a steady cycle; however, a ten year spin-up was able to achieve this. Figure 4.3 shows the relative variation of each of the diagenetic pathways over a one year cycle, following a ten year model spin-up, compared to the mean contribution of that pathway over the year. As would be expected, the oxygen pathway dominates in the early part of the year; however, as the

oxygen concentrations decrease, in line with the increase in POC flux, as seen in Figure 2.3, the relative contribution of the oxic mineralisation pathway decreases, allowing first the denitrification and then the anoxic pathway to dominate. After the POC flux has declined in the second half of the year, and oxygen concentrations start to increase back to their initial values, then the relative contribution of the oxygen pathway also starts to increase. The lag between the maximum POC flux and the maximum rate of the three pathways can clearly be seen. If, as an initial assumption, we take the POC flux used in this run as the approximate cycle seen in the North Sea, then to a first-order estimate we can say that the oxic mineralisation peak occurs 41 days after the maximum POC flux, the denitrification peak occurs a further 49 days later, while the anoxic mineralisation peak occurs just ten days after the denitrification peak.

It should be noted here that although the POC flux does vary with time, there is no algorithm implemented that allows the ratio of fast-to-slow degrading OM within the POC flux to also vary in line with the POC flux. It is known that this ratio does change throughout an annual cycle, with a greater proportion of fast-degrading material during the spring and summer blooms (Hedges *et al.* 1988). This is likely to have an effect on the relative contribution of each of the oxidation pathways, and may also affect fluxes across the SWI. Future modelling work, which could be verified by careful observational studies, could determine the extent to which the overall nutrient budget of a shelf-sea, such as the North Sea, could be affected by the proportion of fast and slow degrading material in OM which reaches the sediment.

4.4 Flux calculations and comparisons with observed data

As the nature of experimental work dictates that it is difficult to obtain full annual profiles of fluxes and rates of processes, the profiles shown in this section should help indicate if previously estimated chemical fluxes for the North Sea Continental Shelf are been accurate. Figure 4.4 shows the changes in the flux of the chemical species during the one-year model run when the mean POC flux is 15 g C m^{-2} yr^{-1}. From this simple idealised POC flux, the fluxes show the trends that might be expected. As the POC flux increases, the flux of oxygen into the sediment increases to fulfil the demand of the oxic mineralisation pathway, although it is worth noting that there is a lag between the peak rate of oxic mineralisation, which is on day 133, and the peak O_2 flux (which is 610 mmol m^{-2} yr^{-1} at day 152). This could imply that, despite the mineralisation pathway reaching its peak, there is still a drawdown of oxygen to satisfy the demand of the reoxidation of the reduced species. As expected, the minimum O_2 flux (237 mmol m^{-2} yr^{-1} at day 338) almost coincides with the point in the year when the mineralisation rate is lowest (day 333). As with the steady-state

model, the remaining three chemical species have a negative flux at all times of the POC cycle (*cf*. Figure 3.12); unsurprisingly, the nitrate and ammonia fluxes show similar patterns, with the greatest fluxes only being four days apart. The lowest magnitude flux of nitrate occurs 25 days later than the flux of ammonia (day 340 and day 315 respectively), which is likely to imply that as the POC flux increases (after the minimum POC flux at day 274), the excess ammonia is released more quickly, as a result of the still low concentrations of oxygen. As oxygen concentrations increase, nitrification occurs leading to the increase in the flux of nitrate out of the sediment. There is a slight lag of two days between the lowest fluxes of oxygen (day 338) and nitrate (day 340).

By integrating the fluxes over the annual POC cycle, we can more easily compare the dynamic model's fluxes with data in the literature taken using observational and experimental methods. The modelled oxygen flux is 5.47 mmol m^{-2} d^{-1}; despite having the same annual average POC flux, this is higher than the annual flux calculated by the steady-state model, when the result is 4.19 mmol m^{-2} d^{-1}. The difference between the two results is caused by the non-linearity of the model. Both of these results compare favourably with previously published data, with fluxes in the Skagerrak being between 1.34 and 24.32 mmol m^{-2} d^{-1} (Bakker and Helder 1993). Both biological and physical activities have been shown to increase the flux of oxygen into sediments. Forster & Graf (1995) showed that different macrofauna species could increase the flux of oxygen via bioirrigation; the oxygen uptake rate by some sedimentary macrofauna has been shown to be up to 64% of the total O_2 flux across the SWI (Polerecky *et al.* 2006). Meanwhile, Booij *et al*. (1991; 1994) showed that increasing the velocity of the overlying water increased the oxygen flux, primarily as a result of irrigation; this is likely to affect fluxes in coastal areas as a result of tidal activity more than offshore locations, where currents are less predictable, and tend to be much slower than tidal- or wind-generated currents (ICES 2008). A further physical event, resuspension, has been shown to decrease the oxygen flux across the SWI (Tengberg *et al.* 2003), and will be discussed in greater detail in Chapter 6.

The general trend for coastal waters, where the water column is almost always totally mixed, is that the oxygen flux increases with increasing water depth, as a result of greater quantities of organic matter being deposited, and hence stimulating greater rates of diagenesis (Giles *et al.* 2007); however, some authors have suggested that there is a water depth below which the oxygen flux begins to increase again; this minimum apex of oxygen flux is in the O_2-minimum zone (Jahnke *et al.* 1990), although this is not seen in all deep sea data (e.g. Epping *et al.* 2002; Lohse *et al.* 1998). However, given that it seems to be almost universally greater than 1000 m, this does not need to be considered with this model of the North Sea. There also appears

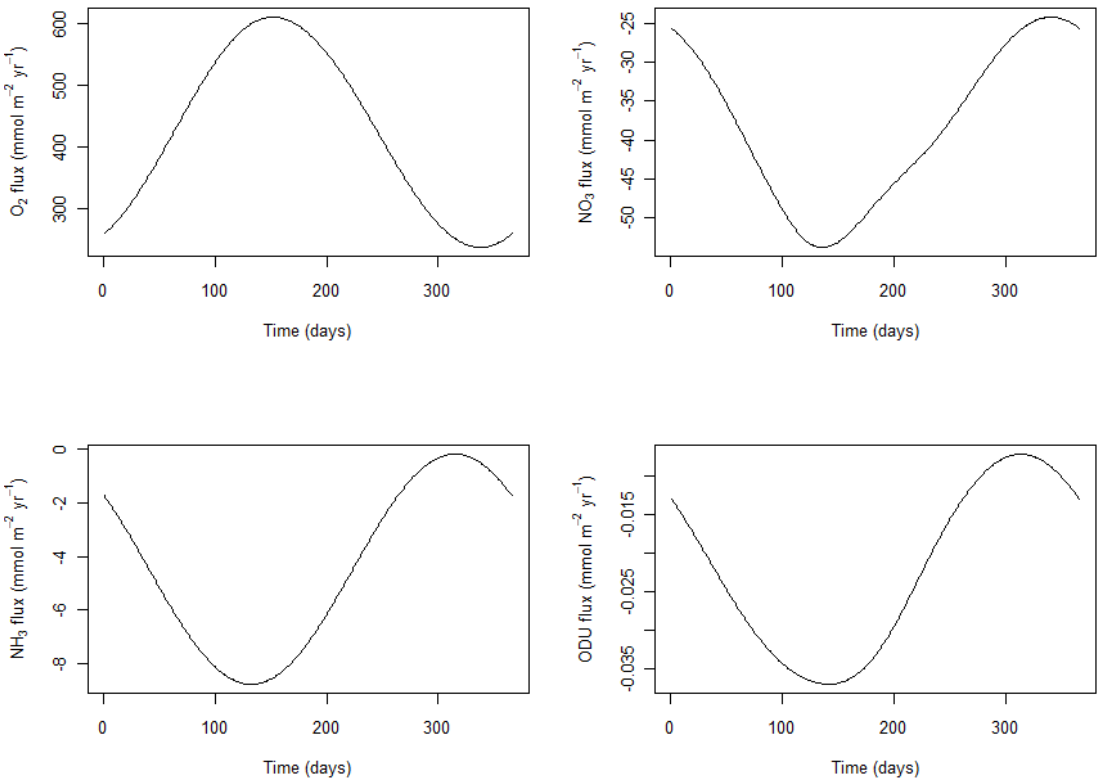

Figure 4.4: Changes in fluxes of the chemical species in the model during an annual cycle (negative fluxes indicate a flux out of the sediment into the overlying water column); the mean imposed POC flux is 15 g C m^{-2} yr^{-1}

to be a large temporal variability in flux data, with the flux generally becoming more negative throughout the spring-bloom (Lohse *et al.* 1996; Overnell *et al.* 1995). Lohse *et al.* (1996) reported values that are in general agreement with those already discussed, showing that the flux of oxygen, at the same site, can be more than 13 times higher in August than in the following February. The highest value is 28.4 mmol m^{-2} d^{-1}, measured in August 1991 in shallow water (25 m) off the Danish coast (although this is not in an area which the authors class as a main deposition area of the North Sea), while the lowest value, 0.8 mmol m^{-2} yr^{-1} was measured during February 1992 in 58 m of water (the deepest sample site in the study, except for one site in the Skagerrak). Linearly extrapolating this value would suggest an annual flux of 292 mmol m^{-2} yr^{-1}, which is lower than minimum value the model currently generates (310 mmol m^{-2} yr^{-1} at day 337) with the imposed mean carbon flux. In shallow waters, the sediment is within the photic zone and so benthic primary production will occur (Meyercordt *et al.* 1999). This can lead to a clear diurnal cycle (McGinnis *et al.* 2008), with a flux of oxygen out of the sediment during the day as a result of photosynthesis, showing a further effect that macrofauna has on nutrient

cycling across the SWI. There is, however, variation between locations, with this diurnal flux not being observed in Pensacola Bay (Murrell *et al.* 2009)

Taking the average depth of the main basin of the North Sea as approximately 100 m (North Sea Task Force 1993; Calow 1999), and taking the fluxes reported in Bakker & Helder (1993) from the stations which are at water depths of between 60 m and 140 m (the mean value of the depths given is 100.3 m), it might seem as though the model underestimates the probable annual flux by as much as 52% (for the steady-state model) and 37% (for the dynamic model). Although this is a relatively arbitrary method of calculating the result, it does go to show that there are perhaps better ways to simulate the POC flux, which I shall discuss later in this chapter. Simplifying the relationship between oxygen flux and the concentration of oxygen in the overlying water even further, Cai & Sayles (1996) derived an equation that linked them linearly; although the equation they presented was obtained by using data from six separate studies, all the field data was from deep sea sites (water depths varied from 60 to 5380 m (Cai and Sayles 1996; Sayles *et al.* 1995; Jahnke *et al.* 1990; Reimers *et al.* 1992; Jahnke *et al.* 1989; Hales *et al.* 1994; Archer and Devol 1992)); however, all but 9 of the 90 study sites where data was taken from were below the O_2-minimum zone defined by Jahnke *et al.* (1990), and thus this relationship would be unsuitable for the shelf-sea environment being discussed in this chapter.

4.5 Effect of POC flux variation

The sinusoidal POC flux profile used during the initial testing is not a particularly realistic representation of the carbon flux to sediments in shelf seas. Although accurate POC fluxes to the benthos are highly variable (Nedwell *et al.* 1993), it is clear that the lowest POC flux should be at the beginning of the year, when the primary productivity in the surface waters are at their lowest levels; higher fluxes will then follow the spring and summer blooms (Gieskes and Kraay 1975). Two approaches were used to try and improve the POC flux over the annual cycle; the first used a simple step-wise approach to approximate the increase in POC flux during spring and summer, while the second used a more complex sinusoidal approach, described by Equation 4.3.

$$f_t = \alpha \times \left(-\cos\left(\frac{2\pi t}{365}\right) + \sin\left(\frac{2\pi t}{365}\right) - \left(2.5 \times \cos\left(\frac{4\pi t}{365}\right)\right) - \left(0.5 \times \sin\left(\frac{4\pi t}{365}\right)\right)\right) + \overline{f} \qquad \text{Eqtn 4.3}$$

where f_t is the flux at time *t*, $\overline{f}$ is the mean flux over a flux cycle (in this case annual), in units of g C m^{-2} yr^{-1}, and α is a coefficient related to $\overline{f}$, in a relationship shown in Equation 4.4.

$$\alpha = 5.59\overline{f} - 4.59 \qquad \text{Eqtn 4.4}$$

Using these two approaches, the resulting annual flux cycles can be seen in Figures 4.5a and 4.5b; Figure 4.5a shows a baseline POC flux of 15 g C m^{-2} yr^{-1}, while Figure 4.5b shows the profile with a mean POC flux of 15 g C m^{-2} yr^{-1}.

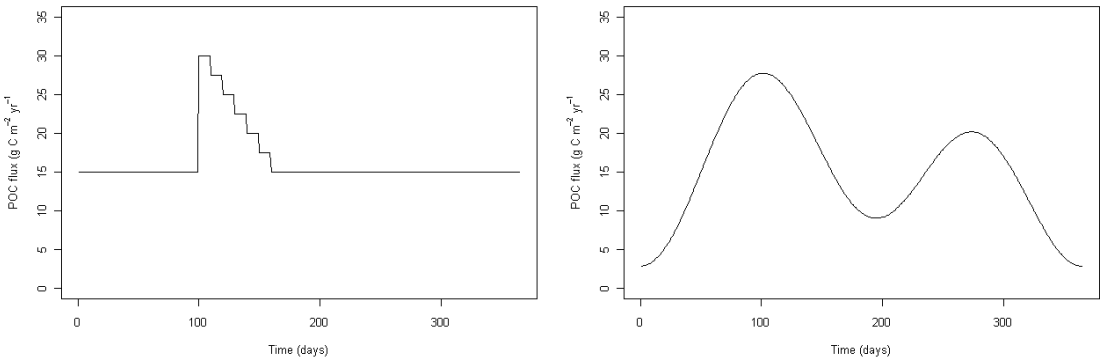

Figure 4.5: POC fluxes using after attempts to improve the realism of the POC flux; **a** (left) shows the stepwise approach, with a baseline POC flux of 15 g C m^{-2} yr^{-1}, while **b** (right) shows the profile described using Equation 4.3

To make comparisons later on in this chapter easier, the four flux profiles used have been given codes as follows: FP1 is the flux profile with no variation in the POC flux with time; FP2 uses the simple, but inaccurate, sinusoidal relationship; FP3 is the step-wise relationship (with the output shown in Figure 4.5a)., and FP4 uses the more complex sinusoidal relationship (with the output shown in Figure 4.5b).

Empirically, it was found that the solutions for FP2, FP3 and FP4 all reached a steady-state within the same timeframe; given that FP4 was the most accurate POC flux that seems to have been used in a coastal ocean early-diagenetic model to date, it would seem sensible to use this in the majority of testing from this point on in the thesis where the dynamic model is used. During runs using mean POC fluxes of 2, 15 and 50 g C m^{-2} yr^{-1}, the difference between day 1 and day 365 of the integrated concentrations of each of the chemical species in the 1 year model run is less than 1%. Figure 4.6 shows the 2D concentration isopleths plots of carbon, oxygen, nitrate and ammonia after a 1 year model run with a mean POC flux of 15 g C m^{-2} yr^{-1}; while Figure 4.7 shows the SWI fluxes of each of the chemical species from three model runs, with varying POC flux.

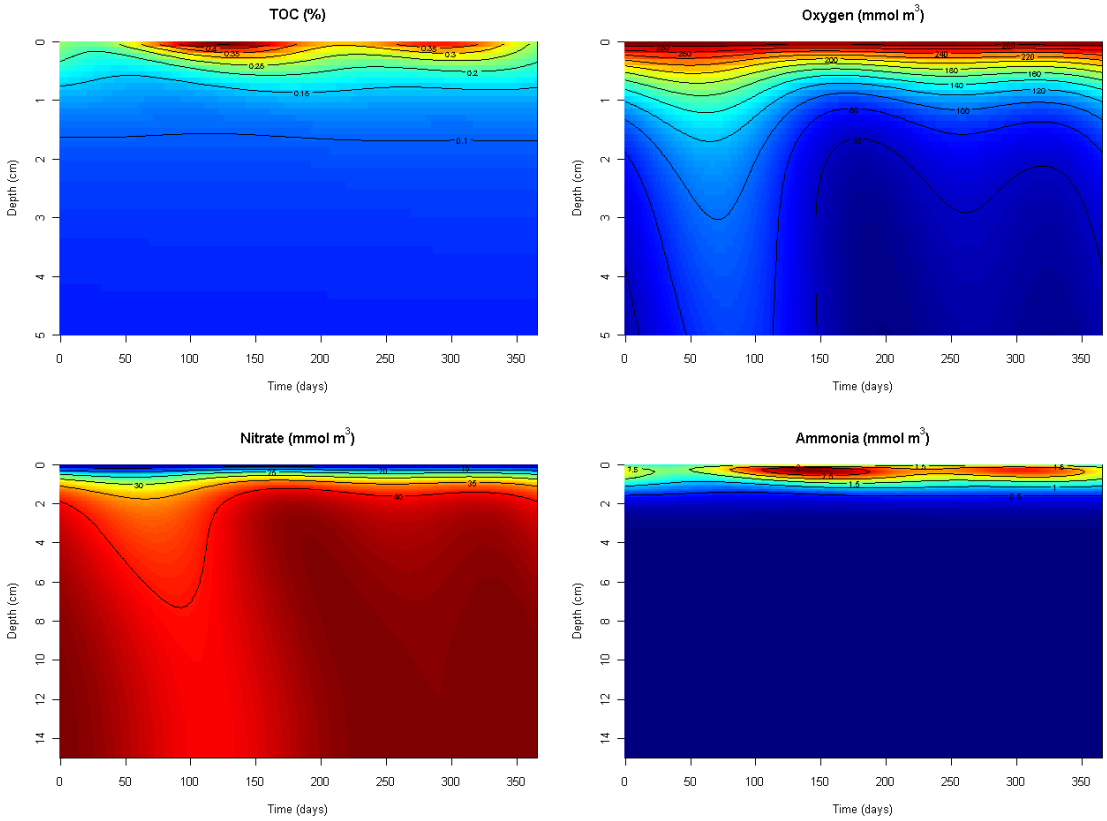

Figure 4.6: Porewater concentration plots of total organic carbon, oxygen, nitrate, and ammonia generated with an imposed mean POC flux of 15 g C m^{-2} yr^{-1} using the carbon flux profile FP4

As can be seen from the concentration profiles, the change in each of the chemical species reflects the variation in the POC flux. As the carbon concentrations in the sediment increase, the oxygen penetration depth (OPD) decreases, the nitrate concentrations decrease and ammonia concentrations in the surface sediments increase. Ammonia concentrations are three times higher in the top two centimetres of the sediment than in the water column (3 mmol m^{-3} compared with 1 mmol m^{-3}); due to the oxygen concentrations not decreasing to zero, nitrification occurs throughout the year leading to a depletion of ammonia but allowing nitrate concentrations to remain just higher than water column concentrations for the vast majority of the year. However, if the POC flux is increased to 50 g C m^{-2} yr^{-1} (concentration profiles not shown), then the expected nitrate peak does return, and remains between 2 and 5 mm throughout the year, before the concentration of nitrate falls to below 0.2 mmol m^{-3} below a depth which fluctuates between 1.4 cm and 3.9 cm. As expected, this also leads to much higher ammonia concentrations. In general, the oxygen concentrations, the OPD and the nitrate peak depth and concentration are similar to the profiles obtained from the steady-state solution. However, the TOC concentrations and ammonia profile are slightly different to the steady-state solution, with the maximum

value of TOC being lower during this dynamic run than during the equivalent steady-state run (0.99% compared with 1.39%), and the maximum ammonia concentration also being lower (75.9 mmol m^{-3} compared with 108.0 mmol m^{-3}). These are both reminders that the dynamic model and steady-state model should not be directly compared, although they are both useful in their own right.

The concentrations calculated by the model do show relatively good agreement with some observations from the North Sea. Profiles of nitrogen species in the southern North Sea from June 1974 show maximum concentrations of 70 mmol m^{-3} for nitrate (the maximum concentration of the nitrate peak, measured at a depth of 6 cm), while the maximum observed ammonia concentration was 40 mmol m^{-3} (Billen 1982; Billen 1978); the relatively deep nitrate peak being due to the high porosity values. Concentrations on 22nd April 1974 show much lower nitrate concentrations, with a maximum value of 20 mmol m^{-3} at 4 cm. This implies that the initial spring bloom occurred in mid-April, while the late summer bloom had not occurred when the June samples were taken. Comparing this data to the OMEXDIA run with the FP4 POC flux initially appears to show remarkable similarity in one respect; for day 115 in the model output, the maximum nitrate concentration is 17.3 mmol m^{-3} if the mean POC flux is 50 g C m^{-2} yr^{-1}; however, this is a difference of 13.5% compared with the observed value, and the depth at which the maximum concentration is found in the model output is 2.5 mm. In addition, the maximum calculated nitrate concentration for day 141 is 16.7 mmol m^{-3}, much lower than the observed concentration of approximately 60 mmol m^{-3}. It should also be noted that sediments in the southern North Sea tend to be relatively sandy, and so some care should be taken when trying to make comparisons with model output, where cohesive environments have been assumed.

The observations by Rutgers van der Loeff (1980a) from the Wadden Sea also show great variation; the winter concentrations of both nitrate and ammonia are much higher than shown in Billen (1978), despite both being carried out in the same region of the North Sea. Rutgers van der Loeff (1980a) reported nitrate concentrations of 81 mmol m^{-3} in an off-shore location in winter, and 30 mmol m^{-3} in summer, while ammonia concentrations of 200 mmol m^{-3} in winter and 300 mmol m^{-3} in summer were observed. These are all much higher concentrations than the model generates under any reasonable POC flux. However, in general, reported carbon concentrations in the North Sea are between 0.03% and 3.83% (e.g. de Haas *et al.* 1997; Al-Raei *et al.* 2009; Klamer *et al.* 2005; van Raaphorst and Malschaert 1996; Slomp *et al.* 1998; Bakker and Helder 1993). Lower values tend to be found in higher porosity sandy sediments, while higher values are observed in cohesive sediments. Reported oxygen penetration depths are 3-20 mm (Cook *et al.* 2007; Bakker and Helder 1993; van der Zee *et al.* 2003; Janssen *et al.* 2005; Rajendran *et al.* 1992; Böttcher *et al.* 2004), although this is

also highly variable – higher porosity sediments have deeper OPDs, which can cause the OPD to vary by as much as an order of magnitude. In addition, bioturbation is also known to affect the OPD (Rajendran *et al.* 1992).

The range of maximum nitrate concentrations are 4 – 80 mmol m^{-3}, while the depth of the nitrate concentration peak ranges from 2 – 30 mm (Lohse *et al.* 1993; Lohse *et al.* 1996; Rutgers van der Loeff 1980a). Maximum ammonia concentrations range from 50 to 150 mmol m^{-3} (van Raaphorst and Malschaert 1996; Van Raaphorst *et al.* 1992), although much higher concentrations are found in coastal and estuarine locations (van Raaphorst and Malschaert 1996).

The fluxes across the SWI over 1 year model runs, after a 10 year spin-up, of oxygen, nitrate, ammonia and ODU are shown in Figure 4.7. Unsurprisingly, the fluxes follow the trends of the POC flux, and are affected by the POC flux. For example, when the POC flux is low, the oxygen flux into the sediment is low, due to the rates of oxic mineralisation in the sediment. As the POC increases (both as the flux imposed is increased and as the POC varies over the course of a 1 year model run), so does the oxygen flux into the sediment. There is also a lag between the maximum POC flux and the maximum oxygen flux; when the mean flux of POC is 50 g C m^{-2} yr^{-1}, the greatest POC flux is the equivalent of 94.3 g C m^{-2} yr^{-1}, at day 103, while the greatest oxygen flux is the equivalent of 1395 mmol m^{-2} yr^{-1}, which is at day 142. This lag is also seen after the second spring bloom; the peak POC flux is on day 275 (68.1 g C m^{-2} yr^{-1}), while the associated peak in oxygen across the SWI corresponds to 1262 mmol m^{-2} yr^{-1} on day 303. The range of the oxygen flux during the 1 year model run is 548.3 mmol m^{-2} yr^{-1}, with the minimum oxygen flux being at day 38.

Similar patterns are seen with the fluxes of ammonia and ODU, where the flux out of the sediment increases following the increase of POC to the sediment. The maximum flux of ammonia across the SWI is the equivalent of -39.7 mmol m^{-2} yr^{-1} at day 145; the values for ODU being the equivalent -127.6 mmol m^{-2} yr^{-1} on day 163. The fluxes for nitrate also show variability, but whereas oxygen, ammonia and ODU have a clear differential between the POC fluxes of 15 and 50 g C m^{-2} yr^{-1}, nitrate does not. For 126 days, from day 119, and for 86 days from day 273, the flux of nitrate across the SWI when the POC flux is 15 g C m^{-2} yr^{-1} is higher than when it is 50 g C m^{-2} yr^{-1}. This is as a result of the increased POC flux utilising much higher concentrations of nitrate through denitrification, and hence decreasing the amount of excess nitrate available to be released to the water column. The concentrations of nitrate do not decrease as greatly when the POC flux is lower, as a result of nitrification.

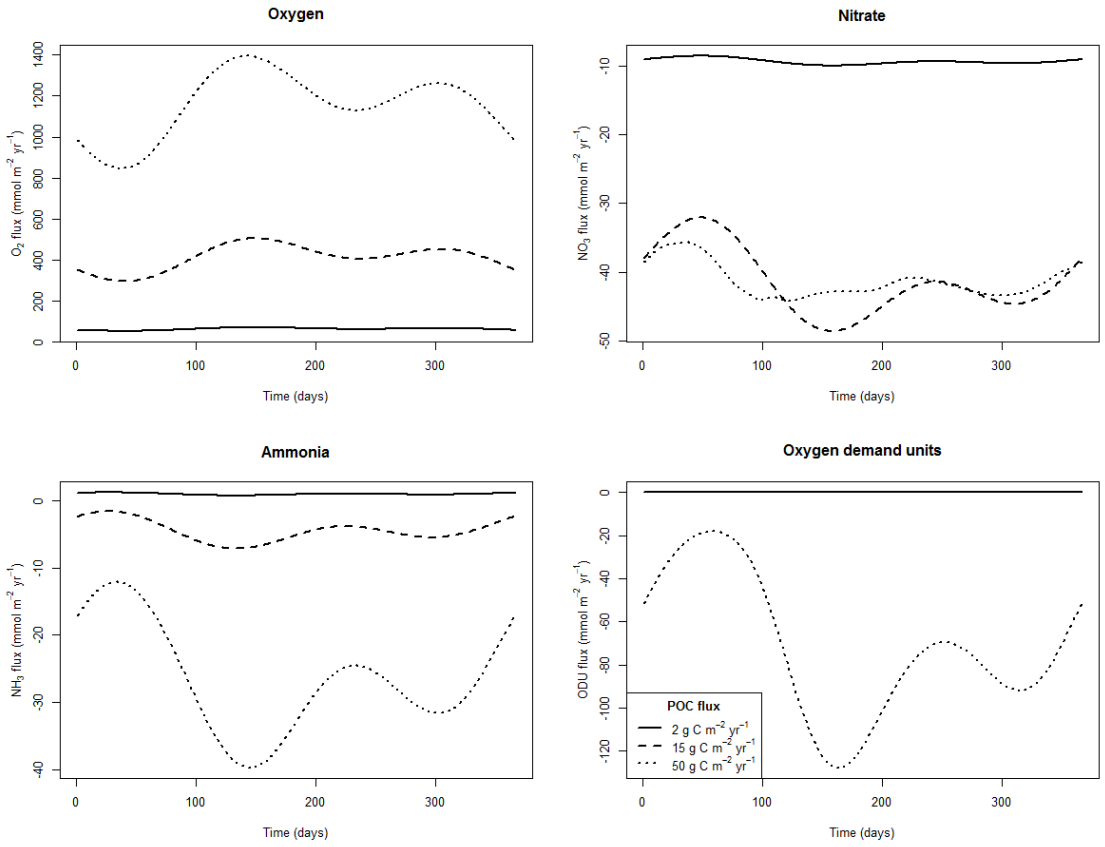

Figure 4.7: Fluxes over 1 year of oxygen, nitrate, ammonia, and ODU calculated from three model runs with an mean POC fluxes of 2, 15 and 50 g C m^{-2} yr^{-1} using the carbon flux profile FP4 (positive values indicate a flux into the sediment)

It is worth remembering that not only are sedimentary environments highly variable (Billen 1978), but it is also difficult to compare a model designed for cohesive environments with sandy sediments, and, as stated in Chapter 3, this brief comparison does help to show that the model is more likely to be useful to calculate fluxes and integrated rates of biogeochemical processes across a whole shelf-system rather than to precisely represent a small number of observed profiles. However, the comparisons made above do show that the model output is able to recreate realistic ranges of concentrations, and as such is suitable to carry out scenario testing and to estimate biogeochemical rates and fluxes over much larger areas, as well as to back-calculate the values of parameters difficult to measure, such as the POC flux or bioturbation coefficient for a sediment.

4.6 Comparison of model output with observational data

By using the results from two of the model runs described above, extrapolation can be used to estimate values of biogeochemical process rates and fluxes across the SWI for the North Sea continental shelf. Table 4.2 shows rates and fluxes for the whole

of the North Sea, if the area of the North Sea is assumed to be 745 950 km^2 (North Sea Task Force 1993; although note that this includes the Skaggerak, Kattegat, and English Channel).

Table 4.2: Estimates of fluxes and total utilisation of oxygen, nitrate and ammonia across the whole of the North Sea following a 1 year model run, with a 10 year model spinup, with mean imposed time-varying POC fluxes of 15 and 50 g C m^{-2} yr^{-1}, when the POC flux profile FP4 is used

		POC flux (g C m^{-2} yr^{-1})	
		15	50
Fluxes (Tmol yr^{-1})	Oxygen	1.12	3.2
	Nitrate	-0.11	-0.11
	Ammonia	-0.01	-0.07
Biogeochemical rates (Tmol yr^{-1})	Oxic mineralisation	0.89	1.76
	Denitrification	2.29×10^{-3}	0.20
	Nitrification	5.8×10^{-2}	0.15

Table 4.2 gives some estimation of values that are currently difficult to find in the literature. The rates of the biogeochemical processes are in units of the electron acceptor, based on the relationships in Table 1 of Soetaert *et al.* (1996b), and represent the total concentration of each oxidant used in the top 15 cm of the sediment across the whole of the North Sea. Unsurprisingly for oxygen, this is similar to the total flux into the sediment, with the remainder of the oxygen being used in secondary oxidation processes. What is also unsurprising, given the results seen in Figure 4.7, is that the total flux of nitrate to the water column is approximately the same whether the POC flux is 15 or 50 g C m^{-2} yr^{-1}. It can also be seen that fluxes of oxygen are approximately linearly proportional to the POC flux, whereas this is not the case for nitrate or ammonia.

The overarching conclusion from Table 4.2 is that this chapter has provided new estimates for the biogeochemical processes within the North Sea sediments. Perhaps most importantly is that sediments appear to provide 0.11 Tmol yr^{-1} of nitrate and 0.072 Tmol yr^{-1} of ammonia, assuming that the mean POC flux is 50 g C m^{-2} yr^{-1}. This means that the total flux of carbon to the benthic environment is 3.7×10^7 tonnes yr^{-1}. When compared with Table 3.2, it can also be seen that the dynamic model gives the same result for the flux of oxygen across the SWI per year, but the dynamic model estimates the flux of nitrate out of the sediment to be approximately an order of magnitude larger than the flux calculated by the steady-state model.

If the model run where the imposed mean POC flux is 50 g C m^{-2} yr^{-1} is considered, the range of the POC flux over the year is 179 nmol C cm^{-2} d^{-1} when the flux is lowest (day 1) to 2153 nmol C cm^{-2} d^{-1} when the flux is highest (day 103). As has been already discussed, the flux profile FP4 is likely to be the most accurate representation of POC flux to the sediment, and so comparisons can be made with observational data. Although it has historically been difficult to get precise measurements of POC fluxes, estimates have been made by using sediment traps, although their accuracy has been questioned (Buesseler 1991), and marine snow catchers (Lampitt *et al.* 1993). Although this does obviously vary with season, the range generally found in the North Sea is 14 – 82 g C m^{-2} yr^{-1} (Boon and Duineveld 1998) with the range used in previous models of similar environments being 40 – 70 g C m^{-2} yr^{-1} (Luff and Moll 2004) The sedimentary concentrations calculated by this model run do seem realistic, and the POC fluxes used fall within observations, thus giving support that this set up of OMEXDIA being used for scenario testing, and the values given in Table 4.2 are a good first-order estimate.

Some comparisons can be made of the total integrated rates of biogeochemical processes (Table 4.2) with previously measured values of oxic mineralisation and denitrification rates. Billen (1978) found that denitrification rates were 3.5 g N m^{-2} yr^{-1}; although no indication of depth integration is given, this leads to 0.18 Tmol N for the North Sea, which is very similar to the magnitude of nitrogen used in denitrification calculated by the model, assuming that a high POC flux is imposed. A slightly lower value of 0.08 Tmol N would be the case using the rates of 12 μmol N m^{-2} hr^{-1} found by Lohse *et al.* (1993), while extrapolating the values found at two sites in the southern North Sea gives a range of 0.01 to 0.15 Tmol N (Van Raaphorst *et al.* 1992).

The published total oxic mineralisation for the North Sea range between 0.52 and 3.5 Tmol O_2 (Bakker and Helder 1993; Upton *et al.* 1993; Osinga *et al.* 1996); however, it should be noted that care should be taken if attempting to extrapolate values taken out of context. Osinga (1996), for example, found that the oxic mineralisation at the Oyster Grounds could be as high as 131 g C m^{-2} yr^{-1}; using just this value to calculate an overall integrated mineralisation for the whole of the North Sea would lead to a value two orders of magnitude larger than that calculated by this model when the POC flux is 50 g C m^{-2} yr^{-1}. However, the oxic mineralisation at the Broad Fourteens site was only 44 g C m^{-2} yr^{-1}, leading to an integrated oxic mineralisation for the North Sea to within the range calculated by the model. It is clear, therefore, that if experimental data is to be used to calculate total rates for biogeochemical processes, some assessment must be made as to whether the value is sensible.

The fact that the model is able to produce values that are well within the ranges observed, despite its relative simplicity, does show that it is a viable method to increase our understanding of shelf-sea biogeochemistry, and to provide deeper knowledge about the cycling of nutrients in the North Sea. Although the flux profile FP4 is still only an estimate of POC flux to the benthic environment, it seems a relatively good approximation. Although its extrapolation here has been applied to the whole of the North Sea, this may be acceptable for a first order-estimate, even though the POC flux is likely to vary between locations. In general, coastal areas have much higher primary production and therefore have higher POC fluxes to the sediment (Stoeck *et al.* 2003). However, areas with deeper water-depths, such as the Skagerrak, tend to have a wider range in primary productivity, leading to more variable benthic POC fluxes and a corresponding range in denitrification rates (Rysgaard *et al.* 2001; Foster and Shimmield 2002; Ståhl *et al.* 2004).

As the model does generate realistic benthic mineralisation rates and oxygen fluxes, the implication is that the remaining biogeochemical processes are also relatively accurate. Thus the estimated net nitrate flux from the sediment to the North Sea is 0.11 Tmol yr^{-1}, and the net ammonia flux is 0.07 Tmol yr^{-1}, which means that sediment contributes more nitrate to the North Sea than the total atmospheric flux by more than an order of magnitude, but approximately the same amount of ammonia. Using values given in Rendell *et al.* (1993), and extrapolating for the total area of the North Sea, atmospheric contribution is approximately 6.3×10^{-3} Tmol yr^{-1}. Meanwhile, from the same study, the total atmospheric flux of ammonia to the North Sea is 1.82×10^{-2} Tmol yr^{-1}.

Relative to sedimentary contributions of total dissolved nitrogen, the total riverine input has been estimated to be 805±237 kT N yr^{-1} (Brion *et al.* 2004) whereas, from the model output presented in Table 4.2, it can be estimated that sediments contribute approximately 21 kT N yr^{-1}. However, sediments have been estimated to be responsible for removing 5-36 kT of nitrogen in SPM deposition, with a mean value of 20±15 kT N yr^{-1}. The net flux of nitrogen therefore seems to be 1 kT N yr^{-1} from the sediment into the North Sea. Although this does not affect the conclusions that the North Sea can vary from being a net contributor to a net importer of nitrogen (Brion *et al.* 2004), it is nonetheless still an important result, and improves knowledge of the complex North Sea system.

Although the conclusions here are, in general, the same as in Chapter 3, it is believed that the potential accuracy gained by using the FP4 flux profile, whilst not greatly reducing model efficiency does give much greater certainty in the results, particularly with regard to temporal detail. This dynamic version of the model will now

be used in Chapter 6 with confidence that the results given are the best estimate that can be gained using current knowledge about the North Sea.

4.7 Summary

Although the equation to describe POC flux in the default version of OMEXDIA may be sufficient to model continental shelf and abyssal plain environments, it was clear that this is unsuitable for the modelling of shelf seas. This Chapter has shown how it is possible to slightly modify OMEXDIA to enable it to model specific environments more accurately, and it is believed to be the first time that an algorithm to describe the specific OM flux pattern in a shelf sea has been implemented into a diagenetic model.

Improving the accuracy of the forcing parameter in OMEXDIA has meant that better estimates can be made about the shelf-wide rates for biogeochemical processes (specifically oxic mineralisation, denitrification and nitrification) and fluxes of the primary chemical species (O2, NO_3^-, and NH_3) across the SWI. However, it is likely that future work, using both modelling and observational approaches, could further improve the calculations made in this chapter. The assumptions made in this chapter have ignored the potential impact of different sedimentary type; the sandy sediments which form a substantial portion of the North Sea (Basford and Eleftheriou 1988), and have different POC content to muddy sediments (Leipe *et al.* 2011), will therefore have a different values for both biogeochemical processes and fluxes across the SWI. Therefore, the implementation of diagenetic processes into a 3D hydrodynamic model is likely to improve upon the estimates provided in this chapter, and could the focus of a future study.

5 Sensitivity Analysis and Genetic Algorithm

The effects of variation in coefficients can provide an indication of the importance of individual parameters (Steele 1975). Specifically, model sensitivity is defined by O'Brien & Wroblewski (1973) as "the displacement from equilibrium the model experiences due to quantitative variation in an individual parameter". Further to this, sensitivity analysis can be subdivided into local and global subtypes (Soetaert and Herman 2009), where local is the result of infinitesimally small changes in a parameter, and global uses parameter values over a much larger range, possibly over the entire reasonable range of a parameter. Here, a set of univariate global sensitivity analyses are carried out to investigate the parameters to which the model is likely to be most responsive.

5.1 Sensitivity Analysis Method

A literature search was carried out in order to find the range of possible values for all parameters used in the model. Where data from the North Sea could not be found, data from other shelf-seas, continental shelves, deep seas, estuaries or lakes has been taken, although the appropriateness of the data was taken into account. Where no experimental data could be found from any environment, parameter values from other models have been taken; in the vast majority of cases, the parameter values in other models have been obtained by parameterisation methods. The data collected during this search is shown in Table 5.1; data taken from models is indicated. Following on from the results and conclusions presented in Chapters 2 and 3, the simpler version of OMEXDIA, which combines the manganese oxide, iron oxide and sulphate pathways for OM oxidation, will be used.

Where independent or wider-ranging data has not been found, either from experimental work or from other models, the values of parameters used in the standard version of OMEXDIA have been checked to be consistent with values used in similar models. Bottom water concentrations of ammonia and ODU were always assumed to be zero due to anoxic conditions not being modelled.

Three sensitivity analysis experiments were carried out. The first one (referred to from now on as experiment SA1) used the values taken from the literature, where these were available. Where no data was available, the lower value was taken as half of the default value, and the upper value taken as double the value. The default values shown in Table 5.1 are mainly the values shown in Tables 6 and 7 of Soetaert *et al.* (1996b), although some values have been taken from experimental work associated

with this project (these data are indicated in Table 5.1). The model was run 52 times – once for the upper and lower value for each of the 26 parameters. For each run, all parameters bar one were set to their default values so that only one parameter was changed; the forcing parameter for the model, *MeanFlux*, was given a default value of 20 g C m^{-2} yr^{-1}. The second experiment (known as experiment SA2a) set the lower value for all parameters to half of the default value, and the upper value to be twice the default value, and the third experiment (experiment SA2b) set the lower and upper values to be 0.1 and 10 times that of the default values. The only slight deviation from the scheme for experiments 2a and 2b was for the parameter *pFast* (the proportion of organic matter which is fast-degrading). As the value of this parameter can only range between 0 and 1, and the model default was 0.86, both doubling and increasing by an order of magnitude was unrealistic. Although the range found in the literature (taken from a previous model) was 0.4 – 1 (Luff and Moll 2004), it was decided to fix the lower and upper limits to 0.1 and 0.99 respectively for both experiments SA2a and SA2b. As the upper values for this parameter using the above rules would not be realistic, and hence an arbitrary value would have to be picked, it was decided that the lower value should also be arbitrarily chosen.

Table 5.1: Parameter values used in the Sensitivity Analysis of OMEXDIA. Experiment SA1 used the lower and upper values shown; Experiments SA2a and SA2b used upper values that were half & double and one order of magnitude either side of the default values for the upper and lower values, except for the exceptions noted in the text; ND = North Dogger site

Name	Description	Units	Model default	Lower value	Upper value	Notes	References
depthPor	Porosity of sediment at depth	–	0.7	0.45	0.9	(a)	1, 2*
biot	Bioturbation	$cm^2\ d^{-1}$	0.0027	0.0002	1		2*, 3*, 4*
mixL	Depth of mixed layer	cm	5	1	5		2*
MeanFlux	POC flux	$g\ C\ m^2\ yr^{-1}$	20000/12*10 0/365	10000/12*1 00/365	80000/12*10 0/365		5*
rFast	Rate of degradation of fast degrading OM	day^{-1}	0.01	0.005	0.02	(b)	
rSlow	Rate of degradation of slow degrading OM	day^{-1}	0.0001	0.00005	0.0002	(b)	
pFast	Fraction of fast degrading OM	–	0.86	0.4	1		5*
w	Advection rate	$cm\ d^{-1}$	2.74E-07	1.37E-07	5.48E-07		
NCrFdet	N:C ratio in fast degrading OM	mol N: mol C	0.16	0.05	3.3	(b, c)	4*, 6, 7*
NCrSdet	N:C ratio in slow degrading OM	mol N: mol C	0.13	0.05	3.3	(b, c)	4*, 6, 7*
bwO2	Bottom water O2 conc (mean of ND experimental data)	$mmol\ m^{-3}$	248.7421	125	750	(d)	8, 9, 10
bwNO3	Bottom water NO_3^- conc (mean of ND experimental data)	$mmol\ m^{-3}$	1.94	0.5	49	(e)	6
bwNH3	Bottom water NH_3 conc (mean of ND experimental data)	$mmol\ m^{-3}$	2.72	0	10.5		6
ksO2oxic	half-sat O2 in oxic mineralisation	$mmol\ O_2\ m^{-3}$	3	1.5	6		
rnit	Max nitrification rate	day^{-1}	20	0.026	1.43		11
kinO2denit	half-sat O2 inhibiting denitrification	$mmol\ O_2\ m^{-3}$	1	0.5	2		
ksNO3denit	half-sat NO_3^- in denitrification	$mmol\ O_2\ m^{-3}$	30	15	60		
ksO2nitri	half-sat O2 in nitrification	$mmol\ O_2\ m^{-3}$	1	0.5	2		
NH3Ads	Adsorption coefficient ammonium	–	1.3	0.4	1.9		12
DispO2	O_2 diffusion coefficient (temp dependent)	–	1.341	0.6705	2.682		

DispNO3	NO_3^- diffusion coefficient (temp dependent)	-	1.81	0.905	3.62
DispNH3	NH_3 diffusion coefficient (temp dependent)	-	1.83	0.915	3.66
ksO2oduox	Half-saturation of O_2 in oxidation of ODU	mmol O_2 m^{-3}			
kinNO3anox	Half-saturation of NO_3^- in inhibition of anoxic mineralisation	mmol $NO_3^-m^{-3}$			
kinO2anox	Half-saturation of O2 in inhibition of anoxic mineralisation	mmol O2 m^{-3}			
rODUox	Rate of ODU oxidation	day^{-1}			
DispODU	Diffusion coefficient of ODU	-			

1. van der Zee *et al*. (2003); 2. Arndt and Regnier (2007); 3. van der Zee *et al*. (2002b); 4. Beck *et al*. (2009); 5. Luff and Moll (2004); 6. Rusch *et al*. (2000); 7. Van Cappellen and Wang (1996); 8. Upton *et al*. (1993); 9. Hall *et al*. (1996); 10. Jenkins and Goldman (1985); 11. van Raaphorst *et al*. (1990); 12. Mackin and Aller (1984)

Notes

(*) value taken from previous model (not taken from observational data)

- Whereas the model defines a decrease in porosity using an exponential decay, from a value of 1 at the sediment-water interface to a value of 0.7 at 15 cm, the experimental data not only shows much lower porosity values (i.e. denser sediment) at depth, but also that the overall decrease through the sediment is often in a much more random manner than can be described by a relatively simple decay function.

- No observational papers give values for the proportion of fast- and slow-degrading organic matter.

- In observations, the ratio of N:C has been shown to vary with depth, although this is not reflected in the model.

- Although 750 mmol m^{-3} would signify a supersaturated solution, supersaturation has been observed highly productive areas (e.g. in [11]) and so it has been included in the model runs carried out here

- [4] only gives values for NO_x; however, NO_2^- concentrations are generally much lower than NO_3^- concentrations. It is considered safe that the majority of NO_x will be NO_3^-Sediment surface temperature

5.2 Sensitivity Analysis Results

For each run of the model, the results of four sets of output (percentage changes of O_2 flux, NO_3^- flux, NH_3 flux and a cost function defined in Equation 5.1) were compared with the output generated when the default model values were used.

$$\sum_i (e_{i1} - e_{i2})^2 \qquad \text{Eqtn 5.1}$$

where *i* is the current layer (from 1 to 100), e_1 is concentration of the chemical species currently being considered (O_2, NO_3^- or NH_3) in the current layer in the standard run and e_2 is the concentration in the current layer in the current sensitivity analysis experiment (SA1, SA2a or SA2b). Equation 5.1 was applied to each chemical species in the model, and the three resulting values were summed to give a final *cost* for the parameter.

Figure 5.1 shows the percentage change that occurred as a result of experiment SA1. The greatest percentage change from the standard run is in the flux of ammonia when the upper value of *NCrFdet* (the ratio between nitrogen and carbon in the fast degrading proportion of organic matter) was used (from 0.16 to 3.3), with the percentage change being 11070%. Although the default version of OMEXDIA has different values for the ratio of nitrogen to carbon in the fast and slow degrading pools of organic matter (0.16 and 0.13 respectively), different values for fast and slow degrading organic matter could not be found in the literature; the lower and upper values (0.05 and 3.3 respectively) were therefore used for both *NCrFdet* and *NCrSdet*. Given the small difference between the default values of *NCrFdet* and *NCrSdet*, but that the change in flux of NH_3 that occurred when *NCrSdet* was given the value of 3.3 was only 739% compared with the percentage change of *NCrFdet* (22896%), it implies that the model is much more sensitive to changes in *NCrFdet* than *NCrSdet*.

The second greatest flux change of all the runs was in the ammonia flux when the upper value was changed for *MeanFlux* (from 20 to 80 g C m^{-2} yr^{-1}), when the percentage change was 1754%. The third, fourth and fifth largest percentage changes were 1001% (NH_3 flux when the *rnit* parameter was assigned the lower value), 875% (NO_3^- flux change when the *NCrFdet* parameter was assigned the upper value) and 522% (NH_3 flux when the *rnit* parameter was assigned the upper value) respectively. All of these five largest percentage changes are as a result of changes in parameters for which literature data has been used.

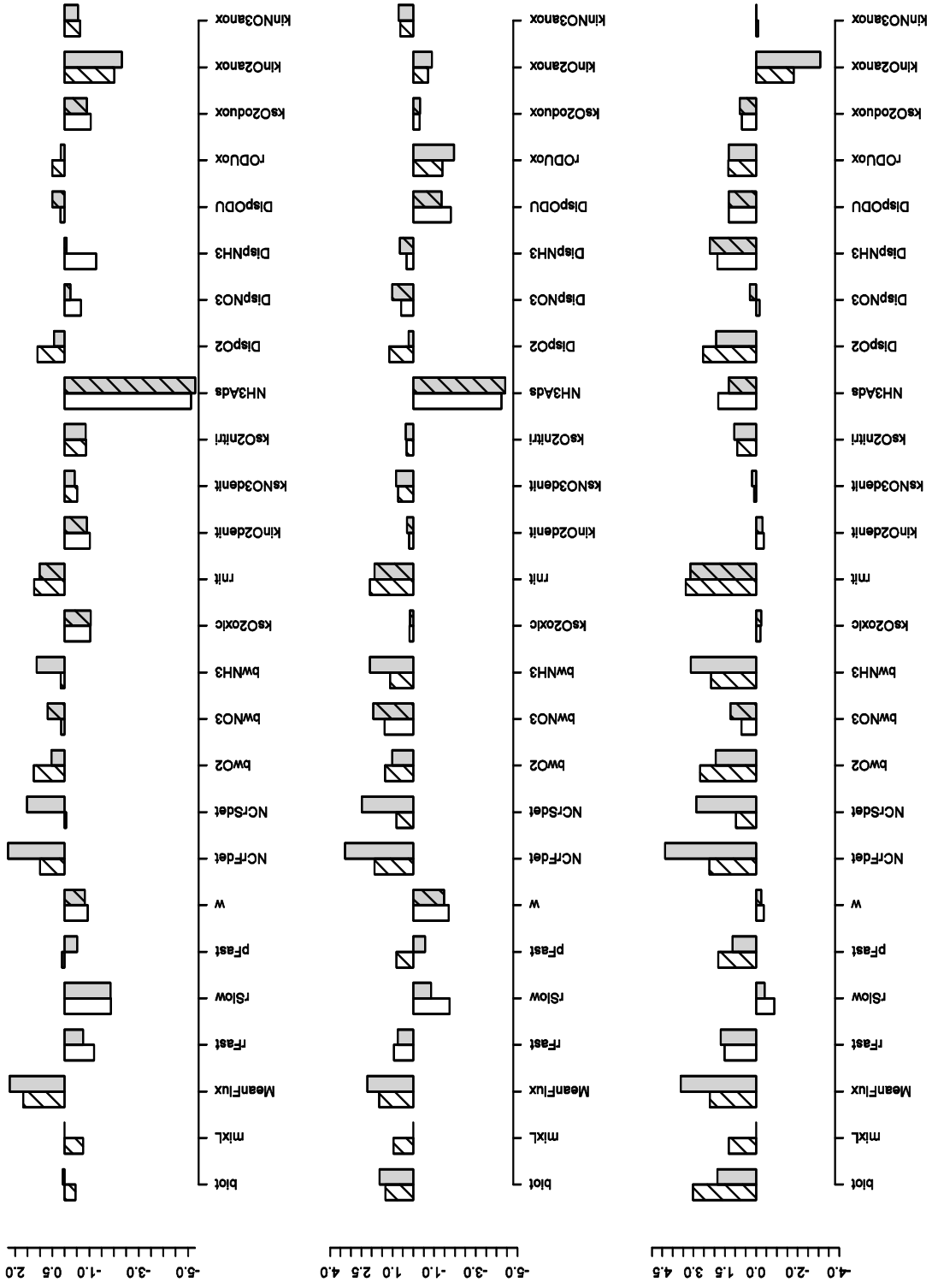

Figure 5.1: Percentage changes in fluxes of oxygen (top), nitrate (middle) and ammonia (bottom) as a result of experiment SA1; white bars denote the percentage flux change as a result of the lower values, while grey bars denote the percentage flux change as a result of the upper values. Note that the absolute calculated values of the have been logged, and the hashed bars indicate values where the flux change was negative

Although there is no clear link between the sensitive parameters, it is interesting to note that the greatest described above are all in the nitrogen compounds, and that the six largest changes are induced by five parameters; four of these five parameters are also related to nitrogen cycling.

Figure 5.2 shows the percentage change from experiment SA2a. The largest change seen here (367%) is in NH_3 flux when the mean flux of organic carbon is changed from the standard run value of 20 g C m^{-2} yr^{-1} to the upper value of 40 g C m^{-2} yr^{-1}. The second largest change (283%) is in the flux of NH_3 when the upper value of *NCrFdet* (0.32 compared to 0.16 in the standard run) is used. It is worth noting here that the largest literature value found for *NCrFdet* was 3.3, 20.6 times larger than the upper value used in SA2a, and hence two times larger than the upper value in experiment SA2b. The change in NH_3 when *pFast* was assigned the lower value (0.1 compared to 0.86) was -211%. Percentages below -100% indicate a change in direction of the flux. In this instance, this corresponds to a change in flux from -2.73 mol m^{-2} d^{-1} to 3.04 mol m^{-2} d^{-1}.

The fourth and fifth largest percentage changes in flux are -182% (the flux of NH_3 as a response to the upper value assigned to bwNH3) and -143% (the flux of NH_3 as a response to the upper value assigned to *rnit*).

The five largest fluxes in the SA2b experiment (shown in Figure 5.3) are NH_3 (7650%) when the upper value of mean flux – 200 g C m^{-2} yr^{-1} – was used, NH_3 (3810%) when the upper value of *NCrFdet* – 1.6 – was used, NH_3 (-1641%) when the upper value of *bwNH3* – 27.2 mmol m^{-3}– was used, NH_3 (527%) when the lower value of *DispO2* – 0.134 – was used and NH_3 (524%) when the lower value of *bwO2* – 24.9 mmol m^{-3} – was used. Despite the model being sensitive to *NCrFdet*, some caution should be applied to this; the default value of 0.16 implies a C:N ratio of 106:17, close to the Redfield Ratio value. However, the upper value used in experiment 2A (0.32) would imply that the ratio is 3.1, which is not in the range of observed ratios (6.6 – 12) given by Martin & Sayles (1994). The upper value used in experiment 2B is particularly unrealistic. The lower value of SA2a, however, gives a ratio of 11.8. This value is within observed ranges, and is parameter with the largest influence on NO_3^- fluxes and the third largest influence on NH_3 fluxes, and so should be considered valid.

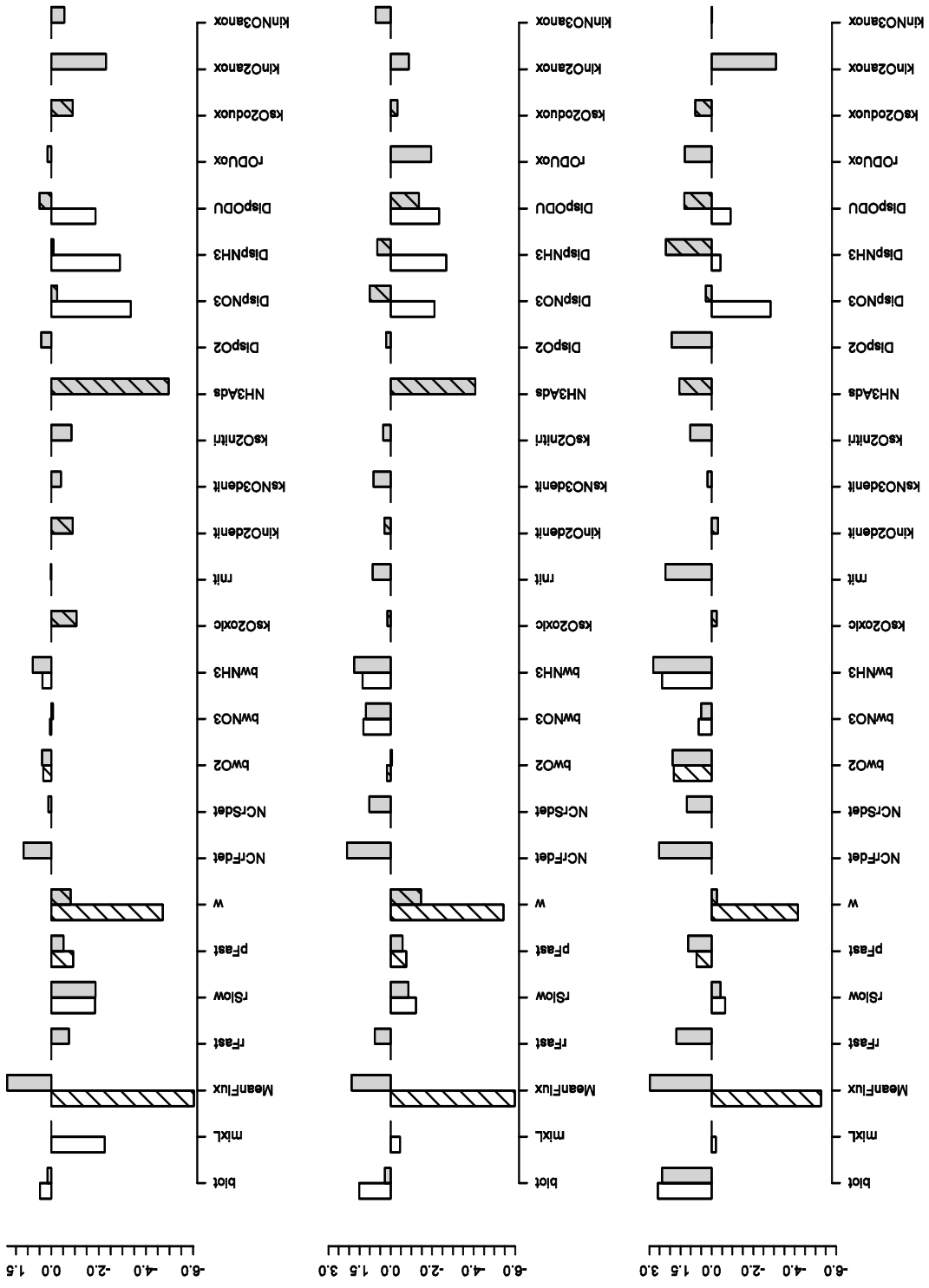

Figure 5.2: Percentage changes in fluxes of oxygen, (top), nitrate (middle) and ammonia (bottom) as a result of experiment SA2a; white bars denote the percentage flux change as a result of the lower values, while grey bars denote the percentage flux change as a result of the upper values. Note that the absolute calculated values of the have been logged, and the hashed bars indicate values where the flux change was negative

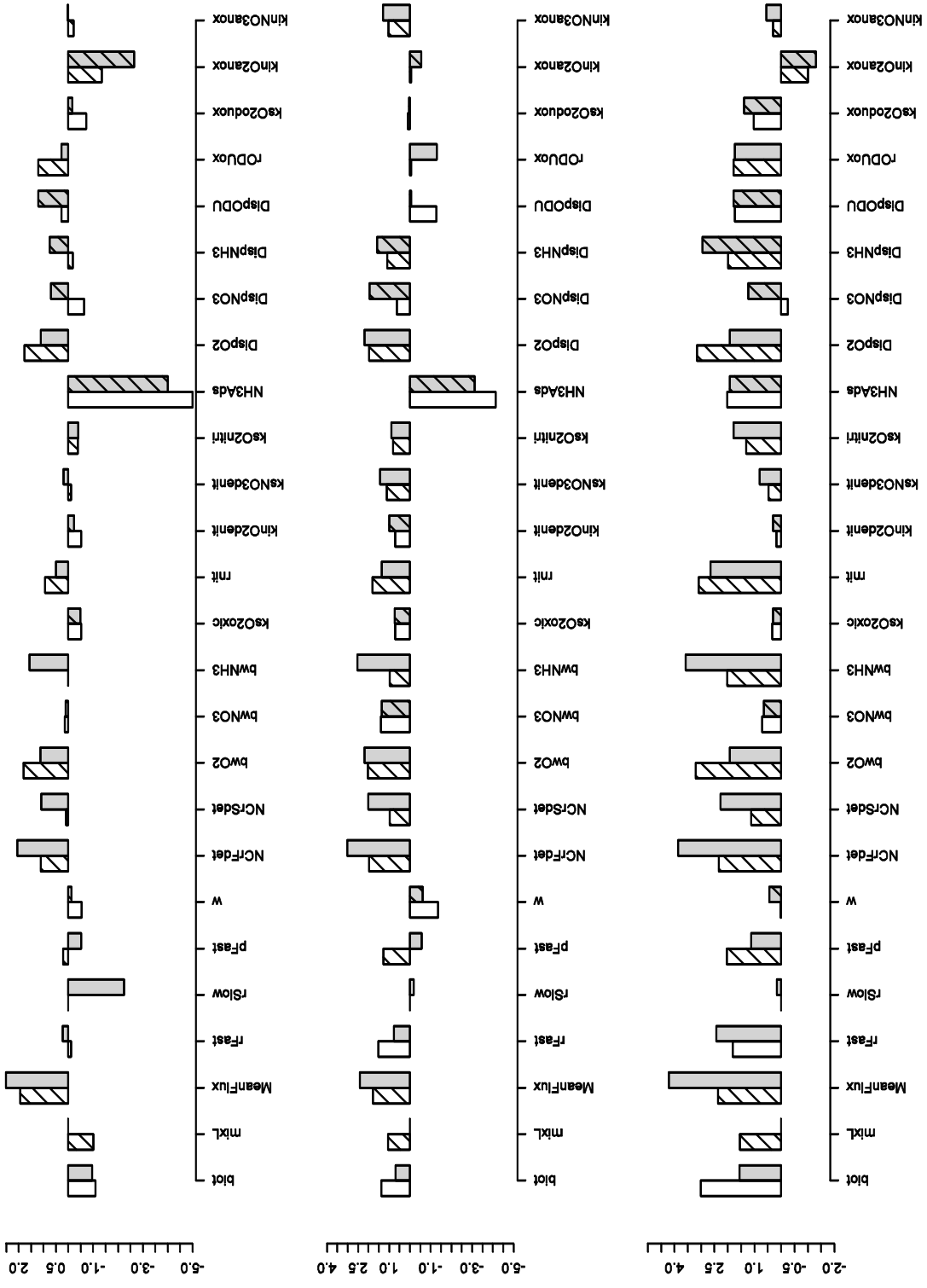

Figure 5.3: Percentage changes in fluxes of oxygen, (top), nitrate (middle) and amonia (bottom) as a result of experiment SA2b; white bars denote the percentage flux change as a result of the lower values, while grey bars denote the percentage flux change as a result of the upper values. Note that the absolute calculated values of the have been logged, and the hashed bars indicate values where the flux change was negative

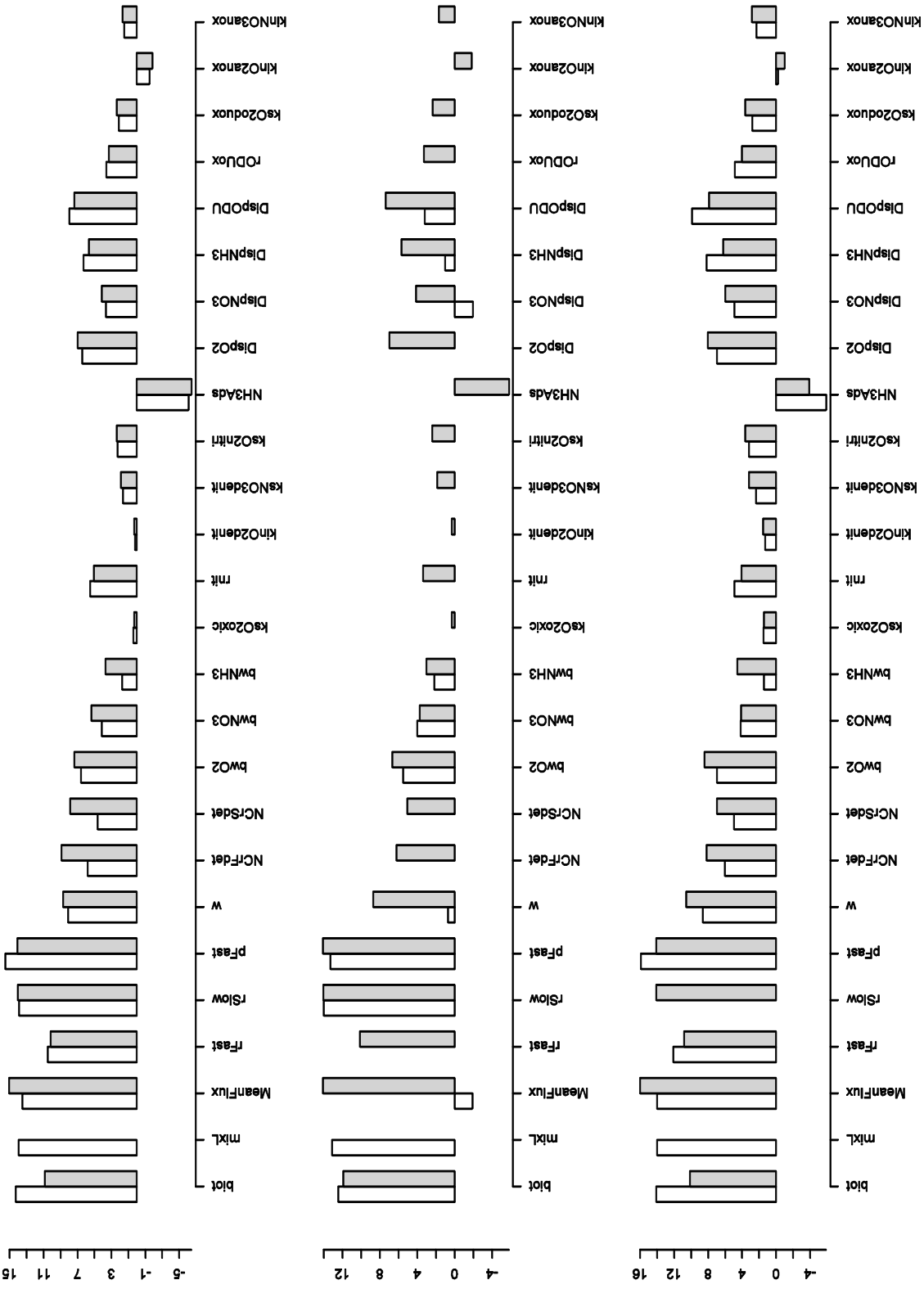

Figure 5.4: Output of logged value of cost function for experiment SA1 (top), SA2a (middle) and SA2b (bottom); white bars denote the percentage flux change as a result of the lower values, while grey bars denote the percentage flux change as a result of the upper values

By comparing the cost functions, we can also get a feel for how much the profiles vary for each of the species. Figure 5.4 shows the results of summing the cost functions for each species for each of the three sensitivity analysis runs respectively. It can be clearly seen that the lower value of *pFast*, the upper value of *MeanFlux* and the lower value of *biot* result in the largest cost functions when the SA1 experiment was carried out. The SA2a experiment, however, had a single parameter which produced the largest result (lower value of *pFast*), with three parameters having a similar effect (upper value of *MeanFlux*, lower value of *rSlow* and upper value of *pFast*). The parameters involved in bioturbation and mixing have much less effect on the output of the SA2b experiment. The upper value of MeanFlux, and the lower values of rSlow and pFast result in the largest cost functions during this experiment.

From judgement by eye, the following six parameters are the ones the model can be deemed to be most sensitive to: *MeanFlux*, *pFast*, *rSlow*, *rFast*, *NCrFdet* and *biot*. To strengthen this argument, Figures 5.5–5.7 show the percent change and absolute fluxes as a result of the three experiments.

The absolute fluxes provide a useful visual check for the percentage change – where the flux of a sensitivity run for a particular parameter is the same as the standard run, the percentage change should be zero. The percentage changes are calculated using Equation 5.2; when a percentage change is less than –100, this indicates that there has been a change in direction of the flux; in these cases, the magnitude is the absolute difference between the result and –100.

$$\frac{flux_{(i,j)} - flux_{(i,std)}}{flux_{(i,std)}} * 100 \qquad \text{Eqtn 5.2}$$

where $flux_{(i,j)}$ is the flux of chemical species *i* in the current run, *j*, of the sensitivity runs and $flux_{(i,\ std)}$ is the flux of *i* in the standard run. The six parameters noted in the previous paragraph as being particularly sensitive to the model dominate the percentage changes in fluxes for each of the chemical species. However, there are also some subtle differences between each of the species which aren't apparent in the combined results shown earlier in this report. For example, *rnit* (the rate of nitrification in the model, given a default value of 20 day^{-1}), unsurprisingly, has a large effect on the fluxes of both NO_3^- and NH_3 – where increasing the value (i.e. making nitrification, the oxidation of ammonia to form nitrate via nitrite, more likely to happen) increases the flux of NO_3^-, as its concentration in the sediment increases, and decreases the flux of NH_3, as its concentration decreases as a result of being consumed in the oxidation reaction.

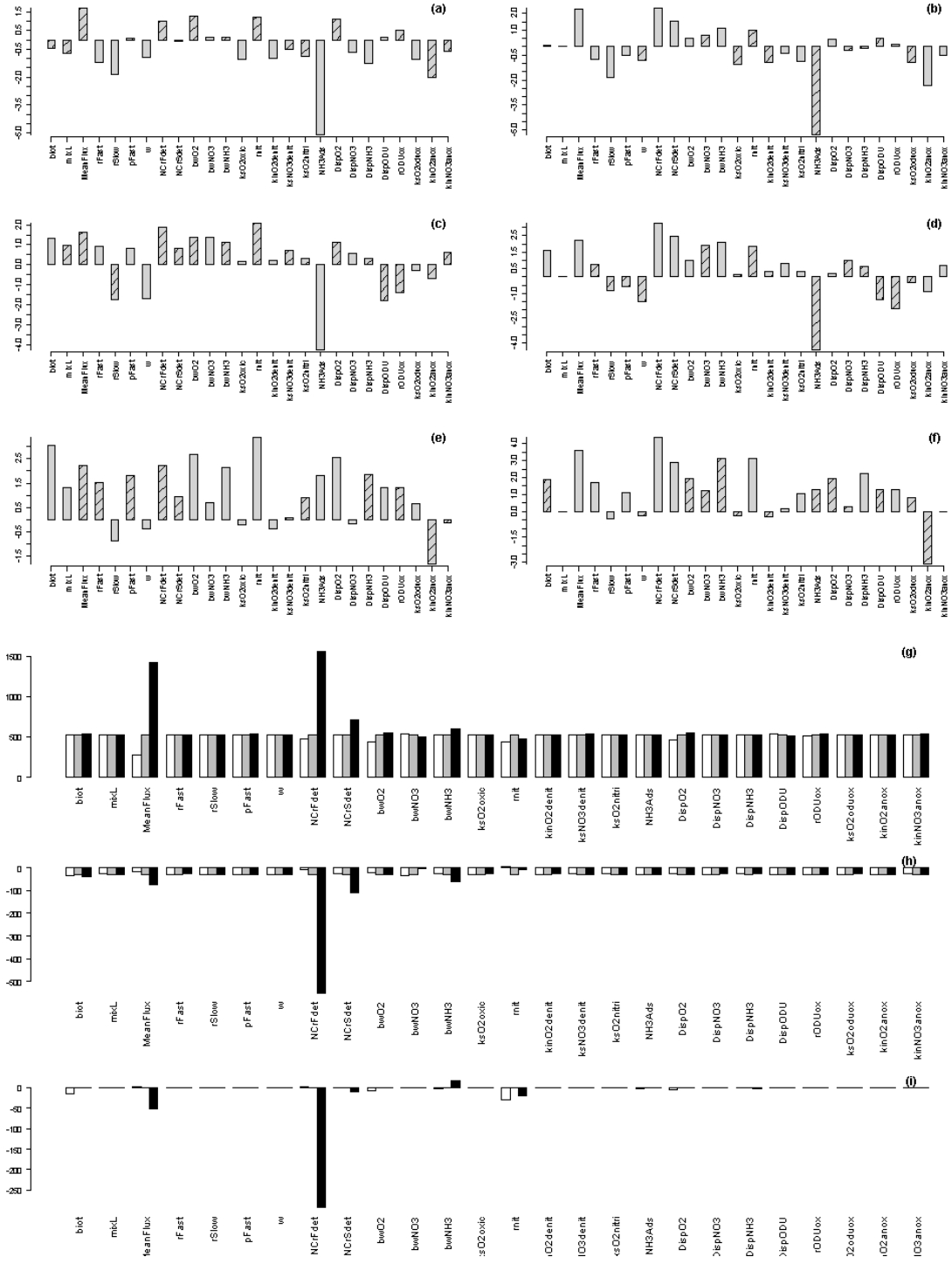

Figure 5.5: Percentage change of oxygen (**a** and **b**), nitrate (**c** and **d**), and ammonia (**e** and **f**) as a result of experiment SA1; **a, c** and **e** show the percentage flux change as a result of the lower values, while **b, d** and **f** show the percentage flux change as a result of the upper values. Note that the absolute calculated values of the have been logged, and the hashed bars indicate values where the flux change was negative; **g**, **h** and **i** show the absolute values of the flux of oxygen, nitrate and ammonia respectively (white bars showing the value from lower values, grey bars from the default model run and black bars from the upper values)

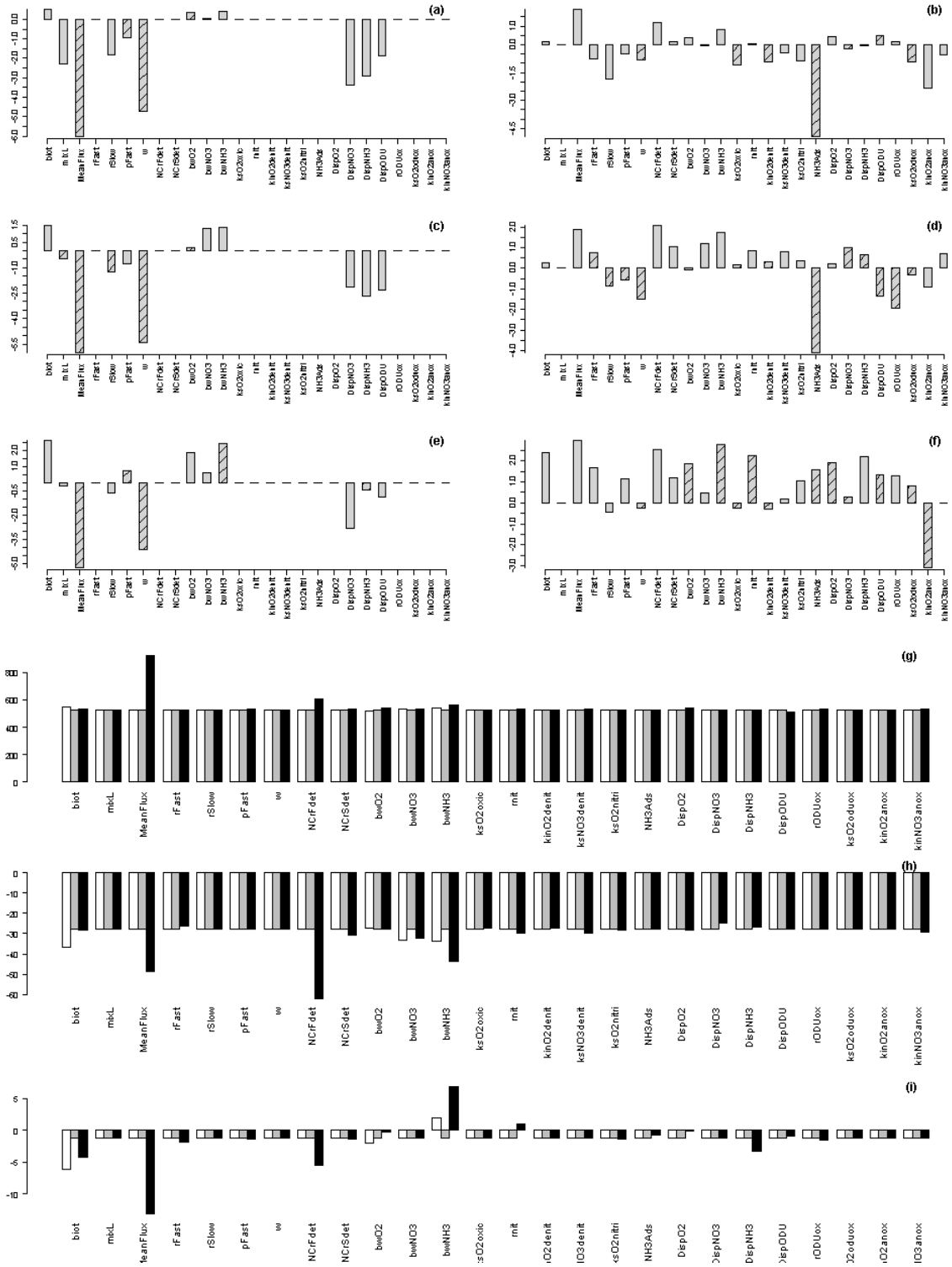

Figure 5.6: Percentage change of oxygen (**a** and **b**), nitrate (**c** and **d**), and ammonia (**e** and **f**) as a result of experiment SA2a; **a, c** and **e** show the percentage flux change as a result of the lower values, while **b, d** and **f** show the percentage flux change as a result of the upper values. Note that the absolute calculated values of the have been logged, and the hashed bars indicate values where the flux change was negative; **g**, **h** and **i** show the absolute values of the flux of oxygen, nitrate and ammonia respectively (white bars showing the value from lower values, grey bars from the default model run and black bars from the upper values)

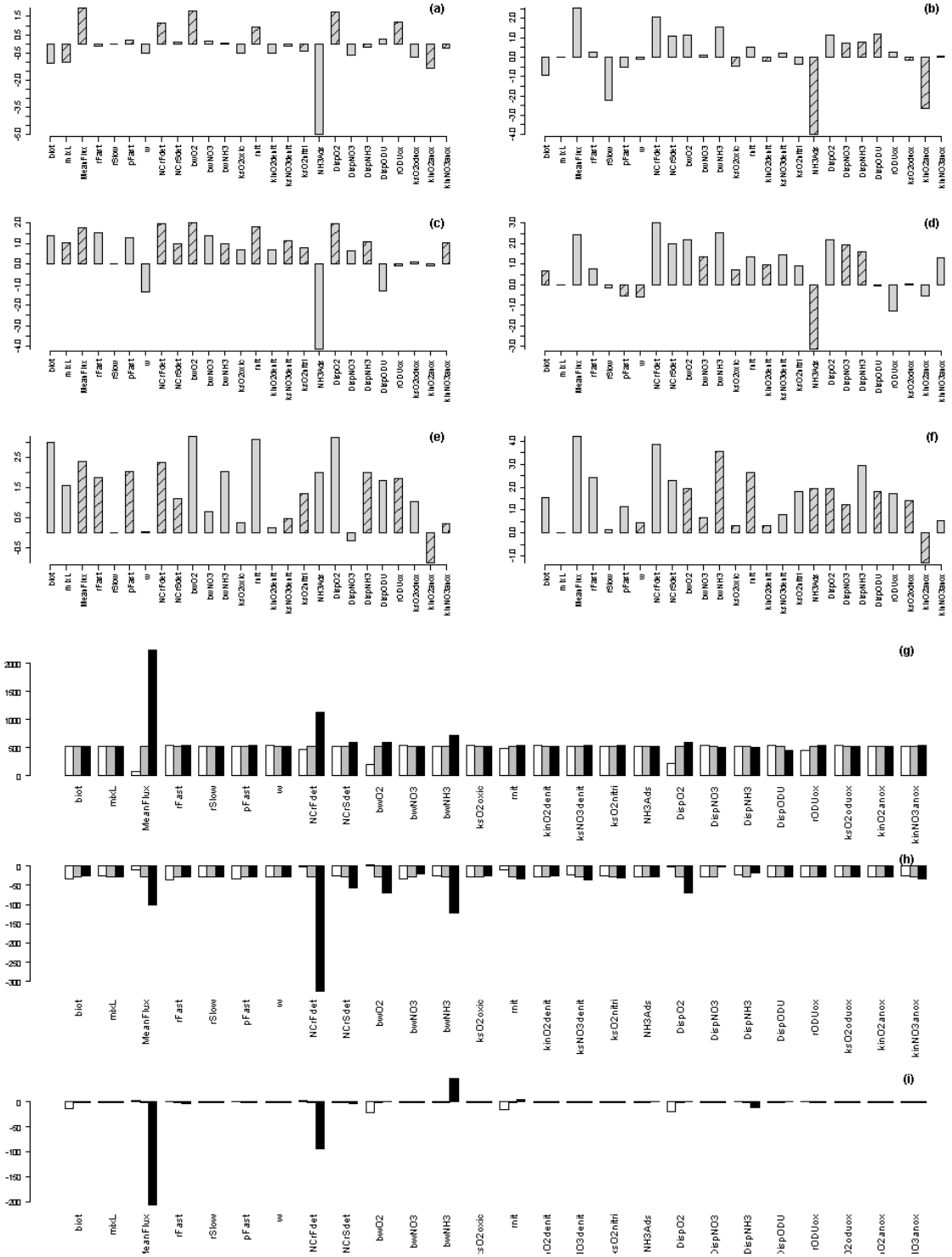

Figure 5.7: Percentage change of oxygen (**a** and **b**), nitrate (**c** and **d**), and ammonia (**e** and **f**) as a result of experiment SA2b; **a, c** and **e** show the percentage flux change as a result of the lower values, while **b, d** and **f** show the percentage flux change as a result of the upper values. Note that the absolute calculated values of the have been logged, and the hashed bars indicate values where the flux change was negative; **g**, **h** and **i** show the absolute values of the flux of oxygen, nitrate and ammonia respectively (white bars showing the value from lower values, grey bars from the default model run and black bars from the upper values)

Decreasing the value of *rnit* has the opposing effect, drastically increasing the flux of NH_3. Somewhat more surprisingly is that the diffusion coefficient of O_2 (*DispO2*, given a default value of 1.341) has a much larger effect than any of the other diffusion coefficients on all of the species. Decreasing the value of *DispO2* has a much larger relative effect on the fluxes of O_2, NO_3^- and NH_3 than increasing it. In the model, all of the diffusion coefficients are linearly related to the temperature, with the equation to calculate *DispO2* shown in Equation 5.3.

$$DispO2 = 0.955 + Temp*0.0386 \qquad \text{Eqtn 5.3}$$

where the value of temperature in the model is set at 10°C. Also relatively surprising is that, especially for the upper value during the SA2a and SA2b experiments, the value of *bwO2*, the bottom water oxygen concentration, has a slightly greater effect on the flux of NO_3^- than O_2, but has virtually no impact on the flux of NH_3. If the impact of changing the value of *bwNO3* is considered, it seems that the model is very unsensitive to it, even with respect to the NO_3^- flux; however, the model is much more sensitive to *bwNH3*, with the fluxes of O_2 and NO_3^- increasing, and the flux of NH_3 decreasing, when the value of this parameter is increased. This is almost certainly again linked to nitrification, with an increase in ammonia in the bottom water causing a lower flux needed to create equilibrium, allowing more NH_3 to be oxidised, and therefore increasing the flux of oxygen from the water column to the sediment, and increasing the flux of nitrate into the water column.

Although the graphs presented above give a good idea of the sensitivity of the parameters, the parameter optimisation, described in Section 5.2 needs some quantification of the sensitivity. A metric was devised to rank the parameters by sensitivity, and the method employed is discussed here. Initially, the values for each parameter were ranked for each of the three approaches, after the parameters had been sorted by the value of their change in flux of chemical species and of their cost function. For example, in Experiment SA2b, the lower and upper values of *MeanFlux* caused the greatest change in the magnitude of the flux of O_2 out of all parameters, and as such, was given a value of 26 for each. Similarly, the values of the lower and upper values for changes in NO_3^- and NH_3 flux, and the cost function were 22, 24, 22, 26, 23 and 26 respectively. The values were summed for each parameter (in this case, the answer being 195). 195 was the largest summed value out of all parameters, and so *MeanFlux* was given a value of 1 (*i.e*, it was the most sensitive parameter in this experiment). This procedure was repeated for Experiment SA2a and Experiment SA2b. The three results were then scored by summing, and then sorted. The resulting

ranked list is shown in Table 5.2, along with their overall ranked score; for example, *MeanFlux* was ranked first in both SA1 and SA2b, and third in SA2a; the sum of these ranks is 5. As seen in Table 5.2, 5 is the lowest overall ranked score of all parameters, and hence the overall rank of *MeanFlux* was one.

Table 5.2: The rank and overall ranked score for each of the parameters using the method described in the text

Parameter	Overall rank	Overall ranked score
Mean carbon flux to the sediment	1	5
O_2 in overlying bottom water	2	10
Nitrogen to Carbon ratio in fast degrading organic matter	3	12
NH_3 in overlying bottom water	4	18
Bioturbation coefficient	4	18
Rate of nitrification	6	22
Proportion of fast degrading organic matter	7	24
O_2 diffusion coefficient	8	26
NO_3^- in overlying bottom water	9	27
NH_3 diffusion coefficient	9	27
Nitrogen to Carbon ratio in slow degrading organic matter	11	28
Rate of oxidation of fast degrading organic matter	11	28
Oxygen demand units diffusion coefficient	13	33
NO_3^- diffusion coefficient	14	36
Half-saturation concentration of NO_3^- in denitrification	15	49
Rate of oxidation of oxygen demand units	15	49
Half-saturation concentration of O_2 in nitrification	17	53
Advection rate	17	53
Rate of oxidation of slow degrading organic matter	19	57
Mixed layer depth	20	58
Half-saturation concentration of NO_3^- inhibiting anoxic mineralisation	21	61
Half-saturation concentration of O_2 in oxidation of ODU	22	66
Half-saturation concentration of O_2 in inhibiting denitrification	22	66
Half-saturation concentration of O_2 in oxic mineralisation	24	67
NH_3 adsorption coefficient	25	71
Half-saturation concentration of O_2 inhibiting anoxic mineralisation	26	78

n.b. where 2 parameters had equal scores, the parameter with lowest variance was ranked more highly

This quantification of the sensitivity supports the conclusions that were made during the earlier visualisation process. In general, the parameters to which the model is most sensitive are those for which there is greatest understanding biogeochemically, are relatively easy to measure both *in-situ* and under controlled laboratory conditions, and which are known to have significant effects in natural systems. For example, the most sensitive parameter is the flux of carbon to the sediment. As this is the forcing parameter (i.e. the parameter which drives the kinetics and biogeochemistry of the rest of the system), it would be expected that the model should be particularly sensitive to it. The next five most sensitive parameters were overlying O_2 concentration, nitrogen:carbon ratio in fast degrading organic matter, overlying NH_3 concentration, bioturbation coefficient and rate of nitrification, which are all parameters for which observational data is available.

5.3 Discussion

These sensitivity analysis experiments have shown that only a small number of the 26 parameters tested have a significant impact on the model outcomes that have been looked at. As an attempt will be made to fit the model to observations carried out on experimental work in the North Sea, it is particularly useful to know which parameters are likely to influence the outcomes most. The fitting experiments will use a range of techniques, and will initially focus on adjusting the six parameters identified in this section, with the hope that most of the fitting will be carried out by only using these parameters. Adjusting the values of the remaining 20 parameters is likely to have a minimal effect on the outcome of the model.

The results from these experiments, however, have shown the impact that changing the values of the parameters in a complex non-linear model has on its outputs. In a simple, linear model with two parameters, it would be expected the outcome by doubling each of them individually would be proportional. However, in OMEXDIA, we see that this does not hold true. The differences between Figures 5.2 and 5.3 show that, even by increasing each of the parameters by a fixed amount (in this case, each of the upper parameters in Figure 5.3 are five times higher than they are in Figure 5.2), but the percentage changes seen are clearly not proportional to each other. This could have a bearing on any fitting experiments, if large changes (on the scale of at least one order of magnitude) to some parameters are needed.

Further sensitivity studies could be made, but would require some modification to OMEXDIA. For example, in the natural environment, the impact of bioturbation on sediment reworking has been observed to be affected by the POC sedimentation rate, with a simple early-diagenetic model showing that varying the imposed bioturbation

mixing rate has little effect at high sedimentation rates, but that at lower sedimentation rates, the relationship between the bioturbation mixing coefficient and the burial efficiency is almost linear (Martin and Sayles 1994). However, even though OMEXDIA calculates a bioturbation profile, based on a mixed layer depth and a bioturbation coefficient, there is no coupling between this and the POC flux. This means that there will be no change in the bioturbation for different POC fluxes. However, as early diagenesis does depend on the bioturbation in the sediment, changing the value of the bioturbation coefficient will alter the organic carbon degradation (and, as a result, the fluxes of O_2, NO_3^- and NH_3).

A further improvement which could be made, but was not done in this work due to time constraints, is the decoupling of all the adsorption linear equations, an example of which is shown in Equation 5.3; a generic form of this equation is shown in Equation 5.4 (Berner 1980; Li and Gregory 1974)

$$D^T = \alpha T + D^0 \qquad \text{Eqtn 5.4}$$

where D^T is the diffusion coefficient in a free solution at T°C, α is an ion-specific coefficient, and D^0 is the zero degree coefficient. By modifying the model, it would be possible to include temperature and the remaining eight parameters (α and D^0 for the diffusion coefficients of O_2, NO_3^-, NH_3 and ODU). These nine parameters could all then be included in the Genetic Algorithm (see Section 5.2), and fitted values could be obtained. However, the calculated values for D^0 (calculated from earlier work presented in Robinson & Stokes (1959), and from which values for α were derived, as published in Soetaert *et al*. (1996b)) are still the most comprehensive set of diffusion coefficients available in the literature; the fact that some (chloride, sulphate, sodium and calcium ions) of the calculated values shown in Table 1 of Li & Gregory (1974) have been verified by experimental work both in sea-water and sediment agar samples, it would be difficult to determine ranges for these parameters, and whether the values obtained would be more or less valid than the values used here. Further to this, there is advice in the literature that there should not be an over-reliance on modelled data. Although models are obviously invaluable in increasing our understanding of the natural environment and its systems, Anderson (2010) argues that mathematics is "'unreasonably effective' at describing phenomenon', and this is especially the case where there are many free parameters due to the model being complex. Anderson (2005, 2010) also warns that models often incorporate processes that aren't fully understood. Although diffusion is a well understood theory which has been backed-up by experimental work, not only by Li & Gregory (1974), but also by numerous other authors, such as Ullman & Aller, (1982), McDuff & Ellis (1979), Krom &

Berner (1980) and Iversen & Jørgensen (1993), I do believe that advice about keeping models as simple as possible should be heeded, and, as such, it can be argued that where reliable real data exists, this should be used if there is no evidence that the model will help determine a more accurate value.

5.4 Parameter Optimisation

One important step in model development is to match model output to experimental data, which is often done via a technique known as *parameter optimisation*. In a parameter optimisation exercise, the values of some of the model parameters are varied until the model output best matches the experimental data. There are a number of optimisation techniques, ranging from simply varying one or more parameters and judging the output visually, to using more complex algorithms such as a Monte Carlo approach or implementing a genetic algorithm (GA), from which the difference between experimental data and model output can be quantified.

As an initial exercise, optimisation was carried out by varying the values of the 6 most sensitive parameters, by choosing values for each of them that seemed sensible based on the results presented in Soetaert *et al*. (1996b), and information in the literature. However, it was quickly concluded that this was an inefficient approach. Due to the highly non-linear relationship between parameters, results could not be predicted, making it difficult to judge the extent that each parameter should be adjusted based on previous model runs.

Previous work has shown that although diagenetic models can replicate experimental results of the environments they have been designed to represent (Soetaert *et al.* 1996b), it is believed no-one has previously used a GA approach although they are common in other branches of ecosystem and biogeochemical modelling (e.g. Ward *et al.* 2010). Due to their use in other environmental modelling scenarios, a GA approach was used for the work in this chapter. Using parameter optimisation to fit model output to experimental data has the benefit of showing that the model is a suitable tool to study this environment, and also enables values of model parameters to be determined. Where these parameters mirror observations taken in the field it can also be used as a method for estimating values for these parameters in other environments, which can be particularly helpful when observational data is difficult to obtain. In particular, as discussed in earlier chapters, OMEXDIA has a number of parameters which have no experimental parallel due to the Monod kinetics employed in OMEXDIA. The use of a GA could help determine values for these parameters which would otherwise be difficult to estimate.

5.4.1 Parameterisation of OMEXDIA

The results of the sensitivity analysis shown earlier in this chapter are an ideal starting point in the use of a GA. The genetic algorithm approach used was a micro genetic algorithm (μGA), which is a technique comparable to natural selection. The method used was the same as described in detail by Ward *et al*. (2010), and the basics are given here. The μGA is allowed to pick a random value within a set range for each of the unconstrained parameters; the parameter vector that this generates is known as a '*species*'. The ranges are given to the algorithm in advance, and are selected to be representative of values which are deemed sensible.

Initially, following on from the result of the sensitivity analysis, the six parameters deemed most sensitive to model output (*MeanFlux*, *pFast*, *rSlow*, *rFast*, *NCrFdet* and *biot*) were used in these optimisation experiments. The ranges for these parameters were decided in different ways; *rFast*, *rSlow*, and *biot* were given values of one order of magnitude either side of the default value used previously, while *pFast*, *NCrFdet*, and *NCrSdet* were given ranges based on extremes found in the literature values for shelf-sea systems (ranges of 0.5–0.99, 0.14–0.2 and 0.10–0.13 respectively); increasing the upper value for the latter three parameters by an order of magnitude would not make sense from a biogeochemical point of view.

The model was run 6 times (*n*), each time with a different random parameter set; 6 is the number of unconstrained parameters as listed above; this set of *n* runs is collectively known as a generation. After each generation, the species with the smallest *misfit* value (i.e. closest to the observational data) is passed unchanged to the next generation. This misfit is calculated in a sum of least squares method, with the sums of the differences between the observational data points and the modelled values at each layer depth being summed to give an integrated misfit value for the entire sediment column for each chemical species (O_2, NO_3^- and NH_3). The integrated misfit values for each of the three chemical species were then also summed to give a final misfit value for each of the species in the generation.

The remaining five species for the next generation are then determined using weighted genetic crossover. Probability, weighted according to the size of their misfit, is used to combine two species (i.e. the lower the misfit of a species, the more likely it is to be picked to be combined with a different species). Combination is analogous to genetic crossover, such that a single random point is picked along the parameter vectors, and all the values past this point are swapped between the two species. This

is repeated until the five remaining species necessary for the next generation have been generated.

After a prescribed number of generations, the species with the lowest misfit value from the final generation is returned as the set of parameters from this GA run that has both the highest accuracy and precision when compared with the experimental data. All of the GA experiments described in this chapter have been run for 5000 generations. 5000 was initially picked as it was likely to be a good compromise between the computational time taken for the algorithm to be run, and the chance of the GA being allowed to run for enough generations to get a set of parameters that represented the data well (pers. comm. A.P. Martin, 2010).

The experimental data used in the GA experiments have been gathered from the North Sea as part of the Marine Ecosystems Connections Program (Cefas 2011). Over the course of three years (2007-2009), a series of cruises were carried out allowing physical, biological and chemical data to be collected at three sites (North Dogger, Oyster Grounds and Sean Gas Fields) at four different times of year (pre-Spring Bloom, post-Spring Bloom, post-Summer bloom / autumn and Winter). The biogeochemical data includes organic carbon content, and concentrations of O_2, NO_3^-, and NH_3. Full site details and some preliminary results can be found in Greenwood et al. (2010). Some additional adaptations to the algorithm described by Ward *et al*. (2010) have been made, to account for idiosyncrasies with the experimental data used. The number of study sites visited, the number of cores taken and the number of repeat measurements for some of the chemical species varied between each different cruise. The genetic algorithm calculates the misfit between the modelled value and the value of all observations at each observed depth for each chemical species. The results for each species are then summed to give a total misfit value for that generation. However, as all observational values are compared with the modelled data, there is potential for bias to occur if the number of profiles for each chemical species is not accounted for, and for those chemical species that had more repeat measurements to have greater influence over the final GA result. To correct for this, the misfit value for each chemical species at each depth is divided by the variance of the observed values at that depth (i.e. the square of the standard deviation divided by the number of valid data points). Care was taken for the data to be corrected for missing data points in the observational data; without this correction, the cost function for a chemical species which had missing data points at a given depth would have been slightly underestimated.

Due to both the nature of the genetic algorithm approach, and the high non-linearity of the model, it is impossible to know, for any given parameter range, whether

the parameters returned after the 5000th generation are in fact the parameters which would give the best fit to the data. As a result of this, each genetic algorithm experiment was repeated ten times with different initial conditions but with no changes in the range of each parameter; it was decided that this number of runs would not be too computationally intensive but would still give a good assessment of the μGA approach.

As it had been established that a suitable fit could not be found with only using six of the parameters, it was decided that an iterative approach would be taken to discover how many parameters would be needed for a suitable optimisation. The experiments were repeated, each time using the three next most sensitive parameters (as determined in the earlier Sensitivity Analysis, and shown in Table 5.2).

Initially, in a similar manner as above, the six most sensitive parameters were used, and allowed to vary by double and half of the default OMEXDIA parameters, except when experimental values from the MEC project were available, when the observed range was used. The default parameters were based on continental slope data, and it was unknown if the values of these parameters, particularly for the parameters involved in the Monod kinetics, are likely to be appropriate for shelf-sea systems. It was therefore decided to allow the constrained parameters some freedom, and they were allowed to vary by ±10%. At the end of each experiment, the profiles generated from each of the 10 repeat runs were visually compared with the observational data. To provide a more object measure, the run which generated the lowest mean misfit value was also the run which produced the profiles which appeared closest when assessed by eye.

For each set of experiments where the magnitude and shape of the calculated profiles did not correlate with the observational data, the number of free parameters was increased by three (each set of three being the three next most sensitive parameters) before rerunning the μGA. This approach was initially chosen to limit the computational effort required; however, it became clear that sensible fits were not being generated when a limited number of parameters were used. This method was followed until all 26 parameters were used (the final experiment used only two more parameters than the previous experiment). No satisfactory fits were found even when all parameters were used with the ranges set as they were. As an example of the output produced, Figure 5.8 shows the output from the 10 repeat runs using all 26 parameters, using the default parameter ranges. It can be seen that none of the modelled profiles generated show good fits to the observed data

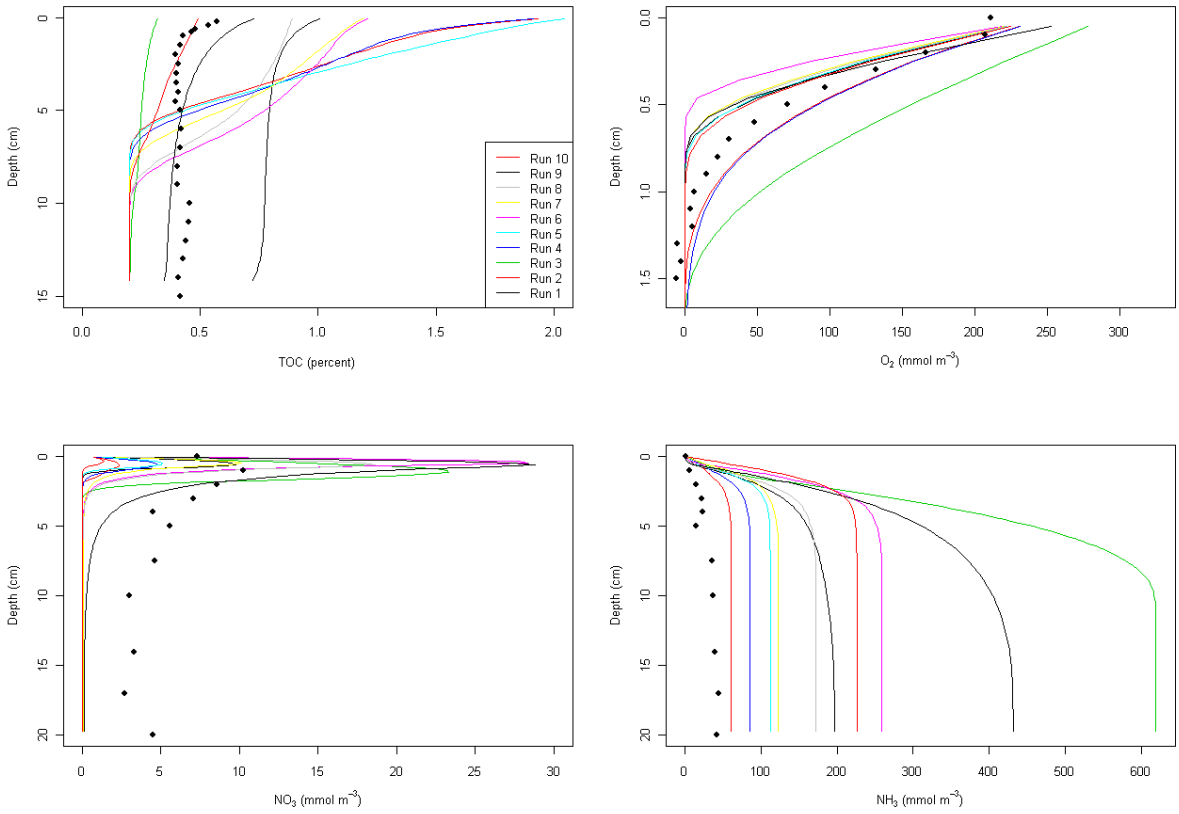

Figure 5.8: Modelled profiles of using default parameter ranges (see text for details); for clarity, the observational data (solid circles) being optimised against are the means of all the observational data used in the optimisation. These are the means of 5 profiles (TOC), 14 profiles (oxygen), 9 profiles (nitrate) and 5 profiles (ammonia) from the North Dogger site in 2008

As a result of this, a final experiment (Experiment 2) was therefore also carried out where all 26 parameters were allowed greater freedom. Once again, an iterative process was used, running the μGA multiple times with all model parameters. After each iteration, the output was assessed visually, and modifications were made to the ranges of the parameter set given by the algorithm. Where the μGA calculated a value for a parameter which was one of the two boundary values of the given range for that parameter, an increased range was given to that parameter, with the increase being double that of that boundary value when the upper boundary was reached, and half when the lower boundary was reached. However, the ranges of those parameters for whose range was that observed in the experiments carried out as part of the MEC project were not increased. By the end of this iterative process, the given ranges of some was up to two orders of magnitude; Table 5.3 contains full details of the parameter set generated using in this run. The final iteration was the one where a representative fit for the data was found, as assessed visually.

Finally, Figure 5.9 shows the decrease in the value of the misfit through the final run of the algorithm, when all 26 parameters were used. As can be seen, the misfit reduces rapidly, and decreases from 684080 after the initial generation to 580590 after the 20th generation; the misfit cost then decreases gradually, to a final value after the 5000th generation run to 557370. This not only shows that the GA method is suitable for generating parameter values that will match experimental data, but that it will do so in a relatively short period of time. A 5000 generation run takes approximately 25 hours on a single processor of IRIDIS, Southampton University's high-performance computing cluster; and so the initial large drop in the misfit value takes less than 10 minutes.

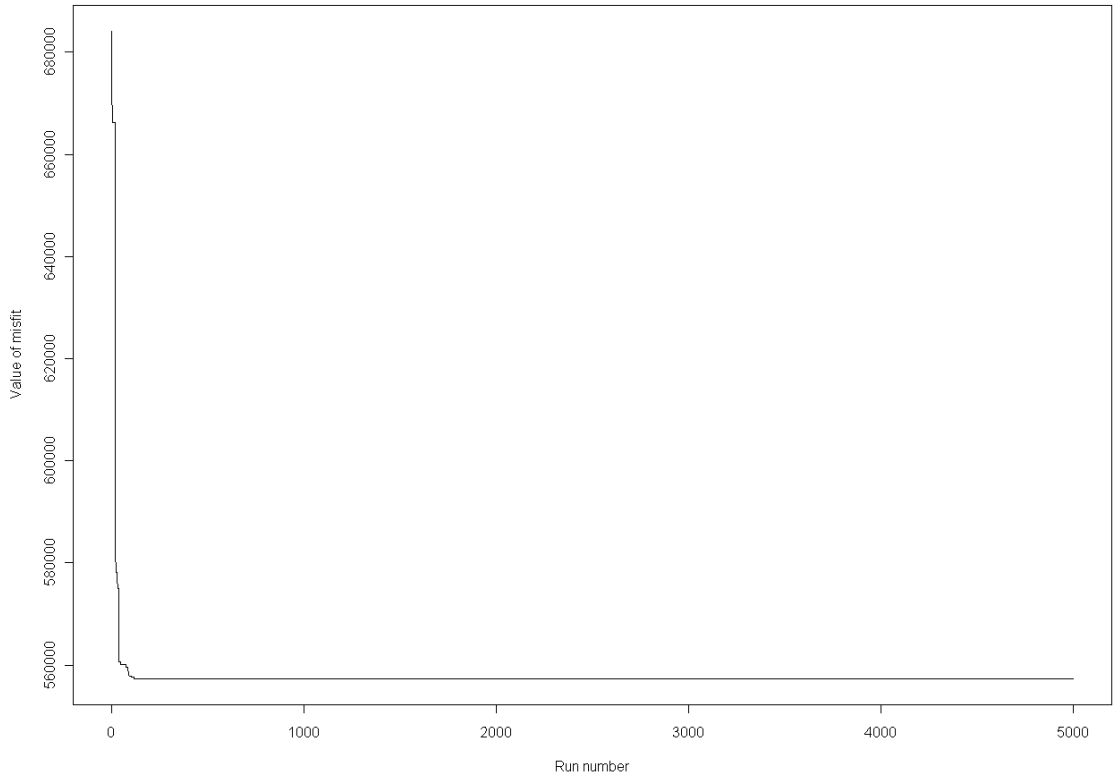

Figure 5.9: Graph to show the decrease in misfit between model output and observational data during a 5000 generation GA experiment

Table 5.3: Results of the Genetic Algorithm experiments described in the text (units as in Table 2.2)

Parameter	GA output (all data)[a]	GA output (2007 data)	Comparisons[b]
Mean carbon flux to the sediment	19.1	16	31–130 [1–3]
O_2 in overlying bottom water	248.27	248.27	–
Nitrogen to Carbon ratio in fast degrading organic matter	0.14	0.14	0.05–0.3 [4–7]
NH_3 in overlying bottom water	0.54	0.25	–
Bioturbation coefficient	0.044	0.039	0.0002–0.2 [5,8–10]
Rate of nitrification	49.14	90	0.86–143 [11,12]
Proportion of fast degrading organic matter	0.952	0.730	–
O_2 diffusion coefficient[c]	1.22	1.19	0.67–0.86 [13]
NO_3^- in overlying bottom water	1.5	0.1	–
NH_3 diffusion coefficient[c]	1.01	1.25	0.432–4.32 [14–19]
Nitrogen to Carbon ratio in slow degrading organic matter	0.13	0.11	0.05–0.3 [4–7]
Rate of oxidation of fast degrading organic matter	0.097	0.1	0.002 to 0.101 [20–24]
Oxygen demand units diffusion coefficient	1.202	1.079	0.328–0.536 [18,25,26]
NO_3^- diffusion coefficient[c]	1.35	1.35	1.73–4.32 [14,27,28]
Half-saturation concentration of NO_3^- in denitrification	106.7	64.29	–
Rate of oxidation of oxygen demand units	0.57	2.14	–
Half-saturation concentration of O_2 in nitrification	100	4.9	–
Advection rate[d]	2.39×10^{-6}	2.14×10^{-6}	6.85×10^{-5} – 1.10×10^{-3} [1,20,21]
Rate of oxidation of slow degrading organic matter	4×10^{-4}	1×10^{-3}	0.002 to 0.101 [27,28,33]
Mixed layer depth	15	9.0	2–20 [2,8,9]
Half-saturation concentration of NO_3^- inhibiting anoxic mineralisation	7.96	4.50	–
Half-saturation concentration of O_2 in oxidation of ODU	9.37	10	–
Half-saturation concentration of O_2 in inhibiting denitrification	10	10	–
Half-saturation concentration of O_2 in oxic mineralisation	29.1	30	–
NH_3 adsorption coefficient	8.71	13	0.8–1.9 [29]
Half-saturation concentration of O_2 inhibiting anoxic mineralisation	0.73	0.1	–

[a] The value of the parameter given by the best fitting genetic algorithm output
[b] Values aren't given where the parameters are formulated purely for the model (e.g. half-saturation constants). Values are also duplicated where experimental work is unable to separate values between separate model parameters (e.g. differentiating between fast and slow degrading organic matter)
[c] n.b. For diffusion coefficients, values have been compared directly with values cited; the coefficient hasn't been compared with theoretical D^Ts (i.e. calculated using equations in Li & Gregory (1974) using T from the papers cited)
[d] diagenetic models tend to use the term 'advection rate', whereas experimental work often measures only 'sedimentation rate'. Given the lack of data in the literature for 'advection rates', for the purposes of comparison here, they are treated as the same parameter so that they can be compared like-for-like (the values shown in the 'comparisons column' are reported 'sedimentation rates'). However, sedimentation only takes into account that material which is accumulated at the sediment-water interface. Advection would normally be interpreted as a function of depth that not only considers sedimentation, but also the impact of compaction that will occur throughout the sediment column. However, in OMEXDIA, advection is a depth-independent parameter, with units of cm d^{-1}. Given that sedimentation rate will include organic matter which will be degraded, whereas advection will be the integrated rate over the whole sediment column, it is not surprising that sedimentation rate is higher than advection rate.

[1] de Haas & van Weering (1997)
[2] Anton *et al.* (1993)
[3] Gargas *et al.* (1980)
[4] Jossain *et al.* (2011) – n.b. this N:C ratio is in water column OM
[5] Beck *et al.* (2009)
[6] Rusch *et al.* (2000)
[7] Van Cappellen & Wang (1996)
[8] Mouret *et al.* (2009)
[9] Arndt & Regnier (2007)
[10] van der Zee *et al.* (2002b)
[11] van Raaphorst *et al.* (1990)
[12] Smits (1980)
[13] Revsbech *et al.* (1980)
[14] Rutgers van der Loeff (1980b)
[15] Kamiyama *et al.* (1976) – n.b. sediment temperatures not given
[16] Emerson *et al.* (1984)
[17] Aller (1980)
[18] Krom & Berner (1980)
[19] Li & Gregory (1974)
[20] Epping *et al.* (2002)
[21] van Weering *et al.* (1987)
[22] Andersen (1996)
[23] Huettel *et al.* (2007)
[24] Westrich & Berner (1984)
[25] Goldhaber *et al.* (1977) n.b. sulphate values used to represent ODU
[26] Iversen & Jørgensen (1993)
[27] Vanderborght & Billen (1975)
[28] Jensen *et al.* (2005)
[29] Mackin & Aller (1984)

5.5 Results from the Genetic Algorithm Experiments

Figure 5.10 shows the result from one μGA run where the resulting profiles match the observational data relatively well. As can be seen in Figure 5.10, the algorithm is mainly able to accurately represent the carbon profile, despite the large differential in profile shape between what would be expected in continental slope and abyssal plain sediments, which OMEXDIA was originally written for, and continental shelf sediments as shown in this thesis. The profiles shown in Chapter 2, where OMEXDIA was run using its default parameter set, show expected profiles for continental slope sediments; however, Figure 5.10 shows that carbon concentrations do not decrease steadily throughout the sediment, and instead decreases from a mean of 0.57% to 0.43% in the top 10 mm before remaining relatively constant. The algorithm is not, however, able to resolve the very fast degradation of the OM in the top 10 mm, with the TOC values decreasing from a maximum of 0.45% in the uppermost layer to a mean value of 0.42% below 10 mm. This is the same mean value as the observations in the sediment below 10 mm. The oxygen profile, which shows the oxygen penetration depth (OPD) as being approximately 12 mm, is correctly represented, as is are the ammonia profiles used in this μGA run. Figure 5.10 also

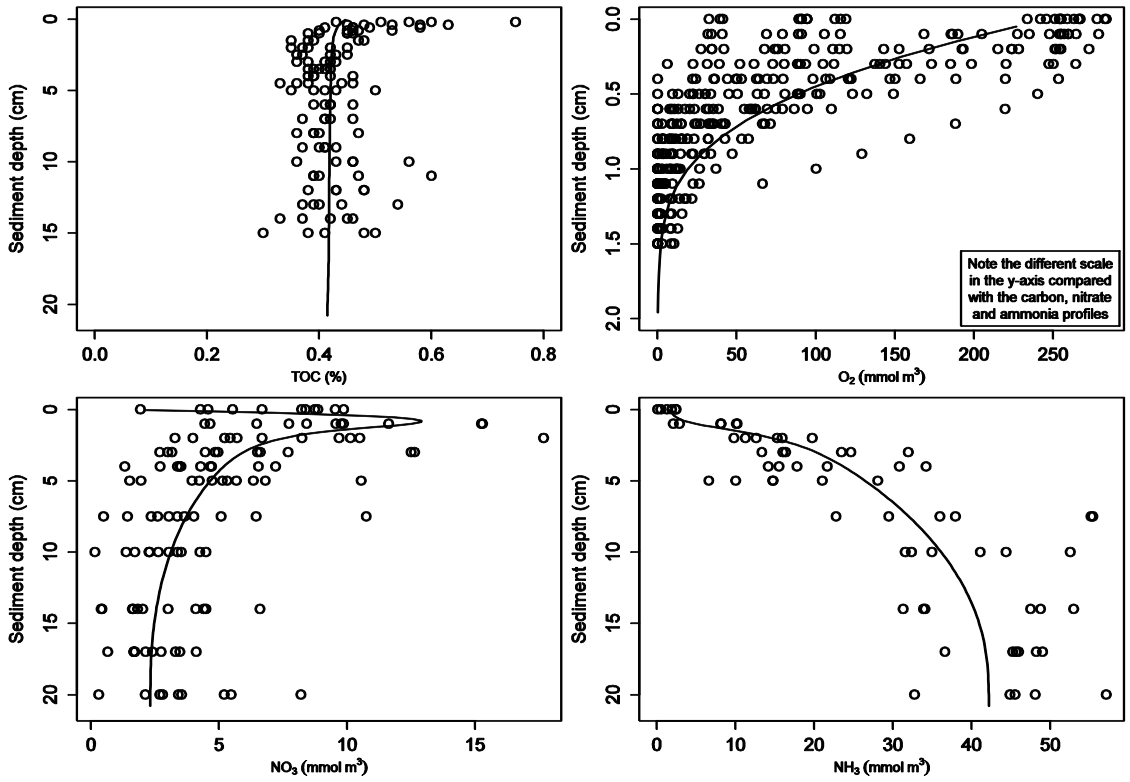

Figure 5.10: Best fitting profiles from Experiment 2, using all available data to fit model output. Note that the profiles show the mean concentrations from multiple cores from each cruise

shows the algorithm's ability to correctly generate both the concentration magnitude (12.9 mmol m^{-3}) and depth (8 mm) of the nitrate peak (which is caused by nitrification in the oxic zone, above the denitrification boundary, and therefore falls within the oxic zone), before the decrease in concentration of nitrate due to its use as an electron acceptor, although there appears to be two outliers in the nitrate peak. The oxygen profiles show some temporal variability, but no variability is seen in the remaining profiles. The variability in the oxygen is as a result of the large quantities of OM being deposited soon after the spring bloom, causing an increase in the consumption of oxygen, and hence decreasing the OPD. In winter, when low primary productivity in the overlying water column decreases the OM flux to the sediment, the OPD is increased. Although it would be possible to generate a parameter set for the individual oxygen profiles, it would not be possible, using the current version of OMEXDIA, to generate a single parameter set that would provide a fit for each of the oxygen profiles and the mean profiles of TOC, NO_3^- and NH_3.

A second GA experiment was carried out, using only North Dogger site data from the 2007 cruises. This allowed us to validate the results against the North Dogger 2008 data, to see if the model had any temporal predictive ability. For this μGA run, the same ranges were used as in the first μGA experiment. The fit from the 2007 data can be seen in Figure 5.11, showing, as would be expected, a relatively good fit; as when using the whole data set, the model does not resolve the very fast decay of OM in the top 10 mm. The TOC profiles do show a sharp decrease in the top 2 mm, particularly in February, from a value of 0.75% to a value of 0.45%. By 6 mm, the mean value of TOC is 0.48%, falling to 0.41% at 150 mm. The relatively high values in the top 2 mm are due to high concentrations of labile organic matter in the oxic zone close to the SWI, before being oxidised by oxygen and nitrate. The model appears to slightly over-estimate the OPD by approximately 3 mm, although this is likely to be affected by the oxygen profile in February 2007, which is almost certainly caused by a worm-hole, significantly increasing the oxygen concentrations that would otherwise be expected. The nitrate peak also seems to be slightly over estimated (the model peak concentration is 9.6 mmol m^{-3}, in comparison with a maximum observed value of 6.68 mmol m^{-3}), although without much higher resolution in vertical profile measurements, this would be difficult to verify. The ammonia profile shows the expected increase in concentration as OM is oxidised, before the concentration stabilises, implying that this is below the depth at which all labile OM has been oxidised. The modelled mean ammonia concentration in this zone is 49.2 mmol m^{-3}, compared to an observed mean value of 51.6 mmol m^{-3}.

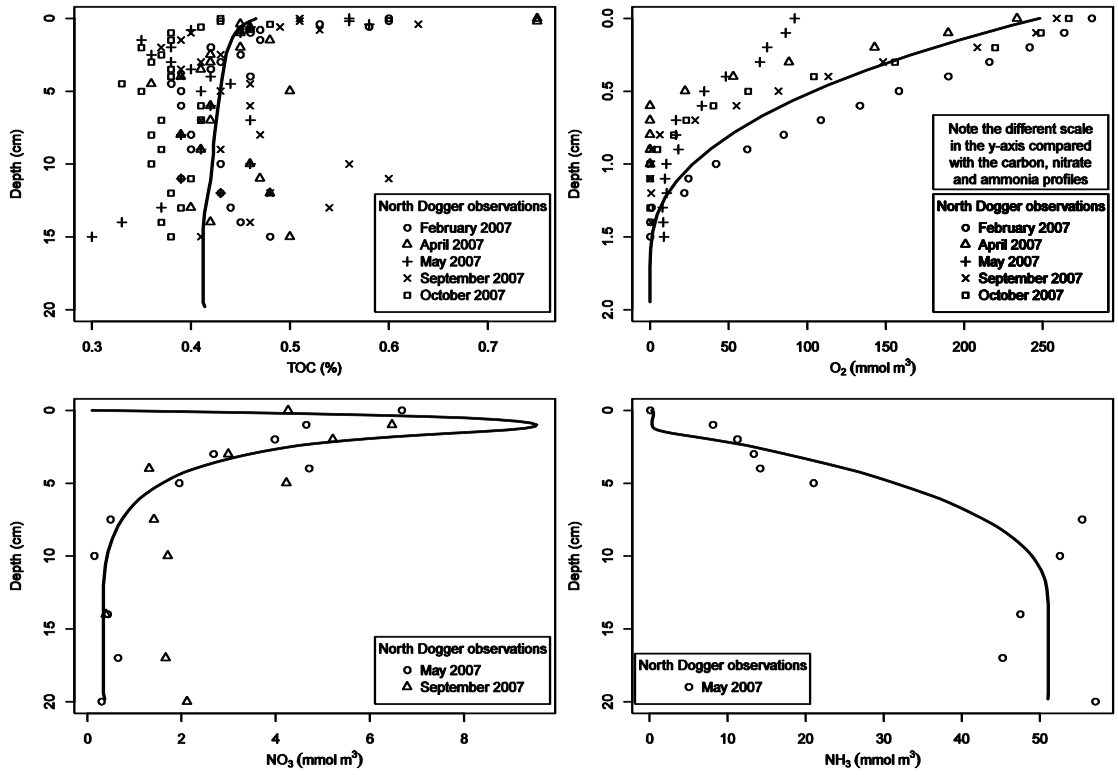

Figure 5.11: Best fitting profiles from Experiment 2, using only 2007 data to fit model output. Note that the profiles show the mean concentrations from multiple cores from each cruise

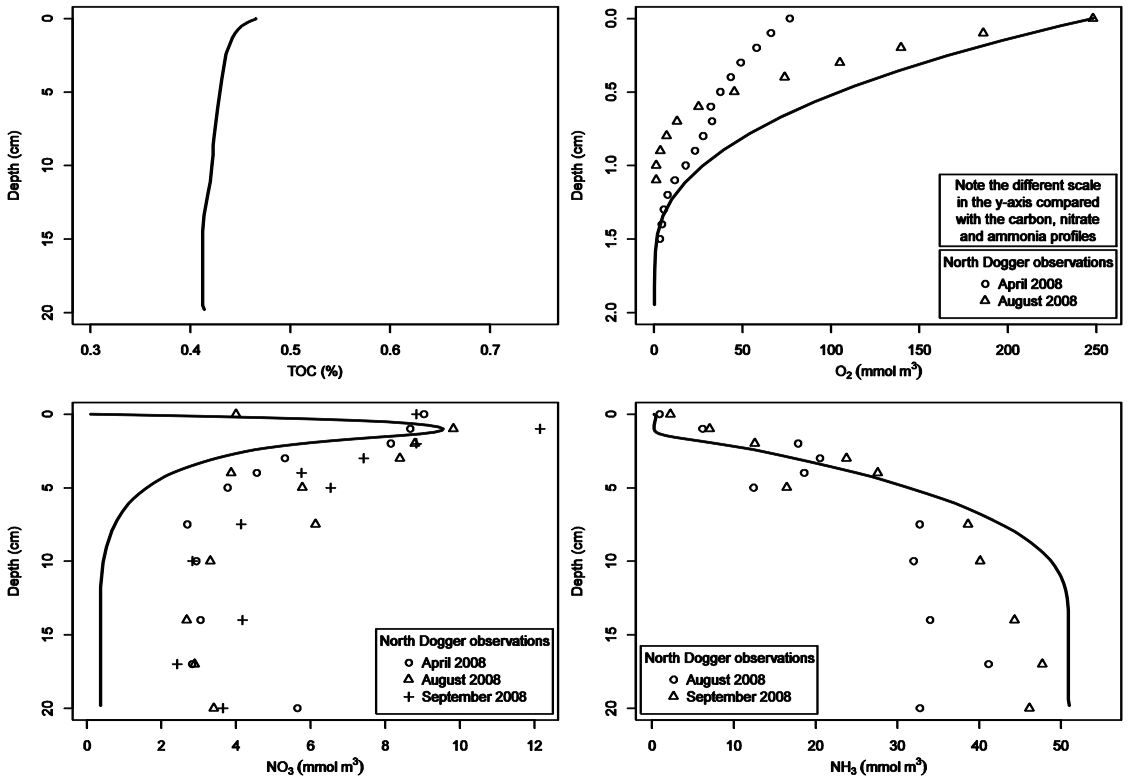

Figure 5.12: Model output profiles from Experiment 3, with 2008 observational data. Note that the profiles show the mean concentrations from multiple cores from each cruise

Figure 5.12 shows model output using the parameter set obtained from this GA run against 2008 data (no TOC data is yet available from the 2008 cruises); however, experimental data from the 2008 cruises replaced the optimised values for three parameters (bottom water concentrations of oxygen, nitrate and ammonia). As no carbon data are yet available from 2008, the N:C ratios have continued to be set as the 0.086 and 0.16 in the slow and fast degrading organic matter respectively. The model slightly overestimates oxygen concentrations for the 2008 data, and also overestimates the OPD by approximately 5 mm. Although the model estimates the concentration (9.6 mmol m^{-3} compared to the observed value of 10.5 mmol m^{-3}) and depth (10 mm) of the nitrate peak well, it slightly underestimates the nitrate concentration in the sediment below this point. Nitrate concentrations never reaching zero in the observations implies that there is sufficient nitrate to oxidise all available labile OM; this is also reflected in the ammonia concentrations, which stabilise at approximately the same depth (75 mm) as nitrate concentrations. The ammonia model profile matches the observations well, with the ammonia concentrations stabilising approximately only 3 mm below the observations. The modelled ammonia concentration in this zone is 50.9 mmol m^{-3}, compared to an observed value of 39.8 mmol m^{-3}.

5.6 Discussion

Although the results shown in this chapter indicate that data from different environments for which it was intended can be fitted to OMEXDIA, this was only achieved at a large computational expense. Each single μGA took approximately 25 hours to complete on a single processor of IRIDIS (the University of Southampton's High Performance Computing Cluster), and more than 50 runs were completed; however, due to the large number of parameters, the wide range of parameter space used, and the fitting algorithm employed by a μGA (Ward *et al.* 2010), there is still unspecified uncertainty as to whether the set of parameters shown here are the best possible fit.

Although there are recognised uncertainties in the methods and limitations in the data, the μGA used here has come very close to recreating the profiles shown by the experimental data despite OMEXDIA originally being designed to fit profiles found in continental margin areas (Soetaert *et al.* 1996b; Soetaert *et al.* 1996a). The observational data used here do not show highly stereotypical profiles for early diagenesis. For example, the largely vertical carbon profiles from the 2007 data do not show a decrease of carbon with depth, as would normally be expected. This is most likely to be attributed to the importance of the benthic fluff layer; benthic fluff

was observed above the sediment-water interface (SWI) during these cruises (pers. comm. E.R. Parker); there is also a wide spread of data at all depths in the sediment column, possibly attributable to the high productivity in both the water column and sediment leading to a relatively large density of macrozoobenthos in these sediments (Baptist *et al.* 2006). The TOC profiles imply that the benthic fluff contains the vast majority of fast degrading organic matter (although it is important to bear in mind that, although OMEXDIA contains three carbon fractions, the reality is that the TOC is composed of large number of carbon compounds degradable over a wide spectrum of time scales). The values of TOC observed between 6 and 150 mm are in line with other observations from similar areas of the North Sea (e.g. Upton *et al.* 1993; van Raaphorst *et al.* 1990; van Raaphorst and Malschaert 1996; Boon and Duineveld 1998; de Haas *et al.* 1997). It is therefore likely that the majority of fast degradable OM is mineralised in the water column, leading to only slow degrading OM being mineralised in the sediment. The profiles of O_2, NO_3^- and NH_3 agree with this interpretation of the TOC profile. The oxic water column is able to mineralise all of the fast degradable TOC that is in the benthic fluff layer, and also leads to an oxic sediment. The oxygen in the sediment is rapidly consumed, by both mineralisation of OM and by oxidation of ammonia to nitrate, leading to the nitrate peak which coincides with the oxic-suboxic boundary. NO_3^- is reduced to NH_3 below this boundary, leading to the slight decrease in TOC as already described, and also leading to the increase of NH_3 as shown in Figure 5.12.

The profiles do show specific patterns. Oxygen in particular shows very strong seasonal trends; as a result of the spring bloom, O_2 concentrations at the SWI drop from 200 mmol m^{-3} in February 2007 to ~90 mmol m^{-3} in April 2007, recovering to pre-spring bloom values by September. However, by a sediment depth of 10 mm, there is little spread in the concentrations of O_2. Perhaps rather surprisingly, there is little seasonal spread of either NO_3^- or NH_3 in both 2007 and 2008. This could be used as an argument that the system is in some sort of quasi-steady state. It should also be noted that Figures 5.10 and 5.11 show the mean profiles, whereas Figure 5.12 shows all data as discrete data points. Given that the genetic algorithm uses each data point, it can be argued that there is bias towards those cruises when more data was collected. The oxygen profile in Figure 5.10 also clearly shows a burrow structure, with increased O_2 concentrations in 1 profile from the SWI down to 13 mm; this may have also slightly affected the fit of the parameters. The fitted parameters led to interpretable model profiles typical of the system studied.

The values of each parameter after being fitted by the μGA are shown in Table 5.3, along with parameter values from the original OMEXDIA model. The values for the five most sensitive parameters show relatively sensible values (e.g. an increase in the bioturbation coefficient from 0.0027 cm^2 d^{-1} to 0.047 cm^2 d^{-1} seems realistic considering the difference in benthic biological activity between low productivity continental slopes and relatively high productivity shallow coastal seas). The estimated bioturbation coefficient also resembles the values derived from experimental work, as shown in Table 5.3. More surprising is the value of the mean POC flux to the sediment of 16 g C m^{-2} yr^{-1}. Compared to previous estimates of carbon fluxes in the North Sea, this is particularly low, with ranges given in the literature for high productivity areas being between 31 and 130 g C m^{-2} yr^{-1} (de Haas and van Weering 1997; Anton *et al.* 1993; Gargas *et al.* 1980). However, this could, again, be explained by the fact that the majority of the fast degradable carbon is mineralised in the water column; if the carbon flux to the benthic fluff layer could be measured, it is highly likely that this would be higher and would be comparable to previous estimates (Bale and Morris 1998; Jago and Jones 1998; Jones *et al.* 1998; Jago *et al.* 2002).

Although all parameter values are listed in Table 5.3, it should be noted that care is needed when attempting to interpret these figures. The vast majority of parameters in the model are associated with the Monod kinetics of the model formulation (Boudreau 1997a), and are parameters that are not routinely measured during observational work. In particular, the half-saturation constant values represent the concentration of the oxidant which can carry out the reaction at 50% of the fastest theoretical rate; the only method to obtain values for these parameters is to fit observed data to model output. It is therefore difficult to make comparisons of the values of these parameters between different environments (e.g. sediment composition, water depth *etc.*). Other parameters, such as the rates of the reactions, do have a more tangible meaning, and it is relatively easy to make comparisons between them and the values obtained in experimental situations. For example, degradation of bacterial matter has been studied with results ranging from 0.002 to 0.101 d^{-1} in oxic coastal environments (Huettel *et al.* 2007; Westrich and Berner 1984; Jensen *et al.* 2005; Andersen 1996; Sun *et al.* 1991), showing that this study's μGA result of 0.0576 d^{-1} for fast degrading organic matter is a realistic estimate; given that previous experimental work has tended to concentrate more on highly labile organic matter, a μGA result of 0.0001 d^{-1} for slow degrading organic matter also seems reasonable. The μGA generated values for five parameters which were outside of the range found in the literature. Three of these parameters were diffusion coefficients (oxygen, nitrate and ODU). The ODU diffusion coefficient in Table 5.3 was compared with the diffusion coefficients for the constituent species of ODU (Mn^{2+}, Fe^{2+} and S^{2-}), and so it is difficult to compare these like-for-like. The optimised value for the

oxygen diffusion coefficient was slightly larger than the values reported in the literature, by 0.36 mmol m^{-2} d^{-1}, while the optimised nitrate diffusion coefficient was smaller than the lowest literature value by 0.38 mmol m^{-2} d^{-1}. Given that the literature range for the oxygen diffusion coefficient is very small, and only from one study in a brackish estuary, and that the range for the nitrate diffusion coefficient is 2.59 mmol m^{-2} d^{-1}, the values generated by the algorithm seem reasonable. The value of advection generated is only 6% lower than the range given in the literature, and so again this seems a reasonable value particularly given the discussion regarding the difference between *advection* and *sedimentation rate* in Note *d* of Table 5.3. However, the value of the NH_3 adsorption coefficient generated is 6.8 times larger than the largest literature reported value for the algorithm using just 2007 data. Although this is a large difference, the range in the literature is from just one study; it is noted in Mackin & Aller (1984) that temperature will have an effect of up to 25% over a 20°C range; it is also noted that high porosity (i.e. sandy) sediments will lead to low adsorption coefficients. It is unknown what effect very low porosity sediments will have, and this is a clear area where further research would help validate the model output. For brevity, a discussion of all remaining parameters is not necessary; however, as shown in Table 5.3, the results provided by this μGA technique does provide a full set of parameter values that are sensible when compared with observational data.

It is important to stress that models are seen only to reflect the processes from natural systems that are well understood; as has already been discussed, although technically feasible, the parameters in the calculation of the diffusion coefficient have not been split up. It would be difficult to determine, in practice, how the sensitivity of α and D^0 affect the model, and also how realistic these effects would be related to diffusion processes in the natural environment. Further to this, decoupling the diffusion equation for each of the chemical species would not only create a further eight parameters (increasing the parameter space even further), but the range of the diffusion coefficient of each of the chemical species would increase by approximately two orders of magnitude, which could lead to optimised values which are significantly outside the range found in the literature. There is no evidence that this increase would give rise to diffusion coefficients that are more realistic than the ones that this work has determined (even though they might actually make the model fit the data better), and is the type of over-fitting (and the type of situation where mathematics could be seen to be 'unreasonably effective') that Anderson (2005, 2010) warns against.

Finally, it is recognised that this work gives detailed results from only one study site. The other two sites primarily studied as part of the Marine Ecosystems Connections project, the Oyster Grounds and Sean Gas Fields, are very different

environments to the North Dogger site (where the observational data shown in this chapter was obtained). In particular, the Sean Gas Field site is very sandy; sandy sediments change the dynamics of the early diagenetic processes due to increased porosity (as a result of larger grain sizes), which increases the OPD (Cai and Sayles 1996). Sandy sediments also tend to be both organic- and ammonia-poor, as well as having lower concentrations of reactive iron (van Raaphorst *et al.* 1990). From a physical chemistry perspective, the nature of sands being neutrally charged, rather than having charged surfaces, as clays do, as a large effect on the concentrations of ions available as a result of the lack of adsorption (Burdige 2006; Libes 1992). The observations from the Sean Gas Field and Oyster Grounds are notably different to the data from the North Dogger Site (pers. comm. E. R. Parker); as such, there was enough variability between the sites that spatial predictability was unlikely to be successful. However, the data from these two sites was not as extensive as from the North Dogger site, and so it is unlikely the algorithm would have produced results which were as conclusive. Future work could allow us to determine whether the parameters generated in this study can be used in a predictive manner, both across different sedimentary environments that are geographically close, and in similar sedimentary environments in different marine areas. However, as this study shows, μGA techniques are a potentially valuable method in generating parameter values that are otherwise difficult to obtain and, as such, are a means towards explaining the processes that may are occurring in complex environments such as coastal marine sediments.

5.7 Summary

This chapter has shown how OMEXDIA can be used in conjunction with observational data. The sensitivity analysis provided a quantitative method to determine the parameters to which the model was most sensitive, and hence provide a way to allow the model to be efficiently manipulated to allow suitable parameter values to be found that would match observations. The sensitivity analysis also re-enforced the implication made in earlier chapters about the complexity of the model. In the use of a genetic algorithm, this chapter, has, for the first time, shown that it is possible to match observational data collected from a sedimentary shelf-sea environment to a diagenetic model. However, the use of the genetic algorithm has highlighted one of the limitations of the model; due to temporal variability it would not be possible for a single parameter set to represent all the individual profiles observed. Future work could implement a similar genetic algorithm approach into the time-dependent version of OMEXDIA which may allow parameters to be varied during model runs, and hence allow a parameter-set range which would generate appropriate profiles.

6 Modelling Nutrient Release During Sediment Resuspension within a Diagenetic Model I: Porewater Re-equilibrium Times

Resuspension has an important role in the wider biogeochemistry of shelf seas through release of particles and porewater solutes into the overlying water column. Diagenetic models can provide information on surface porewater nutrient concentrations, but a method of introducing these nutrients into the overlying water column as a result of resuspension is required. Firstly in this chapter there is a description of the main processes that can lead to resuspension, and then different ways of coupling these resuspension processes with the diagenetic model are investigated.

6.1 Processes of resuspension

Resuspension can happen as a result of both natural and anthropogenic processes. Natural processes can be further subdivided into biological and physical causes, with physical processes being either as a result of tidal or current effects, or storm events.

6.1.1 Physical processes

The processes that affect the resuspension of sediment can be divided into those that happen randomly (or quasi-randomly), and those that are much more regular, with the outcomes on the biology or chemistry of any such resuspension event also being predictable; this is likely to have an impact on the best way to implement resuspension into OMEXDIA. Within the physical events that result in resuspension, tidal, and to a certain extent current, movements are well known and understood, and previous work has shown how it is possible to model and predict correctly the concentrations of suspended particulate matter (SPM) as a result of resuspension over both tidal cycles (Pleskachevsky and Gunther 2008; Sundermann *et al.* 1993) and over longer time periods as a result of ocean (Dobrynin *et al.* 2010; van der Molen *et al.* 2009) and wind (Chung *et al.* 2009) currents; it is unlikely that such models could have been developed without previous detailed measurements being carried out (e.g. Noji *et al.* 2002; Tengberg *et al.* 2003). Over long timescales, relative to a tidal cycle, the

ability to predict the effects of resuspension has the ability for bathymetric change to be modelled (Ganju *et al.* 2009).

Previous work has shown how resuspension purely as a result of tidal processes can affect the fate of organic compounds in the marine environment (Chang and Sanford 2005). Chang & Sanford (2005) found that increasing resuspension does not always increase the dissolved fluxes to the water column, and that prolonged resuspension-deposition cycles (such as tidal events) causes greater mineralisation to occur in the water column than would otherwise be expected. This particularly occurs in environments where the residence time of POC in the water column is longer than rate of degradation. This trend has also been successfully modelled (Wainright and Hopkinson 1997); the modelling study presented by Wainright & Hopkinson (1997) suggests that resuspension events increase total mineralisation of organic matter (OM), rather than shift mineralisation from the benthic to pelagic layer. The porosity of sediment was shown to be the most sensitive parameter in the coupled 1-D hydrodynamic/sediment-contaminant/organic carbon water quality model used by Chang and Sanford (2005). As explained in Chapter 5, due to the way in which OMEXDIA has been written, it is unlikely that in this work, the sensitivity of sediment porosity could be tested.

With regards to the processes which are responsible for the increase in concentration of chemical species in the water column after a resuspension event, desorption has been shown to be responsible for up to 90% of the increase, although for ammonium, which is more relevant to the effects on diagenesis, this falls to 50% (Fitzsimons *et al.* 2006). The remaining increase is predominantly as a result of porewater injection; however, it is clear that concentrations of chemical species are also affected by secondary processes, such as take-up by microfauna and dissimilatory nitrate reduction to ammonium (DNRA) which occur as a result of the increase caused by desorption. Overall, Fitzsimons *et al.* (2006) showed that the tidal cycle reduced the residence time of NH_4^+ in estuarine sediments. Laboratory work seems to have confirmed this, with *in vitro* experiments, designed to simulate the cycle of oxic/anoxic sedimentary conditions resuspension causes, showing that, in general, nitrate concentrations in the overlying water column tend to increase during oxic periods and decrease during anoxic periods, with ammonia showing the opposite trend (Abril *et al.* 2010). However, as already stated, there is likely to large spatial variations with respect to the relative magnitude of tidal cycles to overall resuspension. Tidal currents in Chesapeake Bay were responsible for less than 1 mm of sediment resuspension (Sanford *et al.* 1991).

An important distinction to make with respect to the resuspended material is that it can be divided into two separate parts: sedimentary or benthic fluff. Benthic fluff is high-carbon low-density deposit on the sea bed, and has low shear stress (0.02-0.03 Pa), particularly with respect to the consolidated sedimentary material it lies above (Jago *et al.* 2002). The impact of fluff on the biogeochemistry on the benthic layer is difficult to determine due to the difficulty in sampling and analysing the very low-density material (Naomi Greenwood, pers. comm.); however, the presence of large quantities of benthic fluff has been thought to decrease the oxygen concentrations at the sediment-water interface (SWI), as a result of oxic mineralisation in the water column, and hence decreasing the oxygen penetration depth (OPD), or to send the sediment into an anoxic state (Jago *et al.* 2002; Greenwood *et al.* 2010). Another important observation is that although the erosion rate as a result of tidal currents is reported to be linear with respect to the critical shear stress (Sanford *et al.* 1991), the resulting fluxes are not linear with respect to the quantity of sediment resuspended (Chang and Sanford 2005; Sanford *et al.* 1991).

The remaining physical process which results in resuspension is storm events, which can be thought of to occur quasi-randomly. While the exact periodicity of storms, and the energy associated with them, is difficult to predict on a long time-scale, the average number of storms over an annual cycle, and the total associated energy, can be modelled (Weisse *et al.* 2005). Previous studies on the impact of storm events on the concentration of SPM concentrations as a result of resuspension (Pusceddu *et al.* 2005b) and the potential effects on the biogeochemistry on the sediment and overlying water column (Tengberg *et al.* 2003) have concentrated on the effect of a single storm event. SPM concentrations were found to increase from 2 to 9.8 mg l^{-1} (Pusceddu *et al.* 2005b) following a short-term (less than 48 hour) winter storm; the storm resulted in waves with a significant height of 6 m and a sea surface rise of approximately 0.5 m (Grémare *et al.* 2003). Tengberg *et al.* (2003) used a lander to carry out *in-situ* chamber experiments to measure fluxes and concentrations of various chemical species before and after an imposed resuspension event.

Two experiments were carried out in the same location with only a one-day gap between the two experiments; however, oxygen fluxes as a result of resuspension varied widely between the experiments. During the first experiment, mean oxygen fluxes across the SWI were found to decrease from a mean of -16.6 mmol m^{-2} d^{-1} to a mean value of -9.01 mmol m^{-2} d^{-1}. However, in the second experiment, the mean oxygen flux decreased from -19.3 mmol m^{-2} d^{-1} to -14.8 mmol m^{-2} d^{-1}. The differences are likely to as a result of the differing SPM concentration: in the first experiment, the SPM concentration in the water column increased from 1 to 85 mg l^{-1}, while in the second experiment, the SPM concentrations increased from 4 to 10 mg l^{-1}.

It was estimated that 13 μm of the sediment surface was resuspended in the first experiment, and 2 μm resuspended in the second experiment (Tengberg *et al.* 2003).

Nitrate and ammonia fluxes were also affected by the resuspension, with large variations seen within experiment one between the two chambers that were used. Pre-resuspension fluxes for ammonia were 45.8 μmol m^{-2} d^{-1} in Chamber 1 and 315 μmol m^{-2} d^{-1} in Chamber 2; post-resuspension fluxes increased to 102 μmol m^{-2} d^{-1} and 387 μmol m^{-2} d^{-1} respectively. Nitrite+nitrate fluxes in both chambers increased from -50.7 μmol m^{-2} d^{-1} and -453 μmol m^{-2} d^{-1} to 272 μmol m^{-2} d^{-1} and 700 μmol m^{-2} d^{-1} respectively. The influx of nitrate to the sediment before the resuspension event was assumed to be as a result of the rate of nitrification being lower than that of denitrification, while the change in the direction of the flux after the resuspension was due to the stirring stimulating nitrification in the sediment (Tengberg *et al.* 2003). The variation in these values shows how difficult it can potentially be to determine suitable observations for use in calibrating and validating a new model.

The SPM concentrations after a storm event have been also successfully modelled, with the model described by Liu and Huang (2009) being able to match the observed values of total suspended solids (TSS) with a correlation coefficient of between 0.73 and 0.75 during model verification runs. Hydrodynamic models have also been used to match observations that there is not always a net increase of SPM, but that it can be transported around a small bay depending on wind conditions (Pleskachevsky and Gunther 2008). Seifert *et al.* (2009) used model experiments to calculate the required wind speed to resuspend benthic fluff and SPM through 20 m of water depth. However, the long term (seasonal to annual) impact on the biogeochemistry as a result of storm events has not yet been studied.

Storm events which produce waves with a significant wave height of 3 m have also shown to be capable of resuspending sediments within the 50 m isobath (O'Brien *et al.* 2006); applying this to the North Sea would imply that very few areas of the North Sea Shelf would not be affected by storms of this magnitude (North Sea Task Force 1993). Using a modified version of OMEXDIA, an attempt to model this impact will be made in this chapter, leading to a conclusion about the importance of storms on sediment biogeochemistry over a whole shelf-sea system.

6.1.2 Biological processes

Biological causes of resuspension, as with storm events, can be seen to be a quasi-random process. Although the precise onset of primary production in coastal oceans is difficult to predict (Brandt and Wirtz 2010), model output has estimated that

the total rate of primary production in an area is similar on an interannual cycle (Skogen and Moll 2000). Greater primary productivity in the water column may lead to a greater density of benthic macrofauna (Meyer-Reil 1983), which are responsible for bioturbation and bioirrigation, mixing the sediment in a non-local way (Pope *et al.* 1996; Boudreau 1986; D'Andrea *et al.* 2004), and resulting in resuspension (Madsen *et al.* 1997). The process by which bioturbation results in non-local mixing has also been successfully modelled (Boudreau 1997b). However, there is also a potential feedback loop with resuspension. As has already been discussed, resuspension may increase the levels of some nutrients in the water column, allowing the rates of some bacterially-mediated processes such as DNRA to increase. If this allowed an increase in biomass throughout the whole ecosystem, then even further resuspension would result. This would likely continue until the flux of carbon from the surface waters decreased slowing down the overall rate of early diagenesis. Bioturbation, and resuspension caused by biological activities has also been linked to prolonging the rate of oxic mineralisation of OM in sediment (Barbanti *et al.* 1995).

The population dynamics of some benthic macrofauna species, such as ghost shrimps, show that the total biomass does not significantly decrease during winter (Berkenbusch and Rowden 1998); however, their distribution is very patchy (Rowden *et al.* 1998b). Despite this, experimental work has shown how ghost shrimps are able to expel 33 g (dry-weight) of sediment per day (Rowden *et al.* 1998b), which has the ability to aid erosional processes such as resuspension (Cadée 1976). The results of these experiments led to the calculation of the total annual sediment expulsion at a site characterised with a water depth of 47 m and a median grain size of 100 μm by ghost shrimp as 11 kg m^{-2} yr^{-1} (Morris and Howarth 1998; Rowden *et al.* 1998b). Other studies have looked at the effect benthic worms have had on chemical species. Madesen *et al.* (1997) found that *Capitella* sp. 1 was able to increase the probability of resuspension, leading on from earlier work showing that bioturbation leads to sediment instability by producing a fluid surface that is easily resuspended (Rhoads and Young 1970).

Finally, resuspension also has an impact on the rate of primary production, as a result of the increased TSS limiting light attenuation in the water column (Tian *et al.* 2009). Although it has never been quantified, it is likely that, as a result of the similarity of both the total primary productivity and of the average impact of storms on an area over an annual cycle, the impact of biology on the concentration of SPM and its subsequent effect on sediment biogeochemistry is also similar when considered on annual timescales.

6.1.3 Anthropogenic processes

Some work has been carried out to assess the impact of anthropogenic activities on water column and sediment biogeochemistry as a result of increased sediment transport. The majority of work has concentrated on the impact of either fishing trawlers (e.g. Churchill 1989; Pusceddu *et al.* 2005b; Warnken *et al.* 2003) or dredgers (e.g. Schoellhamer 1996; Hayes *et al.* 2000). As with biological processes and storm events, the lack of regularity of trawling activity (Schoellhamer 1996) throughout a year makes anthropogenic activities quasi-random when considering the long term impact they are likely to have on sediment biogeochemistry. However, enough small scale studies are available in the literature that, as with storm events, an aim of the work in Chapter 7 will be to determine, to a first degree, the impact of anthropogenic activities across the whole North Sea Shelf. As an indication of the potential importance of anthropogenic activities on the benthic system, Schoellhamer (1996) estimated that, over an annual cycle in a shallow estuary, long-waves generated by passing ships that were not actively disturbing sediment resuspends an order of magnitude greater mass than resuspension by wind waves caused by winter storms (1×10^9 kg compared with 9×10^7 kg respectively). The study also showed that trawling activities routinely cause resuspension which results in double the SPM concentration in the water column when compared with a winter storm; observations showed that a storm has the ability to increase in SPM concentration from 28 mg l^{-1} to 130 mg l^{-1},and the SPM concentrations returned to preperturbed values within 2 hours, while trawling caused the SPM concentration to increase to 250 mg l^{-1}, and the SPM concentration did not return to ambient conditions until 8 hours after the final trawling event (Schoellhamer 1996). The effect trawling had on resuspension in the Middle Atlantic Bight appeared to be at least an order of magnitude than that reported by Scheollhamer (1996), with the greatest concentration of SPM being 465 μg l^{-1} as a result of 150 days of trawling of muddy sediments (Churchill 1989); however, no like-for-like comparisons with how long the environment took to return to ambient conditions were presented. Churchill (1989) also found at shallower water depths (below 100 m), currents were responsible for greater amounts of resuspension than trawling activities between January and March 1984, but this trend reversed in deeper waters. Based on this information, and given that the majority of the North Sea is water depths of less than 100 m, it seems as though it would be difficult to directly compare the results from the Middle Atlantic Bight; however, it could also be surmised that as trawling is a prolific activity in the North Sea (CEFAS 2001), trawling could always be responsible for more resuspension than currents.

As would be logically expected, both trawling and dredging operations induce addition of all the chemical species that are present in the top layers of sediment and

which are involved in early diagenetic processes to the overlying water column (Audry *et al.* 2007; Pusceddu *et al.* 2005b). Shrimp trawling has been estimated to mobilise the top 1 cm of sediment in shallow water depths (Warnken *et al.* 2003), and resulted in the ammonium flux increasing by up to a factor of 3; oxygen fluxes appeared to be unaffected by trawling. As already stated, it has been suggested that resuspension by any method causes greater mineralisation to occur in the water column. This hypothesis has been backed up by results presented by Pusceddu *et al.* (2005b), where they show that the quality of organic material in the sediment decreases after a resuspension event; similarly, resuspension has also been shown to decrease the turnover time of OM in the sediment (Pusceddu *et al.* 2005a). A potential side effect from the addition of OM to the water column is that it depletes the oxygen concentration in the water column, both as a result of biological and chemical processes, particularly if the water column is stratified and the resuspended sediments are confined below the pycnocline (Wainright and Hopkinson 1997). As a further side effect, trawling could induce mortality of benthic macrofauna, and further resuspension could then produce a pulse of up to 423 mmol C m^{-2} into the overlying water column (Duplisea *et al.* 2001); this occurs due to the macrobenthos being important carbon consumers in the sediment system. Although they show this happens particularly after resuspension due to trawling, there is no evidence to suggest it should not also happen as a result of either physical or biological resuspension.

Recent research has further suggested that it is not as simple to try and quantify the resuspension attributed to each process independently. Although in the southern North Sea, concentrations of SPM are approximately 3 times higher after a storm event than during calm conditions (Fettweis *et al.* 2010), this is thought to have been influenced by other recent dredging activities. Fettweis *et al.* (2010) found that SPM concentrations could reach 3000 mg l^{-1} at 0.2 metres above the bed following a resuspension event; however, they did find also that there is a lag time of approximately 2 days between the resuspension event and the peak SPM concentration at 2.2 metres above the bed. They also infer that vertical mixing is limited where the SPM concentrations do not greatly increase at 2.2 m above the bed. Their results also show that very soft muddy sediments around navigation channels, which occur as a result of recent deposition following dredging activities, are more likely to be resuspended following storm events than sediments not affected by human activities.

There is also a potentially complex link between biological activity and resuspension by physical means. Both brittle stars and shrimps have been shown to cause instability of the upper few centimeters of North Sea sediment, particularly during summer when productivity is highest. Although experimental work has never

looked at the direct link to quantify the potential impact, this instability could cause enhanced resuspension during storms (Rowden *et al.* 1998a).

6.2 Methods of modelling resuspension

Although the physical results of resuspension (such as the increase in SPM concentration and the effect on light attenuation) have been successfully modelled (e.g. van der Molen *et al.* 2009; Van Duin *et al.* 2001), there has been little work on the impact of resuspension on sedimentary biogeochemistry.

When developing a complex model such as the one described here, where physical and biogeochemical processes both need to be represented, one potential way forward would be to couple a mature physical sediment-transport model with OMEXDIA. However, this is likely to be problematic. The two separate models would have different forcing parameters (bed shear stress for the resuspension model and POC flux for OMEXDIA). Further to this, the domain of the two models would overlap, with both attempting to describe activity that was happening within the top few centimetres of sediment with different sets of variables. The two models also deal with the sediment in fundamentally different ways, with OMEXDIA not needing to incorporate the physics of the sediment in the same manner that sediment transport models do. This differs from the situation which often arises when two models are coupled, where to improve one or both models, the neighbouring environment is also modelled with no overlap, such as models describing the water-column and overlying atmosphere. In these cases, only the boundary conditions and values of these variables between each of the models need to be considered. It was decided that a simpler approach should be taken, particularly since this is the first time that this type of model has been developed; this is also following convention that it is generally good practice that models should be as simple as possible (Anderson 2005).

OMEXDIA does incorporate enough variables relating to the sediment structure that can be used to make a relatively simple representation of the processes which occur during and after resuspension. As the model is initially not directly concerned with the effect of the SPM in the water column (e.g. adsorption), and only on the effects on the biogeochemistry, then a simple way is needed to couple the water column and surface sediment during resuspension.

As discussed in Chapter 2, OMEXDIA has a porosity function which could be used to represent the physical process of resuspension: the layer of sediment which is

resuspended has a much lower porosity than the sediment that was there before the resuspension event, relative to the original SWI, as shown in Figure 6.1.

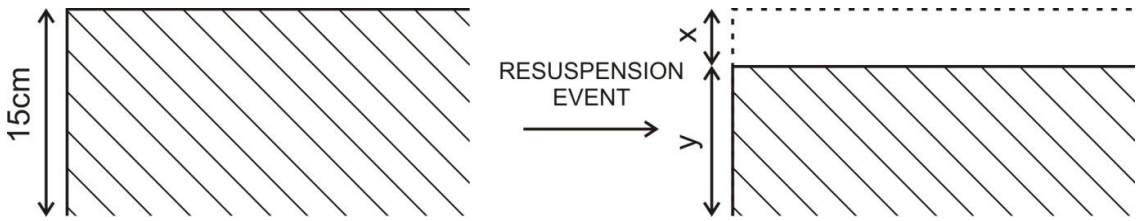

Figure 6.1: Schematic to show the effect of resuspension on the sedimentary column in the model. The model domain is 15 cm; after a resuspension event, the chemical species in the portion of the sediment which has been resuspended (*x*) takes on the concentration of the overlying water column, except for POC which takes on the integrated concentration over *x*, to simulate the mixing which occurs during resettling of resuspended material. The value of porosity through x is not changed, for reasons explained in the text.

It was decided that porosity should not be allowed to change with respect to time during a resuspension event for two primary reasons: the first being that this goes against making the model as simple as possible when trying to find an initial representation for the process; the second being that, as discussed in the introduction of this chapter, SPM concentrations often vary within the time frame of tidal cycles. After individual resuspension events, sediments can settle within a matter of hours; increased water column SPM concentrations are often only seen as a result of continued resuspension events, whether they be physically, biologically or anthropogenically driven. As the default model output time-step is daily, it is unlikely that implementing a more complex method of modifying the porosity of the resuspended sediment would be visible in model output. However, it is recognised that the future development of this model may lead to a version with greater time-resolution being used. If this is the case, then modifying the porosity as described above may become necessary to increase the accuracy of the model.

Leading on from the discussion above, the simplest method for modelling resuspension is to allow the concentrations of all the chemical species in the part of the sedimentary domain that is resuspended to take on the concentration of the overlying water column, which is a fixed value throughout a model run, at the time of resuspension. By using the dynamic version of OMEXDIA, we can then make an estimate of how long the system takes to return to a pre-perturbed state by using both the concentration of the chemical species in the sediment and the flux of each chemical species across the SWI as a tracer.

6.3 Porewater re-equilibrium times after resuspension

In order to simulate real systems, and to be able to make comparisons with previous experimental studies, a suitable method of determining the re-equilibration time of porewater concentrations needs to be established. A number of different metrics can be used to quantify the time taken for the sediment to become re-equilibrated after a resuspension event. Some simple statistical methods will be briefly discussed in this section, from which a decision will be made as to which metric will be used for the remainder of the experiments. For simplicity, the results discussed in this section refer only to model runs where carbon flux into the sediment did not vary over time, and where the mixed layer depth of the sediment is 15 cm. The object of these runs was to choose a suitable metric for use later.

6.3.1 Method 1

The initial method to be evaluated is shown in Equation 6.1. The system is deemed to have reached re-equilibrium when the sum of the difference between a dynamic run and the corresponding steady-state run, integrated over the whole sediment column, is less than a given percentage of the steady-state solution.

$$\sum |dyn_i - SS_i| < \frac{\sum SS}{ratio} \qquad \text{Eqtn 6.1}$$

Where *i* is current layer, *dyn* is the dynamic run output (for the current day), *SS* is the steady-state run, and ratio is the proportion of the SS we want to be the threshold (i.e. the ratio would be 1000 for 0.1%). For each model run (where each run is a different thickness of perturbation), we want to find the first day where the left-hand side of the equation has a lower value than the right hand side.

A slight deviation of this method can be used to determine the point at which the significant chemical species in the model (fast-degrading organic matter, slow-degrading organic matter, O_2, NO_3^- and NH_3) reach a given percentage of the steady-state value. Due to the increased computation required for this, four values were chosen: 90%, 95%, 99% and 99.9%. These values were chosen as they correspond to the primary significance values used in null-hypotheses in standard statistical analysis (NIST/SEMATECH 2012). For each of the chemical species, the time taken to reach the re-equilibrium threshold for each of the percentages can be calculated.

6.3.2 Method 2

An alternative approach for estimating the re-equilibrium time is to determine the time by which the ratio of the concentrations of the chemical species in sediment during a dynamic run compared with a steady-state run are below a given percentage; this is described in Equation 6.2.

$$\left|\left(\frac{\sum dyn}{\sum SS}\right) - 1\right| < percentage \qquad \text{Eqtn 6.2}$$

Where *dyn* is the dynamic run output (for the current day), *SS* is the steady-state run, and percentage is the threshold. For each model run, we want to find the first day where the left hand side of the equation is less than the percentage threshold. This will be the first day when the inequality in Equation 6.2 is true, and as such will be the first day when the sediment can be deemed to have returned to equilibrium.

In both Method 1 and Method 2, each of the layers has to be multiplied by layer thickness and porosity to obtain an accurate value for concentration.

6.4 Results

When we apply these equations to the FDET, O_2, NO_3^- and NH_3 results of resuspension experiments which were carried out for 10 years with perturbation depths of between 0.1 and 14.9 cm, with the threshold of 1000 and 100 for method 1 and, equivalently, percentages of 0.1 and 1 for method 2, then we obtain the graphs shown in Figure 6.2.

It should be noted that, although both metrics use a threshold of 0.1% and 1%, these are not directly equivalent, and hence the result graphs show different results. There are some interesting results from both of these methods. Intuitively, it might be expected that the response time would be either linear or logarithmic. This is the case (or very close to the case) in some of the results (FDET and O_2 using method 1 with both 0.1% and 1% thresholds, NO_3^- for 1% threshold using method 1 and 0.1% using method 2). It is also the case for NO_3^- using method 2 for a 1% threshold – although the fast response times imply a stepwise path to re-equilibrium. The correlation coefficient, allowing for the correlation to pass through the origin, is 0.99. However, there are some responses which need some further discussion.

The difference between the 2 statistical methods is responsible for the difference between the FDET appearing to respond logarithmically by method 1 (and, for example, taking approximately 600 days to re-equilibrate after 5 cm of sediment has been perturbed), whereas method 2 appears to show that FDET re-equilibrates immediately, regardless of the depth of sediment that was perturbed. However, given that all species are being perturbed, the concentration of each species throughout the whole sediment column is given the value of the bottom-water. As we are modelling environments which have oxic bottom waters, the entire sediment column will become very oxic after perturbation (250 – 300 mmol m^{-3} O_2). As FDET is the fraction of organic matter which is fast degrading, it is entirely plausible that all of the FDET is mineralised within the first day, and hence regarded by the output as returning to steady-state immediately. This is most likely to be as a result of method 1 taking the absolute difference between each individual layer; this means that, in method 2, although the overall inventory is the same, the pattern of FDET in the sediment column is not the same. Method 1 does check the pattern of FDET in the column, compared with the SS result; this therefore implies that although the total inventory has been restored, the SS profiles have not. This has potentially interesting consequences for experimental work, where, although solutes are often measured at high resolution, it is common for solid material to be measured over much coarser depth thicknesses. This explanation also gives a reason for the time for re-equilibrium to occur by method 2 being an order of magnitude faster than method 1. It does not, however, provide an explanation for the relatively strange graphs such as the re-equilibrium to 1% for NH_3 using method 1, as seen in Figure 6.2.

By looking at the model output in more detail, some light may be shed on the reasons for the shape of the NH_3 sedimentary re-equilibrium profile. Table 6.1 shows the concentration of ammonia in layers 1, 10 and 100 for perturbation depths of 0.1, 1 and 10 cm, on the last time step of the model run, in the hope that this may give some explanation for the graph shown in Figure 6.2. The concentrations obtained from a steady-state run are also shown for comparison.

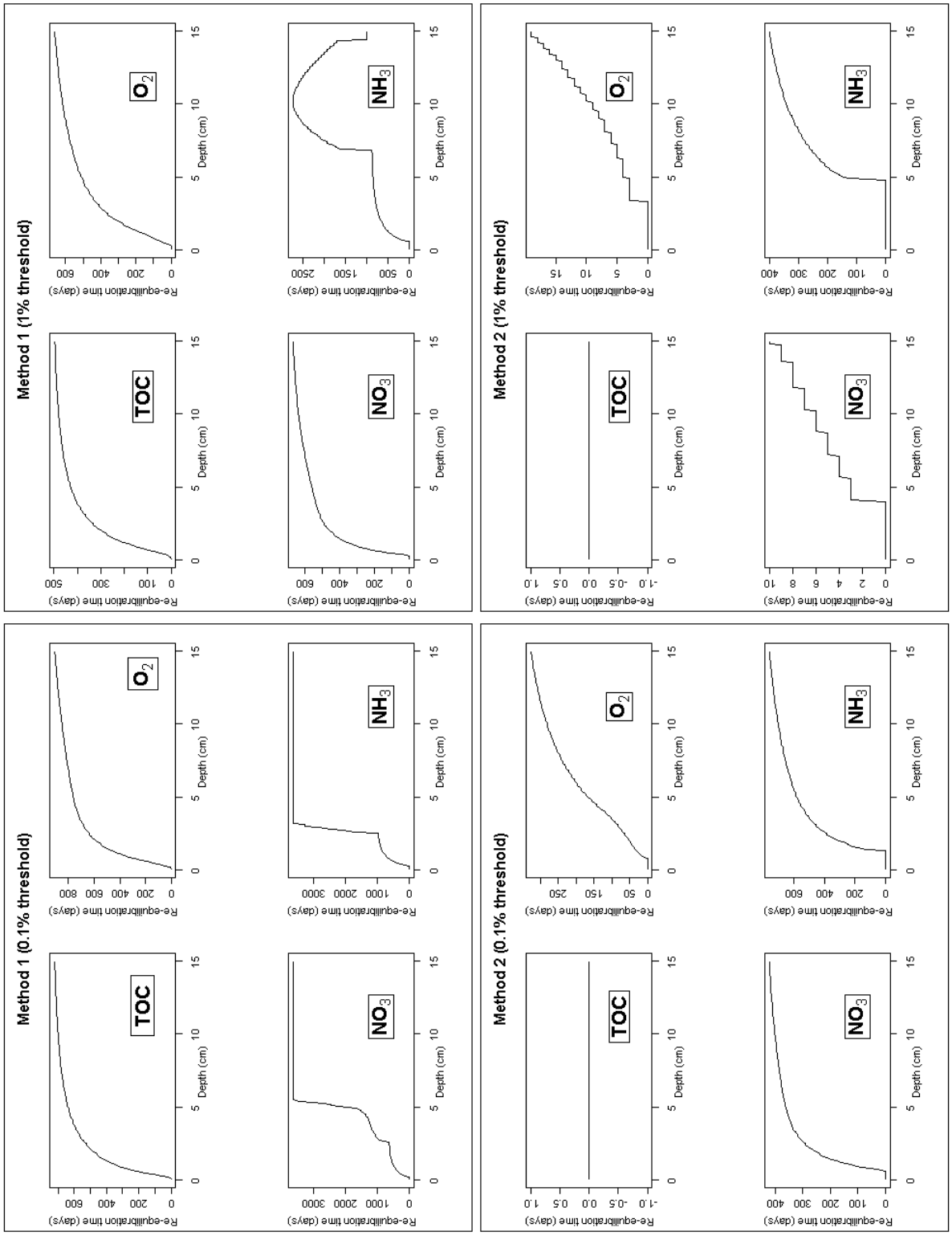

Figure 6.2: Sedimentary re-equilibrium timescales for thresholds of 0.1% and 1% for methods1 and 2

Table 6.1: Concentrations of NH_3 following a 10 year model run

		Concentration of NH_3 at day 3651 (mmol m^{-3})			
		Layer 1	Layer 10	Layer 100	Total sedimentary inventory
Perturbation depth (cm)	0.1	1.67	1.64	30.04	327.03
	1	1.67	1.64	30.04	327.03
	10	1.67	1.65	31.12	335.80
	15	1.67	1.67	45.53	426.81
Steady-state value		1.66	1.64	30.04	327.04

Table 6.1 shows that, when the sediment is perturbed to a depth of 0.1 and 1 centimetres, the sediment is re-equilibrated by the end of the model run, which is consistent with the graph shown in Figure 6.2. Table 6.1 also shows that the sediment is not re-equilibrated by the end of the model run when the sediment is perturbed to a depth of 10 or 15 cm; this is also consistent with Figure 6.2 – an unpredicted consequence of method 1 is therefore that the time taken for re-equilibrium can appear to decrease, but seemingly only when the depth of perturbation is greater than the maximum perturbation depth when re-equilibrium is reached. As can be seen in Figure 6.2, the greatest perturbation depth at which the sediment is re-equilibrated within 10 years is 10.2 cm; the reason why the re-equilibrium time decreases when the perturbation depth is greater than this is likely to be related to the calculation of the total amount of ammonia in each layer – the steady-state value of ammonia in the top layer is 0.1666943 mmol m^{-2}, however this decreased to 0.1666064 mmol m^{-2} at day 3651 when the perturbation depth was 15 cm. Following the discovery of this unexpected deviation, this method could continue to be used, albeit with careful consideration when the concentration of a chemical species within a layer, and the depth of that layer, are both below a value of 1.

If we now update method 2 so that it takes into account the concentrations of each individual layer, rather than the total inventory (described in Equation 6.3), then we can make judgements about how important looking at the whole inventory is when trying to make conclusions about the re-equilibrium time of coastal sediment resuspension events.

$$\sum \frac{|SS_i - dyn_i|}{SS_i} > percentage \qquad \text{Eqtn 6.3}$$

A caveat when using this method is that it will obviously not work if the steady-state value in the current layer is 0; however, due to the computational calculations,

even when concentrations appear to be zero, they are very often infinitesimally small values, allowing the division to occur.

Care has been taken to formulate this equation so that it doesn't suffer from a caveat that many ratio calculations are subject to; that is when a very small value is divided by a relatively much smaller value (but should actually be approximated as zero), the result is an unrealistic large value. Taking the case of equation 6.3, the value of SS will always be larger than the absolute difference between the values of SS and dyn, hence ensuring that the result for each layer will be between 0 and 1. As there are 100 layers in the model domain, the maximum value for the total sum of the dynamic result will be 100. Although this makes an ideal easy comparison with the value of *percentage*, it should be recognised that if the number of layers should be changed, the equation would not have to be normalised to 100 for the percentage comparison to be valid, although it may be argued that it would be good practice for it to be. With method 2a it should be noted that the advantage of subtracting one from the division is that it normalises the result relative to the steady-state result. It should also be noted that although method 2a and 2b are similar, due to the differences in calculating the influence of each layer, the significance of *percentage* is different in each case, and so any results between the two methods cannot be directly compared

Figure 6.3 shows the results from using method 2b. As would be expected, it is clear that the addition of checking each depth layer does have an effect on re-equilibrium time-scales. TOC now does not re-equilibrate instantaneously, presumably as a fact that, although the overall inventory of TOC in the sediment is unchanged, its profile, as a result of oxidation and mixing, is different. However, method 2b shows that the time taken for oxygen re-equilibrium is equal to the number of days in the model run (10 years), implying that oxygen never comes to re-equilbrium following any level of perturbation, something that only happens with nitrate and ammonia after approximately 5 cm of sediment is perturbed. Given that the diffusion coefficient of oxygen in methods 2 and 2b are the same, this initially seems like a strange result. Table 6.2 shows the concentration of oxygen in layers 1, 10 and 100 for perturbation depths of 0.1, 1 and 10 cm, on the last time step of the model run. The concentrations obtained from a steady-state run are also shown for comparison.

As can be seen from Table 6.2, it appears that re-equilibrium has been reached by the end of the model run when the perturbation is 0.1 and 1 cm, and that re-equilibrium has almost been reached when the perturbation depth is 10 cm. The output from the analysis indicating that re-equilibrium is never reached seems to be an artefact of the calculation of the metric.

Table 6.2: Concentrations of O_2 following a 10 year model run

		Concentration of O_2 at day 3651 (mmol m^{-3})			
		Layer 1	Layer 10	Layer 100	Total sedimentary inventory
Perturbation depth (cm)	0.1	277.44	49.20	2.38×10^{-49}	158.30
	1	277.44	49.20	7.99×10^{-153}	158.30
	10	277.44	49.16	1.06×10^{-153}	158.25
Steady-state value		277.44	49.20	1.59×10^{-121}	158.30

A direct conclusion of this discussion is that a decision can be taken on which metric to use for the remainder of the analysis in this chapter. By visualising this data in different ways, further conclusions can be made about the results. Figure 6.4 shows data from percent threshold *vs.* re-equilibrium time, giving an indication of the behaviour that might be expected following a perturbation (either natural or anthropogenic), and therefore estimate the time that it would take for the entire sediment to re-equilibrate to a given threshold following a perturbation event. It must be remembered that, as shown in Chapters 2, 3, and 4, the model is relatively specific for site and time, and that in these early runs, the model only outputs concentration values for whole integer values of days; however, keeping these factors in mind, from Figure 6.4, we can start to interpret the re-equilibrium times. As would be expected, it can be seen that re-equilibrium time increases with increased percentage threshold, although, whereas it might be expected that the re-equilibrium times increase gradually, perhaps following a power or exponential function over all thresholds, it can be clearly seen that this is not the case, and that there seems to be a percentage threshold only after which the re-equilibrium time increases steeply.

Furthermore, Figure 6.4 shows the time needed to re-equilibrate the sediment versus percentage threshold for three different perturbation depths for oxygen, nitrate and ammonia for each of the three methods. We can see that, for example, re-equilibrium is never reached if the required percentage threshold was to be 100%. If the re-equilibrium of O_2 is considered for method 1, then it can be seen that equilibrium is always instantaneous when the percentage threshold is below 100% when the perturbation depth is 1 mm.

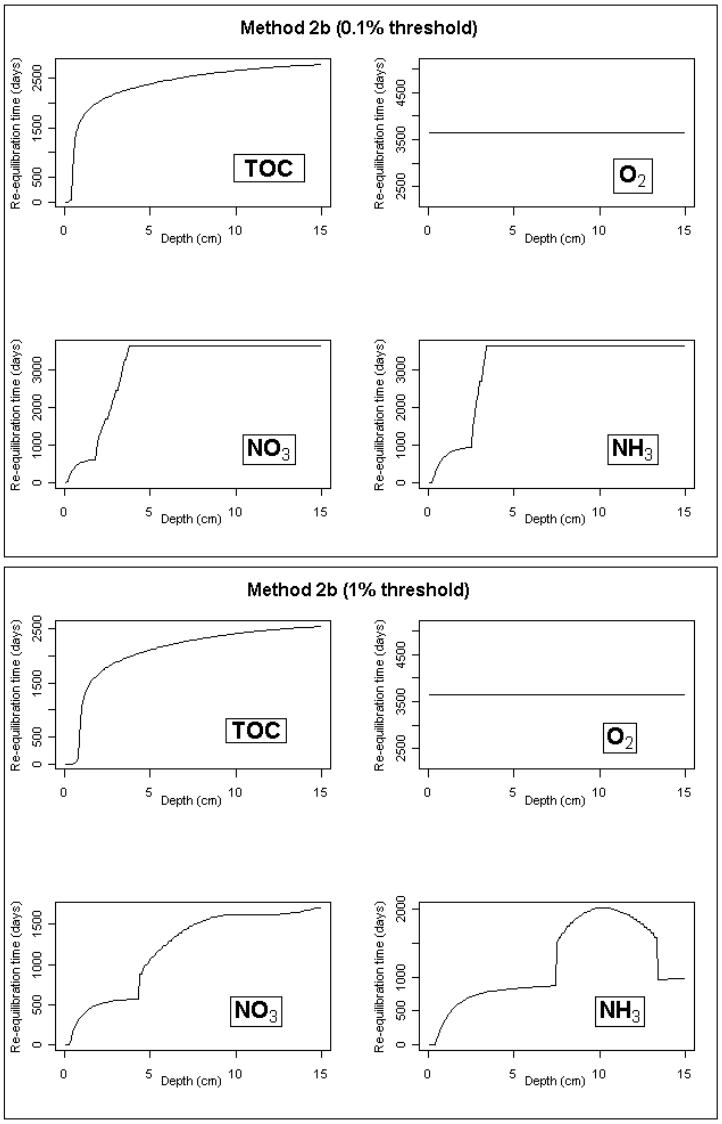

Figure 6.3: Sedimentary re-equilibrium timescales for thresholds of 0.1 and 1% for method 2b

Re-equilibrium stops being instantaneous when the percentage threshold is above 87% when the top 10 mm of sediment is perturbed; re-equilibrium is never instantaneous when the perturbation is 100 mm, although re-equilibrium is always within the timeframe of the model when the threshold is less than 100%. The re-equilibrium timescale ranges from 1 day when the percentage threshold is 1% to 617 days (i.e. 1.7 years) when the threshold is 99%.

Figure 6.4 also shows that method 2 and 2b imply that a perturbation of 100 mm mixes the sediment to such an extent that the concentrations of none of the solute chemical species are within 1% of the steady-state concentrations. This result is not seen in method 1, where only ammonia does not return to re-equilibrium instantaneously at low percentage thresholds when the perturbation depth is 10 mm. Figure 6.3 shows that re-equilibrium is established instantaneously for all chemical species below a threshold of 100% when the perturbation depth is 1 mm, and that re-equilibrium can be established for all percentage thresholds below 100% at the perturbation depths within the timescale of the model. The largest re-equilibrium timescale, 2741 days, is caused by requiring ammonia to be re-equilibrated to a threshold of 99% when the perturbation depth is 100 mm.

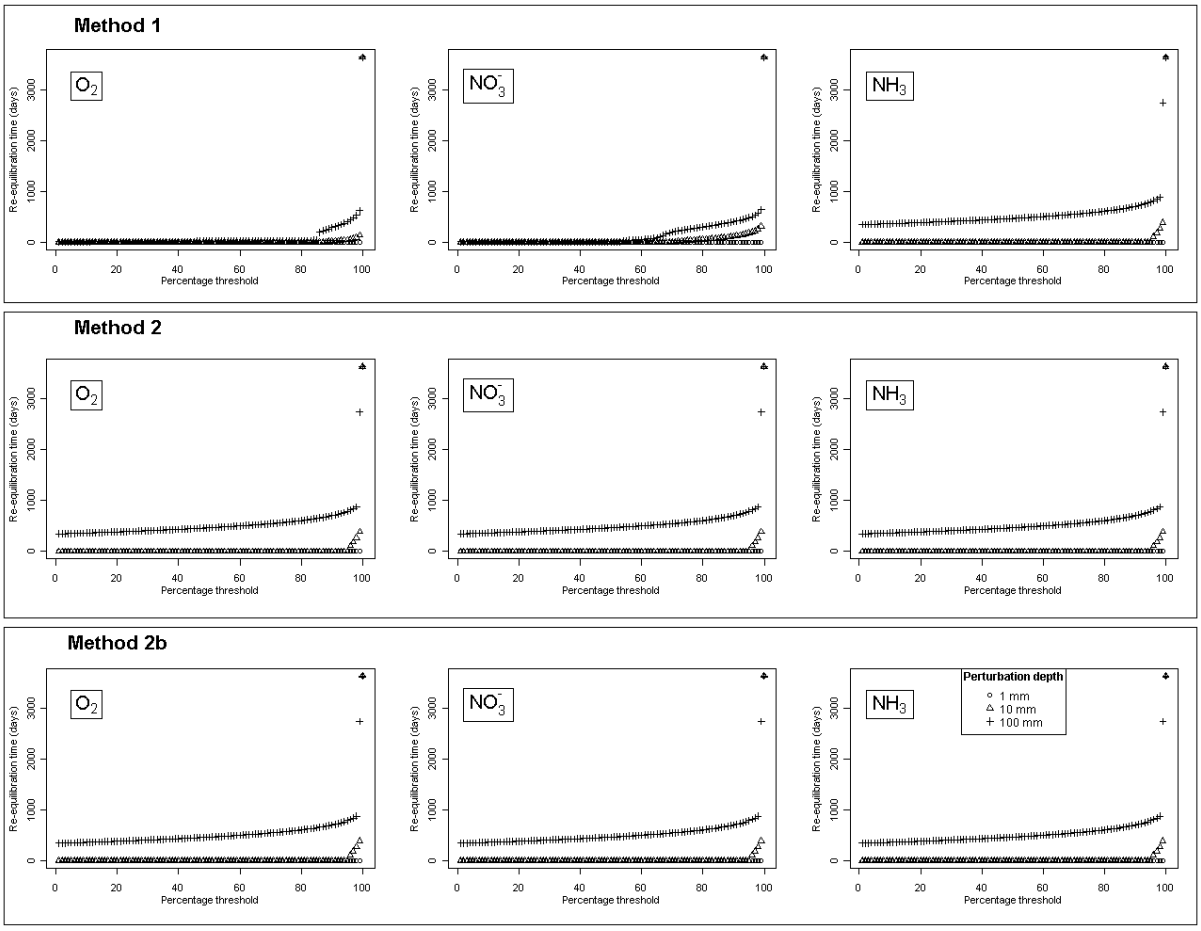

Figure 6.4: Sedimentary re-equilibrium timescales of oxygen, nitrate and ammonia for all integer percentage thresholds between 1 and 100% for methods 1, 2 and 2b when the perturbation depths were 1, 10 and 100 mm

Although in the previous section three different metrics were discussed for calculating re-equilibrium times, and various thresholds associated with re-equilibrium, it makes sense to pick just one of these metrics to use when analysing model runs for the remainder of this chapter. Method 1 has been chosen, primarily for two reasons:

- The graphical results for method 1 are easier to interpret and in general follow a more consistent pattern than those for method 2. For example, the totally instantaneous re-equilibrium of TOC as shown by method 2 is unlikely to be realistic. However, care does need to be taken with interpreting some of the results from method 1, as the re-equilibrium of ammonia in Figure 6.2 shows. Table 6.2 also indicates that there is an as yet inexplicable artefact of method 2b showing that oxygen is reaching equilibrium when Figure 6.3 indicates that re-equilibrium is not reached.

- Method 1 is more intuitive than method 2. In the environmental sciences, when quantifying the change of an environment due to external factors, it is common to compare the difference relative to a standard state, as in method 1. Method 2 also has the disadvantage that results could be obscured if ΣSS was infinitesimally small compared with Σdyn, resulting in very large values.

6.5 Summary

Resuspension can occur as a result of numerous physical, biological and anthropogenic processes, and it is unclear from current knowledge which processes are most important when considering the impact of resuspension on the overall sedimentary environment or the overlying water column. It is, however, clear that within certain geographical areas, there is overwhelming evidence that a particular perturbation event, such as a beam trawl, will have an immense impact on the sediment. It has been recognised that it is difficult to quantify both the impact of re-equilibration, and for re-equilibration of the porewater concentrations of the major chemical species found within shelf-sea sediments.

By implementing a simple first approach to modelling resuspension, this chapter has shown that it is possible for re-equilibrium times of porewater concentrations of oxygen, nitrate and ammonia to be estimated following a perturbation event. A review of different potential methods for estimating re-equilibration times was carried out, and one method (Method 1) was deemed to be more appropriate than the remaining two. The results in this chapter show that re-equilibration time is approximately exponential with respect to the percentage threshold considered. It is clear that re-equilibration to within 99% (or greater) is likely to give unrealistically large re-equilibration times, and as such, a percentage threshold of 95% will be used throughout Chapter 7. In addition, it is clear that re-equilibration timescales are very different for each of the chemical species modelled within OMEXDIA, as a result of the biogeochemical processes involved.

7 A First Approach to Modelling Resuspension within a Diagenetic Model II: Impact of Varying Resuspension Depth & POC Flux

Building on the results that generated a suitable metric in Chapter 6 to determine re-equilibration timescales, a comprehensive set of experiments was carried out to examine the effect varying three key parameters in the model (POC flux, depth of perturbation, and the magnitude of the mixed layer depth) has on re-equilibration times, and how these compare with previous published estimates. However, very little previous work, both theoretical and experimental, has been carried out on establishing the impact of resuspension on the sedimentary environment, and thus this work is an important step forward in improving knowledge about this process.

7.1 Experimental details

In order to gain insights into the system after resuspension events of different magnitudes, a series of model runs were carried out. For each of the following experiments, the dynamic version of OMEXDIA was run for 100 years. The simple method of representing resuspension was implemented, and initially, the time-step at which resuspension occurred was chosen to be day 14. Resuspension was only allowed to occur in the first year of model simulation, after the spin-up run. As described above, resuspension was assumed to be an instantaneous process, so that at time-step (i.e. day) 14, the concentration of each of the solute chemical species in the model (O_2, NO_3^-, NH_3 and ODU) was given the value of the default water-column concentration (300 mmol m^{-3}, 10 mmol m^{-3}, 1 mmol m^{-3} and 0 mmol m^{-3} respectively) in the layers of sediment that were resuspended. The concentration of TOC in each of the layers to be resuspended was given the value of the integrated value over the depth of resuspension, to simulate the redistribution that would occur during the resettling of resuspended material.

All of the experiments described involve individual runs such that the entire range of sediment resuspension can be investigated. The number of model layers resuspended in each run is one greater than in the previous run. However, experiments where all 100 layers (i.e. 15 cm) were resuspended were not carried out as this led to a discontinuity in the model calculations at the bottom boundary. A

description of the distribution of the model layers can be found in Chapter 2. In all, three discrete sets of experiments were conducted.

The first set of experiments carried out used the same experimental structure as seen in Chapter 4. Using the four techniques of varying POC flux (as described in Section 4.5), the modified OMEXDIA model was run with mean POC fluxes of 2, 15 and 50 g C m^{-2} yr^{-1} for 10 years, following a steady-state run. This resulted in 1788 experimental runs being carried out.

Following on from this, a second set of experiments was carried out. For each of the four methods of POC variation, the mixed layer depth was varied to 1, 5 or 15 cm. This was done as some of the results of the Genetic Algorithm experiments (Chapter 5) show that the profiles from the North Dogger site could best be represented by having a much larger mixed layer depth than the original default value in OMEXDIA, which was 5 cm. A mixed layer depth of 1 cm was also chosen as a comparison to see the effect that a much lower mixed later depth would have; this is likely to be the best representation of the sandy sediments of the Southern Central North Sea, such as the Sean Gas Fields, where the sediments have much larger median grain size, greater oxygen penetration depths (OPDs) and lower organic carbon content than the muddy sediments of the Dogger Bank and Oyster Grounds (Neubacher *et al.* 2011). The larger sediment grains are likely to lead to lower rates of resuspension from physical processes, while the lower carbon content and relatively high value of the OPD implies that there is low biological activity, also leading to low resuspension as a result of bioturbation when compared with the North Dogger site discussed in Chapter 5. Each of the experimental runs were run for 100 years.

Finally, a third set of experiments used all permutations of varying the depth of the mixed layer (1, 5 and 15 cm), the mean POC flux (2, 15 and 50 g C m^{-2} yr^{-1}) and the four methods of varying the POC flux. Each was run for 100 years. For these experiments, the stepwise method for POC variation was modified so that the lower value was the mean POC flux but the higher value was 1500 nmol C cm^{-2} d^{-1} (equating to 65.7 g C m^{-2} yr^{-1}).

Over the three sets of experiments, 10281 experimental runs were carried out; each 100 year experimental run took between 20 and 35 minutes, depending on the POC variation technique, and generated a results file of approximately 900 mb.

7.2 Results

7.2.1 Effect of different POC flux forcing patterns

A comparison of the four different POC flux forcing patterns was initially carried out. In this experiment, the mixed layer depth was kept at 5 cm, and three POC fluxes were imposed in the model: 2, 15 and 50 g C m^{-2} yr^{-1}. The model was run for 10 years, with the perturbation depth being at day 14 in year 1. The four POC flux forcing patterns, as described in Chapter 4, have been used. Results from 95% re-equilibrium using method 1 for calculating re-equilibrium timescales are shown.

Figure 7.1 shows the re-equilibrium times of all the chemical species for the experiment when there is no carbon flux variability. It can be seen that the time taken for carbon to re-equilibrate is not related to the flux of carbon; this is due to the mixing of carbon in the sediment during perturbation; although the concentration of carbon will still vary throughout different flux scenarios, this is different to, and as shown here unrelated to, the time taken for that carbon to return to pre-perturbation concentrations. It can be seen that the re-equilibrium times for oxygen, nitrate and ammonia are less straightforward to explain. As would be expected, oxygen re-equilibrates most quickly when the carbon flux is 50 g C m^{-2} yr^{-1}. This is due to the much shallower oxygen penetration depth (OPD) and higher oxic mineralisation rates when the carbon flux is high, meaning that the oxygen is utilised faster and therefore the biogeochemical cycle enables oxygen to return to pre-perturbation concentrations within a shorter time. Re-equilibrium timescales are longest for oxygen when the carbon flux is 15 g C m^{-2} yr^{-1}; however, below a perturbation depth of 7 mm when the carbon flux is 15 g C m^{-2} yr^{-1}, and 10 mm when the carbon flux is 50 g C m^{-2} yr^{-1}, the re-equilibrium is instantaneous. Ammonia re-equilibrates most quickly when the POC flux is 2 g C m^{-2} yr^{-1}, in line with expectations. Lower carbon fluxes result in lower overall concentrations of ammonia (as shown in Chapter 3), meaning that the concentration is most likely to return to steady-state values more quickly. The reason for nitrate re-equilibrating most quickly when the POC flux is highest is the same as the reason given for oxygen; the complex biogeochemistry is also the most likely cause for the nitrate taking longest to re-equilibrate most slowly when the POC flux is 15 g C m^{-2} yr^{-1}, as a result of denitrification; it is possible that due to denitrification, the overall inventory of nitrate in the sedimentary column does return to pre-perturbed values, but the concentration in each sedimentary layer has not returned to their steady-state values. As shown in Figure 3.1, the nitrate peak caused by denitrification is deepest when the POC flux is 15 g C m^{-2} yr^{-1}, making it a sensible conclusion that it also has a significant effect on the overall re-equilibrium timescales of nitrate at this flux. It should also be noted that when the perturbation depth is

greater than 12.3 cm, the re-equilibrium time is longer than the timescale of the model when the POC flux is 15 g C m^{-2} yr^{-1}. As a result of the role of oxygen in denitrification, and of denitrification on the concentration of ammonia, it also likely that the process of denitrification is the reason why both oxygen and ammonia concentrations return to pre-perturbation concentrations most slowly when the POC flux is 15 g C m^{-2} yr^{-1}.

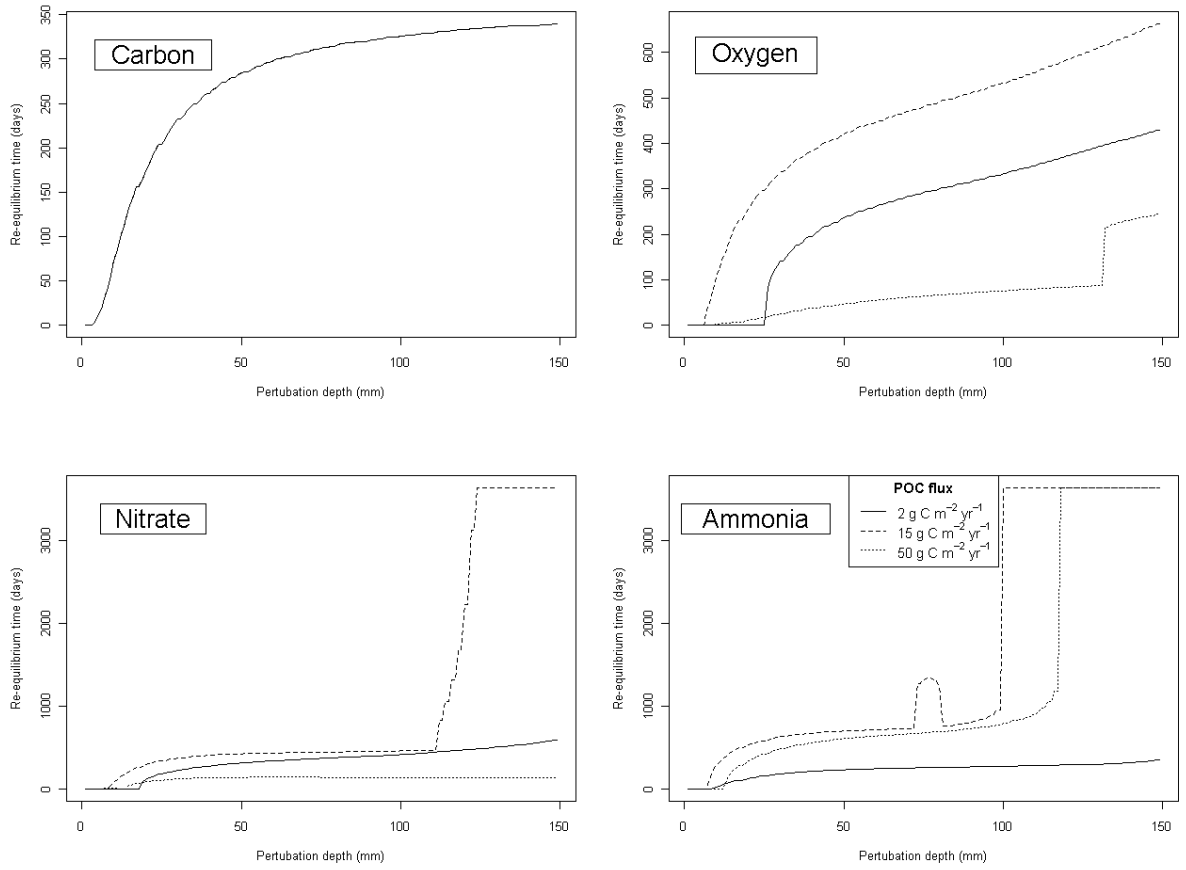

Figure 7.1: Sedimentary re-equilibrium timescales of carbon, oxygen, nitrate and ammonia using method 1 to calculate re-equilibrium timescales when a 95% threshold is considered for 3 different POC fluxes, with no POC flux variation over a range of perturbation depths

If the simple sinusoidal function (flux profile FP2) for carbon flux variability is now considered, then there is evidence that re-equilibrium times change drastically (Figure 7.2). As with using a steady-state carbon flux, the time taken for carbon to re-equilibrate appears not to be related to the carbon flux; however, Figure 7.2 also shows that re-equilibration is not reached within the timescale of the model for any carbon flux, regardless of percentage threshold considered. Ammonia also does not reach equilibrium at any threshold for any POC flux. This is not the case with oxygen, where pre-perturbation event concentrations are reached when the POC flux is 2 g C m^{-2} yr^{-1}; re-equilibrium is not reached when the POC flux is 15 or 50 g C m^{-2} yr^{-1}.

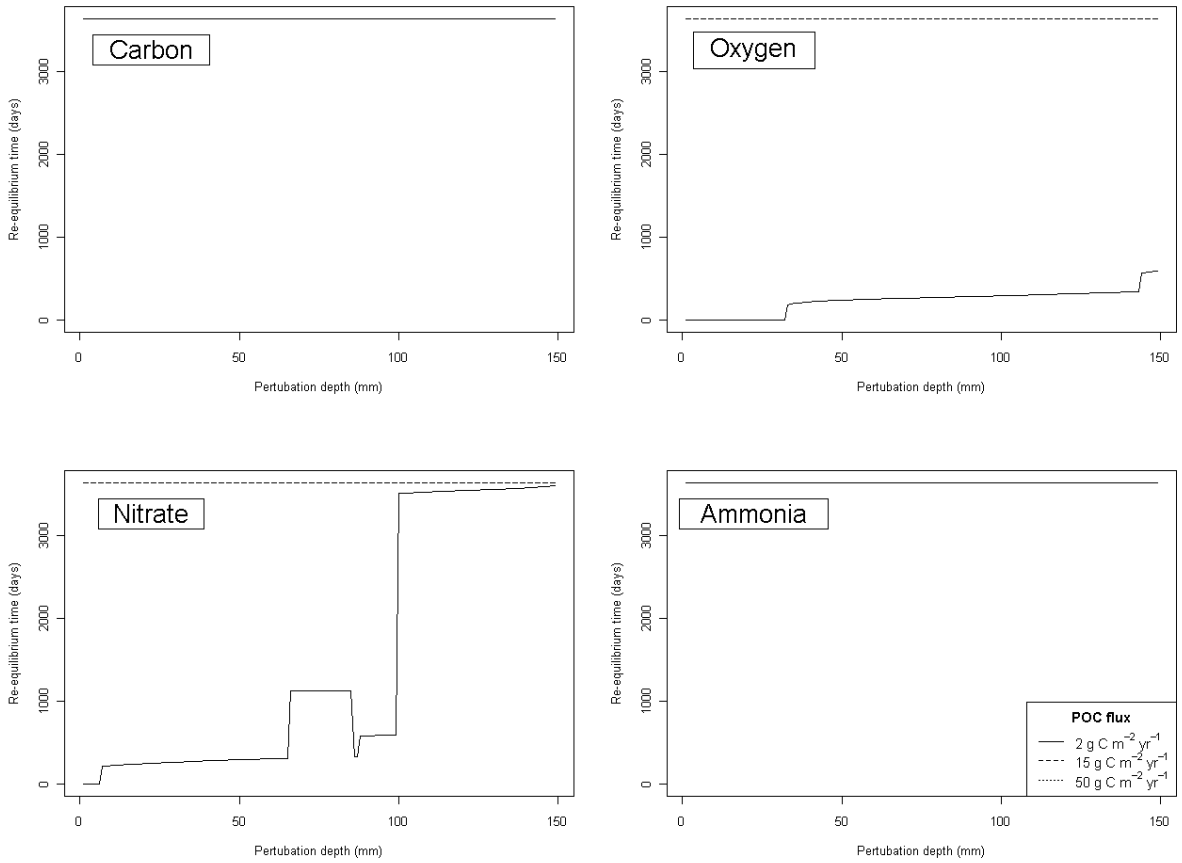

Figure 7.2: Sedimentary re-equilibrium timescales of carbon, oxygen, nitrate and ammonia using method 1 to calculate re-equilibrium timescales when a 95% threshold is considered for 3 different POC fluxes, when a simple sinusoidal POC flux variation was imposed, over a range of perturbation depths

This pattern is repeated in the nitrate re-equilibrium times, where, despite the unexpected decrease in re-equilibrium times when the perturbation depth is 86 mm, re-equilibrium is reached when the POC flux is 2 g C m^{-2} yr^{-1}, but not when it is 15 or 50 g C m^{-2} yr^{-1}. As well as the sudden decrease, the large step in re-equilibrium time from 597 to 3505 days when the perturbation depth is 100 mm is also difficult to explain. However, it should be noted that the comparisons made here are between the concentrations during a dynamic run and the concentrations calculated during a steady-state run. The results presented here show that the concentrations during a dynamic run are unlikely to match those found by running the model to steady-state, and therefore, the second metric used for calculating re-equilibrium, where the total inventory of each chemical species in the sedimentary column is used to check for re-equilibrium, may be a good compromise. Although there is no guarantee that the concentrations in each sedimentary layer will match between the steady-state and dynamic run, it will provide a first-order estimate to re-equilibrium times. Given that

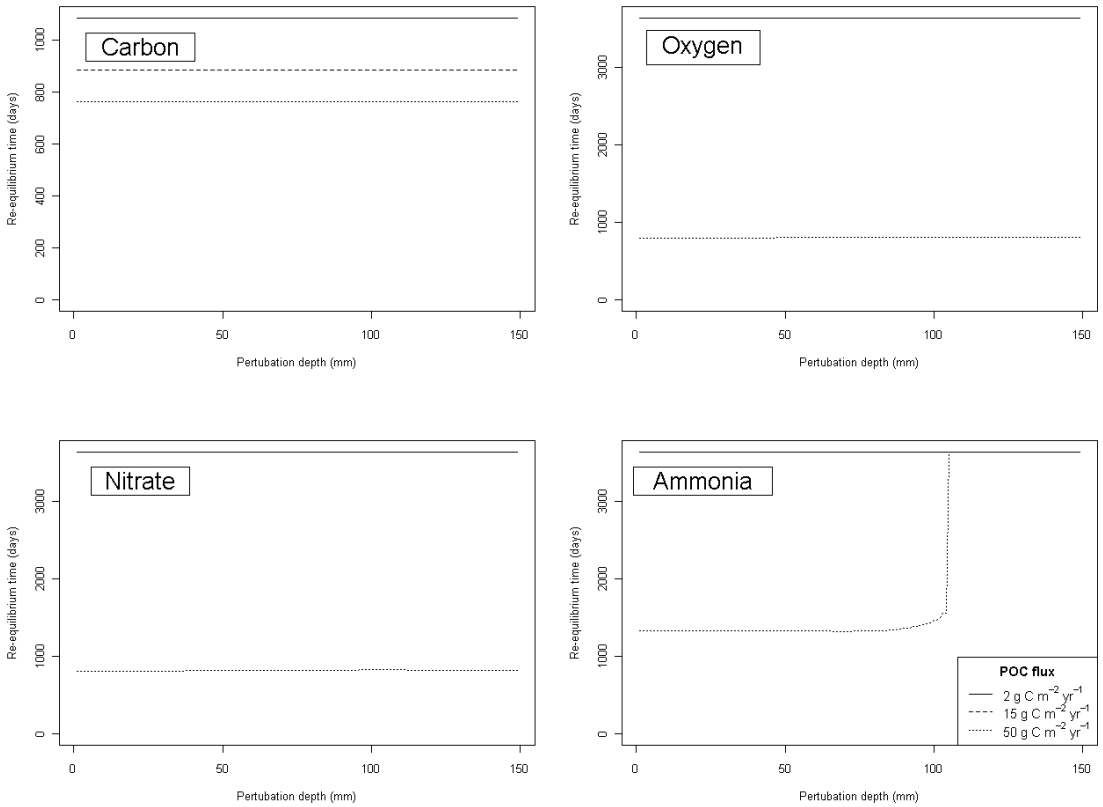

Figure 7.3: Sedimentary re-equilibrium timescales of carbon, oxygen, nitrate and ammonia using method 1 to calculate re-equilibrium timescales when a 95% threshold is considered for 3 different POC fluxes, when a simple stepwise POC flux variation was imposed, over a range of perturbation depths

no work has been done on the re-equilibration times following perturbation events, any estimate provided here will be a good starting point for future work.

Finally, Figures 7.3 and 7.4 show the results when a more realistic carbon flux forcing is attempted, with Figure 7.3 using the more stepwise pattern (FP3), and Figure 7.4 using the complex trigonometric function (FP4). It is worth mentioning at this point that the model using FP3 takes 2 to 3 times longer to run than when the method includes the seemingly more complex trigonometric function shown in Equation 4.3. This is likely to be due to the method used in the model to solve the differential equations being able to solve the equations more efficiently when the steps between two consecutive time steps is very small, rather than the large jump seen when the stepwise perturbation method is used.

When a stepwise approach is taken to the carbon flux profile, the carbon re-equilibrium times do vary depending on the average carbon flux; however, the re-

equilibrium time is not dependent on perturbation depth, with the re-equilibrium times being 1085 days, 883 days and 762 days for POC fluxes of 2, 15 and 50 g C m^{-2} yr^{-1} respectively. Oxygen and nitrate also do not show variation based on the perturbation depth; the re-equilibrium time for oxygen and nitrate when the average POC flux is 50 g C m^{-2} yr^{-1} is 812 days and 825 days respectively. The re-equilibrium time when the average POC flux is 2 or 15 g C m^{-2} yr^{-1} is longer than the timescale of the model for both chemical species. Ammonia concentrations return to pre-perturbed values only when the POC flux is 50 g C m^{-2} yr^{-1} when the perturbation depth is less than 10.5 cm.

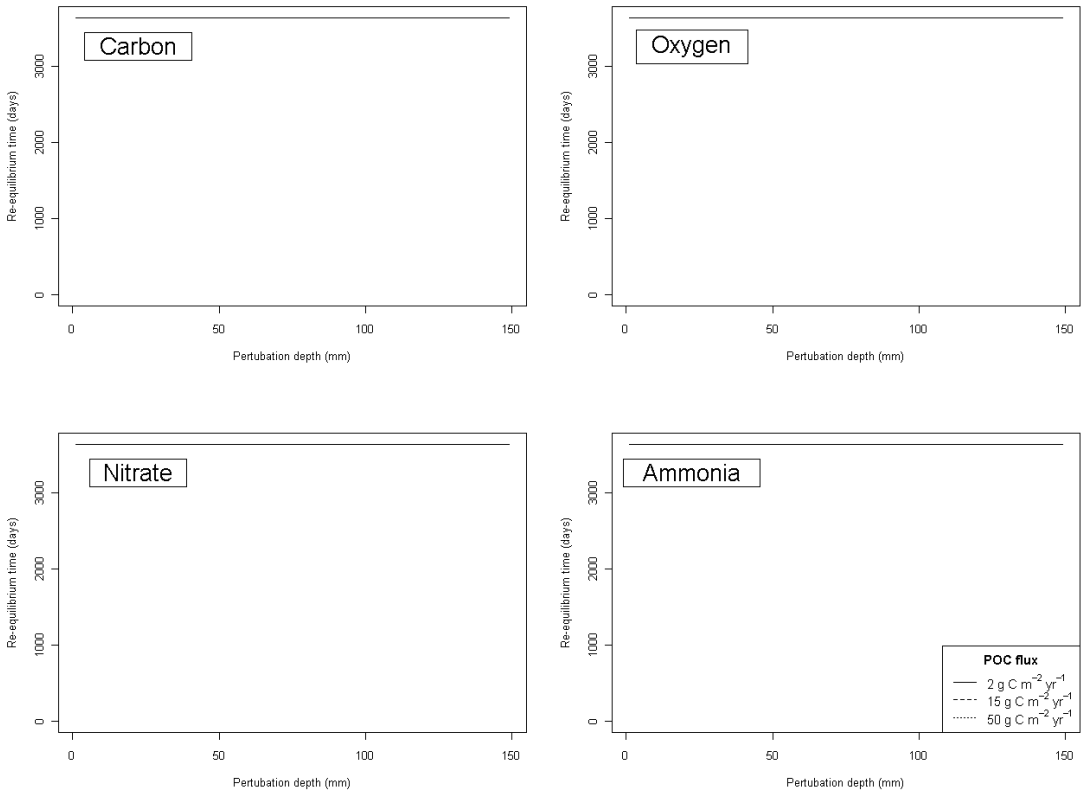

Figure 7.4: Sedimentary re-equilibrium timescales of carbon, oxygen, nitrate and ammonia using method 1 to calculate re-equilibrium timescales when a 95% threshold is considered for 3 different POC fluxes, when a realistic sinusoidal POC flux variation was imposed, over a range of perturbation depths

When the complex trigonometric function is used to describe the POC flux over time, then pre-perturbed values are not reached for any of the chemical species within the timeframe of the model. However, this may be due to the method being used to calculate re-equilibrium requiring the concentration in each layer to be the same, in order for re-equilibrium to deem to have been re-established. As it is possible that method 1 for calculating re-equilibrium times may not be suitable for dynamic runs, method 2 will be used to provide a further estimate of re-equilibrium times. It should

be noted that as method 2b also takes into account the concentration in each sedimentary column, this is also unlikely to reflect re-equilibrium times accurately.

The results for carbon, oxygen and nitrate all show that re-equilibrium is instantaneous for all three POC fluxes for both the simple and more complex trigonometric POC flux functions; however, this is not the case for ammonia which does show an increase in re-equilibration times as perturbation depth increases, but only when the POC flux is 15 g C m^{-2} yr^{-1}; when the POC flux is 2 g C m^{-2} yr^{-1}, re-equilibrium is instantaneous, and when the POC flux is 50 g C m^{-2} yr^{-1}, re-equilibrium is not reached within the timeframe of the model. Figure 7.5 shows the increase in re-equilibrium time versus perturbation depth for ammonia when the POC flux is 15 g C m^{-2} yr^{-1}.

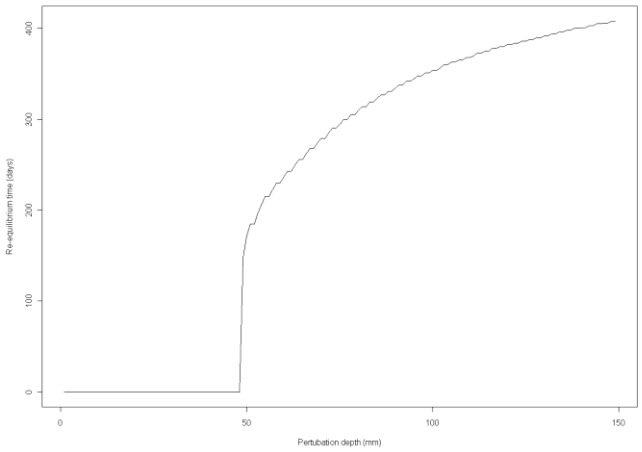

Figure 7.5: Sedimentary re-equilibrium timescales of ammonia using method 2 to calculate re-equilibrium timescales when a 95% threshold is considered for a POC flux of 15 g C m^{-2} yr^{-1}, when a realistic sinusoidal POC flux variation was imposed, over a range of perturbation depths

Re-equilibrium times for all four species using method 2b is 36501 days (the timescale of the model run), which is expected due to this method checking the concentration in each layer. The most likely cause for carbon, oxygen and nitrate appearing to re-equilibrate instantaneously is due to the perturbation event increasing, or, in the case of carbon, not changing the concentration of the species. This may lead to the integrated concentration after the perturbation event being negative, which would result in the percentage difference also being negative. However, the ammonia concentration in the sediment will always decrease during a resuspension event, which will always result in the percentage difference being positive. This makes ammonia the most suitable tracer for use in the calculation of re-equilibrium timescales.

Figure 7.5 shows the re-equilibration pattern that may be expected, with re-equilibrium being instantaneous when the perturbation depth is less than 49 mm, and the re-equilibration time increasing after that in a quasi-logarithmic fashion. The re-equilibration time increases to 408 days when the perturbation depth is 149 mm. However, the sudden jump from an instantaneous re-equilibration to one which takes 148 days between perturbation depths of 49 and 50 mm is difficult to explain. Once again, this is close to the depth of the expected nitrate peak during a steady-state run of the POC flux, but it is unclear why the depth of the nitrate peak should influence the re-equilibrium time after a perturbation to that depth so greatly.

The fluxes of each of the chemical species across the sediment-water interface (SWI) shows that the flux of oxygen, nitrate or ammonia varies immediately after the perturbation event when the depth of perturbation is changed. It is also not unexpected that the flux does not change throughout time when the carbon flux to the model is constant. The flux is the same as calculated when the model is run at steady-state with no perturbation. However, the flux of the three chemical species does vary with changes in both the POC flux and the profile of the POC flux (Figure 7.6).

As can be seen, the POC flux has little effect on the change in the flux of oxygen when compared with the perturbation depth (when the perturbation depth is 100 mm, the change in flux is -72.25%, -83.43% and -82.42% for POC fluxes of 2 g C m^{-2} yr^{-1}, 15 g C m^{-2} yr^{-1} and 50 g C m^{-2} yr^{-1} respectively. A negative flux represents a flux of a species out of the sediment, whereas a change in flux lower than -100% indicates that the flux is in the opposite direction that would be expected. This makes sense for oxygen, as the concentration of oxygen in the water column is much higher than the concentration in the sediment. As a result of this, and that the overall inventory of carbon does not change during a resuspension event, this is the direction of the flux that would be expected. The approximately inverse logarithmic pattern seen is as a result of the concentration profile of oxygen in sediment. As oxygen concentrations decrease as the depth of sediment increases, deeper perturbations will have less of an effect, leading to a levelling off of the increase in the flux.

The peaks in the increase of the nitrate fluxes reflect processes occurring within the sediment. The method used to calculate the percentage change uses the flux in the timestep following the perturbation event. However, the maximum change in flux when the POC flux is 50 g C m^{-2} yr^{-1} is actually 2 timesteps after the perturbation event. This is as a result of the nitrate concentration in the water column being higher than that in the sediment, and so the perturbation event increases the sedimentary concentrations of nitrate. Initially, this excess of nitrate is used in denitrification. However, the excess of nitrate means a flux out of the sediment does need to be

established so that re-equilibrium can occur. Again, this is an unsurprising pattern as the concentration of nitrate is higher in the sediment at these depths than the concentration in the water column. The flux therefore has to be into the water-column, in a change proportional to the sedimentary concentration at the depth of perturbation, for re-equilibration of the sediment to occur. The results shown here imply that there is a critical depth of perturbation at which the imposed concentration is an excess that can be used before a flux needs to be established.

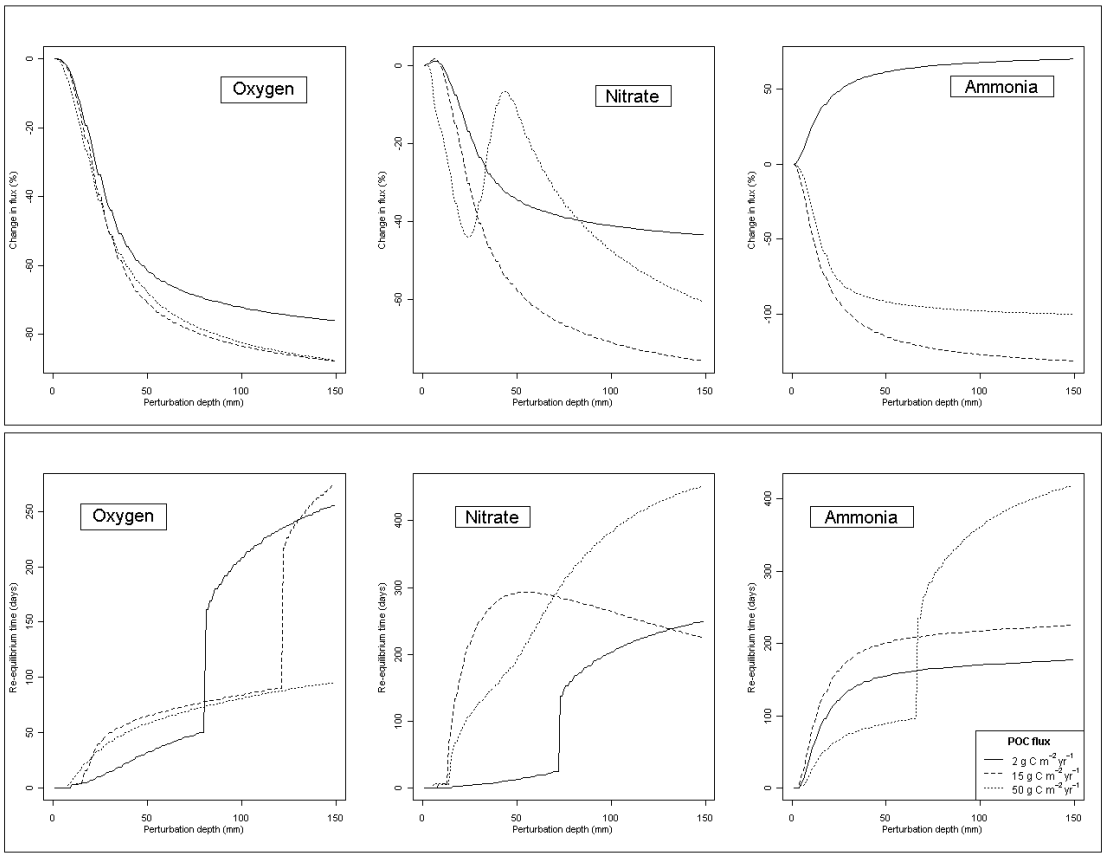

Figure 7.6: The resulting percentage change in flux for oxygen, nitrate and ammonia that a perturbation event causes (upper panel) and the time taken for fluxes to return to re-equilibrium for the three chemical species (lower panel); the results relate to a three different constant POC fluxes

The patterns in the ammonia mirror the concentration profiles of nitrate; a POC flux of 2 g C m^{-2} yr^{-1} results in little ammonia in the sediment due to nitrification, and so the flux resulting from a perturbation event is into the sediment as there is sufficient oxygen for nitrification to occur. However, POC fluxes of 15 and 50 g C m^{-2} yr^{-1} result in relatively high concentrations of ammonia (120 mmol m^{-3} at a depth of 15 cm at the highest POC flux). When this is perturbed, and the resulting sedimentary concentration is reduced to 1 mmol m^{-3}, the biogeochemical processes determine the SWI flux that needs to be established to drive the ammonia concentrations back to pre-perturbation values. At POC flux values of 15 and 50 g C m^{-2} yr^{-1}, ammonia

produced can be distributed throughout the whole sedimentary column, and so the flux across the SWI is much lower than under steady-state conditions: -2.7 mmol m^{-2} d^{-1} compared to -27.06 mmol m^{-2} d^{-1}. Under steady-state conditions, the flux of ammonia would be into the sediment when the POC flux is 2 g C m^{-2} yr^{-1}, although the flux would be small; the positive change in flux under this POC flux is 2 g C m^{-2} yr^{-1} therefore denotes that the flux is larger than would be expected.

The time taken for the fluxes to return to pre-perturbation values is also shown in Figure 7.7. In line with the POC flux not having a large impact on the difference between the change in fluxes observed, varying the POC flux also does not affect the re-equilibrium times as much as the depth of perturbation. When the depth of perturbation is 100 mm, the re-equilibrium time when the POC flux 2, 15 and 50 g C m^{-2} yr^{-1} is 409, 477 and 432 days respectively. The tailing off of the re-equilibrium time follows the same pattern as seen previously. The peak seen in re-equilibrium time when the perturbation depth is 32 mm when the POC flux is 15 g C m^{-2} yr^{-1} may be as a result of the oxygen being used during nitrification. Low and high POC fluxes also help nitrate to re-equilibrate relatively quickly, when compared to intermediate POC fluxes (with re-equilibrium times of 454 and 779 days when the POC flux is 2 and 50 g C m^{-2} yr^{-1} respectively); however, re-equilibrium is not reached within the model timescale when the POC flux is 15 g C m^{-2} yr^{-1} and the perturbation depth is greater than 141 mm. This is as a result of the biogeochemical cycling - at low POC fluxes, nitrate is a relatively unimportant oxidising agent, and so diffusion, which is a relatively fast transport mechanism, will allow the nitrate to re-equilibrate, with very little removal of nitrate occurring through denitrification. At high POC fluxes, the majority of nitrate is used much higher up in the sediment. As a result, following a deeper perturbation event, diffusion will drive nitrate upwards through the sediment to fulfil the demand required by the high POC flux. However, during the intermediate fluxes, nitrate is affected by both nitrification and denitrification. It is significant that the re-equilibrium time is fairly constant until the depth of perturbation is 110 mm, before the re-equilibrium time increases from 349 to 641 days. This is probably as a result of the nitrate peak that would be observed just above this depth. If the entire nitrate peak is not resuspended, then the nitrate still available in the sediment will be able to diffuse upwards, as well as being able to utilise nitrate diffusing into the sediment from the overlying water column. However, if the whole peak is resuspended, then the inventory of nitrate in the sediment immediately following the resuspension event is lower compared with a shallower perturbation, and hence can only rely on diffusion of nitrate downwards from the SWI.

The ammonia re-equilibrium times follow, in general, a more straightforward pattern. Initially, a high POC flux helps ammonia to re-equilibrate faster than the two

lower POC fluxes (as a result of lower concentrations of ammonia due to nitrification), however, when the depth of perturbation is greater than 23 mm, re-equilibrium times increase as the concentration of ammonia at these depths increases correspondingly. When the perturbation depth is 149 mm, the re-equilibrium time is 312, 368 and 695 days for POC fluxes of 1, 15 and 50 g C m^{-2} yr^{-1} respectively.

The re-equilibrium times for each of the three chemical species when a varying POC flux is introduced were calculated. Comparing the value with the value of the flux is meaningless; not only might a false positive be the result (i.e. the first time a flux value is found that matches the steady-state value, and hence regarded as having returned to an equilibrium, might not be the 'correct' value of the flux for that time-step during a normal dynamic run), but also, as a result of the calculation of the flux in the model, no time-step might generate the value of the steady-state flux, resulting in an implication that re-equilibrium has never been reached. Therefore, the flux from the resuspension model was compared with a run when no perturbation was imposed. Re-equilibrium was deemed to have been reached at the timestep when the flux of O_2 was within a given threshold relative to the same timestep in a model run with no perturbation.

As observed previously, re-equilibration time of the oxygen flux is much more dependent on perturbation depth than the imposed POC flux, with the re-equilibrium time being 79 days, 100 days and 92 days for POC fluxes of 2, 15 and 50 g C m^{-2} yr^{-1} when the depth of perturbation is 149 mm. When the more complex flux profile is considered, the re-equilibrium time is 109 and 100 days respectively when the POC flux is 15 and 50 g C m^{-2} yr^{-1}, but 240 days when the POC flux is 2 g C m^{-2} yr^{-1}. The longer re-equilibration time for oxygen when the POC flux is low is most likely as a result of the deeper OPD. This follows the pattern that when the perturbation depth is less than 120 mm, the re-equilibrium time when the POC is 2 g C m^{-2} yr^{-1} is lower than at the higher POC fluxes. This result comes about due to residual oxygen remaining in the sediment; at low POC fluxes, oxygen utilisation rates are lower, increasing re-equilibrium times accordingly.

For both imposed POC flux patterns, an increase in re-equilibrium time, followed by a slight increase for nitrate can be seen; this is due the nitrate peak caused by denitrification present in the sediment. The pattern for nitrate when the POC flux is 50 g C m^{-2} yr^{-1} is the same for both POC flux profiles, due to the shallow nitrate peak. It is also an indication that when the POC flux is high, the flux of nitrate is more dependent on the POC flux than the annual pattern of the POC. A similar pattern is also seen between the two POC flux profiles when the POC flux is 2 g C m^{-2} yr^{-1}. The increase in re-equilibrium times when the depth of perturbation is greater than 120 mm is as a

result of the more complex biogeochemical cycling that comes about when POC flux is more variable. However, the results when the more complex flux profile is used shows that when the perturbation depth is above 27 mm, the re-equilibrium time, nitrate takes longer to return to re-equilibrium when the POC flux is 15 g C m^{-2} yr^{-1} relative to 50 g C m^{-2} yr^{-1}. This again is due to the more complex biogeochemical cycling that occurs. As shown in Chapter 2, when the more complex POC flux is imposed, the overall inventory of nitrate is greater when the POC flux is 15 g C m^{-2} yr^{-1} than when it is 50 g C m^{-2} yr^{-1}, as a result of the deeper nitrate peak. The total inventory of nitrate is also more variable over time when considering the more complex POC flux compared with the simpler flux. An increase in time taken for re-equilibrium is therefore unsurprising.

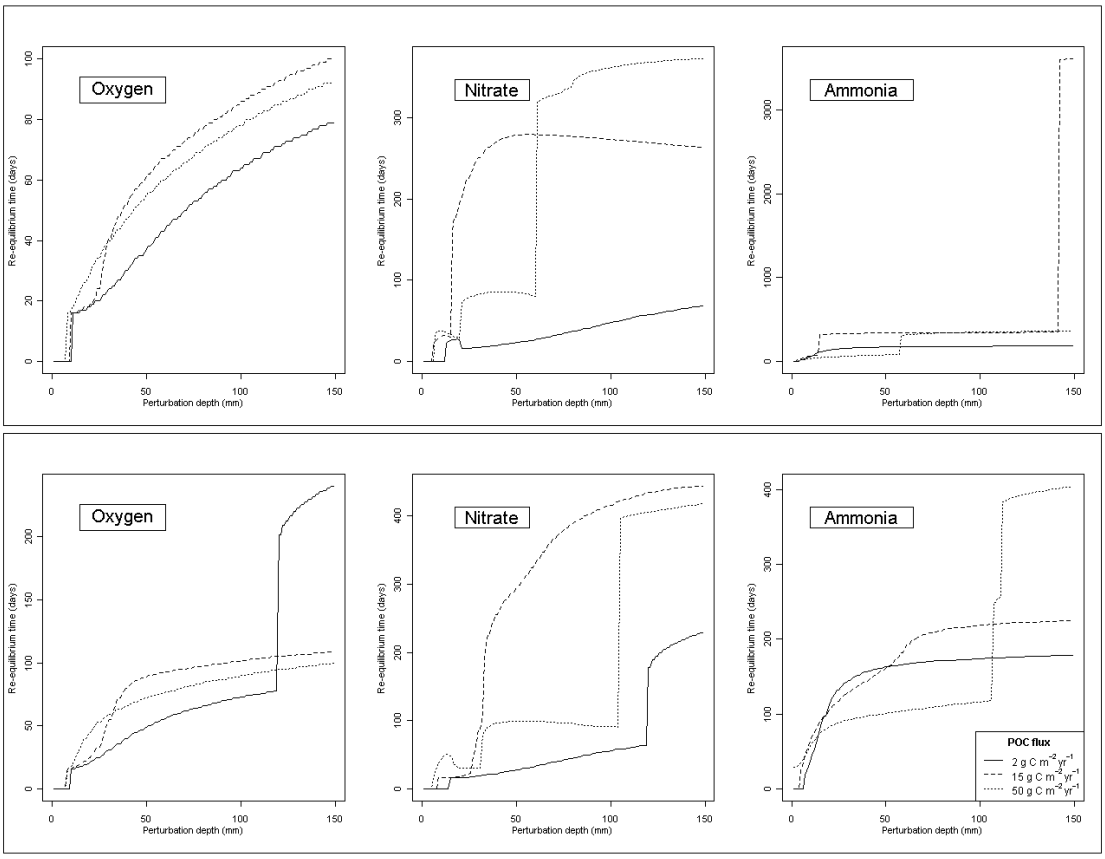

Figure 7.7: The time taken for fluxes of oxygen, nitrate and ammonia to return to re-equilibrium for the three chemical species (lower panel); for flux profiles FP2 (upper panel) and FP4 (lower panel); the results relate to a three different POC fluxes when a 95% threshold was considered

The process of nitrification results in decreased concentrations of ammonia, but occurs when the concentrations of oxygen are highest. The impact that this has on ammonia concentrations is the cause of the re-equilibrium time of ammonia being higher for POC fluxes of 2 and 15 g C m^{-2} yr^{-1} compared to a POC flux of 50 g C m^{-2} yr^{-1}

when the imposed perturbation depth of the sediment is 107 mm for the flux profile FP4. When the perturbation depth is greater than this, it seems that the high concentrations of ammonia caused by the high POC flux has more of an impact than the cycling of nutrients that nitrification causes. This leads to the observation that when deep perturbations of the sediment are considered, re-equilibrium times are more dependent on fluxes of POC than of any other biogeochemical cycling that occurs within the sediment. For the flux profile FP4, when 149 mm of sediment is resuspended, the re-equilibrium times for nitrate are 178 days, 225 days and 404 days respectively when the POC fluxes are 2, 15 and 50 g C m^{-2} yr^{-1}. It appears that the complex flux profile also helps ammonia to re-equilibrate. When the simpler single sinusoidal POC flux is imposed (FP2), then the re-equilibration time jumps from 347 days to 3605 days when the depth of perturbation is 142 mm and the mean POC flux is 15 g C m^{-2} yr^{-1}. It is difficult to explain this break, and also causes the maximum re-equilibrium times to not follow the expected patterns for deep perturbation depths. This leads to a conclusion that the more complex flux profile does, on the whole, provide potentially a more realistic picture of the impact of different perturbations under varying mean POC fluxes. This result will be further considered throughout this chapter.

Although not shown, re-equilibrium times when the threshold is increased to 99% are also generally within the timescale of the model. However, as with the results discussed above, when the simpler flux is imposed with a mean POC flux of 15 g C m^{-2} yr^{-1}, ammonia has a large jump in re-equilibrium time from 689 days to 1048 days when the perturbation depth is 37 mm, quickly rising to 3631 days when the resuspension depth is 149 mm. This correlates with a similar jump in the nitrate re-equilibrium times. This jump is not seen when the imposed mean POC flux is 2 or 50 g C m^{-2} yr^{-1}, when the re-equilibrium times for nitrate are 425 and 756 days respectively, and for ammonia are 261 and 697 days respectively. Once again, oxygen re-equilibration is dependent on resuspension depth rather than POC flux; this is reflected in the re-equilibrium times of 420 days, 452 days and 423 days when the mean POC flux is 2, 15 and 50 g C m^{-2} yr^{-1} respectively. These are almost the same re-equilibrium times when the more complex flux profile is considered (440, 438 and 455 days). The flux profile FP4 also does not cause the discontinuity in either nitrate or ammonia re-equilibrium times, with the re-equilibrium times being 446, 618 and 766 days for nitrate, and 312, 416 and 616 days for ammonia for mean POC fluxes of 2, 15 and 50 g C m^{-2} yr^{-1} respectively. It is also worth stating at this stage that the non-linearity in the re-equilibrium times between a 95% and 99% threshold are due to the model non-linearity. The non-linearity means that concentrations of the chemical species cannot be interpolated, and, as such, re-equilibration times also cannot be accurately interpolated between different thresholds. It can also be clearly seen in

Figure 7.7 that, even when the depth of perturbation is 149 mm, all of the lines are either positively or negatively trending, implying that a change in any parameter of variable value is likely to affect the re-equilibrium time.

As a result of the output seen for the flux patterns of FP4, only results for FP4 will be described for the remainder of this chapter. Although FP3 was a good stepping stone to developing a more realistic carbon flux over annual timescales, the encouraging results shown by FP4, as well as its slightly more realistic pattern (with a gradual increase in flux throughout the spring, rather than a large increase in flux via one step) means that its results are also likely to be more realistic, as well as being easier to interpret. It was also found during the course of the model runs that the runs where flux profile FP2 was used did not run significantly faster than those where FP4 was used. Therefore, although a full quantitative analysis on the results between FP2 and FP4 has not been carried out, there appears to be no drawbacks in using FP4. The results discussed throughout the remainder of this chapter will therefore use the output from model runs where FP4 was imposed, rather than FP2.

It is also clear that re-equilibrium timescales for fluxes across the SWI, as opposed to timescales for the re-equilibrium of the concentration in the entire sedimentary column, are easier to both calculate and interpret. Therefore, flux re-equilibrium times will be considered for the remainder of this chapter.

7.2.2 Effect of different mixed layer depth

Repeat experiments were conducted with mixed layer depths of 1, 5 and 15 cm, with the model being allowed to run for 100 years. One perturbation event was included in the model run, at day 14. Figure 7.8 shows the re-equilibrium times versus perturbation depth for carbon, oxygen, nitrate and ammonia when a steady POC flux was 15 g C m^{-2} yr^{-1} was imposed.

Figure 7.8 provides some interesting insights; firstly, it can be seen that carbon re-equilibration time is not related to the depth of the mixed layer. This is similar to Figure 6.1, where carbon re-equilibration was not related to the flux of POC to the sediment. Overall, carbon re-equilibration follows a pattern which is to be expected – that the time taken for re-equilibration does increase with depth, and, as the concentrations of organic matter decrease to infinitesimally small values as it gets mineralised in the sediment, the time taken for re-equilibration at these depths levels off. The depth of perturbation at which the re-equilibration time starts to level off, 46 mm, is also the approximate depth at which carbon concentrations decrease to values close to zero. Figure 7.10 shows the carbon re-equilibration time when the POC flux

is 2 and 50 g C m^{-2} yr^{-1}. The re-equilibrium time profile flattens off at approximately the same depth of perturbation as when the POC flux was 15 g C m^{-2} yr^{-1}. The re-equilibrium times when the resuspended depth is 149 mm for all three carbon fluxes are 349 days, 340 days and 340 days when the mixed layer depths are 1, 5 and 15 cm respectively. It can be concluded that the time for re-equilibration for carbon is not linked to either the depth of the mixed layer or to the flux of POC to the sediment. Instead, it seems that by far the most important parameter is just the depth of perturbation.

The remaining three chemical species show that the re-equilibrium time is dependent on the mixed layer depth, with re-equilibrium taking longest when the mixed layer depth is 1 cm (Figure 7.8). The shortest re-equilibrium times occur when the mixed layer depth is 15 cm. However, the fact that nitrate and ammonia do not re-equilibrate within the model time scale of 36500 days when the depth of the mixed layer is either 1 or 5 cm detracts slightly from the re-equilibrium time when the mixed layer depth is 15 cm.

The re-equilibrium times under these conditions are 563 days, 477 days and 845 days respectively for oxygen, nitrate and ammonia when the perturbation depth is 15 cm, and therefore it should be noted that re-equilibrium still takes between 1 and 3 years for these species under the conditions shown here. Re-equilibrium is instantaneous when the perturbation depth is less than 7, 9 and 10 mm for the three chemical species respectively, with the re-equilibrium time profiles showing the same shape as for carbon – for the same reason that at depth, the concentration of all the species becomes insignificant. The inability of nitrate and ammonia to reach pre-perturbation values within the timeframe of the model above perturbation depths of 60 and 63 mm respectively shows the importance of biological mixing in the role of sedimentary biogeochemical cycling. Although the large step in the re-equilibrium time, from approximately 2 years to more than 100 years (given that 100 years is the timescale of the model run) of these two chemical species coincides with the approximate depth of the nitrate peak, the reason for the increase in re-equilibrium time is unclear.

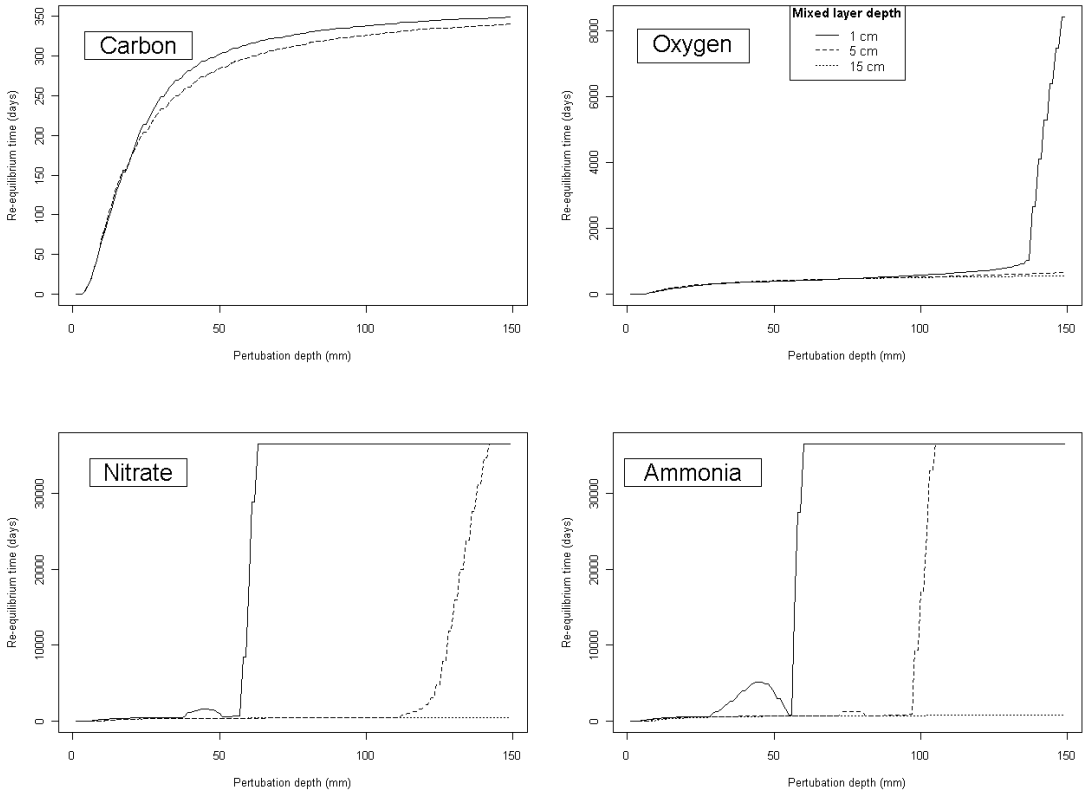

Figure 7.8: Sedimentary re-equilibrium timescales of carbon, oxygen, nitrate and ammonia using method 1 to calculate re-equilibrium timescales when a 95% threshold is considered for 3 different mixed layer depths, when a steady POC flux of 15 g C m^{-2} yr^{-1} was imposed, over a range of perturbation depths

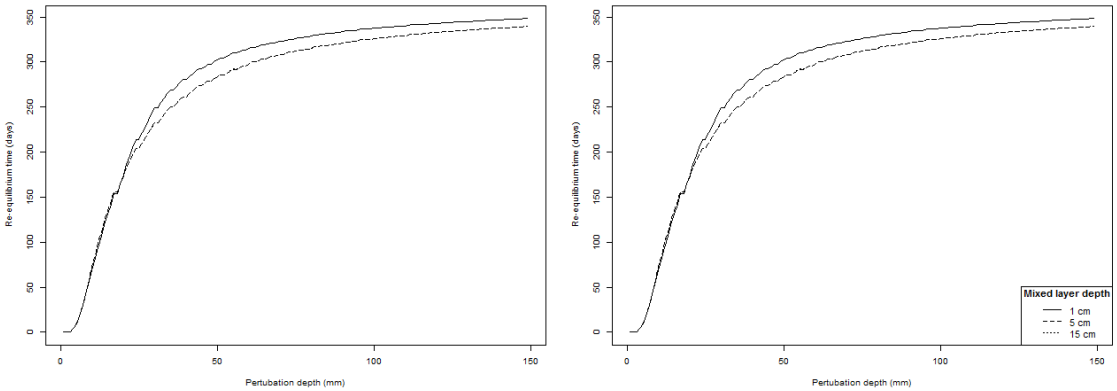

Figure 7.9: Sedimentary re-equilibrium timescales of carbon using method 1 to calculate re-equilibrium timescales when a 95% threshold is considered for 3 different mixed layer depths, when a steady POC flux of 2 g C m^{-2} yr^{-1} (left panel) and 50 g C m^{-2} yr^{-1} (right panel) was imposed, over a range of perturbation depths

A comparison between the total inventory and the steady-state value shows the re-equilibrium times for this experiment for ammonia when the more complex trigonometric carbon flux profile (FP4) is used (Figure 7.11). Re-equilibrium time for carbon, oxygen and nitrate is zero across all perturbation depths, for the reasons already discussed. Once again, re-equilibration is instantaneous when the depth of perturbation is below 51, 49 and 47 mm respectively for mixed layer depths of 1, 5 and 15 cm; when the depth of perturbation is greater than this, the time taken for the sediment to return to pre-perturbed values increases logarithmically. There is a large re-equilibration timestep between the final perturbation depth when re-equilibration is instantaneous, and the first perturbation depth at which re-equilibration is not instantaneous (see also Figure 7.5)

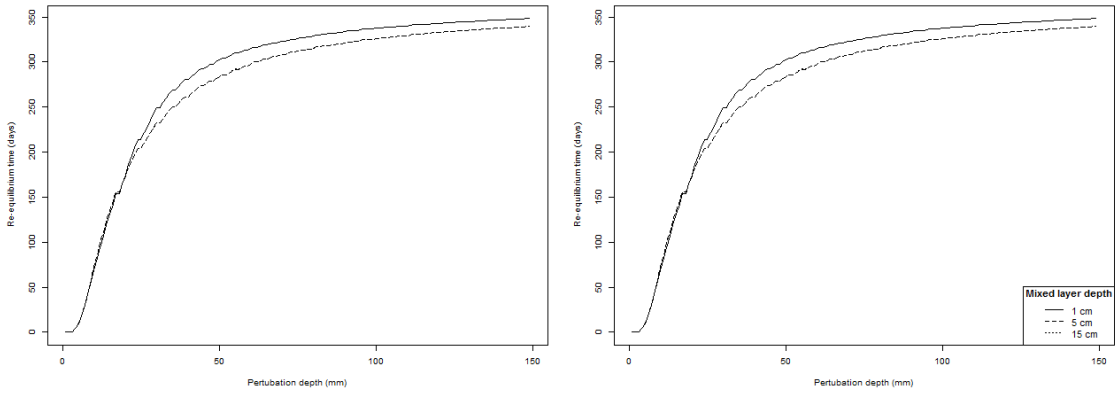

Figure 7.10: Sedimentary re-equilibrium timescales of carbon using method 1 to calculate re-equilibrium timescales when a 95% threshold is considered for 3 different mixed layer depths, when a steady POC flux of 2 g C m^{-2} yr^{-1} (left panel) and 50 g C m^{-2} yr^{-1} (right panel) was imposed, over a range of perturbation depths

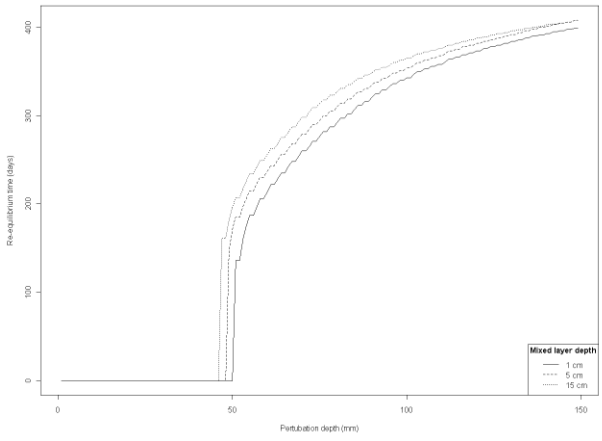

Figure 7.11: Sedimentary re-equilibrium timescales of ammonia using method 2 to calculate re-equilibrium timescales using a 95% threshold for 3 different mixed layer depths, when the flux profile FP2, with an average POC flux of 15 g C m^{-2} yr^{-1} was imposed, over a range of perturbation depths

The effect of changing the mixed layer depth on the fluxes can also be examined. For brevity, only the effect on constant fluxes and on FP4 are discussed here. Figure 7.12 shows the re-equilibrium time needed for the SWI fluxes of oxygen,

nitrate and ammonia for the three mixed layer depths and the three POC fluxes that were investigated, for a constant POC flux when a 95% threshold was used.

In general, re-equilibrium time is not linked to the mixed layer depth; however, it can be seen that both the imposed POC flux and the perturbation depth are important, and changing the mixed layer depth does not affect the perturbation time. The large peak seen in the nitrate re-equilibrium time when the POC flux is 15 g C m^{-2} yr^{-1} and the mixed layer depth is 1 cm is as a result of the nitrate peak in the sediment. This pattern is not seen when the POC flux is either 2 or 50 g C m^{-2} yr^{-1} due to no nitrate peak forming (in the former case) or the peak being much more shallow, and hence higher biogeochemical process rates driving the peak back to pre-perturbed values more quickly in the latter case.

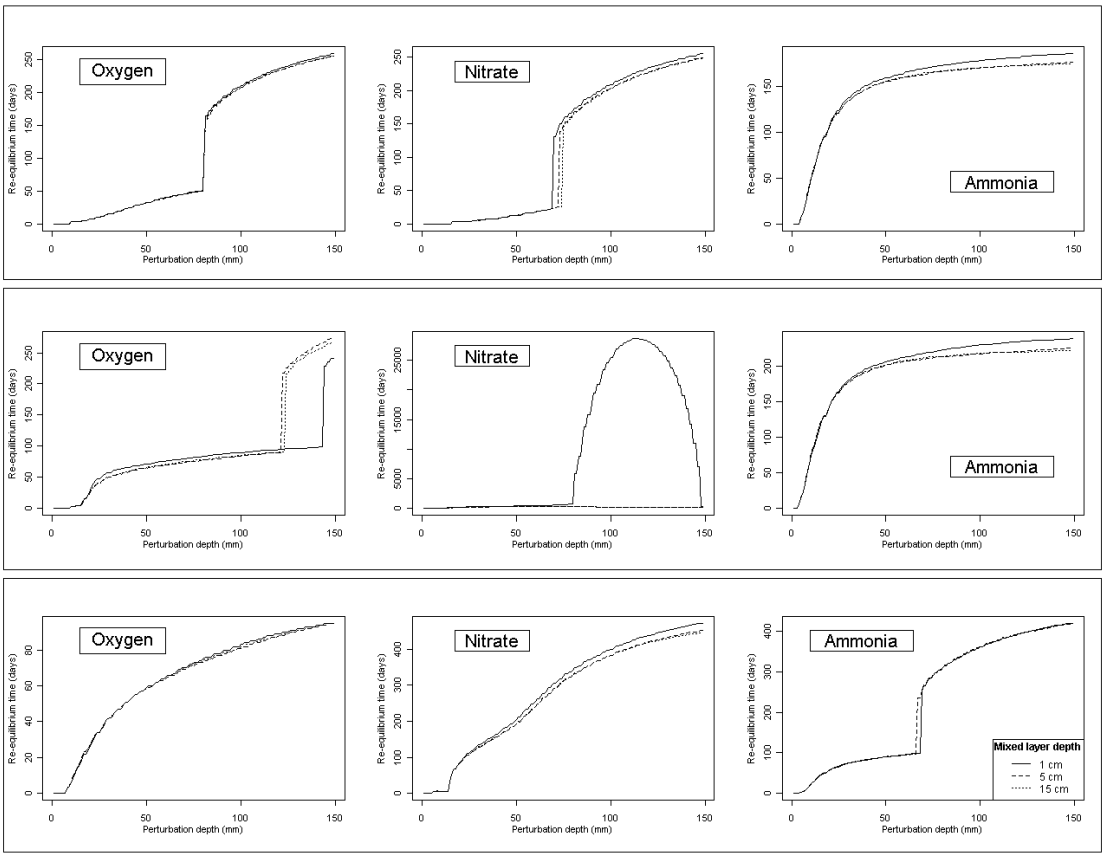

Figure 7.12: The time taken for fluxes of oxygen, nitrate and ammonia to return to re-equilibrium for the three chemical species (lower panel) for constant POC fluxes of 2 g C m^{-2} yr^{-1} (upper panel), 15 g C m^{-2} yr^{-1} (middle panel) and 50 g C m^{-2} yr^{-1} (lower panel); the results relate to the three mixed layer depths considered using a 95%

Although the mixed layer depth has an influence on the distribution on the chemical species, the results from this experiment show that it has very little overall influence on the general biogeochemical process. The only reason why nitrate takes so

long to re-equilibrate (and shows the peak in re-equilibrium times when the perturbation depth is 114 mm) when the mixed layer depth is 1 cm is likely to be due to the enhanced variability in the nitrate peak that a lack bioturbation causes. It shows that bioturbation may have an important role in the distribution of nutrients under certain conditions, leading to lower re-equilibration times when the mixed layer depth is 5 or 15 cm. However, as the profiles for all other nutrients under all other conditions are more easily resolved, and less affected by multiple processes at different depth levels, the effect of bioturbation is minimal compared with the other processes of diffusion and microbially-mediated chemical reactions.

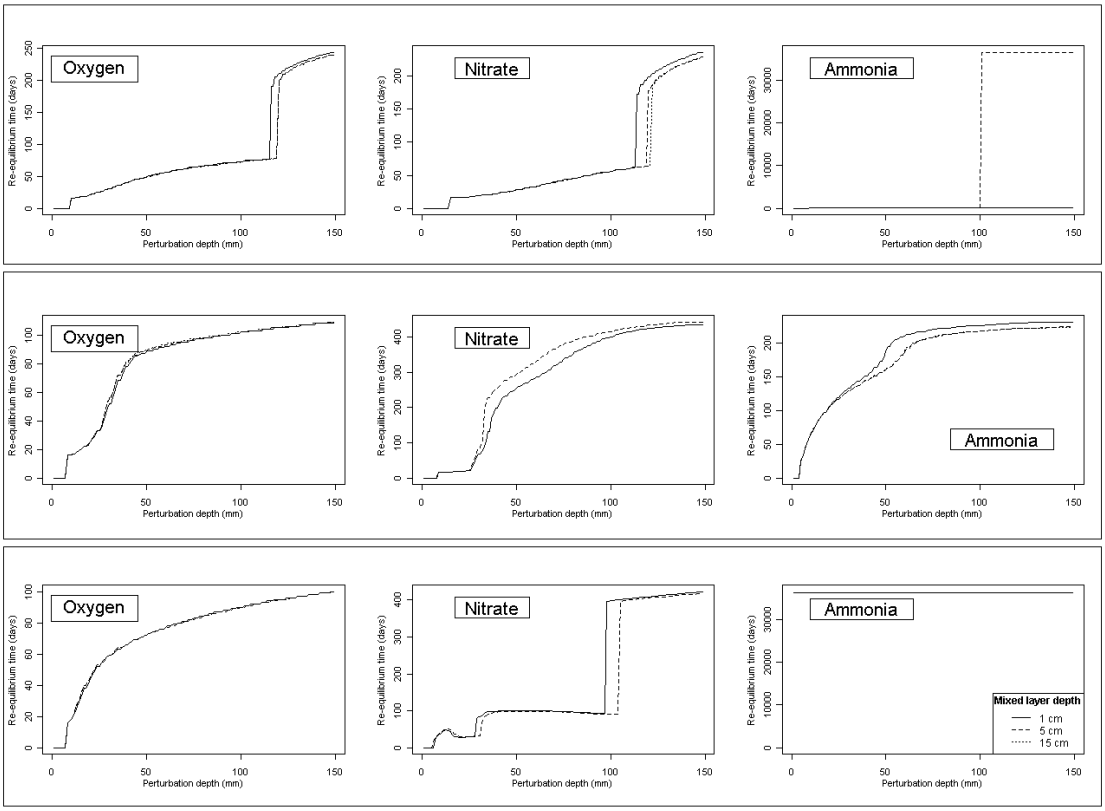

Figure 7.13: The time taken for fluxes of oxygen, nitrate and ammonia to return to re-equilibrium for the three chemical species for mean POC fluxes of 2 g C m^{-2} yr^{-1} (upper panel), 15 g C m^{-2} yr^{-1} (middle panel) and 50 g C m^{-2} yr^{-1} (lower panel), using the flux profile FP4; the results relate to the three mixed layer depths considered using a 95% threshold

It should be noted from Figure 7.13 that the results for nitrate when the POC flux is 15 and 50 g C m^{-2} yr^{-1} with a model mixed layer depth of 15 mm are not shown; the re-equilibrium time for nitrate across all perturbation depths for both of these POC fluxes was greater than the time scale of the model, and would have distorted the results when the mixed layer depth was 1 and 5 cm. Once again, it can be seen that in general, the mixed layer depth has very little influence on the re-equilibrium time. The overall range of re-equilibrium times between a run with a constant POC flux and

a run with a variable POC flux is also very similar, although the pattern in re-equilibrium times is clearly different. The majority of patterns seen have already been discussed in this chapter, particularly with respect to the approximate logarithmic shape of the graphs, the large steps seen in the oxygen and nitrate re-equilibrium times when the POC flux is 2 g C m^{-2} yr^{-1}, and the initial rise and fall of the nitrate re-equilibrium time when the POC flux is 50 g C m^{-2} yr^{-1}. However, some observations between the two sets of plots warrant some further discussed. As a result of nitrate being unable to return to pre-perturbation patterns, it is unsurprising that ammonia also fails to return to a quasi-steady state; it is also unsurprising that this observation, in both the nitrate and ammonia re-equilibration times, is also observed in the run where the mixed layer depth was 1 cm with a mean POC flux of 50 g C m^{-2} yr^{-1}. However, it is not observed in the run with a mean POC flux of 2 g C m^{-2} yr^{-1}, as the biogeochemistry of the conditions dictates that no nitrate peak is produced. It seems to be the complex nature of the processes causing the nitrate peak which means that solely physical transport mechanisms are unable to recreate this profile within the model timescale of 100 years, and that the enhanced transport given by bioturbation is needed for re-equilibration to proceed.

The change in the fluxes of oxygen, nitrate and ammonia for the two flux profiles considered in these results follow the same general patterns as the re-equilibrium times. Figures 7.14 and 7.15 confirm that the mixed layer depth has little effect on the fluxes of the chemical species following a resuspension event. There are some exceptions to this general rule though; when a constant POC flux is imposed, a mixed layer depth of 5 cm may drive changes in the flux of ammonia when the POC flux is 50 g C m^{-2} yr^{-1}. A high POC flux should indicate that concentrations of ammonia in the sediment are comparatively high; it would therefore be expected that when the sediment is perturbed, and the ammonia concentration is decreased throughout the whole sedimentary column, the flux would be greatest. The result seen here could indicate either that under specific conditions, the mixed layer depth in the model does have the ability to rapidly redistribute nutrients; however, it could also be as the result of a discontinuity in the model. This could only be confirmed with more extensive testing of the model and, ideally, observational data. The very small difference seen when the POC flux is 2 g C m^{-2} yr^{-1}, which is as a result nitrification occurring due to lower POC fluxes encouraging nitrification as a result of excess oxygen being available in the sediment, are insignificant when compared with the ammonia flux changes seen when the POC flux is 50 g C m^{-2} yr^{-1}. The effect of changing the POC flux can be seen here, with change in flux of nitrate showing the same pattern when the POC flux is 2 or 15 g C m^{-2} yr^{-1}, as a result of the water column nitrate concentration being higher than the sedimentary concentrations. The low percentage change in nitrate flux when the perturbation depth is 43 mm is as a result of the concentration of nitrate at the depth

of resuspension approximately matching the water column concentration. The remaining plots in Figure 7.15 show the same patterns as the ones in Figure 7.14, for the reasons already discussed. The overarching conclusion is that the depth of the mixed layer does not affect the outcome of perturbation events.

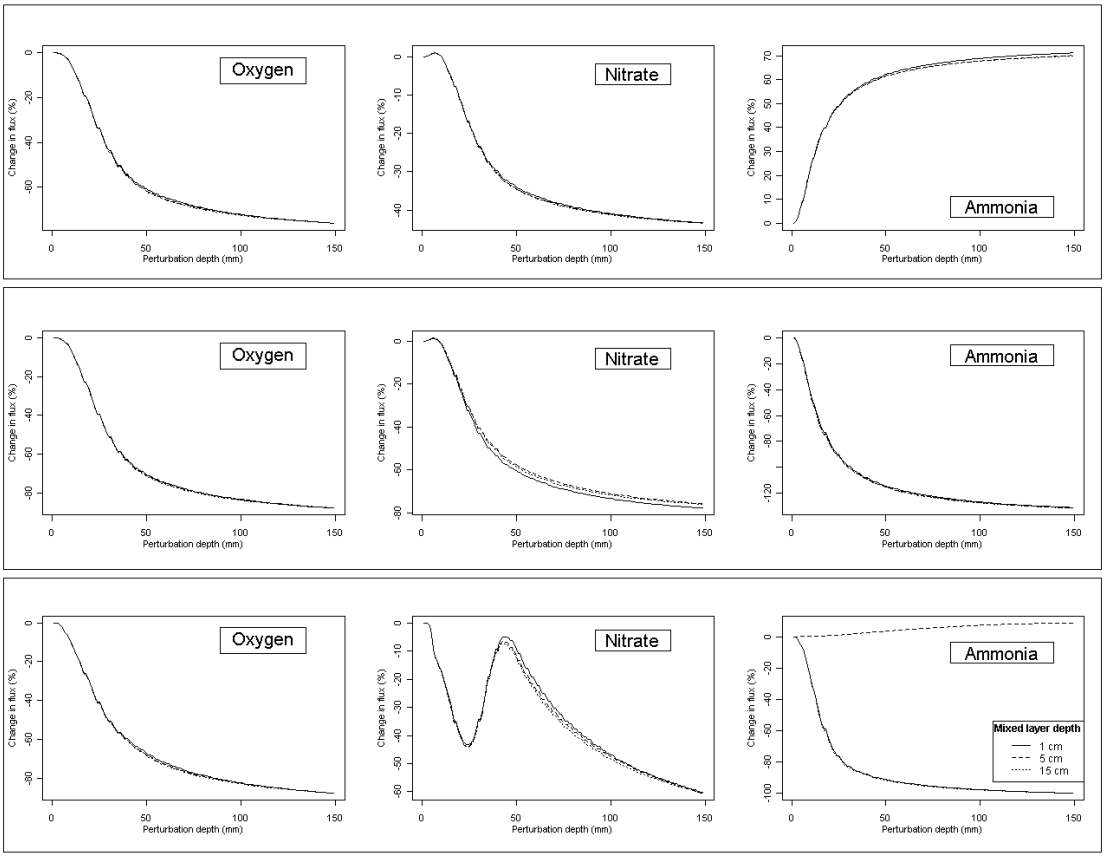

Figure 7.14: The resulting percentage change in flux for oxygen, nitrate and ammonia that a perturbation event causes when a constant POC flux of 2 g C m^{-2} yr^{-1} (upper panel), 15 g C m^{-2} yr^{-1} (middle panel) and 50 g C m^{-2} yr^{-1} (lower panel) is imposed; the results relate to the three different mixed layer depths when a 95% threshold was considered

When a variable flux profile is imposed on the model, the change in flux of oxygen is similar as to when the POC flux was constant; however, fluxes of nitrate and ammonia do vary. The change in flux is the same when a mean POC flux of 2 or 15 g C m^{-2} yr^{-1} is imposed, but the magnitude of the change is much greater when the POC flux is 50 g C m^{-2} yr^{-1} and the mixed layer depth is 15 cm. This increase is due to the conditions of the sediment immediately preceding the perturbation event. The flux profile FP4 has a minimum POC flux at the beginning of the year, which will correspond with a buildup of nitrate in the sedimentary column throughout the autumn of the previous year when the POC flux is decreasing. A perturbation event will increase the concentration of nitrate, leading to a situation when nitrate needs to

diffuse out of the sediment in order for pre-perturbation concentrations to be re-established. The difference seen between the fluxes of nitrate between a mixed layer depth of either 1 or 5 cm and a mixed layer depth of 15 cm is the only result where mixed layer depth does appear to affect the results of a perturbation event. It is likely that the depth of the mixed layer does effect the distribution of nitrate under these conditions, hence leading to the results observed.

There is a similarity between the change in flux of ammonia and ammonia's re-equilibration time, in that a large jump is seen at a perturbation depth of 101 mm when the POC flux is 2 g C m^{-2} yr^{-1} and the mixed layer depth is 5 cm. The assumption is that this is due to a slight discontinuity in the model, particularly as the change in flux is not directly related to the re-equilibrium time.

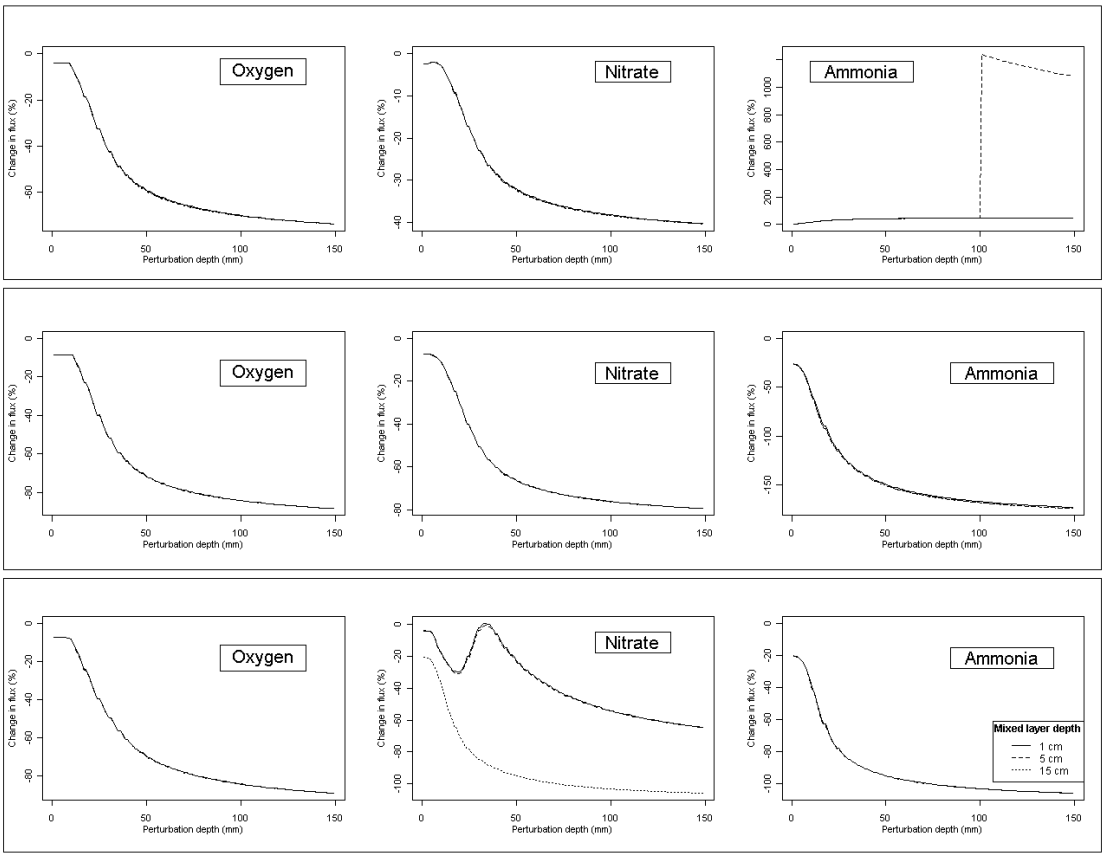

Figure 7.15: The resulting percentage change in flux for oxygen, nitrate and ammonia that a perturbation event causes when a mean POC flux of 2 g C m^{-2} yr^{-1} (upper panel), 15 g C m^{-2} yr^{-1} (middle panel) and 50 g C m^{-2} yr^{-1} (lower panel) imposing the flux profile FP4; the results relate to the three different mixed layer depths when a 95% threshold was considered

7.2.3 Effect of different POC forcing fluxes

The results, and plots, presented so far in this chapter can be used to make inferences about the importance of different POC fluxes to the sediment; these results will be augmented with further results given in this section. As has been seen throughout Chapters 3, 4 and 5, due to the highly non-linear nature of the model, a linear change in one parameter is very unlikely to result in a linear change of one metric of output; however, some general comments can be made. It is clear that the magnitude of the POC flux does have an effect. This is confirmed in Figure 7.15, which explicitly shows the change in flux as a result of varying POC flux. To verify that mixed layer depth does not have an effect, the results of all three mixed layer depths are shown, but it is clear that the plot for each nutrient from each panel will be the same. Table 7.1 also shows quantitatively that lack of effect that changing the mixed layer depth has, by showing the standard deviation of the mixed layer depths for each of the POC fluxes. In order to provide a comparison, the equivalent standard deviation when applied to variance of the effect of changing the POC flux is shown in Table 7.2. The small values of the standard deviations in Table 7.1, relative to those in Table 7.2, show the lack of variation that mixed layer flux has.

Table 7.1: Standard deviation of the percentage change in flux (mmol m^{-2} yr^{-1}) of each of the chemical species for the three POC imposed fluxes associated with varying the mixed layer depth

	POC flux (g C m^{-2} yr^{-1})		
	2	15	50
Oxygen	34.1	10.0	2.4
Nitrate	31.0	63.6	4.4
Ammonia	45.0	27.3	6.8

Table 7.2: Standard deviation flux of the percentage change in flux (mmol m^{-2} yr^{-1}) of each of the chemical species for the three POC imposed fluxes associated with varying the POC flux

	Mixed layer depth (cm)		
	1	5	15
Oxygen	779.0	685.0	424.0
Nitrate	773.9	628.0	429.4
Ammonia	778.8	655.2	427.5

By viewing the change in flux in each of the nutrients following a perturbation event during runs with different mean carbon fluxes, an idea of importance of the carbon flux can be obtained (Figure 7.16). It can be clearly seen that the POC flux has more of an influence on the perturbation of the sedimentary system than mixed layer depth does; based on the results of the previous section showing how little effect the mixed layer depth has, it is not surprising that the three graphs for each nutrient look similar, and therefore the discussions here will focus on the graphs which show the results when the mixed layer depth is 5 cm. The exception to this is that a mixed layer depth of 5 cm does change the flux of ammonia when the POC flux is 50 g C m^{-2} yr^{-1}, for reasons already discussed.

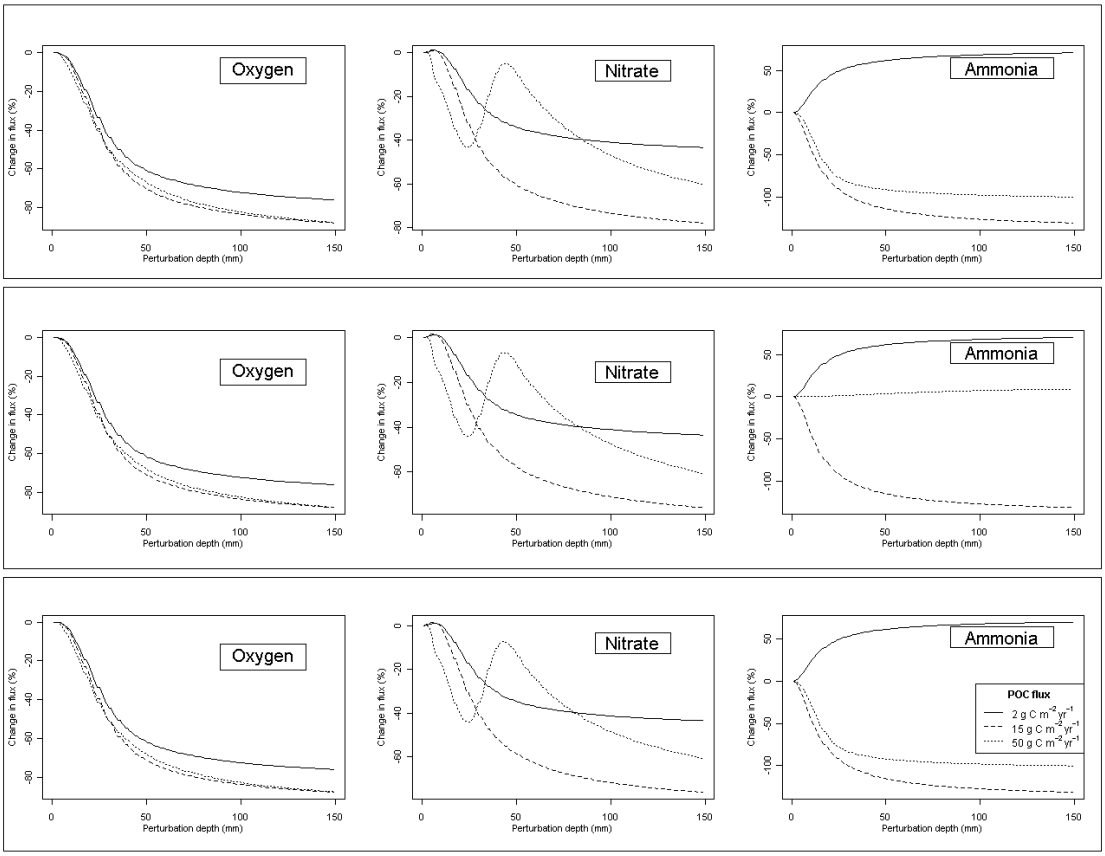

Figure 7.16: The resulting percentage change in flux for oxygen, nitrate and ammonia that a perturbation event causes when mixed layer depths of 1 cm (upper panel), 5 cm (middle panel) and 15 cm (lower panel) were set; the results relate to the three different constant POC fluxes when a 95% threshold was considered

The patterns of the results are as expected, based on the results from the previous sections in this chapter. Oxygen fluxes are out of the sediment, and increase as the depth of perturbation increases in order to reach equilibrium. The profiles for the oxygen variation when the POC flux is 15 and 50 g C m^{-2} yr^{-1} are similar due to only a narrow difference in the OPD at these two POC fluxes (1 and 4 cm respectively).

When the POC flux is much lower, the OPD is comparatively much deeper; from Chapter 2, it can be seen that oxygen concentrations remain above 240 mmol m^{-3} throughout the whole sedimentary column, as a result of sufficient oxygen being available to oxidise all available organic matter. The peak seen in the change in nitrate when the POC flux is 50 g C m^{-2} yr^{-1}, as already discussed, is as a result of the calculation used here using the flux in the day immediately after the perturbation event; a high POC flux means that the greatest change in flux is only seen two days after the event. Perturbation events during lower POC fluxes do not show a peak in flux as there is an immediate excess of nitrate, and so a flux is established. The reasons for the patterns seen in the ammonia fluxes have already been discussed in this chapter.

When the perturbation depth is 5 cm, increasing the imposed POC flux from 2 to 15g C m^{-2} yr^{-1} leads to an increase in the flux of oxygen by 9.52 percentage points; increasing the POC flux to 50 g C m^{-2} yr^{-1} leads to a slight decrease of 3.12 percentage points. The similar fluxes between the O_2 flux when the POC flux is 15 and 50 g C m^{-2} yr^{-1} is due to the OPD being shallower than 5 cm for both of these fluxes; the slight decrease in the magnitude of the flux at the highest POC flux is almost certainly as a result of the increased oxygen availability in the sediment being utilised for organic matter mineralisation of the redistributed carbon. When the perturbation depth is 10 cm, the changes in fluxes are 11.2 and -1.0 percentage points, and 11.8 and 0.2 percentage points when the perturbation depth is 15 cm. The highest nitrate change in flux is -77.8% when the perturbation depth is 149 mm, which occurs when the POC flux is 15 g C m^{-2} yr^{-1}. The maximum variation in flux when the POC flux is 2 g C m^{-2} yr^{-1} is 43.2%, while the maximum variation when the POC flux is 50 g C m^{-2} yr^{-1} is -60.2%. The extreme POC fluxes lead to lower change in flux of nitrate if the entire sedimentary column is perturbed compared to a POC flux of 15 g C m^{-2} yr^{-1} due to lower variability in nitrate concentration when integrated over the whole sedimentary column. Meanwhile, a POC flux of 2 g C m^{-2} yr^{-1} leads to a flux of ammonia of up to 70.1% (from 1.0 mmol m^{-2} d^{-1} to 1.7 mmol m^{-2} d^{-1}), when the perturbation depth is 149 mm; if the POC flux is increased to 50 g C m^{-2} yr^{-1}, the flux decreases from -27.1 mmol m^{-2} d^{-1} to -0.4 mmol m^{-2} d^{-1}.

The effect on re-equilibrium times by varying the POC flux show the same patterns as previously discussed. Figure 7.17 shows the re-equilibration times when the mixed layer depth is 5 cm; the patterns seen when the mixed layer depth is 1 or 15 cm are the same as a mixed layer depth of 5 cm, with the exception of a POC flux of 15 g C m^{-2} yr^{-1}, when the mixed layer depth was 1 cm, which echoes the profile in Figure 7.12. From Figure 7.17, it can be seen that POC flux does, as expected, have an influence on the re-equilibrium of the chemical fluxes. Oxygen re-equilibrates fastest

after shallow perturbations when the POC flux is low, as a result of the sedimentary concentrations being close to those in the water-column. However, when the perturbation is deeper, a high POC flux helps re-equilibration to occur more quickly, because of the shallow OPD. It can be seen that re-equilibration is non-linear with respect to POC flux; when the perturbation depth is 149 mm, the re-equilibration time is 255 and 273 days when the POC flux is 2 and 15 g C m^{-2} yr^{-1} respectively, but is only 95 days when the POC flux is 50 g C m^{-2} yr^{-1}. The opposite pattern is seen in the nitrate flux re-equilibration times, which show that re-equilibration occurs in 249 and 225 days respectively when the POC flux is 2 and 15 g C m^{-2} yr^{-1} if 149 mm is perturbed, compared with 452 days if the POC flux is 50 g C m^{-2} yr^{-1}, as a result of the high concentrations of nitrate imposed at the bottom of the sedimentary column compared with pre-perturbation values. Ammonia flux re-equilibration times level off approximately at the same perturbation depths at which concentrations of ammonia start to become constant with depth; however, when the POC flux is 2 g C m^{-2} yr^{-1}, the ammonia flux takes longer to return to a pre-resuspension event value than might have been expected and it appears that the increase throughout the sedimentary column of approximately 0 to 1 mmol m^{-3} is enough to disrupt the biogeochemical processes such that it takes 106 days for re-equilibrium to occur when the perturbation is only 20 mm.

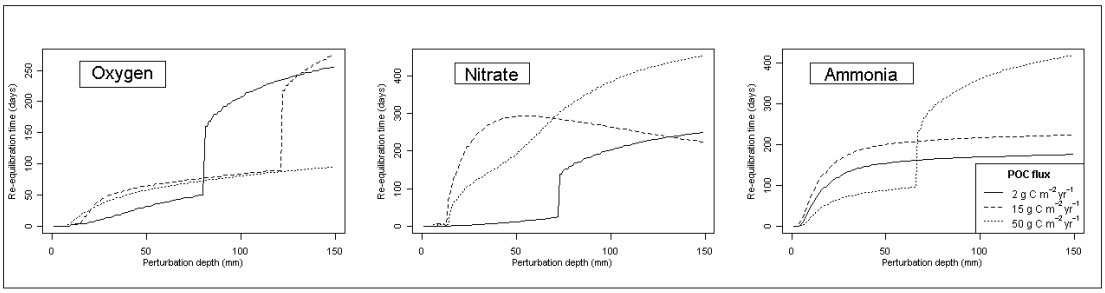

Figure 7.17: The re-equilibration time for the fluxes of oxygen, nitrate and ammonia that a perturbation event causes when mixed layer depths of 5 cm was set; the results relate to the three different constant POC fluxes when a 95% threshold was considered

Finally, the effect of a variable POC flux will be briefly discussed. However, as the mixed layer depth, in general, has very little effect, only the results from the runs where the mixed layer depth was 5 cm will be discussed.

The re-equilibrium times in Figure 7.18 show that oxygen takes 73, 102 and 90 days to return to pre-perturbed values for POC fluxes of 2, 15 and 50 g C m^{-2} yr^{-1} respectively, when the depth of perturbation is 100 mm. If the perturbation depth is reduced to 20 mm, then the re-equilibrium times are 21, 25 and 45 days respectively.

It is likely that the re-equilibrium time is longest when the POC flux is 15 g C m^{-2} yr^{-1} when the depth of resuspension is 100 mm as at this depth the nitrate peak will also have been disturbed, and therefore this will need to be re-established in order for the fluxes of each of the chemical species to return to pre-perturbed states. However, when the perturbation is shallower, this is not the case, and the biogeochemical processes are able to drive the system back to equilibrium more quickly. This is also reflected in the nitrate graph, where a perturbation event of 10 mm leads to re-equilibrium times of 0, 16 and 43 days for the three increasing POC fluxes, while a perturbation event of 100 mm leads to re-equilibrium times of 56, 416 and 91 days. The much longer time for the re-equilibrium when the POC flux is 15 g C m^{-2} yr^{-1} is a reflection of the time needed for the nitrate peak to be re-established. As has been implied earlier in this chapter, and is clear from the graph, re-equilibrium times are not linear either with respect to POC flux or perturbation depth. Once again, there appears to be some discontinuities in the model, leading to the jumps in re-equilibration times seen when the perturbation depths are 100 mm, 104 mm, and 119 mm. The model also seems unable to resolve the re-equilibrium times for ammonia when the POC flux is 2 or 50 g C m^{-2} yr^{-1}. However, the re-equilibrium times when the POC flux is 15 g C m^{-2} yr^{-1} seem reasonable, and follow similar patterns to the nitrate and oxygen graphs, with an approximately linear increase from 0 to 225 days.

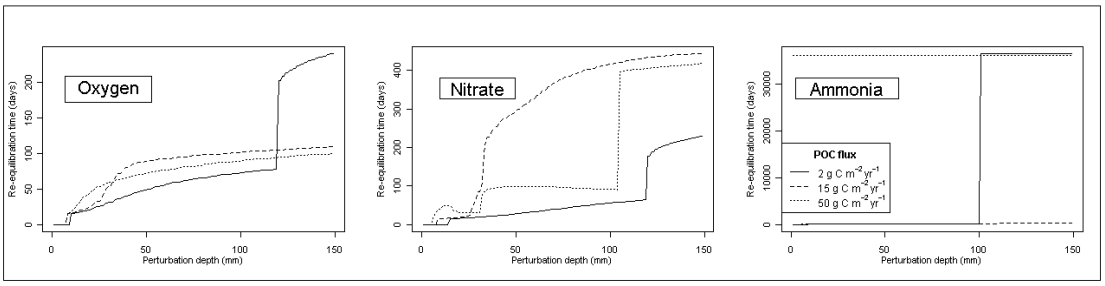

Figure 7.18: The re-equilibration time for the fluxes of oxygen, nitrate and ammonia that a perturbation event causes when a mixed layer depth of 5 cm was set; the results relate to the three different POC fluxes when the FP4 POC flux was imposed and a 95% threshold was considered

With the exception of the discontinuity seen in the ammonia flux when the POC flux is 101 mm, the patterns seen in the fluxes of the chemical species broadly follow the patterns seen previously, despite the imposed time-varying carbon flux (Figure 7.19). As with a constant POC flux, increasing the perturbation depth from 10 to 50 mm causes an increase in the magnitude of the flux of O_2 from -8.5% to -71.8%; however, these reflect an absolute change in fluxes of 46.1 mmol m^{-2} d^{-1} and 242.4 mmol m^{-2} d^{-1}. During a steady-state run, the absolute changes in fluxes are 26.5 mmol m^{-2} d^{-1} and 297.6 mmol m^{-2} d^{-1}; the increased absolute flux during the shallower

perturbation is unsurprising, as the beginning of the year represents a period of low POC flux, and so oxygen, which is consumed during nitrification, is depleted, leading to a greater relative difference between the sedimentary and water-column when comparing a steady-state and non-steady state run. However, at deeper perturbation depths, the time-varying POC flux run has a slightly lower absolute flux as a result of the overall build-up of oxygen in the sediment, leading to a slightly lower difference between the oxygen concentrations at this depth and the water column values.

Increasing the POC flux from 2 to 50 g C m^{-2} yr^{-1} leads to the nitrate flux being reduced by an extra 15 percentage points when the perturbation is 10 mm, but only an extra 15.9 percentage points when the perturbation is 100 mm.

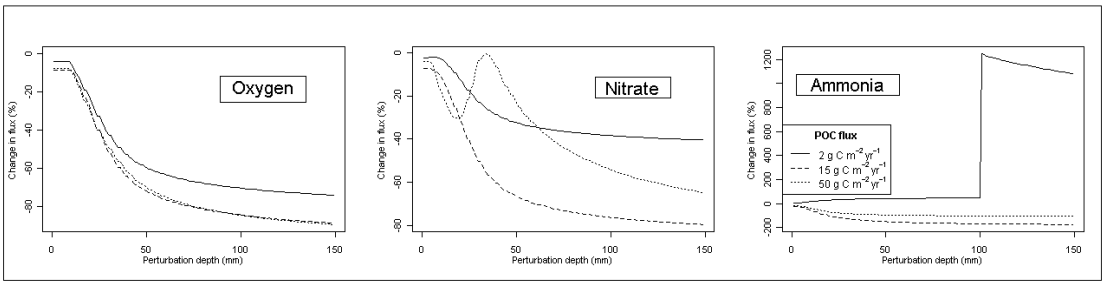

Figure 7.19: The resulting percentage change in flux for oxygen, nitrate and ammonia that a perturbation event causes when a mixed layer depth of 5 cm was set; the results relate to the three different POC fluxes when the FP4 POC flux was imposed and a 95% threshold was considered

7.2.4 Effect of perturbation depth

The results presented in the above sections have shown re-equilibrium times as a function of depth perturbation, and the variation of fluxes across the SWI as a result of different perturbation depths, and so a summary of these results can be discussed here. The main conclusion is that the depth of perturbation has a complex and non-linear, but clearly significant effect on both of the outputs measured in the experiments discussed. Excluding the runs where discontinuities are apparent, increasing perturbation depths from 10 to 100 mm when the mean POC flux is 15 g C m^{-2} yr^{-1}, a time-varying POC flux is imposed, and the mixed layer depth is 5 cm increases the magnitude in the change of flux from -8.8% to -84.3%; increasing the perturbation depth even further to 14.9 mm only increases the magnitude in the flux to -88.4%. Similarly, for nitrate, the equivalent percent changes in the fluxes are -11.0%, -76.2% and -79.5%.

If a brief comparison is made with a steady-state run with all other parameters kept, then the equivalent change in fluxes are -6.3%, -83.4% and -87.8% for oxygen, and 0.5%, -71.0% and -75.8% for nitrate. The similar fluxes for oxygen and nitrate at 100 and 149 mm are as a result of the depletion of the chemical species with depth. There is a very small change in the nitrate flux (-34.76 mmol m^{-2} d^{-1} compared to -34.95 mmol m^{-2} d^{-1}, although it should be noted that the flux is -36.5 mmol m^{-2} d^{-1} in the next timestep) when the perturbation depth is 10 mm, caused by the fact the water column concentration and sedimentary concentrations integrated across the depth of perturbation are very similar. The small amount of extra nitrate imposed during the perturbation is diffused out of the sediment. During deeper resuspension events, the imposed nitrate is utilised in denitrification; although the integrated concentration of nitrate will be higher following a perturbation event than under steady-state conditions, the biogeochemical processes cause the nitrate to be cycled within the sediment before it is diffused across the SWI, leading to a decrease in the flux before equilibrium is re-established.

7.2.5 Closing remarks of results

The decision as to when to impose the perturbation event in the model was relatively arbitrary, although day 14 was chosen as corresponding with the middle of January, when the chance of high energy storms is relatively high as a result of low pressure weather systems, compared with the majority of the rest of the year (Flocas 1988); the North Sea has also specifically been found to have a higher intensity of low pressure systems than areas in the central North Atlantic (Beersma *et al.* 1997). As there is no evidence in the literature that trawling events are biased towards a particular season (e.g. Piet *et al.* 2000; Frid *et al.* 2000), a first order approximation can be made that January is more likely to endure a resuspension event than most other months in the year. It should also be noted that, when considering a variable POC flux over time, the effect of any resulting perturbation event will be dependent on the state of the sediment at that time. In the simulations considered here, it is clear that different results will have been achieved had the perturbation been imposed on any other day of the year.

It should also be remembered that comparisons, both in terms of percentage changes and absolute values, should be made in context. For example, the steady-state flux of ammonia when the mixed layer depth is 5 cm and the POC flux is 15 g C m^{-2} yr^{-1} is 4.16 mmol m^{-2} d^{-1}, and that the percentage flux change following a perturbation event is -80.9% if the perturbation is 20 mm. However, the absolute decrease in flux is relatively small at 3.37 mmol m^{-2} d^{-1}; the change in flux of oxygen in the same simulation was 119.6 mmol m^{-2} d^{-1}, although this represents a percentage

change of -28.5%. Extrapolating these values suggests that in the 100 days following the resuspension event in this simulation, the total flux of ammonia across the SWI will be 2.6 mol m^{-2}, compared with a flux of 3.5 mol m^{-2} that would be expected under normal conditions. This compares with a flux of 3.5 mol m^{-2} following a perturbation event of 149 mm and a POC flux of 50g C m^{-2} yr^{-1}, as opposed to 4.2 mol m^{-2} that would otherwise be expected.

Finally, and perhaps most importantly, it should be noted that the imposing a physical process on a complex biogeochemical system is likely to cause some surprising results, is likely to be difficult to interpret, and the interactions between all parameters will vary in such a way that attempting to explain them succinctly will be very difficult. As an example, Figure 7.20 shows the oxygen, nitrate, and ammonia fluxes in the 15 days before and 100 days following the perturbation event where the mixed layer depth is 5 cm and the mean POC flux was 15 g C m^{-2} yr^{-1}. The plots show output from two separate runs, one where the POC flux is constant and one where the POC flux is variable over time, following the FP4 profile. Although the profiles displayed do follow, as expected, the approximate same patterns as the profiles describing re-equilibrium times, it is clear that process is very non-linear, and that describing and discussing the outcomes from all changed parameters would result in a consistent conclusion. The results outlined here are only a first attempt at understanding the effect of a resuspension event.

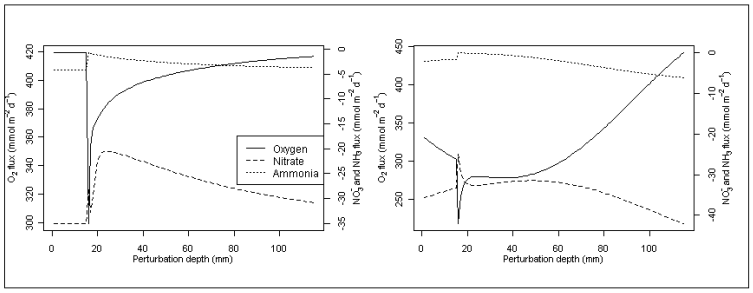

Figure 7.20: The resulting absolute fluxes for oxygen, nitrate and ammonia that a perturbation event causes when a mixed layer depth of 5 cm and a mean POC flux of 15 g C m^{-2} yr^{-1} was set; the results relate to a constant POC flux (left panel) and a time-varying POC flux using the FP4 pattern was imposed (right panel)

7.3 Comparison of model output with field data

The Marine Ecosystems Connection project has conducted experimental work to assess the impact of resuspension events on both biogeochemical and physical processes in coastal environments (Couceiro *et al.* 2012; Couceiro et al. in press; Thompson *et al.* 2011). The work described in this Chapter, along with the

experimental work, is the first time that a coupled experimental-modelling approach has been used to estimate the wider effect of resuspension events of different magnitudes.

The experimental work was carried out both *in-situ* and under controlled laboratory conditions. However, the majority of the work was carried out on much shorter timescales than possible with the modelling work presented in this chapter. The experimental work typically concentrated on resuspension depths of less than 10 mm (Courceiro, pers. comm.); however, the nature of the experimental work meant that POC fluxes were not recreated. The experiments resulted in re-equilibrium times of less than 36 hours, when steady-state conditions were not modified. In particular, in laboratory experiments, a high sedimentary carbon content (~3.1%) caused nitrate fluxes to drop from 83.6 to 70.7 mmol m^{-2} yr^{-1}; although the absolute values are higher in the experimental work than the modelling results presented in this chapter, where the equivalent values are a drop from 42.4 to 35.2 mmol m^{-2} yr^{-1}, it should be noted that the experimental values here relate to a flux following a perturbation of 19 mm which has followed a much more shallow (less than 3 mm) perturbation event of five hours.

The *in-situ* experiments, carried out using an annular flume at the Oyster Grounds site in the North Sea (Couceiro *et al.* 2012), were an opportunity to discover if similar patterns were observed in natural environments. Although re-equilibrium times were not established, the experiments did consider the variation in the flux of nitrate, phosphate and dissolved silicate caused by an imposed perturbation. When 1.56 mm of sediment was resuspended, the change in flux on nitrate was 5.1%, whilst when 7.1 mm of sediment was resuspended, the resultant change in the nitrate flux was 9.0%. This relative change in flux is very similar to the value calculated by the model if the mixed layer depth is 5 cm during a run where the mean POC flux was 50 g C m^{-2} yr^{-1}, and the FP4 flux profile was imposed, which is a particularly encouraging result. The results from the *in-situ* annular flume also indicated that an increase in shear stress that was below the critical threshold (i.e. the stress required for resuspension to occur) also had an effect on the flux of nutrients across the SWI.

In general, the re-equilibrium times of the chemical species observed in the laboratory experiments correlate well with the modelling results, where the general conclusion that can be made is that regardless of POC flux, chemical species measured or method used for the calculation of re-equilibrium, the time taken for the re-equilibrium of each of the chemical species at comparable perturbation depths is deemed to be instantaneous, which, due to the time-steps used in the model, is actually just a maximum re-equilibration time of one day. Two early conclusions can

therefore be made; since the model is able match the results of the experimental work, modelling is an appropriate tool to carry out further experiments. Secondly, the model may also be a suitable means by which to examine the potential impact of specific events by extrapolation of results. The results presented in this chapter, with the varying of a number of parameters, have been much more extensive than any experimental work would be able to achieve.

7.4 Comparisons with previous work

The majority of previous work on resuspension, both modelling and experimental, has concentrated on the physical processes involved, rather than the effect on the ecosystem or biogeochemistry of the system. However, some studies can provide data for the output presented here to be compared with.

There have been a handful of studies to date which have attempted to model the effect of trawling on sediment biogeochemistry. A relative simple model which only considered organic and inorganic carbon found that the proportion of carbon mineralisation by aerobic processes accounted for 0.37 under standard conditions, but increased to 0.54 under heavily trawled conditions (Duplisea *et al.* 2001). This modelling study compared CO_2 production stoichiometrically with observed fluxes of total nitrogen. The observed nitrogen fluxes used for comparison were 7–33 μmol m^{-2} hr^{-1} (note that a positive value here indicates a flux out of the sediment); the model seemed to overestimate CO_2 production, but it was acknowledged that the lack of processes which utilise nitrate and ammonia may have an influence on this. If it is assumed that nitrite+nitrate and ammonia are the two largest components of total N (Nedwell *et al.* 1993), then some comparisons can be made with the results provided by the model in this chapter. If the constant POC flux runs are considered, then the total nitrogen flux under steady-state conditions if the mixed layer depth was 5 cm and the POC flux was 2 g C m^{-2} yr^{-1} was -8.5 mmol m^{-2} d^{-1} which is approximately an order of magnitude larger than the upper observed value. Despite the lack of nitrogen in their model, Duplisea *et al.* (2001) estimated that a trawling event of 6 cm could release 5.6 mmol m^{-2} d^{-1} of nitrate. However, the model in this chapter reduces the nitrate flux under these conditions by 21.6 mmol m^{-2} d^{-1}, from -34.9 mmol m^{-2} d^{-1} to -13.3 mmol m^{-2} d^{-1}, as a result of the carbon mixing occurring in the sediment driving denitrification in deeper sediment.

In a separate modelling study, the European Regional Seas Ecosystem Model (ERSEM) was modified to provide an approximate time for the system to return to pre-perturbed values following simulated trawling events (Allen and Clarke 2007).

Although this model used an ecosystem model rather than biogeochemical model, some similarities can be seen. The ERSEM approach examined both single and multiple trawling events, but simulated the events in a separate manner to the approach used in this chapter, with the most obvious difference being that whereas OMEXDIA was set such that the sedimentary concentrations were set to water-column values, the ERSEM approach was to remove the oxic layer by setting it to zero. Although it should be noted that the ERSEM model used a less stringent re-equilibrium threshold of 80%, both approaches give similar results, with the ERSEM approach showing that re-equilibrium (to an 80% threshold) is reached in between 0 and 400 days, depending on specific parameters used. During simulations where multiple trawling events were allowed to occur (up to five a year for a five year period) in the approach using the ERSEM model, the maximum re-equilibration time was approximately 5 years; excluding simulations where the model seemed to fail to reach a steady-state, the maximum time taken for the sediment to return to pre-perturbed values in the output presented in this chapter is 443 days. An increase by a factor of four for the increased perturbation does not seem unreasonable. It is encouraging that the range seen in both studies is similar, and goes some way to producing data that can be used to validate both future experimental and modelling studies.

Comparisons can also be made with the limited previous experimental studies that have been conducted. Trimmer et al (2005) found no relationship between trawling and pore-water concentrations over the long-term. Although this agrees with results which suggested that concentrations of chlorophyll and dissolved porewater concentrations of nitrate and ammonia returned to pre-trawl values within 7 hours when a furrow of 15 cm was dredged (Falcão *et al.* 2003), it does not agree with output from the modified OMEXDIA.

Tidal areas have been known to be affected by continuous resuspension as a result of tidal currents; the depth of the resuspension has been estimated to be on the order of a few millimetres or less (Sanford *et al.* 1991), therefore, from the results of this modelling work, and the laboratory work mentioned, it is likely that any biogeochemical changes to the sediment as a result of such resuspension are likely to be minor, and will return to steady-state values before the next tidal cycle. Re-equilibration times are consistently less than 1 day for all model simulations with a constant POC flux when the perturbed depth is not more than 5 mm.

7.4.1 Further consequences

Both the sign of the change in flux, and the magnitude of the flux, can also be used to make an inference about the potential impact on the biogeochemistry of the

water column, and hence on the wider ecosystem. In general, it can be seen that as the depth of resuspension increases, the flux of oxygen into the sediment decreases; when the depth of perturbation is 149 mm, the re-equilibrium time is approximately 18 months, this implies that oxygen will be diffusing into the sediment at a lower rate than would happen under normal steady-state conditions. As the concentration of oxygen is increased relative to steady-state conditions, both oxic mineralisation and nitrification rates are likely to be higher in the water column during this period. If a perturbation event of 50 mm is considered when the POC flux is a constant 15 g C m^{-2} yr^{-1}, the integrated decrease in the flux of oxygen out of the water column is 4.5 mol m^{-2}, whilst the decrease in nitrate flux out of the sediment is 2.3 mol m^{-2}. By taking the value of a trawl as 0.449 km^2 (Hiddink *et al.* 2006), then each trawl could account for a decrease of 1.03×10^6 moles of nitrate to the sediment over the 292 days it takes for the sediment to return to re-equilibrium. This decrease could have wide-ranging consequences for the ecosystem of shelf seas – decreasing the potential availability of nitrate in the bottom waters could lead to anoxic conditions and higher concentrations of sulphides as a result of reduced rates of denitrification. To put into perspective the potential importance of these events, over the time taken for the sediment to return to re-equilibrium, the average daily reduction in nitrate flux to the water column is an order of magnitude higher than the atmospheric total nitrogen flux to the North Sea, assuming that the atmospheric flux is 0.19 mmol m^{-2} d^{-1} (de Leeuw *et al.* 2003). Assuming a Redfield C:N ratio of 6.625, this is a decrease in carbon fixation of 52 mmol C m^{-2} d^{-1}.

An interesting observation is the time taken for the change in flux to be propagated through the sediment as a result of a resuspension event. The resuspension event was consistently imposed on day 14 of the model run; however, when the perturbation depth is greater than 8 mm the maximum change in flux, of all species, did not occur until day 16. This implies that biogeochemical processes occurred within the sediment to attempt to manage the changed nutrient fluxes, before diffusion drove the flux of the nutrients across the SWI. This may be an artefact of the model dynamics as a result of the organic matter being mixed throughout the sedimentary column during a resuspension event; amplified POC concentrations at depth, when oxygen concentrations have also been increased would encourage oxic mineralisation, as well as denitrification and nitrification. The diffusion coefficient values of 1.341 (for oxygen) and the bioturbation coefficient of 365^{-1} cm^2 d^{-1} may lead to a delay in the dissemination of the fluxes across the sedimentary layers. It is likely that the result is it is a consequence of the mixing that occurs in this model, and therefore is unlikely to appear in the output of the previously published models by Allen & Clarke (2007) and Duplisea *et al.* (2001). However, the result would be

relatively easy to confirm with laboratory experiments, and could help development of our knowledge of stressed biogeochemical systems.

7.5 Summary

The modified OMEXDIA model presented in this chapter has presented for the first time an attempt to study the effects of sediment resuspension on sedimentary biogeochemistry by using an early-diagenetic model. The modified model assumed that physical processes were instantaneous, and as such, relationships such as the Stoke's Settling Velocity and the Rouse parameter did not need to be included in the model. Instead, the model assumed that a resuspension event takes the porewater concentrations of each of the chemical species resolved in the model to bottom water concentrations. A limited set of parameters were then modified to test the model under different scenarios.

The change in flux of each of the chemical species, and the time taken for fluxes to return to pre-perturbation values, were generally used to measure the impact of a resuspension event. The results clearly show that variation of the biological mixed layer depth has very little effect on the biogeochemistry of the sediment; however, the imposed mean POC flux, the perturbation depth and the time-varying pattern of the imposed POC flux do all have significant impacts. Increasing either the mean POC flux or the perturbation depth does, in the vast majority of simulations run, increase the impact that the resuspension event has on the biogeochemistry. However, the results show, in line with the discussions throughout this thesis, that the model is non-linear, making it inappropriate to use parametric methods to determine the relationships between parameters.

Although it is difficult to determine relationships between the model parameters which were varied to obtain the results in this chapter, the closeness of model results to previous measurements and estimates of perturbation impacts on benthic and pelagic systems suggests that the model could be used to run specific simulations to increase knowledge about the overall nutrient budget of shelf seas.

8 Conclusions and future work

An early-diagenetic model, OMEXDIA, was used to model the benthic environment of the North Sea continental shelf. Although OMEXDIA was originally primarily written for continental slope and abyssal plain environments (Soetaert *et al.* 1996b), the results discussed in Chapters 3 and 4 show that it is equally capable of producing realistic concentration profiles, rates of biogeochemical processes and fluxes of oxygen, nitrate and ammonia for the North Sea. Values calculated by the model are, without exception, within boundaries of previously measured values, with oxygen penetration depths of 1-10 mm, nitrate peaks of 5-30 mm, and ammonia concentrations at depth of 40 - 100 mmol m^{-3}. Given a steady-state run of the model with a POC flux of 15 g C m^{-2} yr^{-1}, the model calculated oxygen fluxes of 1529 mmol m^{-2} yr^{-1} into the sediment, nitrate fluxes of 117 mmol m^{-2} yr^{-1} out of the sediment, and ammonia fluxes of 15 mmol m^{-2} yr^{-1} out of the sediment. ODU, the parameter describing the reduced species of all remaining suboxic and anoxic pathways, combines the remaining suboxic pathways, is not released into the overlying water column until the POC flux reached 22.9 g C m^{-2} yr^{-1}. The model was also used to calculate the relative contribution of each of the mineralisation pathways, with comparison made to literature data. The results showed that oxygen was consistently the most important electron acceptor in the degradation of organic matter, under the conditions simulated, with oxygen being the sole electron acceptor when the POC flux was below 11.9 g C m^{-2} yr^{-1}. A further test for the model was to see if it could predict POC fluxes from the calculated contribution of each biogeochemical pathway alone. For example, sulphate reduction has been calculated, from observations, to contribute up to 80% of total OM oxidation in Skagerrak sediments; by optimising the model parameters to recreate this contribution, a range of possible values for POC flux may be estimated. However, this form of model calibration is not likely to be possible without higher resolution observations in the environment.

An important result from the model runs described in Chapter 4 is that imposing a more accurate time-varying seasonal carbon flux than has been used before verifies estimates of total fluxes of oxygen and nitrate across the sediment-water interface (SWI) for the entire North Sea, with the estimate here being that the total oxygen flux is 3.2 Tmol yr^{-1}, the total nitrate flux is 0.11 Tmol yr^{-1}, and the total ammonia flux is 0.07 Tmol yr^{-1} (with the net fluxes of nitrate and ammonia being out of the sediment, into the overlying water column). However, some of the recent extensive estimation of nutrient budgets in the North Sea (e.g. Brion *et al.* 2004) assume that sediments are only a sink for nutrients; the use of early-diagenetic models, such as OMEXDIA, show that more accurate representation of the sediment quantify the flux of nutrients in

both directions across the SWI. Although the results from OMEXDIA presented in Chapter 4 do not change the overall conclusions about whether the North Sea is a sink or source of nutrients, the use of models do enhance knowledge about the overall potential impact on ecosystems; studying the effect of processes involving sediment on the ecosystem in greater detail, by quantifying the impact that the fluxes have on water column biogeochemistry, using a modelling approach could be a feature of a future project.

It appears, given the ability of OMEXDIA to replicate observed concentration profiles and fluxes, that the ODU component in OMEXDIA is a good estimate for the suboxic diagenetic pathways. Although the results presented here show that it is difficult for extra biogeochemical processes to be included within OMEXDIA, a different approach may enable the ODU component to be split up into its constituent biogeochemical pathways (i.e. reduction of manganese oxide, iron oxide, and sulphate, and associated reoxidation reactions), as van Cappellen & Wang (1996) showed was possible. In addition, it may also be possible to include further biogeochemical processes which are not already implemented, such as to expand the nitrogen cycling (inclusion of dissimilatory nitrate reduction to ammonium (DNRA) and anammox), the cycling of phosphorous and trace metals of interest (e.g. Cd, Cu, Co, Ni, U, Mo and V), and recently discovered oxidation pathways (Schippers and Jørgensen 2001). It may be that the complex, non-linear nature of the model means that a steady-state solution cannot be obtained with an iterative steady-state solver using a Jacobian matrix, and instead a time-dependent solver, such as Runge-Kutta 4, may be necessary. However, only extensive testing of the model would verify whether this is the case.

Furthermore, there are various other processes which have an impact on the wider biogeochemistry of shelf seas that are not included in OMEXDIA. Although bioturbation is included in OMEXDIA, bioirrigation, where infaunal burrow networks are flushed with water originating from the sediment-water interface, is not; bioturbation has been modelled as an independent process (Meile *et al.* 2001; Meysman *et al.* 2006), but to my knowledge has not yet been included in a full diagenetic model. Similarly, expanding the carbon cycling aspect of OMEXDIA could allow future work to implement dynamic TOC degradation, so that the impact of bloom events on diagenetic activities and the overall cycling of shelf seas can be estimated more accurately. However, as discussed in detail in Chapters 3 and 4, increasing the complexity may result in the model becoming unstable to such an extent that model runs may be difficult to conduct.

The sensitivity analysis carried out confirmed that the parameters for which the model was most sensitive were the most important biogeochemical parameters, and

are the parameters for which most observational data is available. These parameters were the mean flux of carbon to the sediment, the proportion of fast decaying organic matter, the rate of degradation of both fast and slow decaying organic matter, the ratio of nitrogen to carbon in fast decaying organic matter, and the bioturbation coefficient. The results of the sensitivity analysis were then used to help set up a genetic algorithm that generated values of parameters that would fit model output to observed values. It was found that the complexity of both the model and the data meant that all 27 model parameters needed to be used in order a representative fit to be found. However, only data from one study site, the North Dogger site, was used. It was recognised that the lack of data available from the other two sites visited as part of the Marine Ecosystems Connections (MEC) project would almost certainly prevent a suitable set of parameters being found for these alternative sites. In addition, OMEXDIA was primarily developed to model cohesive sediments, and the vast majority of previous applications of OMEXDIA have been in this type of environment (e.g. Epping *et al.* 2002; Gypens *et al.* 2008; Herman *et al.* 2001; Hochard *et al.* 2010); the physical properties of the two remaining MEC sites (Oyster Ground and Sean Gas Fields) are very different, with much higher porosity values (pers. comm. C.E.L. Thompson, 2009). It may be possible to adapt OMEXDIA to be able to model these environments, and with enough suitable data to run a genetic algorithm, differences in the biogeochemistry between the sandy and cohesive sediments may be determined. A comparison between data assimilation techniques could also be carried out. With a genetic algorithm having been shown to successfully generate parameters which are able to produce realistic concentration profiles, methods such as a Monte Carlo approach could be used. Although this may not inherently improve knowledge about the biogeochemistry of the sediment, it may enable decisions to be made on which data assimilation method may be most appropriate for future models, or lead to improvements in one, or both, methods.

The version of OMEXDIA published by Soetaert *et al.* (1996b) was modified so that the effect of resuspension events on sedimentary biogeochemistry could be investigated. The inclusion of resuspension was approximated to an instantaneous perturbation and deposition of sedimentary material, and in doing so, the interstitial waters to the depth of perturbation took the concentration values of the overlying water column. Although this is undoubtedly a major simplification of the physical processes which occur during resuspension, the results showed remarkable similarity both with previous modelling work (*c.f.* Allen and Clarke 2007) and with results from the limited experimental work (Couceiro *et al.* 2012), with re-equilibrium being instantaneous when the perturbation depth is typically less than 10 mm. Re-equilibrium times with increasing perturbation depth and POC flux follow non-linear patterns. However, as it is a simplification, there is much scope for improvements to make the model more realistic. The simulations run in this thesis only had one

perturbation event imposed, whereas an algorithm to impose multiple resuspension events, of varying perturbation depth, but weighted towards specific times of the year would likely be the most realistic method of simulating resuspension events in the majority of the North Sea. In addition, as a result of the model timestep being in days, perturbations in which re-equilbrium occurs in less than 24 hours have a re-equilibrium which appears to be instantaneous, and the change in flux cannot be estimated. However, when the perturbation is deeper than 10 mm, fluxes rise non-linearly in response to increasing perturbation depth. A perturbation depth of 50 mm leads to a change in flux of oxygen of approximately 65%, while a perturbation depth of 100 mm leads to change in flux of approximately 85%. Peaks in the flux of nitrate with increasing perturbation depth are as a result of the nitrate peak in the sediment. The direction of the flux of ammonia is dependent on the POC flux – low POC fluxes lead to positive change in fluxes, whereas higher POC fluxes result in the percentage change being negative.

This simple modification does not consider the physical parameters of the sediment, and it is likely that a more robust model could be constructed; initially, this could be achieved by increasingly the complexity associated with resuspension using the parameters in OMEXDIA, such as varying the porosity with time. However, coupling OMEXDIA to a physical resuspension model may also be possible. Although the coupling of physical resuspension models is not trivial (Franks 2002), this may provide a better method for estimating the effect of resuspension on both the sedimentary environment and the overlying water column.

The model timestep used in OMEXDIA throughout this thesis is days. The model in this form has therefore been most useful predicting the effect of irregular, infrequent events which cause deep perturbation of the sediment. However, there has been little study of the effect of tidal cycles on overlying water columns. Estuarine sediments tend to have high levels of both carbon (Bourgoin and Tremblay 2010) and nitrate, as a result of fertiliser run-off (Jickells *et al.* 2000), and so should almost certainly be treated differently to shelf-sea systems, despite the simplifications in some previous work (Hydes *et al.* 1999). The experimental work from the MEC project did consider the levels of resuspension that is most likely to be consistent with tidal currents (i.e. 1 – 5 mm (Jonge and Beusekom 1995)), with the sediment used in the experiments coming from the Solent (pers. comm. F. Couceiro, 2010). It is likely that OMEXDIA could be modified to simulate estuarine environments, and for the time resolution of the model to be increased, ideally to hourly intervals. The experimental work could serve to calibrate the modified model. No work has been carried out on the re-equilibrium times of sediments perturbed by continued tidal cycles, and so the assumption is that the biogeochemistry of estuarine sediments is very similar to that of

offshore locations. However, a re-equilibration time which is longer than a tidal cycle would show that estuarine sediments would need to be treated as special cases when considering the cycling of nutrients.

Finally, a brief comment about the use of models such as OMEXDIA should be made. The literature concerning the biogeochemistry of shelf seas, such as the North Sea, is littered with examples showing that observations can be different depending not only on season, which may be expected, but also, less predictably, on variables such as location and water depth (where observations may not show a pattern with respect to water depth). As a specific example, the concentration of manganese oxides in the majority of North Sea sediments is negligible, but at specific sites in the Skagerrak, the manganese oxide pathway dominates the degradation of organic matter (Arnosti and Holmer 2003). To enable a model to create the profiles seen at this site would obviously require a different parameter set to the 'average' parameter set for the whole of the North Sea, but it would almost certainly be possible to generate, using a genetic algorithm, a set of parameters that would replicate the observations seen at any given site. However, for a model to describe the general dynamics of the entire shelf-sea system, a set of parameters should be chosen that seem to match the *average* fluxes and profiles of individual sites. Parameter sets that were not carefully chosen may over- or under-estimate the concentrations and fluxes of the key chemical species when integrated over the whole of the shelf-sea system. As such, OMEXDIA in its current form can either model specific environments, or provide estimates of fluxes (and total sedimentary) inventories) of chemical species across the whole system, but not both. However, this could be overcome if OMEXDIA was coupled to a 3D water-column biogeochemical-hydrodynamic model, such as the European Regional Seas Ecosystem Model (Baretta *et al.* 1995). This would not only allow spatial variation in parameters used in OMEXDIA, but also enable the effect of sediment on the whole ecosystem to be studied. Although it would increase the complexity, coupling the modified OMEXDIA model, dealing with resuspension events, may allow the overall impact of all perturbation events, both natural and anthropogenic, to be estimated.

Appendix: Data Collection & Management

A series of cruises was carried out on the *Cefas Endeavour* in the North Sea, with observations taken in three areas (Dogger Bank, Oyster Grounds and Sean Gas Fields). Additional sampling was undertaken in the Tyne and Thames estuaries. Figure A1 shows the location of the sampling sites.

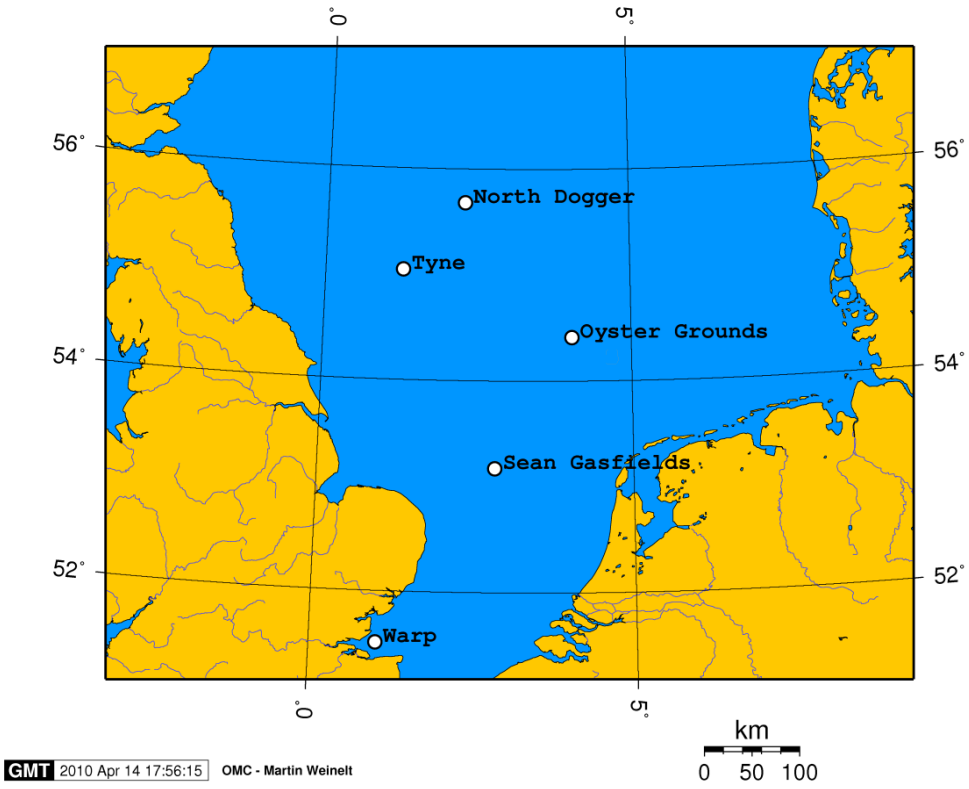

Figure A1: Map to show location of North Sea sampling sites used in the MEC project

Nine cruises were carried out over the course of two years (2007–2009) to capture seasonal ecosystem activity (i.e. winter, post-spring bloom, summer and autumn). Sediment and porewater samples were taken using a NIOZ box-corer so that both concentrations and fluxes of all relevant chemical species (O_2, NO_3^-, NH_4^+, $Fe(OH)_3$, Fe^{2+}, SO_4^{2-}, S^{2-}, PO_4^{3-}) could be measured in the laboratory. Oxygen penetration depths were measured from a box-core aboard the ship. Physical characteristics, including size classification of the sediments, at each site were taken. An annular flume (*Voyager II*: 2.2 m diameter, working channel width of 15 cm and depth of 30 cm) was used *in situ* to artificially induce resuspension, with water samples taken so that concentrations of SPM and nutrients could be measured. The flume works by way of eight paddles being rotated by a motor in a stepwise manner enabling current speeds

to be manipulated over the sediment. The flume was used to specifically investigate the resuspension characteristics of the sediment.

A much smaller annular flume (diameter of 30 cm, working channel width of 4.5 cm and depth of 20 cm) was used in the laboratory using sediment collected in a box-corer at each site. Using a similar technique as on the large *in situ* flume, resusupension was induced by increasing the water current in a step-wise fashion. Water samples were taken and concentrations of chemical species (TOC, O_2, NO_3, NH_4^+) and physical parameters (velocity and SPM concentration) were measured during different current speeds. Further parameters, such as the critical threshold velocities, could then be calculated from these measurements.

A.1 Data management

A relational database was built to store, access and manipulate the large amount of data generated by the experimental work. The database aided the calibration and validation of the model (Chapter 5).

Using a MySQL database supplied by the NOCS IT Group, easily accessible via standard SSH software, a database was built which links together cruises, sites and all experimental data. The database adheres to the Fifth Normal Form (Connolly and Begg 2002). Care was also been taken to maintain data integrity. Figure A2 shows the basic structure of the database. It is worth noting that the many-to-many relationship between Sites and Cruises (i.e. many cruises visited each site multiple times) is solved by using the SiteData table, and this table also stores parameters (such as water temperature) that are individual for a specific cruise's visit to a specific site. Storing data in this way means it is much easier to output and view in a variety of ways

Within the development of the model the database was used to help with model calibration and validation. By having the experimental data stored in such a logical manner means that it is easy to either loop through or select values of interest during calibration experiments.

As described in Section 2.3, the R language is being used to develop the model; the most straightforward method found to access MySQL from R is to use rJava coupled with the Java Database Connector (JDBC), using the RJDBC package. Although this requires an Open Database Connection (ODBC), it does mean that simple SQL statements can be executed using just three lines of code:

```
require(RJDBC)
con<- dbConnect(JDBC("sun.jdbc.odbc.JdbcOdbcDriver"),
                      "jdbc:odbc:PhD_DB")
print(dbGetQuery(conn, "select * from Sites"))
```

This code will print all the information that is stored in the Sites table. Due to the ease with which data can be accessed, it follows that it would then be simple to write code that would then use all the data sequentially to change the forcing parameters in the model in separate runs. The output from each run can then be compared and statistically analysed to calculate the set of parameters most likely to produce the output most similar to the observed.

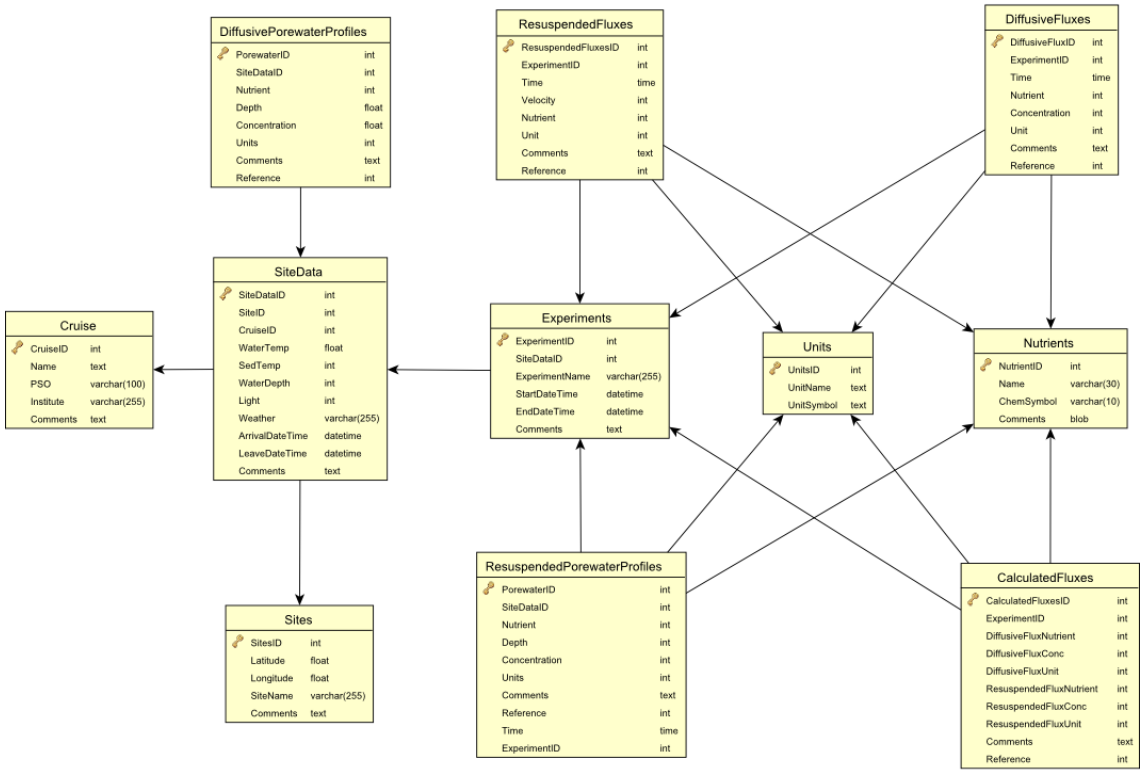

Figure A2: Relationships between the tables in the database storing the experimental data

References

Abdul-Rashid MK, Riley JP, Fitzsimons MF, Wolff GA (1991) Determination of volatile amines in sediment and water samples. Anal Chim Acta 252:223-226

Abril G, Commarieu M-V, Etcheber H, Deborde J, Deflandre B, Zivaðinovic MK, Chaillou G, Anschutz P (2010) *in vitro* simulation of oxic/suboxic diagenesis in an estuarine fluid mud subjected to redox oscillations. Estuar Coast Shelf Sci 88 (2):279-291

Al-Raei A, Bosselmann K, Böttcher M, Hespenheide B, Tauber F (2009) Seasonal dynamics of microbial sulfate reduction in temperate intertidal surface sediments: controls by

temperature and organic matter. Oc Dynam 59 (2):351-370

Allen JI, Clarke KR (2007) Effects of demersal trawling on ecosystem functioning in the North Sea: a modelling study. Mar Ecol Prog Ser 336:63-75

Aller RC (1980) Quantifying solute distributions in the bioturbated zone of marine sediments by defining an average microenvironment. Geochim Cosmochim Acta 44 (12):1955-1965. doi:10.1016/0016-7037(80)90195-7

Aller RC (1990) Bioturbation and Manganese Cycling in Hemipelagic Sediments. Philosophical Transactions of the Royal Society of London Series A, Mathematical and Physical Sciences 331 (1616):51-68. doi:10.1098/rsta.1990.0056

Almroth E, Tengberg A, Andersson JH, Pakhomova S, Hall POJ (2009) Effects of resuspension on benthic fluxes of oxygen, nutrients, dissolved inorganic carbon, iron and manganese in the Gulf of Finland, Baltic Sea. Cont Shelf Res 29 (5-6):807-818

Andersen FØ (1996) Fate of organic carbon added as diatom cells to oxic and anoxic marine sediment microcosms. Mar Ecol Prog Ser 134:225-233. doi:10.3354/meps134225

Anderson TR (2005) Plankton functional type modelling: running before we can walk? J Plankton Res 27 (11):1073-1081. doi:10.1093/plankt/fbi076

Anderson TR (2010) Progress in marine ecosystem modelling and the "unreasonable effectiveness of mathematics". J Mar Syst 81 (1-2):4-11

Anschutz P, Sundby B, Lefrançois L, Luther GW, III, Mucci A (2000) Interactions between metal oxides and species of nitrogen and iodine in bioturbated marine sediments. Geochim Cosmochim Acta 64 (16):2751-2763

Anton KK, Liebezeit G, Rudolph C, Wirth H (1993) Origin, distribution and accumulation of organic carbon in the Skagerrak. Mar Geol 111 (3-4):287-297

Aplin AC, Macquaker JHS (1993) C-S-Fe Geochemistry of some Modern and Ancient Anoxic Marine Muds and Mudstones. Philosophical Transactions of the Royal Society of London Series A - Mathematical Physical and Engineering Sciences 344 (1670):89-100

Archer D, Devol A (1992) Benthic Oxygen Fluxes on the Washington Shelf and Slope: A Comparison of *in situ* Microelectrode and Chamber Flux Measurements. Limnol Oceanogr 37:614-629

Arndt S, Regnier P (2007) A model for the benthic-pelagic coupling of silica in estuarine ecosystems: sensitivity analysis and system scale simulation. Biogeosciences 4 (3):331-352

Arnosti C, Holmer M (2003) Carbon cycling in a continental margin sediment: contrasts between organic matter characteristics and remineralization rates and pathways. Estuar Coast Shelf Sci 58 (1):197-208. doi:10.1016/s0272-7714(03)00077-5

Atkins PW, de Paula J (2002) Physical Chemistry. 7 edn. Oxford University Press, New York

Attrill MJ, Edwards M (2008) Reply to Haddock, S.H.D.: "Reconsidering Evidence for Potential Climate-Related Increases in Jellyfish". Limnol Oceanogr 53 (6):2763-2766. doi:10.2307/40058365

Attrill MJ, Wright J, Edwards M (2007) Climate-related Increases in Jellyfish Frequency Suggest a More Gelatinous Future for the North Sea. Limnol Oceanogr 52 (1):480-485. doi:10.2307/40006097

Audry S, Blanc G, Schafer J, Chaillou G, Robert S (2006) Early diagenesis of trace metals (Cd, Cu, Co, Ni, U, Mo and V) in the freshwater reaches of a macrotidal estuary. Geochim Cosmochim Acta 70 (9):2264-2282. doi:10.1016/j.gca.2006.02.001

Audry S, Blanc G, Schäfer J, Robert S (2007) Effect of estuarine sediment resuspension on early diagenesis, sulfide oxidation and dissolved molybdenum and uranium distribution in the Gironde estuary, France. Chem Geol 238 (3-4):149-167

Baker A, Spencer RGM (2004) Characterization of dissolved organic matter from source to sea using fluorescence and absorbance spectroscopy. Sci Total Environ 333 (1-3):217-232. doi:10.1016/j.scitotenv.2004.04.013

Bakker JF, Helder W (1993) Skagerrak (northeastern North Sea) oxygen microprofiles and porewater chemistry in sediments. Mar Geol 111 (3-4):299-321

Bale AJ, Morris AW (1998) Organic carbon in suspended particulate material in the North Sea: Effect of mixing resuspended and background particles. Cont Shelf Res 18 (11):1333-1345. doi:10.1016/s0278-4343(98)00046-6

Baptist MJ, van Dalfsen J, Weber A, Passchier S, van Heteren S (2006) The distribution of macrozoobenthos in the southern North Sea in relation to meso-scale bedforms. Estuar Coast Shelf Sci 68 (3-4):538-546. doi:10.1016/j.ecss.2006.02.023

Barbanti A, Bergamini M, Frascari F, Miserocchi S, Ratta M, Rosso G (1995) Diagenetic processes and nutrient fluxes at the sediment-water interface, northern Adriatic Sea, Italy. Mar Freshw Res 46 (1):55-67. doi:doi:10.1071/MF9950055

Baretta JW, Ebenhöh W, Ruardij P (1995) The European regional seas ecosystem model, a complex marine ecosystem model. Neth J Sea Res 33 (3-4):233-246

Basford D, Eleftheriou A (1988) The benthic environment of the North Sea (56° to 61°N). Journal of the Marine Biological Association of the UK 68 (01):125-141

Beck M, Dellwig L, Schnetger B, Brumsack HJ (2008a) Cycling of trace metals (Mn, Fe, Mo, U, V, Cr) in deep pore waters of intertidal flat sediments. Geochim Cosmochim Acta 72 (12):2822-2840. doi:10.1016/j.gca.2008.04.013

Beck M, Dellwig O, Kolditz K, Freund H, Liebezeit G, Schnetger B, Brumsack HJ (2007) In situ pore water sampling in deep intertidal flat sediments. Limnology and Oceanography: Methods 5:136-144

Beck M, Dellwig O, Liebezeit G, Schnetger B, Brumsack H-J (2008b) Spatial and seasonal variations of sulphate, dissolved organic carbon, and nutrients in deep pore waters of intertidal flat sediments. Estuar Coast Shelf Sci 79 (2):307-316. doi:10.1016/j.ecss.2008.04.007

Beck M, Köster J, Engelen B, Holstein J, Gittel A, Könneke M, Riedel T, Wirtz K, Cypionka H, Rullkötter J, Brumsack H-J (2009) Deep pore water profiles reflect enhanced microbial activity towards tidal flat margins. Oc Dynam 59 (2):371-383

Beersma JJ, Rider KM, Komen GJ, Kaas E, Kharin VV (1997) An analysis of extra-tropical storms in the North Atlantic region as simulated in a control and 2 × CO2 time-slice experiment with a high-resolution atmospheric model. Tellus A 49 (3):347-361. doi:10.1034/j.1600-0870.1997.t01-2-00003.x

Bender ML, Heggie DT (1984) Fate of organic carbon reaching the deep sea floor: a status report. Geochim Cosmochim Acta 48 (5):977–986. doi:10.1016/0016-7037(84)90189-3

Berkenbusch K, Rowden AA (1998) Population dynamics of the burrowing ghost shrimp *Callianassa filholi* on an intertidal sandflat in New Zealand (Decapoda: Thalassinidea). Ophelia 49 (1):55–69. doi:10.1080/00785326.1998.10409373

Berner RA (1964) An idealized model of dissolved sulfate distribution in recent sediments. Geochim Cosmochim Acta 28 (9):1497–1503. doi:10.1016/0016-7037(64)90164-4

Berner RA (1970) Sedimentary pyrite formation. Am J Sci 268 (1):1–23

Berner RA (1971) Principles of chemical sedimentology. McGraw-Hill, New York

Berner RA (1975) Diagenetic models of dissolved species in the interstitial waters of compacting sediments. Am J Sci 275 (1):88–96

Berner RA (1976) Inclusion of adsorption in the modelling of early diagenesis. Earth Planet Sci Lett 29 (2):333–340

Berner RA (1980) Early diagenesis: a theoretical approach. Princeton series in geochemistry. Princeton University Press, Princeton, N.J.

Berner RA (1982) Burial of Organic Carbon and Pyrite Sulfur in the Modern Ocean: its Geochemical and Environmental Significance. Am J Sci 282:451–473

Berner RA (1984) Sedimentary pyrite formation: An update. Geochim Cosmochim Acta 48 (4):605–615

Billen G (1978) A budget of nitrogen recycling in North Sea sediments off the Belgian coast. Estuarine and Coastal Marine Science 7 (2):127–146

Billen G (1982) An Idealized Model of Nitrogen Recycling in Marine Sediments. Am J Sci 282:512–541

Blackford JC, Gilbert FJ (2007) pH variability and CO2 induced acidification in the North Sea. J Mar Syst 64 (1–4):229–241. doi:10.1016/j.jmarsys.2006.03.016

Boetius A, Ravenschlag K, Schubert CJ, Rickert D, Widdel F, Gieseke A, Amann R, Jorgensen BB, Witte U, Pfannkuche O (2000) A marine microbial consortium apparently mediating anaerobic oxidation of methane. Nature 407 (6804):623–626

Bonazzi A (1919) On Nitrification. III. The Isolation and Description of the Nitrite Ferment. Botanical Gazette 68 (3):194–207

Bonnin J, Van Raaphorst W (2004) Silicic acid enrichment in the deep water of the Faeroe–Shetland Channel. Deep Sea Research Part I: Oceanographic Research Papers 51 (11):1493–1515

Booij K, Helder W, Sundby B (1991) Rapid redistribution of oxygen in a sandy sediment induced by changes in the flow velocity of the overlying water. Neth J Sea Res 28 (3):149–165

Booij K, Sundby B, Helder W (1994) Measuring the flux of oxygen to a muddy sediment with a cylindrical microcosm. Neth J Sea Res 32 (1):1–11

Boon AR, Duineveld GCA (1998) Chlorophyll a as a marker for bioturbation and carbon flux in southern and central North Sea sediments. Mar Ecol Prog Ser 162:33–43. doi:10.3354/meps162033

Boon AR, Duineveld GCA, Kok A (1999) Benthic Organic Matter Supply and Metabolism at Depositional and Non-depositional Areas in the North Sea. Estuar Coast Shelf Sci 49 (5):747–761

Böttcher ME, Hespenheide B, Brumsack H-J, Bosselmann K (2004) Stable isotope biogeochemistry of the sulfur cycle in modern marine sediments: I. seasonal dynamics in a temperate intertidal sandy surface sediment. Isot Environ Health Stud 40 (4):267 - 283

Boudreau BP (1986) Mathematics of tracer mixing in sediments; I, Spatially-dependent, diffusive mixing. Am J Sci 286 (3):161-198

Boudreau BP (1992) A kinetic model for microbic organic-matter decomposition in marine sediments. FEMS Microbiol Lett 102 (1):1-14

Boudreau BP (1994) Is Burial Velocity a Master Parameter for Bioturbation. Geochim Cosmochim Acta 58 (4):1243-1249

Boudreau BP (1996) A method-of-lines code for carbon and nutrient diagenesis in aquatic sediments. Comput Geosci 22 (5):479-496

Boudreau BP (1997a) Diagenetic models and their implementation : modelling transport and reactions in aquatic sediments. Springer, Berlin; New York

Boudreau BP (1997b) A one-dimensional model for bed-boundary layer particle exchange. J Mar Syst 11 (3-4):279-303

Boudreau BP (1998) Mean Mixed Depth of Sediments: The Wherefore and the Why. Limnol Oceanogr 43 (3):524-526

Boudreau BP (2000) The mathematics of early diagenesis: From worms to waves. Reviews of Geophysics 38 (3):389-416

Boudreau BP, Mucci A, Sundby B, Luther GW, Silverberg N (1998) Comparative diagenesis at three sites on the Canadian continental margin. J Mar Res 56:1259-1284

Boudreau BP, Ruddick BR (1991) On a reactive continuum representation of organic matter diagenesis. Am J Sci 291 (5):507-538

Bourgoin L-H, Tremblay L (2010) Bacterial reworking of terrigenous and marine organic matter in estuarine water columns and sediments. Geochim Cosmochim Acta 74 (19):5593-5609. doi:DOI: 10.1016/j.gca.2010.06.037

Brandt G, Wirtz KW (2010) Interannual variability of alongshore spring bloom dynamics in a coastal sea caused by the differential influence of hydrodynamics and light climate. Biogeosciences 7 (1):371-386

Brion N, Baeyens W, de Galan S, Elskens M, Laane RWPM (2004) The North Sea: source or sink for nitrogen and phosphorus to the Atlantic Ocean? Biogeochemistry 68:277-296

Brockmann UH, Laane RWPM, Postma H (1990) Cycling of Nutrient Elements in the North Sea. Neth J Sea Res 26 (2-4):239-264

Brown J, Colling A, Park D, Phillips J, Rothery D, Wright J (1989) Ocean Chemistry and Deep-Sea Sediments. Pergamon Press, Oxford

Buesseler KO (1991) Do upper-ocean sediment traps provide an accurate record of particle flux? Nature 353 (6343):420-423

Burdige DJ (2006) Geochemistry of marine sediments. Princeton University Press, Princeton, NJ

Burdige DJ, Zheng SL (1998) The biogeochemical cycling of dissolved organic nitrogen in estuarine sediments. Limnol Oceanogr 43 (8):1796-1813

Cadée GC (1976) Sediment reworking by arenicola marina on tidal flats in the Dutch Wadden Sea. Neth J Sea Res 10 (4):440-460. doi:10.1016/0077-7579(76)90020-x

Cai W-J, Sayles FL (1996) Oxygen penetration depths and fluxes in marine sediments. Mar Chem 52 (2):123-131. doi:10.1016/0304-4203(95)00081-x

Calow P (1999) Blackwell's concise encyclopedia of environmental management. Blackwell Science, Oxford, England

Canfield DE (1993) Organic matter oxidation in marine sediments. In: Wollast R, MacKenzie FT, Chou L (eds) Interactions of C, N, P & S: Biogeochemical cycles and Global Change. Springer-Verlag, Berlin, pp 333-363

Canfield DE, Jørgensen BB, Fossing H, Glud R, Gundersen J, Ramsing NB, Thamdrup B, Hansen JW, Nielsen LP, Hall POJ (1993a) Pathways of organic carbon oxidation in three continental margin sediments. Mar Geol 113 (1-2):27-40. doi:10.1016/0025-3227(93)90147-n

Canfield DE, Thamdrup B, Hansen JW (1993b) The anaerobic degradation of organic matter in Danish coastal sediments: Iron reduction, manganese reduction, and sulfate reduction. Geochim Cosmochim Acta 57 (16):3867-3883

Canuel EA, Martens CS (1996) Reactivity of recently deposited organic matter: Degradation of lipid compounds near the sediment-water interface. Geochim Cosmochim Acta 60 (10):1793-1806. doi:10.1016/0016-7037(96)00045-2

Carr M-E, Friedrichs MAM, Schmeltz M, Noguchi Aita M, Antoine D, Arrigo KR, Asanuma I, Aumont O, Barber R, Behrenfeld M, Bidigare R, Buitenhuis ET, Campbell J, Ciotti A, Dierssen H, Dowell M, Dunne J, Esaias W, Gentili B, Gregg W, Groom S, Hoepffner N, Ishizaka J, Kameda T, Le Quéré C, Lohrenz S, Marra J, Mélin F, Moore K, Morel A, Reddy TE, Ryan J, Scardi M, Smyth T, Turpie K, Tilstone G, Waters K, Yamanaka Y (2006) A comparison of global estimates of marine primary production from ocean color. Deep Sea Research Part II: Topical Studies in Oceanography 53 (5-7):741-770

CEFAS (2001) Strategic Environmental Assessment (SEA2) North Sea Fish and Fisheries. Technical Report TR003, August 2001.

Cefas (2011) Cefas: Marine Ecosystem Connections. http://cefas.defra.gov.uk/our-science/ecosystems-and-biodiversity/marine-ecosystem-connections.aspx. Accessed 04/08/2011

Cha HJ, Lee CB, Kim BS, Choi MS, Ruttenberg KC (2005) Early diagenetic redistribution and burial of phosphorus in the sediments of the southwestern East Sea (Japan Sea). Mar Geol 216 (3):127-143

Chang M-L, Sanford LP (2005) Modeling the effects of tidal resuspension and deposition on early diagenesis of contaminants. Aquat Ecosyst Health Manag 8 (1):41 - 51

Chauvand L, Jean F, Ragueneau O, Thouzeau G (2000) Long-term variation of the Bay of Brest ecosystem: benthic-pelagic coupling revisited. Marine Ecology-Progress Series 200:35-48

Chen C-TA, Liu K-K, Macdonald R (2003) Continental Margin Exchanges. In: Fasham M (ed) Ocean Biogeochemistry: A synthesis of the Joint Global Ocean Flux Study (JGOFS). Springer-Verlag, Berlin,

Chen K, Giblin PJ, Irving A (1999) Mathematical explorations with MATLAB. Cambridge University Press, Cambridge [England]; New York

Chung EG, Bombardelli FA, Schladow SG (2009) Modeling linkages between sediment resuspension and water quality in a shallow, eutrophic, wind-exposed lake. Ecol Model 220 (9-10):1251-1265

Churchill JH (1989) The effect of commercial trawling on sediment resuspension and transport over the Middle Atlantic Bight continental shelf. Cont Shelf Res 9 (9):841-865. doi:10.1016/0278-4343(89)90016-2

Conley DJ, Björck S, Bonsdorff E, Carstensen J, Destouni G, Gustafsson BG, Hietanen S, Kortekaas M, Kuosa H, Markus Meier HE, Müller-Karulis B, Nordberg K, Norkko A, Nürnberg G, Pitkänen H, Rabalais NN, Rosenberg R, Savchuk OP, Slomp CP, Voss M, Wulff F, Zillén L (2009) Hypoxia-Related Processes in the Baltic Sea. Environ Sci Technol 43 (10):3412-3420. doi:10.1021/es802762a

Connolly TM, Begg CE (2002) Database systems : a practical approach to design, implementation, and management. International computer science series. Addison-Wesley, Harlow, England; New York

Cook PLM, Wenzhofer F, Glud RN, Janssen F, Huettel M (2007) Benthic solute exchange and carbon mineralization in two shallow subtidal sandy sediments: Effect of advective pore-water exchange. Limnol Oceanogr 52 (5):1943-1963

Cornwell JC, Morse JW (1987) The characterization of iron sulfide minerals in anoxic marine sediments. Mar Chem 22 (2-4):193-206. doi:10.1016/0304-4203(87)90008-9

Couceiro F, Fones G, Thompson C, Statham P, Sivyer D, Parker R, Kelly-Gerreyn B, Amos C (2012) Impact of resuspension of cohesive sediments at the Oyster Grounds (North Sea) on nutrient exchange across the sediment-water interface. Biogeochemistry:1-16. doi:10.1007/s10533-012-9710-7

Cowling E, Galloway J, Furiness C, Erisman J Optimizing Nitrogen Management in Food and Energy Production and Environmental Protection. In: Report from the Second International Nitrogen Conference, Washington DC, 14-18 October 2001 2002. Ecological Society of America, pp 1-9

D'Andrea AF, Lopez GR, Aller RC (2004) Rapid physical and biological particle mixing on an intertidal sandflat. J Mar Res 62 (1):67-92. doi:10.1357/00222400460744627

Dauwe B, Middelburg JJ (1998) Amino Acids and Hexosamines as Indicators of Organic Matter Degradation State in North Sea Sediments. Limnol Oceanogr 43 (5):782-798

Davies JM, Payne R (1984) Supply of Organic-Matter to the Sediment in the Northern North-Sea During a Spring Phytoplankton Bloom. Marine Biology 78 (3):315-324

de Haas H, Boer W, van Weering TCE (1997) Recent sedimentation and organic carbon burial in a shelf sea: the North Sea. Mar Geol 144 (1-3):131-146

de Haas H, van Weering TCE (1997) Recent sediment accumulation, organic carbon burial and transport in the northeastern North Sea. Mar Geol 136:173-187

de Leeuw G, Spokes L, Jickells T, Skjøth CA, Hertel O, Vignati E, Tamm S, Schulz M, Sørensen L-L, Pedersen B, Klein L, Schlünzen KH (2003) Atmospheric nitrogen inputs into the North Sea: effect on productivity. Cont Shelf Res 23 (17-19):1743-1755. doi:10.1016/j.csr.2003.06.011

Degens ET, Mopper K (1976) Organic Material in Marine Sediments. In: Riley JP, Chester R (eds) Chemical Oceanography, vol 6. Academic Press, London, pp 59-113

Dellwig O, Bosselmann K, Kolsch S, Hentscher M, Hinrichs J, Bottcher ME, Reuter R, Brumsack HJ (2007) Sources and fate of manganese in a tidal basin of the German Wadden Sea. J Sea Res 57 (1):1-18. doi:10.1016/j.seares.2006.07.006

Dhakar SP, Burdige DJ (1996) A coupled, non-linear, steady-state model for early diagenetic processes in pelagic sediments. Am J Sci 296 (3):296-330

Diaz RJ, Rosenberg R (2008) Spreading Dead Zones and Consequences for Marine Ecosystems. Science 321 (5891):926-929. doi:10.1126/science.1156401

Dobrynin M, Gayer G, Pleskachevsky A, Günther H (2010) Effect of waves and currents on the dynamics and seasonal variations of suspended particulate matter in the North Sea. J Mar Syst 82 (1-2):1-20

Doney SC, Fabry VJ, Feely RA, Kleypas JA (2009) Ocean Acidification: The Other CO2 Problem. In: Annual Review of Marine Science, vol 1. Annual Review of Marine Science. Annual Reviews, Palo Alto, pp 169-192. doi:10.1146/annurev.marine.010908.163834

Dugdale RC, Wilkerson FP, Minas HJ (1995) The role of a silicate pump in driving new production. Deep Sea Research Part I: Oceanographic Research Papers 42 (5):697-719

Duplisea DE, Jennings S, Malcolm SJ, Parker R, Sivyer DB (2001) Modelling potential impacts of bottom trawl fisheries on soft sediment biogeochemistry in the North Sea. Geochem Trans 2 (14):112-117

Eisma D, Kalf J (1987) Distribution, Organic Content and Particle-Size of Suspended Matter in the North-Sea. Neth J Sea Res 21 (4):265-285

Emerson S, Jahnke R, Bender M, Froelich P, Klinkhammer G, Bowser C, Setlock G (1980) Early diagenesis in sediments from the eastern equatorial Pacific, I. Pore water nutrient and carbonate results. Earth Planet Sci Lett 49 (1):57-80

Emerson S, Jahnke R, Heggie D (1984) Sediment-water exchange in shallow water estuarine sediments. J Mar Res 42:709-730. doi:10.1357/002224084788505942

Epping E, van der Zee C, Soetaert K, Helder W (2002) On the oxidation and burial of organic carbon in sediments of the Iberian margin and Nazaré Canyon (NE Atlantic). Prog Oceanogr 52 (2-4):399-431

Eppley RW (1989) New production: History, Methods, Problems. In: Berger WH, Smetacek VS, Wefer G (eds) Productivity of the Ocean: Present and Past. John Wiley & Sons, Chichester, pp 85-97

Fabiano M, Danovaro R (1994) Composition of organic matter in sediments facing a river estuary (Tyrrhenian Sea): relationships with bacteria and microphytobenthic biomass. Hydrobiologia 277 (2):71-84. doi:10.1007/BF00016755

Falcão M, Gaspar MB, Caetano M, Santos MN, Vale C (2003) Short-term environmental impact of clam dredging in coastal waters (south of Portugal): chemical disturbance and subsequent recovery of seabed. Mar Environ Res 56 (5):649-664. doi:10.1016/s0141-1136(03)00069-2

Fang T-H, Chen J-L, Huh C-A (2007) Sedimentary phosphorus species and sedimentation flux in the East China Sea. Cont Shelf Res 27 (10-11):1465-1476

Feely RA, Sabine CL, Hernandez-Ayon JM, Ianson D, Hales B (2008) Evidence for Upwelling of Corrosive "Acidified" Water onto the Continental Shelf. Science 320 (5882):1490-1492. doi:10.1126/science.1155676

Fenchel T, Glud RN (2000) Benthic primary production and O2-CO2 dynamics in a shallow-water sediment: Spatial and temporal heterogeneity. Ophelia 53 (2):159-171. doi:10.1080/00785236.2000.10409446

Fettweis M, Francken F, Van den Eynde D, Verwaest T, Janssens J, Van Lancker V (2010) Storm influence on SPM concentrations in a coastal turbidity maximum area with high anthropogenic impact (southern North Sea). Cont Shelf Res 30 (13):1417-1427. doi:DOI: 10.1016/j.csr.2010.05.001

Fitzgerald WF, Lamborg CH, Hammerschmidt CR (2007) Marine biogeochemical cycling of mercury. Chem Rev (Washington, DC, U S) 107 (2):641-662. doi:10.1021/cr050353m

Fitzsimons MF, Dawit M, Revitt DM, Rocha C (2005) Effects of early tidal inundation on the cycling of methylamines in inter-tidal sediments. Mar Ecol Prog Ser 294:51-61

Fitzsimons MF, Millward GE, Revitt DM, Dawit MD (2006) Desorption kinetics of ammonium and methylamines from estuarine sediments: Consequences for the cycling of nitrogen. Mar Chem 101 (1-2):12-26. doi:DOI: 10.1016/j.marchem.2005.12.006

Flocas AA (1988) Frontal depressions over the Mediterranean sea and central southern Europe. Les perturbations frontales au-dessus de la mer Méditerranée et de l'Europe centrale méridionale. Méditerranée:43-52

Forster S, Graf G (1995) Impact of irrigation on oxygen flux into the sediment: intermittent pumping by Callianassa subterranea and “piston-pumping” by Lanice conchilega. Marine Biology 123 (2):335-346

Foster JM, Shimmield GB (2002) 234Th as a tracer of particle flux and POC export in the northern North Sea during a coccolithophore bloom. Deep Sea Research Part II: Topical Studies in Oceanography 49 (15):2965-2977. doi:10.1016/s0967-0645(02)00066-8

François R (1987) A Study of the Extraction Conditions of Sedimentary Humic Acids to Estimate Their True in-situ Sulfur-Content. Limnol Oceanogr 32 (4):964-972

Franks PJS (2002) NPZ Models of Plankton Dynamics: Their Construction, Coupling to Physics, and Application. Journal of Oceanography 58:379-387

Frid CLJ, Harwood KG, Hall SJ, Hall JA (2000) Long-term changes in the benthic communities on North Sea fishing grounds. ICES Journal of Marine Science: Journal du Conseil 57 (5):1303-1309. doi:10.1006/jmsc.2000.0900

Froelich PN, Bender ML, Luedtke NA (1982) The Marine Phosphorous Cycle. Am J Sci 282:474-511

Froelich PN, Klinkhammer GP, Bender ML, Luedtke NA, Heath GR, Cullen D, Dauphin P, Hammond D, Hartman B, Maynard V (1979) Early oxidation of organic matter in pelagic sediments of the eastern equatorial Atlantic: suboxic diagenesis. Geochim Cosmochim Acta 43:1075-1090

Gagnon C, Mucci A, Pelletier É (1996) Vertical distribution of dissolved sulphur species in coastal marine sediments. Mar Chem 52 (3-4):195-209

Ganju NK, Schoellhamer DH, Jaffe BE (2009) Hindcasting of decadal-timescale estuarine bathymetric change with a tidal-timescale model. J Geophys Res 114 (F4):F04019. doi:10.1029/2008jf001191

Gargas E, Mortensen E, Ærtjeberg-Nielsen G (1980) Production and photosynthetic efficiency of phytoplankton in the open Danish waters 1975-1977. Orphelia 1:Suppl. 123-144

Gieskes WWC, Kraay GW (1975) The phytoplankton spring bloom in Dutch coastal waters of the North Sea. Neth J Sea Res 9 (2):166-196. doi:10.1016/0077-7579(75)90014-9

Giles H, Pilditch CA, Nodder SD, Zeldis JR, Currie K (2007) Benthic oxygen fluxes and sediment properties on the northeastern New Zealand continental shelf. Cont Shelf Res 27 (18):2373-2388

Glud RN (2008) Oxygen dynamics of marine sediments. Mar Biol Res 4 (4):243-289. doi:10.1080/17451000801888726

Goering JJ, Cline JD (1970) A note on Denitrification in Seawater. Limnol Oceanogr 15 (2):306-309

Goldhaber MB, Aller RC, Cochran JK, Rosenfeld JK, Martens CS, Berner RA (1977) Sulfate reduction, diffusion, and bioturbation in Long Island Sound sediments; report of the FOAM Group. Am J Sci 277 (3):193-237. doi:10.2475/ajs.277.3.193

Goloway F, Bender M (1982) Diagenetic Models of Interstitial Nitrate Profiles in Deep Sea Suboxic Sediments. Limnol Oceanogr 27 (4):624-638

Goni MA, Teixeira MJ, Perkey DW (2003) Sources and distribution of organic matter in a river-dominated estuary (Winyah Bay, SC, USA). Estuar Coast Shelf Sci 57 (5-6):1023-1048. doi:10.1016/s0272-7714(03)00008-8

Greenwood N, Parker ER, Fernand L, Sivyer DB, Weston K, Painting SJ, Kröger S, Forster RM, Lees HE, Mills DK, Laane RWPM (2010) Detection of low bottom water oxygen concentrations in the North Sea; implications for monitoring and assessment of ecosystem health. Biogeosciences 7 (4):1357-1373. doi:10.5194/bg-7-1357-2010

Grémare A, Amouroux J-M, Cauwet G, Charles F, Courties C, De Bovée F, Dinet A, Devenon JL, De Madron XD, Ferre B, Fraunie P, Joux F, Lantoine F, Lebaron P, Naudin J-J, Palanques A, Pujo-Pay M, Zudaire L (2003) The effects of a strong

winter storm on physical and biological variables at a shelf site in the Mediterranean. Oceanologica Acta 26 (4):407–419

Gross MG, Gross E (1996) Oceanography: a View of the Earth. 7 edn. Prentice-Hall Inc., London

Grunwald M, Dellwig O, Beck M, Dippner JW, Freund JA, Kohlmeier C, Schnetger B, Brumsack H-J (2009) Methane in the southern North Sea: Sources, spatial distribution and budgets. Estuar Coast Shelf Sci 81 (4):445–456

Gunnars A, Blomqvist S, Martinsson C (2004) Inorganic formation of apatite in brackish seawater from the Baltic Sea: an experimental approach. Mar Chem 91 (1-4):15–26

Gutiérrez D, Gallardo VA, Mayor S, Neira C, Vásquez C, Sellanes J, Rivas M, Soto A, Carrasco F, Baltazar M (2000) Effects of dissolved oxygen and fresh organic matter on the bioturbation potential of macrofauna in sublittoral sediments off Central Chile during the 1997/1998 El NiÃ±o. Mar Ecol Prog Ser 202:81–99. doi:10.3354/meps202081

Gypens N, Lancelot C, Soetaert K (2008) Simple parameterisations for describing N and P diagenetic processes: Application in the North Sea. Prog Oceanogr 76 (1):89–110. doi:10.1016/j.pocean.2007.10.003

Hales B, Emerson S, Archer D (1994) Respiration and Dissolution in the Sediments of the Western North Atlantic: Estimates from Models of *in situ* Microelectrode Measurements of Porewater Oxygen and pH. Deep-Sea Research Part I 41:695–719

Hall POJ, Hulth S, Hulthe G, Landen A, Tengberg A (1996) Benthic nutrient fluxes on a basin-wide scale in the Skagerrak (north-eastern North Sea). J Sea Res 35 (1-3):123–137

Hammond DE, McManus J, Berelson WM, Kilgore TE, Pope RH (1996) Early diagenesis of organic material in equatorial Pacific sediments: Stoichiometry and kinetics. Deep-Sea Research Part II-Topical Studies in Oceanography 43 (4-6):1365–1412

Hartnett HE, Keil RG, Hedges JI, Devol AH (1998) Influence of oxygen exposure time on organic carbon preservation in continental margin sediments. Nature 391 (6667):572–575

Hayes DF, Crockett TR, Ward TJ, Averett D (2000) Sediment Resuspension during Cutterhead Dredging Operations. Journal of Waterway, Port, Coastal, and Ocean Engineering 126 (3):153–161

Hedges JI, Clark WA, Cowie GL (1988) Fluxes and Reactivities of Organic Matter in a Coastal Marine Bay. Limnol Oceanogr 33 (5):1137–1152

Henrichs SM (1992) Early diagenesis of organic matter in marine sediments: progress and perplexity. Mar Chem 39 (1-3):119–149

Herman PMJ, Soetaert K, Middelburg JJ, Heip C, Lohse L, Epping E, Helder W, Antia AN, Peinert R (2001) The seafloor as the ultimate sediment trap--using sediment properties to constrain benthic-pelagic exchange processes at the Goban Spur. Deep Sea Research Part II: Topical Studies in Oceanography 48 (14-15):3245–3264

Hiddink JG, Jennings S, Kaiser MJ (2006) Indicators of the Ecological Impact of Bottom-Trawl Disturbance on Seabed Communities. Ecosystems 9:1190–1199

Hochard S, Pinazo C, Grenz C, Evans JLB, Pringault O (2010) Impact of microphytobenthos on the sediment biogeochemical cycles: A modeling approach. Ecol Model 221 (13-14):1687–1701. doi:DOI: 10.1016/j.ecolmodel.2010.04.002

Holling CS (1959) Some Characteristics of Simple Types of Predation and Parasitism. The Canadian Entomologist 91 (7):385–398. doi:doi:10.4039/Ent91385-7

Huettel M, Cook P, Janssen F, Lavik G, Middelburg JJ (2007) Transport and degradation of a dinoflagellate bloom in permeable sublittoral sediment. Mar Ecol Prog Ser 340:139–153. doi:10.3354/meps340139

Hyacinthe C, Anschutz P, Carbonel P, Jouanneau JM, Jorissen FJ (2001) Early diagenetic processes in the muddy sediments of the Bay of Biscay. Mar Geol 177 (1–2):111–128

Hyacinthe C, Van Cappellen P (2004) An authigenic iron phosphate phase in estuarine sediments: composition, formation and chemical reactivity. Mar Chem 91 (1–4):227–251

Hydes DJ, Kelly-Gerreyn BA, Le Gall AC, Proctor R (1999) The balance of supply of nutrients and demands of biological production and denitrification in a temperate latitude shelf sea – a treatment of the southern North Sea as an extended estuary. Mar Chem 68 (1–2):117–131

ICES (2008) ICES-FishMap: Factors affecting the distribution of North Sea fish http://www.ices.dk/marineworld/ices-fishmap.asp. Accessed 7th March 2012

Iversen N, Jørgensen BB (1993) Diffusion coefficients of sulfate and methane in marine sediments: Influence of porosity. Geochim Cosmochim Acta 57 (3):571–578

Jago CF, Bull CFJ (2000) Quantification of errors in transmissometer-derived concentration of suspended particulate matter in the coastal zone: implications for flux determinations. Mar Geol 169 (3–4):273–286

Jago CF, Jones SE (1998) Observation and modelling of the dynamics of benthic fluff resuspended from a sandy bed in the southern North Sea. Cont Shelf Res 18 (11):1255–1282

Jago CF, Jones SE, Latter RJ, McCandliss RR, Hearn MR, Howarth MJ (2002) Resuspension of benthic fluff by tidal currents in deep stratified waters, northern North Sea. J Sea Res 48 (4):259–269

Jahnke RA (1996) The Global Ocean Flux of Particulate Organic Carbon: A Real Distribution and Magnitude. Global Biogeochem Cycles 10 (1):71–88

Jahnke RA, Emerson SR, Reimers CE, Schuffert J, Ruttenberg K, D. A (1989) Benthic Recycling of Biogenic Debris in the Eastern Tropical Atlantic Ocean. Geochim Cosmochim Acta 53:2947–2960

Jahnke RA, Reimers CE, Craven DB (1990) Intensification of recycling of organic matter at the sea floor near ocean margins. Nature 348:50–54

Janssen F, Huettel M, Witte U (2005) Pore-Water Advection and Solute Fluxes in Permeable Marine Sediments (II): Benthic Respiration at Three Sandy Sites with Different Permeabilities (German Bight, North Sea). Limnol Oceanogr 50 (3):779–792

Jenkins WJ, Goldman JC (1985) Seasonal oxygen cycling and primary production in the Sargasso Sea. J Mar Res 43 (2):465–491

Jensen HS, Mortensen PB, Andersen FØ, Rasmussen E, Jensen A (1995) Phosphorous Cycling in a Coastal Marine Sediment, Aarhus Bay, Denmark. Limnol Oceanogr 40 (5):908–917

Jensen MM, Holmer M, Thamdrup B (2005) Composition and diagenesis of neutral carbohydrates in sediments of the Baltic–North Sea transition. Geochim Cosmochim Acta 69 (16):4085–4099. doi:10.1016/j.gca.2005.01.021

Jensen MM, Thamdrup B, Rysgaard S, Holmer M, Fossing H (2003) Rates and regulation of microbial iron reduction in sediments of the Baltic–North Sea transition. Biogeochemistry 65 (3):295–317

Jickells T, Andrews J, Samways G, Sanders R, Malcolm S, Sivyer D, Parker R, Nedwell D, Trimmer M, Ridgway J (2000) Nutrient fluxes through the Humber estuary – Past, present and future. AMBIO: A Journal of the Human Environment 29 (3):130–135

Joassin P, Delille B, Soetaert K, Harlay J, Borges AV, Chou L, Riebesell U, Suykens K, Grégoire M (2011) Carbon and nitrogen flows during a bloom of the coccolithophore Emiliania huxleyi: Modelling a mesocosm experiment. J Mar Syst 85 (3-4):71-85. doi:DOI: 10.1016/j.jmarsys.2010.11.007

Jones SE, Jago CF, Bale AJ, Chapman D, Howland RJM, Jackson J (1998) Aggregation and resuspension of suspended particulate matter at a seasonally stratified site in the southern North Sea: physical and biological controls. Cont Shelf Res 18 (11):1283-1309

Jonge VNd, Beusekom JEEv (1995) Wind-and Tide-Induced Resuspension of Sediment and Microphytobenthos from Tidal Flats in the Ems Estuary. Limnol Oceanogr 40 (4):766-778

Jørgensen BB (1996) Material flux in the sediment. In: Eutrophication in Coastal Marine Ecosystems, vol 52. Coastal Estuarine Studies. AGU, Washington, DC, pp 115-135. doi:10.1029/CE052p0115

Jørgensen BB, Bang M, Blackburn TH (1990) Anaerobic Mineralization in Marine-Sediments from the Baltic-Sea-North-Sea Transition. Marine Ecology-Progress Series 59 (1-2):39-54

Kamiyama K, Okuda S, Kawai A (1976) Studies on the Release of Ammonium Nitrogen from the Bottom Sediments in Fresh Water Bodies Part 1: A Preliminary Experiment Using an Annular Channel. Jpn J Limnol 37 (2):59-66

Kasih GAA, Chiba S, Yamagata Y, Shimizu Y, Haraguchi K (2008) Modeling early diagenesis of sediment in Ago Bay, Japan: A comparison of steady state and dynamic calculations. Ecol Model 215 (1-3):40-54. doi:DOI: 10.1016/j.ecolmodel.2008.02.025

Katsev S, Rancourt DG, L'Heureux I (2004) dSED: a database tool for modeling sediment early diagenesis. Comput Geosci 30 (9-10):959-967. doi:10.1016/j.cageo.2004.06.005

Kazancı C (2007) EcoNet: A new software for ecological modeling, simulation and network analysis. Ecol Model 208 (1):3-8. doi:10.1016/j.ecolmodel.2007.04.031

Kelly-Gerreyn BA, Hydes DJ, Trimmer M, Nedwell DB (1999) Calibration of an early diagenesis model for high nitrate, low reactive sediments in a temperate latitude estuary (Great Ouse, UK). Marine Ecology-Progress Series 177:37-50

Khalil K, Rabouille C, Gallinari M, Soetaert K, DeMaster DJ, Ragueneau O (2007) Constraining biogenic silica dissolution in marine sediments: A comparison between diagenetic models and experimental dissolution rates. Mar Chem 106 (1-2):223-238

Klamer HJC, Leonards PEG, Lamoree MH, Villerius LA, Åkerman JE, Bakker JF (2005) A chemical and toxicological profile of Dutch North Sea surface sediments. Chemosphere 58 (11):1579-1587. doi:10.1016/j.chemosphere.2004.11.027

Knauer GA (1993) Productivity and new production of the oceanic systems. In: Wollast R, MacKenzie FT, Chou L (eds) Interactions of C, N, P and S Biogeochemical Cycles and Global Change. Springer-Verlag, New York, pp 211-231

Koretsky C, Meile C, Van Cappellen P (2002) Quantifying bioirrigation using ecological parameters: a stochastic approach[dagger]. Geochem Trans 3 (1):17

Kremling K, Wilhelm G (1997) Recent increase of the calcium concentrations in Baltic Sea waters. Mar Pollut Bull 34 (10):763-767

Kristensen E (2000) Organic matter diagenesis at the oxic/anoxic interface in coastal marine sediments, with emphasis on the role of burrowing animals. Hydrobiologia 426 (1):1-24. doi:10.1023/A:1003980226194

Krom MD, Berner RA (1980) The Diffusion Coefficients of Sulfate, Ammonium, and Phosphate Ions in Anoxic Marine Sediments. Limnol Oceanogr 25 (2):327-337

Laës A, Blain S, Laan P, Ussher SJ, Achterberg EP, Treguer P, de Baar HJW (2007) Sources and transport of dissolved iron and manganese along the continental margin of the Bay of Biscay. Biogeosciences 4 (2):181-194

Lampitt RS, Wishner KF, Turley CM, Angel MV (1993) Marine snow studies in the Northeast Atlantic Ocean: distribution, composition and role as a food source for migrating plankton. Marine Biology 116 (4):689-702. doi:10.1007/bf00355486

Langston WJ, Burt GR, Pope ND (1999) Bioavailability of Metals in Sediments of the Dogger Bank (Central North Sea): A Mesocosm Study. Estuar Coast Shelf Sci 48 (5):519-540

Leipe T, Tauber F, Vallius H, Virtasalo J, Uścinowicz S, Kowalski N, Hille S, Lindgren S, Myllyvirta T (2011) Particulate organic carbon (POC) in surface sediments of the Baltic Sea. Geo-Mar Lett 31 (3):175-188. doi:10.1007/s00367-010-0223-x

Leivuori M, Vallius H (1998) A case study of seasonal variation in the chemical composition of accumulating suspended sediments in the central gulf of Finland. Chemosphere 36 (10):2417-2435

Lerman A (1979) Geochemical processes : water and sediment environments. Wiley, New York

Li Y-H, Gregory S (1974) Diffusion of ions in sea water and in deep-sea sediments. Geochim Cosmochim Acta 38 (5):703-714. doi:10.1016/0016-7037(74)90145-8

Libes SM (1992) An Introduction to Marine Biogeochemistry. John Wiley & Sons, Inc., New York

Liu X, Huang W (2009) Modeling sediment resuspension and transport induced by storm wind in Apalachicola Bay, USA. Environmental Modelling & Software 24 (11):1302-1313

Lohse L, Epping EHG, Helder W, van Raaphorst W (1996) Oxygen pore water profiles in continental shelf sediments of the North Sea: Turbulent versus molecular diffusion. Marine Ecology-Progress Series 145 (1-3):63-75

Lohse L, Helder W, Epping EHG, Balzer W (1998) Recycling of organic matter along a shelf-slope transect across the NW European Continental Margin (Goban Spur). Prog Oceanogr 42 (1-4):77-110

Lohse L, Malschaert JFP, Slomp CP, Helder W, van Raaphorst W (1993) Nitrogen cycling in North Sea sediments: interaction of denitrification and nitrification in offshore and coastal areas. Mar Ecol Prog Ser 101:283-296

Luff R, Moll A (2004) Seasonal dynamics of the North Sea sediments using a three-dimensional coupled sediment-water model system. Cont Shelf Res 24 (10):1099-1127. doi:10.1016/j.csr.2004.03.010

Mackin JE, Aller RC (1984) Ammonium adsorption in marine sediments. Limnol Oceanogr 29 (2):250-257

Mackin JE, Swider KT (1989) Organic matter decomposition pathways and oxygen consumption in coastal marine sediments. J Mar Res 47:681-716

Madsen SD, Forbes TL, Forbes VE (1997) Particle mixing by the polychaete *Capitella* species. 1: Coupling fate and effect of a particle-bound organic contaminant (fluoranthene) in a marine sediment. Marine Ecology-Progress Series 147 (1-3):129-142. doi:10.3354/meps147129

Martin WR, Sayles FL (1994) Seafloor Diagenetic Fluxes. In: Material Fluxes on the Surface of the Earth. National Academy Press, Washington D.C., pp 143-164

McDuff RE, Ellis RA (1979) Determining diffusion coefficients in marine sediments; a laboratory study of the validity of resistivity techniques. Am J Sci 279 (6):666-675

McGinnis DF, Berg P, Brand A, Lorrai C, Edmonds TJ, Wuest A (2008) Measurements of eddy correlation oxygen fluxes in shallow freshwaters: towards routine applications and analysis. Geophys Res Lett 35 (4):L04403-04401-04405. doi:10.1029/2007gl032747

McManus JP, Prandle D (1997) Development of a model to reproduce observed suspended sediment distributions in the southern North Sea using Principle Component Analysis and Multiple Linear Regression. Cont Shelf Res 17 (7):761-778

McNichol AP, Aluwihare LI (2007) The Power of Radiocarbon in Biogeochemical Studies of the Marine Carbon Cycle: Insights from Studies of Dissolved and Particulate Organic Carbon (DOC and POC). Chem Rev (Washington, DC, U S) 107:443-466

Meile C, Berg P, Van Cappellen P, Tuncay K (2005) Solute-specific pore water irrigation: Implications for chemical cycling in early diagenesis. J Mar Res 63 (3):601-621

Meile C, Koretsky CM, Van Cappellen P (2001) Quantifying bioirrigation in aquatic sediments: An inverse modeling approach. Limnol Oceanogr 46 (1):164-177

Mendes P (1993) GEPASI: a software package for modelling the dynamics, steady states and control of biochemical and other systems. Computer applications in the biosciences : CABIOS 9 (5):563-571. doi:10.1093/bioinformatics/9.5.563

Meyer-Reil LA (1983) Benthic response to sedimentation events during autumn to spring at a shallow water station in the Western Kiel Bight. Marine Biology 77 (3):247-256. doi:10.1007/bf00395813

Meyercordt J, Gerbersdorf S, Meyer-Reil L-A (1999) Significance of pelagic and benthic primary production in two shallow coastal lagoons of different degrees of eutrophication in the southern Baltic Sea. Aquat Microb Ecol 20 (3):273-284. doi:10.3354/ame020273

Meysman FJR, Boudreau BP, Middelburg JJ (2003a) Relations between local, nonlocal, discrete and continuous models of bioturbation. J Mar Res 61:391-410

Meysman FJR, Boudreau BP, Middelburg JJ (2005) Modeling reactive transport in sediments subject to bioturbation and compaction. Geochim Cosmochim Acta 69 (14):3601-3617

Meysman FJR, Galaktionov OS, Gribsholt B, Middelburg JJ (2006) Bio-irrigation in permeable sediments: An assessment of model complexity. J Mar Res 64 (4):589-627

Meysman FJR, Middelburg JJ, Herman PMJ, Heip CHR (2003b) Reactive transport in surface sediments. I. Model complexity and software quality. Comput Geosci 29 (3):291-300

Middelburg JJ (1989) A simple rate model for organic matter decomposition in marine sediments. Geochim Cosmochim Acta 53 (7):1577-1581

Middelburg JJ (1991) Organic Matter Decomposition in the Marine Environment. In: Nierenberg WA (ed) Encyclopedia of earth system science, vol 3. Academic press, San Diego; New York; London,

Millero FJ (2006) Chemical Oceanography. CRC Marine Science Series, Third edn. CRC Press, Boca Raton, FL

Moodley L (1990) Southern North Sea seafloor and subsurface distribution of living benthic foraminifera. Neth J Sea Res 27 (1):57-71. doi:10.1016/0077-7579(90)90034-e

Morris AW, Howarth MJ (1998) Bed stress induced sediment resuspension (SERE 88/89). Cont Shelf Res 18 (11):1203-1213. doi:10.1016/s0278-4343(98)00040-5

Mortimer RJG, Harris SJ, Krom MD, Freitag TE, Prosser JI, Barnes J, Anschutz P, Hayes PJ, Davies IM (2004) Anoxic Nitrification in Marine Sediments. Mar Ecol Prog Ser 276:37-51

Mouret A, Anschutz P, Lecroart P, Chaillou G, Hyacinthe C, Deborde J, Jorissen F, Deflandre B, Schmidt S, Jouanneau J-M (2009) Benthic geochemistry of manganese in the Bay of Biscay, and sediment mass accumulation rate. Geo-Mar Lett 29 (3):133-149

Murrell MC, Campbell JG, Hagy Iii JD, Caffrey JM (2009) Effects of irradiance on benthic and water column processes in a Gulf of Mexico estuary: Pensacola Bay, Florida, USA. Estuar Coast Shelf Sci 81 (4):501-512

Nedwell DB, Parkes RJ, Upton AC, Assinder DJ (1993) Seasonal Fluxes across the Sediment-Water Interface, and Processes within Sediments. Philosophical Transactions: Physical Sciences and Engineering 343 (1669):519-529

Neubacher EC, Parker ER, Trimmer M (2011) Short-term hypoxia alters the balance of the nitrogen cycle in coastal sediments. Limnol Oceanogr 56 (2):651-665

NIST/SEMATECH (2012) e-Handbook of Statistical Methods. http://www.itl.nist.gov/div898/handbook/. Accessed 01 April 2012

Noji TT, Noji CIM, Klungsoyr J (2002) The role of sedimentation and resuspension for the transport of sediments and contaminants in the Skagerrak. Hydrobiologia 469 (1-3):99-108

North Sea Task Force (1993) North Sea Quality Status Report 1993. Oslo and Paris Commissions, London. Olsen & Olsen, Fredensborg, Denmark

O'Brien JJ, Wroblewski.J.S. (1973) Simulation of Mesoscale Distribution of Lower Marine Trophic Levels off West Florida. Investigacion Pesquera 37 (2):193-244

O'Brien MC, Macdonald RW, Melling H, Iseki K (2006) Particle fluxes and geochemistry on the Canadian Beaufort Shelf: Implications for sediment transport and deposition. Cont Shelf Res 26 (1):41-81. doi:10.1016/j.csr.2005.09.007

Osinga R, Kop AJ, Duineveld GCA, Prins RA, Van Duyl FC (1996) Benthic mineralization rates at two locations in the southern North Sea. J Sea Res 36 (3-4):181-191

OSPAR (2010) Quality Status Report 2010. OSPAR Commission, London

Overnell J, Edwards A, Grantham BE, Harvey SM, Jones KJ, Leftley JW, Smallman DJ (1995) Sediment-Water Column Coupling and the Fate of the Spring Phytoplankton Bloom in Loch Linnhe, a Scottish Fjordic Sea-loch. Sediment Processes and Sediment-Water Fluxes. Estuar Coast Shelf Sci 41 (1):1-19

Parry ML, Canziani OF, Palutikof JP, van der Linden PJ, Hanson CE (2007) Climate change 2007: impacts, adaptation and vulnerability. Intergovernmental Panel on Climate Change,

Passier HF, Luther GW, III, de Lange GJ (1997) Early diagenesis and sulphur speciation in sediments of the Oman Margin, northwestern Arabian Sea. Deep Sea Research Part II: Topical Studies in Oceanography 44 (6-7):1361-1380

Pedersen TF, Price NB (1982) The geochemistry of manganese carbonate in Panama Basin sediments. Geochim Cosmochim Acta 46 (1):59-68. doi:10.1016/0016-7037(82)90290-3

Pederstad K, Roaldset E, Rønningsland TM (1993) Sedimentation and environmental conditions in the inner Skagerrak-outer Oslofjord. Mar Geol 111 (3-4):245-268

Pejrup M, Valeur J, Jensen A (1996) Vertical fluxes of particulate matter in Aarhus Bight, Denmark. Cont Shelf Res 16 (8):1047-1064

Petzold L (1983) Automatic Selection of Methods for Solving Stiff and Nonstiff Systems of Ordinary Differential Equations. SIAM Journal on Scientific and Statistical Computing 4 (1):136-148

Piet GJ, Rijnsdorp AD, Bergman MJN, van Santbrink JW, Craeymeersch J, Buijs J (2000) A quantitative evaluation of the impact of beam trawling on benthic fauna in the southern North Sea. ICES Journal of Marine Science: Journal du Conseil 57 (5):1332-1339. doi:10.1006/jmsc.2000.0915

Pleskachevsky A, Gunther H Modeling of suspended particulate matter transport in coastal areas. In: 2008 IEEE/OES US/EU-Baltic International Symposium (BALTIC), Tallinn, Estonia, 27-29 May 2008. IEEE, pp 8 pp.-8 pp. doi:10.1109/baltic.2008.4625511

Polerecky L, Volkenborn N, Stief P (2006) High Temporal Resolution Oxygen Imaging in Bioirrigated Sediments. Environ Sci Technol 40 (18):5763-5769. doi:10.1021/es060494l

Pope RH, Demaster DJ, Smith CR, Seltmann H (1996) Rapid bioturbation in equatorial Pacific sediments: evidence from excess ^{234}Th measurements. Deep Sea Research Part II: Topical Studies in Oceanography 43 (4-6):1339-1364. doi:Doi: 10.1016/0967-0645(96)00009-4

Postma H (1981) Exchange of materials between the North Sea and the Wadden Sea. Mar Geol 40 (1-2):199-213. doi:10.1016/0025-3227(81)90050-5

Press WH, Teukolsky SA, Vetterling WT, Flannery BP (1992) Numerical recipes in FORTRAN : the art of scientific computing. Cambridge University Press, Cambridge [England]; New York, NY, USA

Pusceddu A, Fiordelmondo C, Danovaro R (2005a) Sediment Resuspension Effects on the Benthic Microbial Loop in Experimental Microcosms. Microb Ecol 50 (4):602-613. doi:10.1007/s00248-005-5051-6

Pusceddu A, Gremare A, Escoubeyrou K, Amouroux JM, Fiordelmondo C, Danovaro R (2005b) Impact of natural (storm) and anthropogenic (trawling) sediment resuspension on particulate organic matter in coastal environments. Cont Shelf Res 25 (19-20):2506-2520. doi:10.1016/j.csr.2005.08.012

Radach G, Berg J, Hagmeier E (1990) Long-term changes of the annual cycles of meteorological, hydrographic, nutrient and phytoplankton time series at Helgoland and at LV ELBE 1 in the German Bight. Cont Shelf Res 10 (4):305-328. doi:10.1016/0278-4343(90)90054-P

Ragueneau O, Tréguer P, Leynaert A, Anderson RF, Brzezinski MA, DeMaster DJ, Dugdale RC, Dymond J, Fischer G, François R, Heinze C, Maier-Reimer E, Martin-Jézéquel V, Nelson DM, Quéguiner B (2000) A review of the Si cycle in the modern ocean: recent progress and missing gaps in the application of biogenic opal as a paleoproductivity proxy. Global and Planetary Change 26 (4):317-365

Rajendran A, Kumar MD, Bakker JF (1992) Control of manganese and iron in Skagerrak sediments (northeastern North Sea). Chem Geol 98 (1-2):111-129. doi:10.1016/0009-2541(92)90094-I

Rauch M, Denis L (2008) Spatio-temporal variability in benthic mineralization processes in the eastern English Channel. Biogeochemistry 89 (2):163-180. doi:10.1007/s10533-008-9191-x

Redfield AC (1934) On the proportions of organic derivations in sea water and their relation to the composition of plankton. In: Daniel RJ (ed) James Johnstone Memorial Volume. University Press of Liverpool, Liverpool, pp 177-192

Redfield AC (1958) The Biological Control of Chemical Factors in the Environment. Am Sci 46 (3):205-222

Reimers CE, Jahnke RA, McCorkle DC (1992) Carbon fluxes and burial rates over the continental slope and rise off central California with implications for the global carbon cycle. Global Biogeochem Cycles 6 (2):199-224. doi:10.1029/92gb00105

Rendell AR, Ottley CJ, Jickells TD, Harrison RM (1993) The atmospheric input of nitrogen species to the North Sea. Tellus B 45 (1):53-63. doi:10.1034/j.1600-0889.1993.00005.x

Revsbech NP, Sorensen J, Blackburn TH, Lomholt JP (1980) Distibution of Oxygen in Marine Sediments Measured with Microelectrodes. Limnol Oceanogr 25 (3):403-411

Rhoads DC, Young DK (1970) The Influence of Deposity-feeding Organisms on Sediment Stability and Community Trophic Structure. J Mar Res 28 (2):150-178

Riebesell U (2004) Effects of CO_2 Enrichment on Marine Phytoplankton. Journal of Oceanography 60 (4):719-729

Riebesell U, Zondervan I, Rost B, Tortell PD, Zeebe RE, Morel FMM (2000) Reduced calcification of marine plankton in response to increased atmospheric CO2. Nature 407 (6802):364-367

Robinson RA, Stokes RH (1959) Electrolyte Solution. 2 edn. Butterworths,

Rowden AA, Jago CF, Jones SE (1998a) Influence of benthic macrofauna on the geotechnical and geophysical properties of surficial sediment, North Sea. Cont Shelf Res 18 (11):1347-1363. doi:10.1016/s0278-4343(98)00047-8

Rowden AA, Jones MB, Morris AW (1998b) The role of Callianassa subterranea (Montagu) (THALASSINIDEA) in sediment resuspension in the North Sea. Cont Shelf Res 18 (11):1365-1380. doi:10.1016/s0278-4343(98)00048-x

Rusch A, Huettel M, Forster S (2000) Particulate organic matter in permeable marine sands - Dynamics in time and depth. Estuar Coast Shelf Sci 51 (4):399-414

Rutgers van der Loeff MM (1980a) Nutrients in the Interstitial Waters of the Southern Bight of the North Sea. Neth J Sea Res 14 (2):144-171

Rutgers van der Loeff MM (1980b) Time variation in interstitial nutrient concentrations at an exposed subtidal station in the Dutch Wadden sea. Neth J Sea Res 14 (2):123-143. doi:10.1016/0077-7579(80)90018-6

Rysgaard S, Fossing H, Jensen MM (2001) Organic matter degradation through oxygen respiration, denitrification, and manganese, iron, and sulfate reduction in marine sediments (the Kattegat and the Skagerrak). Ophelia 55 (2):77-91

Salomons W, Mook WG (1981) Field observations of the isotopic composition of particulate organic carbon in the southern North Sea and adjacent estuaries. Mar Geol 41 (3-4):M11-M20. doi:10.1016/0025-3227(81)90079-7

Sanford LP, Panageotou W, Halka JP (1991) Tidal resuspension of sediments in northern Chesapeake Bay. Mar Geol 97 (1-2):87-103. doi:Doi: 10.1016/0025-3227(91)90020-5

Sayles FL, Smith SP, E. GJ (1995) Deep ocean sludge disposal, sediment oxygen consumption and sediment redox profiles at deep water municipal dump site 106. Journal of Marine Environmental Engineering 3:99-130

Schenau SJ, De Lange GJ (2001) Phosphorus regeneration vs. burial in sediments of the Arabian Sea. Mar Chem 75 (3):201-217

Schippers A, Jørgensen BB (2001) Oxidation of pyrite and iron sulfide by manganese dioxide in marine sediments. Geochim Cosmochim Acta 65 (6):915-922

Schlesinger WH (1997) Biogeochemistry: An Analysis of Global Change. Academic Press, San Diego, CA

Schoellhamer DH (1996) Anthropogenic Sediment Resuspension Mechanisms in a Shallow Microtidal Estuary. Estuar Coast Shelf Sci 43 (5):533-548. doi:10.1006/ecss.1996.0086

Schoemann V, de Baar HJW, de Jong JTM, Lancelot C (1998) Effects of phytoplankton blooms on the cycling of manganese and iron in coastal waters. Limnol Oceanogr 43 (7):1427-1441

Schulz HD, Dahmke A, Schinzel U, Wallmann K, Zabel M (1994) Early diagenetic processes, fluxes, and reaction rates in sediments of the South Atlantic. Geochim Cosmochim Acta 58 (9):2041-2060

Schwarzenbach RP, Gschwend PM, Imboden DM (1993) Environmental organic chemistry. Wiley, New York

Seifert T, Fennel W, Kuhrts C (2009) High resolution model studies of transport of sedimentary material in the south-western Baltic. J Mar Syst 75 (3-4):382-396

Seitzinger SP, Nixon SW, Pilson MEQ (1984) Denitrification and Nitrous Oxide Production in a Coastal Marine Ecosystem. Limnol Oceanogr 29 (1):73-83

Skogen MD, Moll A (2000) Interannual variability of the North Sea primary production: comparison from two model studies. Cont Shelf Res 20 (2):129-151. doi:10.1016/s0278-4343(99)00069-2

Slomp CP, Malschaert JFP, Lohse L, Van Raaphorst W (1997) Iron and manganese cycling in different sedimentary environments on the North Sea continental margin. Cont Shelf Res 17 (9):1083-1117

Slomp CP, Malschaert JFP, Raaphorst Wv (1998) The Role of Adsorption in Sediment-Water Exchange of Phosphate in North Sea Continental Margin Sediments. Limnol Oceanogr 43 (5):832-846

Slomp CP, Van der Gaast SJ, Van Raaphorst W (1996) Phosphorus binding by poorly crystalline iron oxides in North Sea sediments. Mar Chem 52 (1):55-73

Smith KL, Baldwin RJ, Williams PM (1992) Reconciling particulate organic carbon flux and sediment community oxygen consumption in the deep North Pacific. Nature 359 (6393):313-316

Smith WO, Codispoti LA, Nelson DM, Manley T, Buskey EJ, Niebauer HJ, Cota GF (1991) Importance of Phaeocystis blooms in the high-latitude ocean carbon cycle. Nature 352 (6335):514-516

Smits JGC (1980) Microbial decomposition of organic matter and nutrient regeneration in natural waters and sediments (report on literature study). In: report no. R1310-5. Delft Hydraulics, Delft, pp 1-117

Soetaert K, Herman PMJ (2009) A practical guide to ecological modelling: using R as a simulation platform. Springer, Dordrecht

Soetaert K, Herman PMJ, Middelburg JJ (1996a) Dynamic response of deep-sea sediments to seasonal variations: A model. Limnol Oceanogr 41 (8):1651-1668

Soetaert K, Herman PMJ, Middelburg JJ (1996b) A model of early diagenetic processes from the shelf to abyssal depths. Geochim Cosmochim Acta 60 (6):1019-1040

Soetaert K, Meysman FJR (2011) ReacTran: Reactive transport modelling in 1D, 2D and 3D. R package version 1.3.1, http://CRAN.R-project.org/package=ReacTran,

Soetaert K, Middelburg JJ, Wijsman JWM, Herman PMJ, Heip C (2002) Ocean Margin Early Diagenetic Processes and Models. In: Wefer G, Billet D, Hebbeln D, Jørgensen BB, Schlüter M, van Weering TCE (eds) Ocean Margin Systems. Springer, Berlin,

Soetaert K, Petzoldt T, Setzer RW (2009) deSolve: General solvers for initial value problems of ordinary differential equations (ODE), partial differential equations (PDE) and differential algebraic equations (DAE).

Soetaert K, Petzoldt T, Setzer RW (2010) Solving Differential Equations in R: Package deSolve. Journal of Statistical Software 33 (9):1-25

Ståhl H, Tengberg A, Brunnegård J, Bjørnbom E, Forbes TL, Josefson AB, Kaberi HG, Hassellöv IMK, Olsgard F, Roos P, Hall POJ (2004) Factors influencing organic carbon recycling and burial in Skagerrak sediments. J Mar Res 62 (6):867-907

Stahlberg C, Bastviken D, Svensson BH, Rahm L (2006) Mineralisation of organic matter in coastal sediments at different frequency and duration of resuspension. Estuar Coast Shelf Sci 70 (1-2):317-325. doi:10.1016/j.ecss.2006.06.022

Steele JH (1975) Biological Modelling II. In: Nihoul JCJ (ed) Elsevier Oceanography Series, vol Volume 10. Elsevier, pp 207-216

Stoeck T, Kroencke I, Garland JL (2003) Carbon utilization profiles of microbial communities in southern and central North Sea sediments in relation to environmental variables. Senckenb Marit 32 (1-2):11-23

Stumm W, Morgan JJ (1996) Aquatic Chemistry. Environmental Science and Technology. Wiley-Interscience, New York

Sun M, Aller RC, Lee C (1991) Early diagenesis of chlorophyll-a in Long Island Sound sediments: A measure of carbon flux and particle reworking. J Mar Res 49:379-401

Sundermann J, Prandle D, Lankester R, McCave IN (1993) Suspended Particulate Matter in the North Sea: Field Observations and Model Simulations [and Discussion]. Philosophical Transactions: Physical Sciences and Engineering 343 (1669):423-430

Tengberg A, Almroth E, Hall P (2003) Resuspension and its effects on organic carbon recycling and nutrient exchange in coastal sediments: in situ measurements using new experimental technology. J Exp Mar Biol Ecol 285-286:119-142. doi:Doi: 10.1016/s0022-0981(02)00523-3

Tett PB, Joint IR, Purdie DA, Baars M, Oosterhuis S, Daneri G, Hannah F, Mills DK, Plummer D, Pomroy AJ, Walne AW, Witte HJ, Howarth MJ, Lankester R (1993) Biological Consequences of Tidal Stirring Gradients in the North Sea. Philosophical Transactions of the Royal Society of London Series A: Physical and Engineering Sciences 343 (1669):493-508. doi:10.1098/rsta.1993.0061

Thamdrup B, Dalsgaard T (2000) The fate of ammonium in anoxic manganese oxide-rich marine sediment. Geochim Cosmochim Acta 64 (24):4157-4164. doi:10.1016/s0016-7037(00)00496-8

Thamdrup B, Fossing H, Jørgensen BB (1994) Manganese, iron and sulfur cycling in a coastal marine sediment, Aarhus bay, Denmark. Geochim Cosmochim Acta 58 (23):5115-5129

Thomas H, Bozec Y, de Baar HJW, Elkalay K, Frankignoulle M, Schiettecatte LS, Kattner G, Borges AV (2005) The carbon budget of the North Sea. Biogeosciences 2 (1):87-96

Thompson CEL, Couceiro F, Fones GR, Helsby R, Amos CL, Black K, Parker ER, Greenwood N, Statham PJ, Kelly-Gerreyn BA (2011) In situ flume measurements of resuspension in the North Sea. Estuar Coast Shelf Sci 94 (1):77-88. doi:10.1016/j.ecss.2011.05.026

Thornton SF, McManus J (1994) Application of Organic Carbon and Nitrogen Stable Isotope and C/N Ratios as Source Indicators of Organic Matter Provenance in Estuarine Systems: Evidence from the Tay Estuary, Scotland. Estuar Coast Shelf Sci 38 (3):219-233. doi:10.1006/ecss.1994.1015

Tian T, Merico A, Su J, Staneva J, Wiltshire K, Wirtz K (2009) Importance of resuspended sediment dynamics for the phytoplankton spring bloom in a coastal marine ecosystem. J Sea Res 62 (4):214-228

Trimmer M, Peterson J, Sivyer DB, Mills C, Young E, Parker ER (2005) Impact of long-term benthic trawl disturbance on sediment sorting and biogeochemistry in the southern North Sea. Mar Ecol Prog Ser 298:79-94

Tsunogai S, Noriki S (1991) Particulate fluxes of carbonate and organic carbon in the ocean. Is the marine biological activity working as a sink of the atmospheric carbon? Tellus B 43 (2):256-266. doi:10.1034/j.1600-0889.1991.00018.x

Ullman WJ, Aller RC (1982) Diffusion coefficients in nearshore marine sediments. Limnol Oceanogr 27 (3):552-556

Upton AC, Nedwell DB, Parkes RJ, Harvey SM (1993) Seasonal Benthic Microbial Activity in the Southern North-Sea - Oxygen-Uptake and Sulfate Reduction. Marine Ecology-Progress Series 101 (3):273-281

Van Cappellen P, Wang Y (1996) Cycling of Iron and Manganese in Surface Sediments: A General Theory for the Coupled Transport and Reaction of Carbon, Oxygen, Nitrogen, Sulfur, Iron, and Manganese. Am J Sci 296:197–243

van der Molen J, Bolding K, Greenwood N, Mills DK (2009) A 1-D vertical multiple grain size model of suspended particulate matter in combined currents and waves in shelf seas. J Geophys Res 114 (F1):F01030. doi:10.1029/2008jf001150

van der Weijden CH (1992) Early Diagenesis and Marine Pore Water. In: Wolf KH, Chilingarian GV (eds) Diagenesis, III. Developments in sedimentology. 47. Elsevier, Amsterdam, pp 13–134

van der Zee C, Slomp CP, van Raaphorst W (2002a) Authigenic P formation and reactive P burial in sediments of the Nazaré canyon on the Iberian margin (NE Atlantic). Mar Geol 185 (3–4):379–392

van der Zee C, van Raaphorst W, Helder W (2002b) Fe redox cycling in Iberian continental margin sediments (NE Atlantic). J Mar Res 60 (6):855–886

van der Zee C, van Raaphorst W, Helder W, de Heij H (2003) Manganese diagenesis in temporal and permanent depositional areas of the North Sea. Cont Shelf Res 23 (6):625–646. doi:10.1016/s0278-4343(03)00024-4

Van Duin EHS, Blom G, Los FJ, Maffione R, Zimmerman R, Cerco CF, Dortch M, Best EPH (2001) Modeling underwater light climate in relation to sedimentation, resuspension, water quality and autotrophic growth. Hydrobiologia 444 (1):25–42. doi:10.1023/a:1017512614680

van Raaphorst W, Kloosterhuis H, T., Cramer A, Bakker KJM (1990) Nutrient Early Diagenesis in the Sandy Sediments of the Dogger Bank Area, North Sea: Pore Water Results. Neth J Sea Res 26 (1):25–52

Van Raaphorst W, Kloosterhuis HT, Berghuis EM, Gieles AJM, Malschaert JFP, Van Noort GJ (1992) Nitrogen cycling in two types of sediments of the Southern North sea (Frisian front, broad fourteens): field data and mesocosm results. Neth J Sea Res 28 (4):293–316

van Raaphorst W, Malschaert JFP (1996) Ammonium adsorption in superficial North Sea sediments. Cont Shelf Res 16 (11):1415–1435

van Raaphorst W, Philippart CJM, Smit JPC, Dijkstra FJ, Malschaert JFP (1998) Distribution of suspended particulate matter in the North Sea as inferred from NOAA/AVHRR reflectance images and in situ observations. J Sea Res 39 (3–4):197–215

Van Weering TCE, Berger GW, Kalf J (1987) Recent Sediment Accumulation in the Skagerrak, North-Eastern North-Sea. Neth J Sea Res 21 (3):177–189

Vanderborght J-P, Billen G (1975) Vertical Distribution of Nitrate Concentration in Interstitial Water of Marine Sediments with Nitrification and Denitrification. Limnol Oceanogr 20 (6):953–961

Velegrakis AF, Michel D, Collins MB, Lafite R, Oikonomou EK, Dupont JP, Huault MF, Lecouturier M, Salomon JC, Bishop C (1999) Sources, sinks and resuspension of suspended particulate matter in the eastern English Channel. Cont Shelf Res 19 (15–16):1933–1957

Vink S, Chambers RM, Smith SV (1997) Distribution of phosphorus in sediments from Tomales Bay, California. Mar Geol 139 (1–4):157–179

Wainright SC, Hopkinson CS, Jr (1997) Effects of sediment resuspension on organic matter processing in coastal environments: A simulation model. J Mar Syst 11 (3–4):353–368. doi:10.1016/s0924-7963(96)00130-3

Wang YF, Van Cappellen P (1996) A multicomponent reactive transport model of early diagenesis: Application to redox cycling in coastal marine sediments. Geochim Cosmochim Acta 60 (16):2993–3014

Ward BA, Friedrichs MAM, Anderson TR, Oschlies A (2010) Parameter optimisation techniques and the problem of underdetermination in marine biogeochemical models. J Mar Syst 81 (1-2):34-43. doi:10.1016/j.jmarsys.2009.12.005

Warington R (1878) On Nitrification. Journal of the Chemical Society 33:44-51

Warnken KW, Gill GA, Dellapenna TM, Lehman RD, Harper DE, Allison MA (2003) The effects of shrimp trawling on sediment oxygen consumption and the fluxes of trace metals and nutrients from estuarine sediments. Estuar Coast Shelf Sci 57 (1-2):25-42

Watson PG, Frickers T (1995) Sediment-Water Exchange of Nutrients in the Southern North-Sea Adjacent to the Humber Estuary. Ophelia 41:361-384

Weissberg HL (1963) Effective Diffusion Coefficient in Porous Media. J Appl Phys 34 (9):2636-2639

Weisse R, von Storch H, Feser F (2005) Northeast Atlantic and North Sea Storminess as Simulated by a Regional Climate Model during 1958-2001 and Comparison with Observations. Journal of Climate 18 (3):465-479. doi:10.1175/jcli-3281.1

Westrich JT, Berner RA (1984) The Role of Sedimentary Organic Matter in Bacterial Sulfate Reduction: The G Model Tested. Limnol Oceanogr 29 (2):236-249

Williams PJ, le B. (1998) The balance of plankton respiration and photosynthesis in the open oceans. Nature 394:55-57

Williams PJ, le B., Bowers DG (1999) Regional Carbon Imbalances in the Oceans. Science 284 (1735b)

Winogradsky S (1890) Recherches sur les Organismes de la Nitrification. Computer Rendu 110:1013-1016

Winterwerp JC, van Kesteren WGM (2004) Introduction to the physics of cohesive sediment in the marine environment. Developments in Sedimentology. Elsevier, Amsterdam

Wright J, Colling A, Open University. Oceanography Course T (1995) Seawater: its composition, properties, and behaviour. Pergamon Press, in association with the Open University, Oxford [England]; New York